Responsive organocatalysis in soft materials

Trausel, Fanny

DOI
10.4233/uuid:c9b50bd1-2db6-4003-827b-883f11c18742

Publication date
2018

Document Version
Final published version

Citation (APA)
Trausel, F. (2018). *Responsive organocatalysis in soft materials*. [Dissertation (TU Delft), Delft University of Technology]. https://doi.org/10.4233/uuid:c9b50bd1-2db6-4003-827b-883f11c18742

Responsive organocatalysis in soft materials

Proefschrift

ter verkrijging van de graad van doctor
aan de Technische Universiteit Delft
op gezag van de Rector Magnificus prof. dr. ir. T.H.J.J. van der Hagen,
voorzitter van het College voor Promoties,
in het openbaar te verdedigen op

donderdag 13 september 2018 om 15:00 uur

door
Fanny TRAUSEL

Master of Science in Chemistry,
Universiteit Leiden
geboren te Dordrecht, Nederland

Dit proefschrift is goedgekeurd door de

promotor: Prof. dr. J.H. van Esch

promotor: Dr. R. Eelkema

Samenstelling promotiecommissie:

Rector Magnificus	voorzitter
Prof. dr. J.H. van Esch	Technische Universiteit Delft
Dr. R. Eelkema	Technische Universiteit Delft

Onafhankelijke leden:

Prof. dr. U. Hanefeld	Technische Universiteit Delft
Dr. S.A. Bonnet	Universiteit Leiden
Prof. dr. S.R. Harutyunyan	Rijksuniversiteit Groningen
Prof. dr. L.J. Prins	Università Degli Studi di Padova
Prof. dr. S.J. Picken	Technische Universiteit Delft, reservelid

Andere leden:

Prof. dr. F. Kapteijn	Technische Universiteit Delft

The work described in this thesis was carried out in the Advanced Soft Matter (ASM) group at Delft University of Technology, Faculty of Applied Sciences, Department of Chemical Engineering. This research has been funded by a VIDI grant from the Netherlands Organization for Scientific Research (NWO) and by an ERC consolidator grant from the European Research Council.

ISBN: 978-94-6186-947-0

Geprint door: Gildeprint, Enschede
Cover design: Annelies Kitsz

Table of contents

Chapter 1

Introduction

1.1 Control over material formation by the activation of catalysts

Cells react to the environment by changing the activity of enzymes in response to chemical signals (Fig. 1.1). Because catalysts such as enzymes lower the activation energy of reactions without being consumed themselves, by controlling the activity of catalysts one can control the reaction rates in a system. Enzymes are activated or deactivated in two different ways: 1) in a covalent fashion by phosphorylation[1] and 2) in a non-covalent manner by allosteric activation or inhibition.[2] Inspired by nature, we would like to make catalysts that can be activated or deactivated by chemical or physical signals and that can control the properties of materials. In parallel with the methods found in nature we applied a covalent method using protecting groups and a non-covalent method that uses host-guest chemistry to control the activation of catalysts. Artificial catalysts that can be activated by signals from the environment can be used to control the formation and properties of soft materials, which would, for instance, have applications in tissue engineering or drug delivery and can ultimately lead to communication between artificial chemical systems.[3, 4, 5]

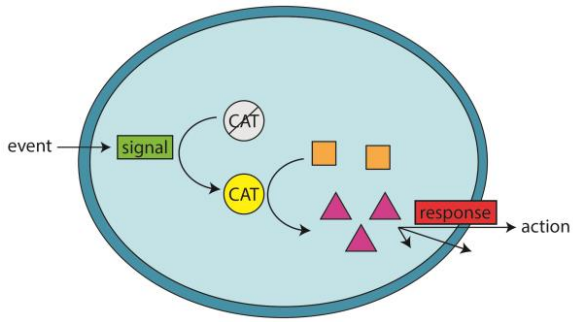

Figure 1.1: Signal transduction in cells as an example where nature responds to signals from the environment: the signal activates a catalyst which changes the rate of a reaction. The resulting compounds are, for example, building blocks for a material or hormone molecules for the response to the event.[6]

The aim of the research described in the thesis is to introduce signal response in materials using catalysis. This goal can be divided into two challenges: 1) to develop materials for which the properties can be controlled by catalysis, and 2) to develop catalysts that can be activated by signals from the environment. First I will explain how we can design materials that can be controlled by catalysis and provide examples from the literature and from this

group where we have accomplished this. Second, I will discuss examples from the literature of catalysts that can be activated by signals and I will present the two different strategies we used to design catalyst systems that can respond to signals from the environment.

1.2 Materials that can be controlled by catalysis

A material that can be controlled by catalysis must contain chemical bonds whose formation are susceptible to catalysis.[7, 8] In the search for materials that can respond to the environment most research is focused on supramolecular materials: the non-covalent interactions can relatively easily be controlled by changing the temperature, solvent or pH. Thermodynamic control, however, has its limitations. First of all, many supramolecular materials remain in kinetically trapped (metastable) states: the rate of formation has a large impact on the properties of these materials. A second reason is that thermodynamic control is typically limited to physical stimuli such as temperature or light.

Kinetic control over supramolecular material formation is challenging because non-covalent interactions are formed (nearly) without activation energy. The formation of a covalent bond typically requires an activation energy which can be lowered by a catalyst. By changing the activation energy by catalysis, one can control the reaction rates. Therefore we have to incorporate covalent bonds that are susceptible to catalysis to enable kinetic control over the formation and properties of materials (Fig. 1.2).

To incorporate covalent bonds that are susceptible to catalysis in a material, we can use click chemistry. Click reactions generally have a high yield, unreactive by-products, require simple reaction conditions such as ambient temperatures and can often use water as solvent.[9] Click reactions are commonly used for bioconjugation, to functionalize biological molecules.[10] The most famous click reaction is the copper-catalysed azide–alkyne cycloaddition.[11] This reaction requires a Cu^{I} catalyst. Ring-opening reactions with, for instance, epoxides and thiols are other examples of click reactions: these are catalysed by base.[12] The thiol-Michael click reaction is also catalysed by base and is increasingly used in materials that are controlled by catalysis.[13]

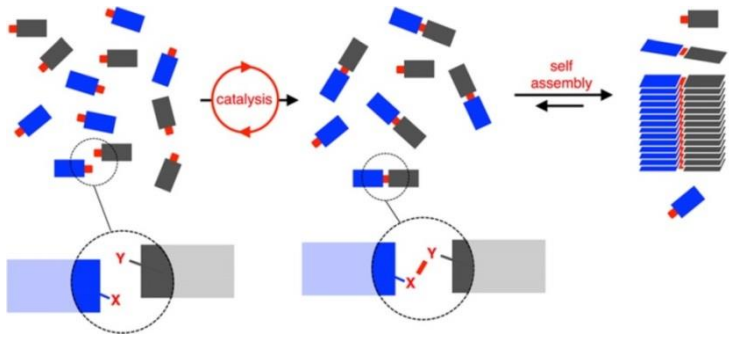

Figure 1.2: Catalysis controlled material formation. Non-assembling building blocks (blue and dark grey) react through covalent bond formation (red) using a catalyst and form a self-assembled structure. The formation rate and properties of this material are controlled by catalysis. Reprinted from reference 7.[7]

Two click reactions that can be controlled by H^+ and amine organocatalysts, are oxime formation[14, 15, 16] and hydrazone formation.[17, 18, 19, 20]

The most famous organocatalyst for hydrazone and oxime formation is aniline **1.1** (Fig. 1.3a). Aniline acts as a nucleophilic catalyst and adds to the aldehyde to form an imine intermediate. Attack of the hydrazide (or hydroxylamine) results in elimination of aniline and the formation of the hydrazone or oxime product.[20] Aniline is not a very efficient catalyst for hydrazone or oxime formation: superstoichiometric amounts (10, sometimes up to 2000, equivalents) are used and the reaction rate is often only increased up to 10-fold.[18]

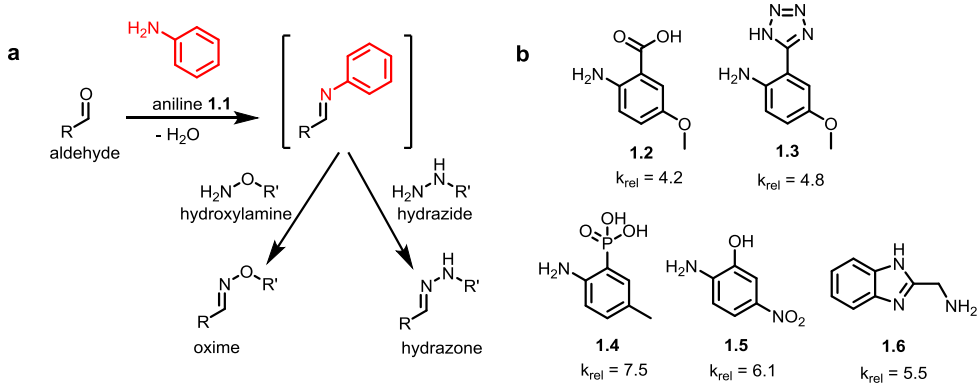

Figure 1.3: Hydrazone and oxime formation. (**a**) Hydrazone formation between an aldehyde and hydrazide and oxime formation between an aldehyde and a hydroxylamine, both reactions are catalysed by acid and by aniline **1.1**. (**b**) Other catalysts for hydrazone (and possibly oxime) formation. The numbers underneath the catalysts indicate the increased catalytic activity with respect to the aniline catalyst (activity catalyst / activity aniline).[20]

In Chapter 5 we provide an overview of different hydrazone reactions and their response to aniline catalysis. In the groups of Kool and Distefano many new organocatalysts for hydrazone or oxime formation were found with activities that are several times higher than aniline (Fig. 1.3b).[15, 19]

Click chemistry is increasingly used to design materials that can be controlled by catalysis. Most often, these materials are designed as polymer networks or covalently cross-linked polymer gels. Hydrazone and oxime chemistry is suitable to use in hydrogels because the reaction takes place in water and can be controlled by acid or amine catalysis. The Becker group developed a hydrogel based on oxime formation.[21] They showed that the rate of formation has a profound influence on the properties of the gels (Fig. 1.4a). The same accounts for hydrazone gels from McKinnon: the amount of acid catalyst does not only change the formation rate but also the resulting gel properties (Fig. 1.4b).[22] In Chapter 2 we show how we control the formation and properties of a polymer gel featuring hydrazone bonds that was developed in our group.

Thiol-Michael addition is another interesting candidate to make materials that can respond to catalysis. The rate of the reaction can be tuned by adjusting the pKa of the thiol and the electron deficiency of the electrophile, and the reaction is catalysed by base.[23] A thiol-Michael polymer network that can be controlled by catalysis was developed in the Bowman group. They even went a step further and used a pro-catalyst that can be activated by light to control where and when this material was formed, by selectively activating the catalyst (Fig. 1.4c).[24]

It is relatively straightforward to control covalently cross-linked polymer gels or networks by catalysis: one just has to control the formation of the covalent bonds that are already there. Conversely, supramolecular gels made from low molecular weight gelators (LMWGs) are usually formed with non-covalent interactions that require (almost) no activation energy. A low molecular weight gelator is a small gelator molecule that above a threshold concentration (the critical gelation concentration) aggregates into fibers, which entangle and form a gel network. A general strategy to enable control over supramolecular gel formation is to design the gelator molecule in such a way that it forms in situ by a reaction between two water-soluble building blocks. The building blocks should not assemble by themselves and the reaction between the building blocks should be susceptible to catalysis.[7]

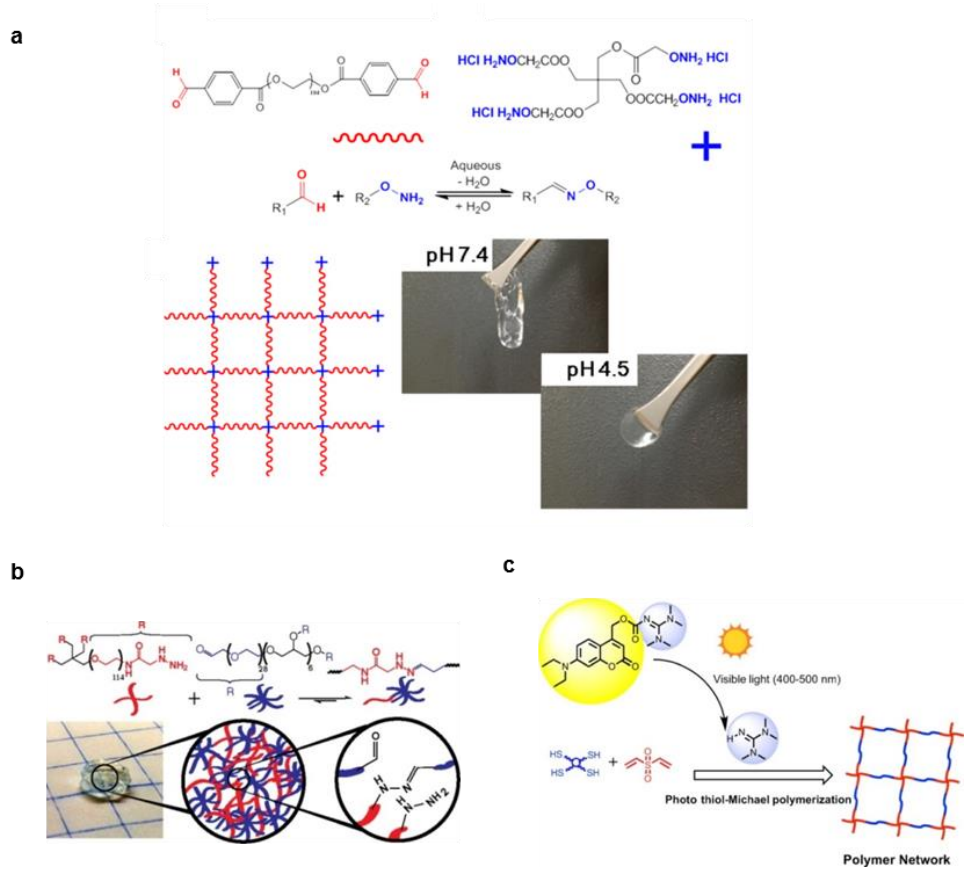

Figure 1.4: Materials that can be controlled by catalysis. (**a**) The properties of a gel featuring oxime bonds is controlled by acid catalysis.[21] Reprinted from reference 21. (**b**) A gel featuring hydrazone bonds is controlled by acid catalysis.[22] Reprinted from reference 22. (**c**) The formation of a polymer network featuring thiol-Michael bonds is controlled by a visible-light-sensitive photobase generator.[24] Reprinted from reference 24.

In our group, control over supramolecular gel formation was obtained by incorporating a hydrazone bond into a previously reported cyclohexanetrisamide-based gelator.[25] The gelator is formed in situ by combining two water-soluble building blocks that react when catalysed by aniline or acid. When the gelator is formed, it stacks into fibers and forms a gel network (Fig. 1.5a).[26] By adjusting the pH or the amount of aniline, the gelation time and the mechanical properties could be tuned: without catalyst at pH 7 the resulting gels were weak, whereas at pH 5 or with aniline catalyst, the resulting gels were formed faster and were stronger (Fig. 1.5b – f).

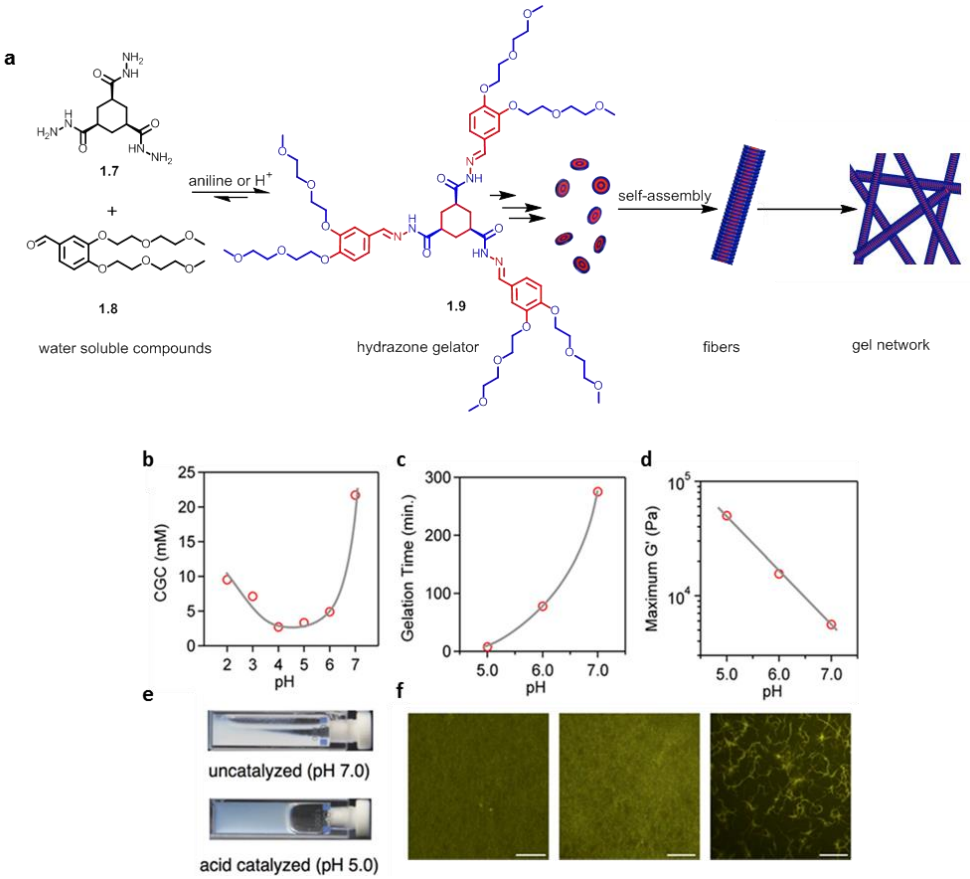

Figure 1.5: Supramolecular gel formation controlled by catalysis. (**a**) The trishydrazone gelator is formed from two water-soluble building blocks that react when catalysed by aniline and acid and form a gelator that stacks into fibers and forms a gel network. (**b**) The critical gelation concentration is determined by the amount of acid catalyst. (**c**) The gelation time depends on the amount of acid catalyst. (**d**) The maximum gel stiffness depends on the amount of acid catalyst. (**e**) The uncatalysed gel is much weaker than the acid catalysed gel. (**f**) The morphology of the gel depends on the catalyst, from left to right: with acid, with aniline, without catalyst.[7, 26] Reproduced from reference 26 and 7.

1.3 Artificial catalysts that can respond to signals

Enzymes are very efficient catalysts, but their application can be limited because of strict operating conditions, a specific set of substrates and chemical stability. In contrast, artificial catalysts can be designed specifically for a wide range of reactions and reaction conditions. Although very common in nature, only a few examples of artificial catalysts that can respond to signals from the environment have been reported.[27] Many of these catalysts use light as a signal: light forms a simple to apply signal that enables spatial control.[28] There are many molecular switches that change conformation when irradiated with light (Fig. 1.6a).[29] The conformational change can be used in a corporative switch in which two catalytic groups are brought together to activate the catalyst (Fig. 1.6b).[30] Another method to design a light-switchable catalyst is to block the catalytic site in the cis form and to unblock this catalytic site when switching to the trans form (Fig. 1.6c). Azobenzenes transform from trans- to the cis when they are irradiated with ultraviolet light. Removing the light-source gives back the trans-form. Azobenzenes can be turned into light-switchable catalysts based on cooperative interactions between the catalytic binding sites and the substrate.[31, 32, 33, 34] The catalytic activity is switched on in the cis-form, because only in this form are the catalytic binding sites close enough to bind the substrates. Another use of azobenzenes is to control the supramolecular encapsulation of the catalyst: by switching the azobenzene from trans to cis, the azobenzene prevents the catalyst from leaving a host molecule or supramolecular structure.[35, 36]

Light-switchable catalysis was also used to control the stereoselectivity of reactions: the bis(oxazoline) complex only binds Cu^{I}-ion in a bidentate fashion when activated by light in the cis-form and forms a rigid chiral environment for the cyclopropanation of styrene.[37] A unidirectional rotary motor was used as a light-switchable catalyst, by bringing two cooperating catalytic groups together in the 'on' position and by separating them in the 'off' position.[38] Another example where photoisomerization is used to control the activity of a catalyst, are photo-switchable N-heterocyclic carbenes, that catalyse transesterification.[39] Very simple catalysts that can be activated by light are photo-bases and photo-acids.[40, 41] As we saw in paragraph 1.2, bases are catalysts for thiol-Michael addition and acids for oxime and hydrazone formation.

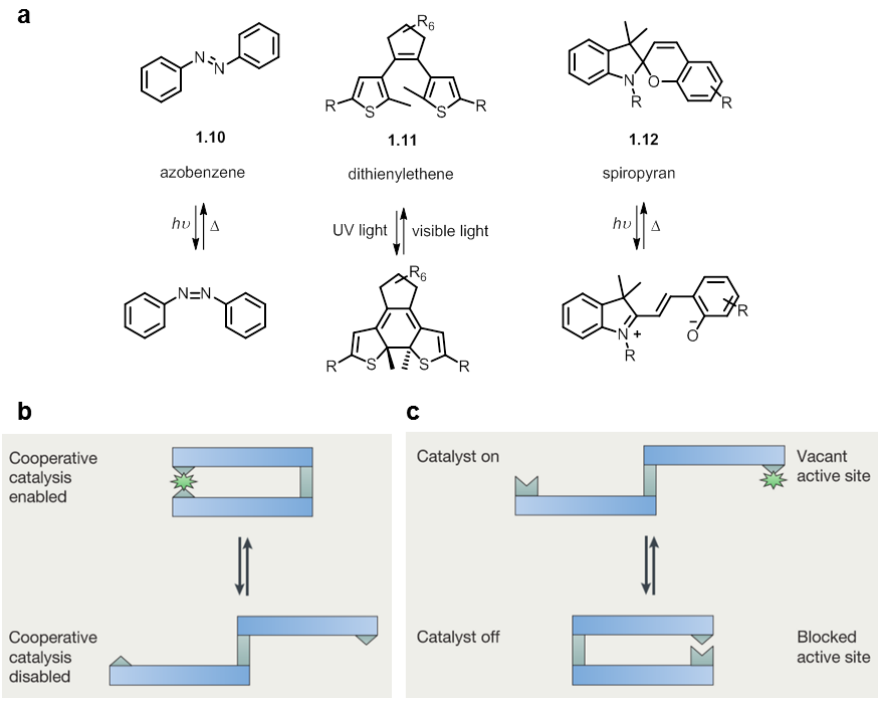

Figure 1.6: Examples of two-state light-switchable catalysts. (**a**) Examples of molecular light-switches.[29] (**b**) A cooperative switch: by bringing the two catalytic sites together the catalyst gets activated. (**c**) A blocking switch: by bringing the two sites together the active site of the catalyst gets blocked.[30] Reprinted from reference 29 and 30.

A light-switchable acid catalyst was used in our group to control the formation of the trishydrazone gel (Fig. 1.5a, Fig. 1.7).[42] Irradiation with light reversibly activates the catalyst, which catalyses gelator formation and when a photomask was used, resulted in patterned formation of the gel (Fig. 1.7a). Irradiation with light induces a ring-closing reaction, which changes the photo-acid from a weak acid to a stronger acid (Fig. 1.7b). The photo-acid was used to obtain spatial control over gel formation to form micro-scale structures (Fig. 1.7c).

Only a few catalysts that can be activated by chemical signals are reported. The Leigh group reported a pH switchable catalyst within a rotaxane. The catalyst contains two different catalytic centres: an imine catalyst and a hydrogen bonding catalyst.

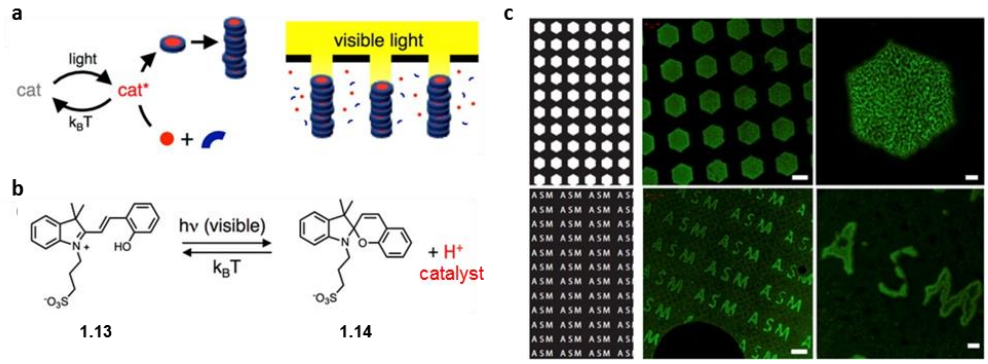

Figure 1.7: A light-switchable acid catalyst was used to gain spatial control over gel formation. (**a**) Light reversibly activates the photo-acid which catalyses gelator formation and when a photomask is used, results in patterned gel formation. (**b**) Irradiation with light induces a ring-closing reaction, which changes the photo-acid from a weak acid to a stronger acid. (**c**) When irradiating though a photomask (left), patterned gel structures were formed.[42] Reprinted from reference 42.

Switching the rotaxane between the two different catalytic centres results in the formation of two different Michael addition products (Fig. 1.8a).[43]

A catalyst that can be activated using Cl^- ions was reported in the Mirkin group. When the catalyst is activated it catalyses a Michael addition as well as the ring opening of lactide (Fig. 1.8b).[44] The switchable catalysts reported in the Schmittel group can be switched between four states with Fe^{2+} and Cu^+ cations, the two active states catalysed a two-step reaction: an azide-alkyne click reaction followed by a Michael addition (Fig. 1.8c).[45]

The chemically activated catalysts described here can efficiently be switched from an inactive state to an active state, often reversible, and sometimes even catalyse different reactions. However, a disadvantage of the catalysts described here, is that they often suffer from complex and non-generic design. Therefore, we developed a more generic method to design covalently protected catalysts (paragraph 1.4) and non-covalently protected catalysts (paragraph 1.5) that can be activated by chemical and physical signals. For the covalent method we used self-immolative chemistry to design pro-catalysts with a signal-labile protecting group (paragraph 1.4). For the non-covalent method we used host-guest chemistry to change the activity of organocatalysts by reversible molecular encapsulation (paragraph 1.5).

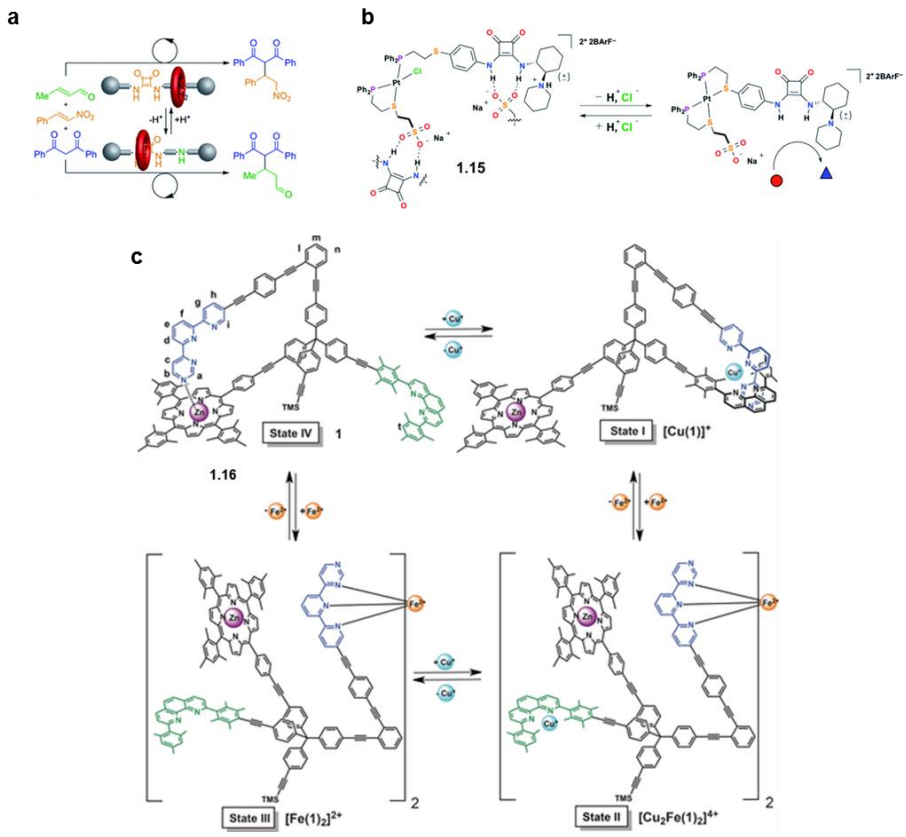

Figure 1.8: Examples of pro-catalysts that can be controlled by chemical signals. (**a**) A rotaxane-based pH switchable organocatalyst that can be switched between imine catalysis and hydrogen bonded catalysis to result in two different Michael products.[43] Reprinted from reference 43. (**b**) A chemically activated catalyst for a Michael addition and for the ring opening of lactide.[44] Reprinted from reference 44. (**c**) A four state catalyst that can be switched using Fe^{2+} and Cu^{+} cations. The two active states catalyse a two-step reaction: an azide-alkyne click reaction followed by a Michael addition.[45] Reprinted from reference 45.

1.4 A covalent approach to design catalysts that can respond to signals

A generic method to design organocatalysts that can be activated by chemical or physical signals is by protecting the active centres of these catalysts with a signal-labile group using self-immolative chemistry. A self-immolative molecule contains a signal-labile group that

is cleaved by a specific signal and results in fragmentation and the release of an output molecule. Many pro-drugs have been developed that release a drug when the relevant signal is applied. Self-immolative chemistry can also be used for signal amplification, by incorporating more than one output molecule per signal labile group, for example by using self-immolative dendrimers or polymers.[46, 47] Another method to accomplish signal amplification is when the output molecule acts as the chemical signal to release more output molecules.[48, 49] There are numerous possibilities for self-immolative groups that are cleaved by chemical signals, such as hydrogen peroxide, hydrogen sulphide, fluoride and a wide range of enzymes and antibodies, or by light (Table 1.1).

Table 1.1: Examples of signal-labile protecting groups that undergo self-immolation.[47]

Signal	Structure	Signal	Structure
H_2O_2	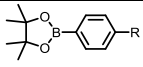	Near Infrared irradiation	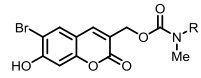
H_2O_2	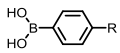	antibody 38C2	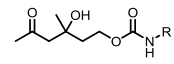
H_2S, PR_3	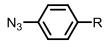	β-glucuronidase	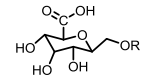
F^-		nitroreductase + NADH	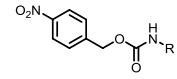
UV-irradiation	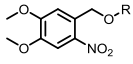	Penicillin Acylase	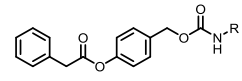

Another method to use self-immolative chemistry to design protected catalysts is by blocking a ligand for an organometallic catalyst with a signal-labile group, as was demonstrated in the Frost group (Fig. 1.9).[50] Enzyme catalysed dephosphorylation induced the self-immolative reaction and release of the ligand which coordinates to form the active organometallic catalyst that was used to catalyse transfer hydrogenation.

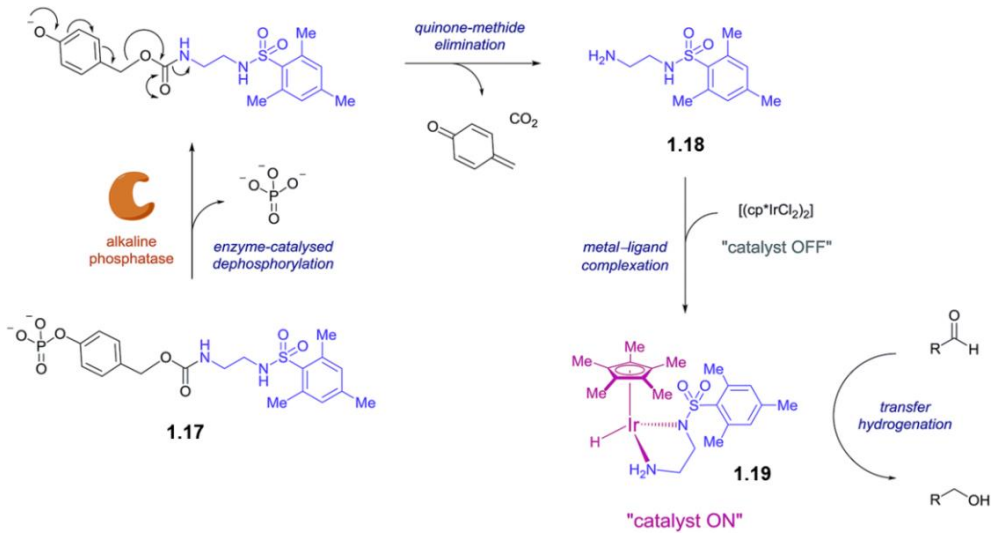

Figure 1.9: Self-immolative chemistry is used to block the binding of a ligand to form an organometallic catalyst for transfer hydrogenation. Enzyme catalysed dephosphorylation induces the self-immolative reaction and release of the ligand which can coordinate to form the active organometallic catalyst.[50] Reprinted from reference 50.

The general strategy to design an organocatalyst that can be activated by a signal to control a catalysed target reaction, is based on the following considerations:

1) The catalytic centre of the organocatalyst should allow protection with a self-immolative moiety: organocatalysts which have a primary, secondary or tertiary amine or an alcohol as a catalytic centre are promising candidates. It should be possible to activate the catalyst in a short time (depending on the timescale of the reaction) under the same conditions as are required for the catalysed target reaction;
2) All reagents, the catalyst and the pro-catalyst should be soluble in the same solvent and the solvent should be compatible with the signal and the self-immolative reaction;
3) The signal that activates the catalyst should not hinder the catalysed target reaction (too much);
4) The pro-catalyst should be stable under the conditions used in the catalysed target reaction and should not release the catalyst without signal;
5) The chemical target reaction should be susceptible to catalysis (show at least a 2-fold increase in reaction rate upon addition or activation of the catalyst).

Primary amine catalysts that can be protected with a self-immolative group are for instance aniline (Fig. 1.3a, Chapter 2) or other amine-catalysts for hydrazone formation (Fig. 1.3b). An example of a secondary amine catalyst is proline, which catalyses the aldol reaction and Michael addition (Chapter 3). Tertiary amines are protected in the form of charged quaternary amines. Examples of tertiary amine catalysts are triethylamine or DABCO (1,4-diazabicyclo[2.2.2]octane) for acylation or for the polymerisation of urethane. A carbamate or carbonate group can be included in the structure to stimulate the release of the catalyst.[51] However, for tertiary amines, including a carbonate or carbamate group might be unnecessary and even make the molecule too unstable.[52] All in all, self-immolative chemistry provides a generic tool to design many different organocatalysts that can be activated by a wide variety of chemical and physical signals.

1.5 A non-covalent approach to design catalysts that can respond to signals

The advantage of a non-covalent approach to design catalysts that can respond to signals from the environment is that non-covalent interactions between a host and a guest molecule can easily be undone by adding a stronger binding guest. Already since the 80s molecular encapsulation is known to change the reactivity of guest molecules.[53, 54] Host-guest chemistry is for example used to stabilize guest molecules to increase the lifetime and to enable safe handling of toxic or explosive compounds.[55, 56, 57] Another application in which the change of reactivity of guest molecules upon binding is used, is supramolecular catalysis.[58, 59] The Nitschke group found that the reactivity of guest molecules depends on the shape and the size of the host molecule.[60] Molecular encapsulation in a supramolecular cage was even used to tune the activity of anti-cancer drugs.[61] A commercially available host molecule that is known to bind strongly to a wide range of guests is the cucurbituril molecule. This macrocycle is formed of a ring of glycouril monomers and is available in different sizes (Fig. 1.10).[62] Cucurbit[7]uril (CB[7]), that contains 7 glycouril units, is the most water-soluble of the cucurbiturils (up to 20 mM) that also binds to a wide range of guests.[63]

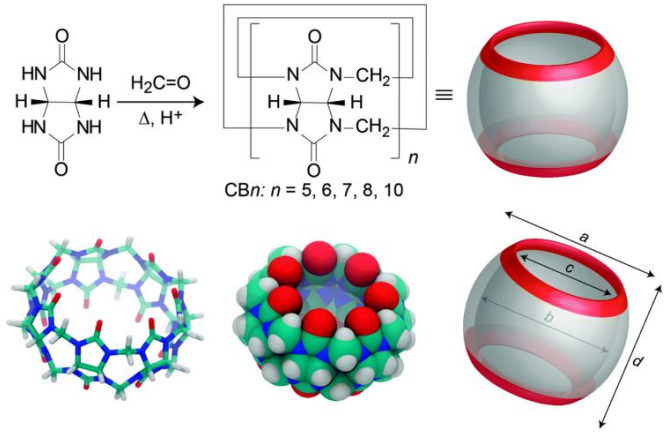

Figure 1.10: The macromolecular host molecule cucurbit[n]uril consists of glycouril units.[62] Reprinted from reference 62.

Curcurbiturils also change the reactivity of guest molecules. CB[7] was, for example, found to stabilize radical cations in a rotaxane made of oligoaniline and CB[7], indicating that molecular encapsulation changes the oxidation potential of the guest.[64] Disulphide and Se-Se bonds are stabilized by CB[6].[65, 66] Cucurbiturils were also used to mediate photochemical reactions, resulting in different stereoisomers.[67, 68, 69] Cucurbiturils are increasingly used as supramolecular catalysts.[70] Already in 1983, Mock demonstrated that CB[6] catalyses the azide-alkyne click reaction.[53] CB[8] was found to catalyse the photodimerization of coumarins.[71] By changing the pKa of guest molecules, CB[6] and CB[7] could act as acid catalysts in the acid catalysed hydrolysis of amides and oximes.[72] CB[7] and CB[8] were also shown to catalyse desilylation in the presence of Ag(I) salts.[73] Recently, CB[7] was used as a supramolecular catalyst for a Diels-Alder reaction.[74] All in all, the reactivity of guest molecules clearly changes upon molecular encapsulation by cucurbiturils. Therefore it is likely that molecular encapsulation will also change the catalytic activity of organocatalysts. An advantage of using host-guest chemistry to change the activity of organocatalysts is that this effect can be undone by releasing the catalyst from the molecule by replacing it with a stronger binding guest. Controlled release from cucurbituril can be done by changing the pH, by adding cations, such as Na^+ or Ca^{2+} or by changing the temperature.[75] However, as changing the conditions will also change the reaction rates, a better method to release the organocatalyst from the cucurbituril is by

competitive binding with a stronger binding (and non-reactive) guest. Signal response can be introduced if the super guest itself forms a relevant chemical signal or if the binding constant of this super guest can be altered by chemical or physical signals. In the Scherman group, methylviologens could be switched electrochemically and photochemically and changed the binding constant of the compounds to CB[8].[76] The Pischel group reported a switchable host-guest system with CB[7]: irradiation with light induces the proton-release photoreaction with 2-nitrobenzaldehyde and lowers the pH, which increases the binding constant of guest **1.20**, which results in the release of guest **1.21** by competitive binding (Fig. 1.11a).[77] The same group reported other super guests **1.23** and **1.25** that are activated by a light-triggered self-immolative reaction (Fig. 1.11b). Upon irradiation with light the super-guests **1.24** and **1.26** are cleaved and releases the guest by competitive binding with CB[7].[78]

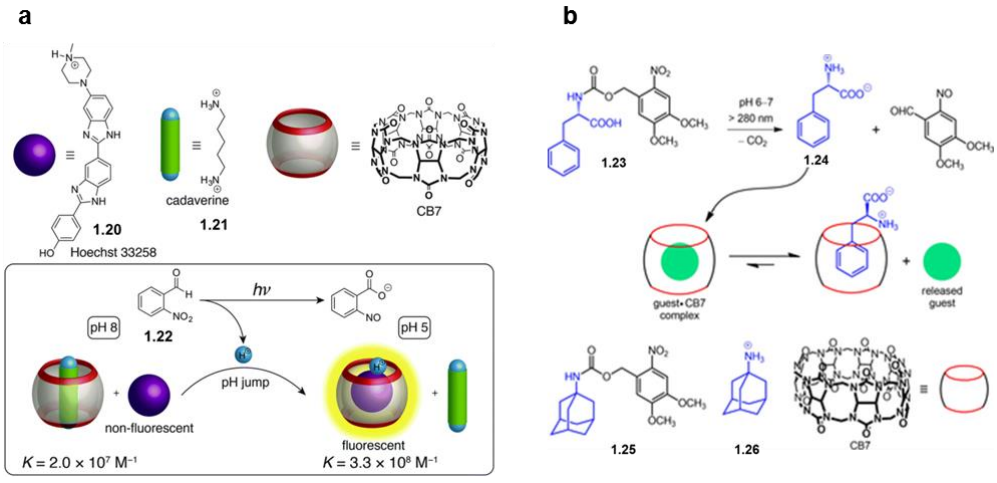

Figure 1.11: Signal-triggered formation of super guests that result in the release of the current guest in cucurbituril. (**a**) By using a photo-acid, the pH is lowered, which increases the binding constant of guest **1.20** that leads to release of guest **1.21** by competitive binding.[77] Reprinted from reference 77. (**b**) The super guests **1.24** and **1.26** are formed by a self-immolative reaction, leading to the release of the current guest.[78] Reprinted from reference 78.

Only a few examples are reported where host-guest chemistry is used to change the activity of catalysts. The Rotello group used CB[7] to block access to organometallic catalysts

embedded in the corona of gold-nanoparticles. Addition of a stronger binding guest removes the CB[7] from the nanoparticles and makes the catalysts available again.[79] Recently they applied pH responsive gold-nanoparticles with embedded organometallic catalysts in the corona to image biofilm-associated infections.[80] Isaacs and Jayawickramarajah used CB[7] indirectly to control the activation of a protein: CB[7] binds to a DNA strand and the protein inhibitor. Addition of ATP (adenosine triphosphate) induces self-assembly of the DNA to a small molecule, which leads to the release of the protein inhibitor.[81]

The large binding constants and wide variety of guests, make cucurbiturils interesting candidates to design host-guest systems to control the activity of organocatalysts.

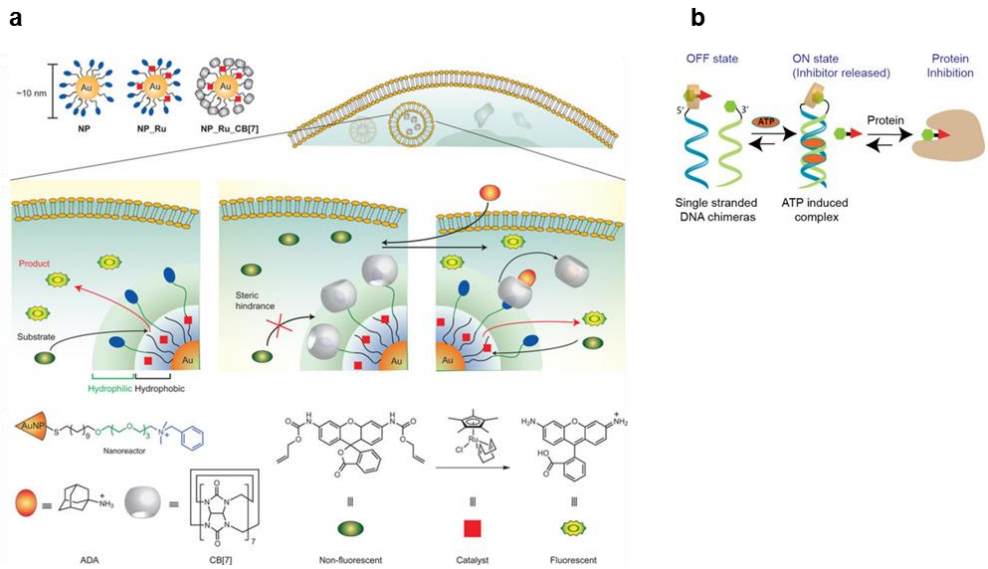

Figure 1.12: Using cucurbiturils to change the activity of catalysts. (**a**) Cucurbit[7]uril (CB[7]) was used to reversibly block an organometallic catalyst on a gold nanoparticle.[79] Reprinted from reference 79. (**b**) Cucurbituril was used indirectly to control the activity of an enzyme: addition of ATP (adenosine triphosphate) induces self-assembly of a small DNA strand with a small molecule, which results in release of a protein inhibitor.[81] Reprinted from reference 81.

To make a host-guest system to control the activity of an organocatalyst, we have to keep in mind the following considerations:

1) All reagents, catalysts, the host and the super guest should be soluble in the same solvent.
2) The host must bind strongly enough to the catalysts so that ≥99% of the catalyst molecules are bound at operating conditions.
3) The activity of the catalysts should change upon binding with the host.
4) The signal must bind several orders of magnitude stronger than the catalysts.
5) All reagents and the resulting product should not bind to the host, or several orders of magnitude less than the catalyst.

For cucurbiturils, the only practical solvent one can use is water.[63] It is also important to notice that the buffer concentrations should not be too high, because cations, such as Na^+ and Ca^{2+} inhibit binding of other guests.[82] Using these considerations, we found a host-guest system to control the activity of two organocatalysts for hydrazone formation, which is described in Chapter 4.

1.6 Research aim

The aim of the work described in this thesis is to explore the possibilities of developing responsive catalysts to make materials that can respond to signals from the environment. We investigated two different methods to develop organocatalysts that can be activated by chemical or physical signals: a covalent method using self-immolative chemistry for the design of the catalysts and a non-covalent method using host-guest chemistry to control the catalytic activity upon binding. In Chapter 2 '*Chemical signal activation of an organocatalyst enables control over soft material formation'*, we describe an organocatalyst that is activated by a chemical signal and that was used to control reaction rates and the formation of a supramolecular gel and a polymer gel. We used self-immolative chemistry to design the protected aniline organocatalyst that is activated by the chemical signal hydrogen peroxide and that catalyses hydrazone formation. Upon activation of the catalyst the rate of hydrazone formation increases 10-fold almost instantly. Activation of the organocatalyst increases the formation rate and stiffness of a supramolecular gel and a polymer gel, both featuring hydrazone bonds.

To explore the versatility of the self-immolative design of organocatalysts, we report three different protected organocatalysts that control two different reactions in Chapter 3: '*Selective activation of organocatalysts by specific signals'*. Using the same self-immolative design we developed three different protected prolines that are activated by three different signals and that control two different reactions. We report one pro-proline that is activated by the chemical signal hydrogen peroxide, the second is activated by light and the third is activated by the enzyme Penicillin Acylase. The three pro-prolines were used to control an aldol reaction: upon activation the reaction rate increased 2.5-fold. The pro-proline activated by hydrogen peroxide was used to control a Michael addition: without activation the reaction did not take place, addition of the chemical signal induced an immediate response and a conversion of almost 90% in 8 hours.

A non-covalent method to control the activity of organocatalysts is described in Chapter 4: '*Reversible control over catalytic activity through host-guest chemistry'*. Cucurbit[7]uril (CB[7]) decreases the activity of one organocatalyst whereas it increases the activity of another organocatalyst. Binding of CB[7] to the organocatalysts changes the rate of hydrazone formation and addition of a stronger binding guest restores the reaction rate to the original value. We were able to control the rate of a hydrazone reaction precisely by adjusting the ratio of CB[7] and the catalyst and we developed a kinetic model that can predict the reaction rates based on the concentrations of catalyst and CB[7].

For a material to be controlled by catalysis, it has to feature covalent bonds whose formation is susceptible to catalysis. In this work we describe supramolecular gels and polymer gels, both featuring hydrazone bonds, for which gel properties can be changed by activation of aniline catalysis. In order to gain more insight into how the aniline catalyst influences the rate of hydrazone formation, an overview of different hydrazone formation reactions and their response aniline catalysis is reported in Chapter 5: '*Aniline catalysed hydrazone formation reactions show a large variation in reaction rates and catalytic effects*'. We found that reaction rates can vary with orders of magnitude and some reaction do not show any response to aniline catalysis whereas other reactions show an up to 50-fold increase in reaction rate.

In essence, we have described different methods to develop catalysts that can respond to signals and provided an example where a responsive catalyst is applied to introduce signal response in materials.

1.7 References

1. Burnett, G., Kennedy, E.P. The enzymatic phosphorylation of proteins. *J. Biol. Chem.* **211**, 969-980 (1954).
2. Traut, T. *Allosteric regulatory enzymes*. Springer (2008).
3. Ooi, H.W., Hafeez, S., van Blitterswijk, C.A., Moroni, L., Baker, M.B. Hydrogels that listen to cells: A review of cell-responsive strategies in biomaterial design for tissue regeneration. *Mater. Horizons* **4**, 1020-1040 (2017).
4. Oliva, N., Conde, J., Wang, K., Artzi, N. Designing hydrogels for on-demand therapy. *Acc. Chem. Res.* **50**, 669-679 (2017).
5. Buwalda, S.J., Vermonden, T., Hennink, W.E. Hydrogels for therapeutic delivery: Current developments and future directions. *Biomacromolecules* **18**, 316-330 (2017).
6. Lodish, H.B., Matsudaira, A., Kaiser, P., Kris, A., Krieger, M., Scott, M. P., Zipursky, S.L., Darnell, J. *Molecular cell biology*. W.H.Freeman & Co Ltd (2003).
7. Trausel, F., Versluis, F., Maity, C., Poolman, J.M., Lovrak, M., van Esch, J.H., Eelkema, R. Catalysis of supramolecular hydrogelation. *Acc. Chem. Res.* **49**, 1440-1447 (2016).
8. Eelkema, R., van Esch, J. H. Catalytic control over the formation of supramolecular materials. *Org. Biomol. Chem.* **12**, 6292-6296 (2014).
9. Kolb, H. C., Finn, M. G., Sharpless, K. B. Click chemistry: Diverse chemical function from a few good reactions. *Angew. Chem. Int. Ed. Engl.* **40**, 2004-2021 (2001).
10. McKay, C. S., Finn, M. G. Click chemistry in complex mixtures: Bioorthogonal bioconjugation. *Chem. Biol.* **21**, 1075-1101 (2014).
11. Spiteri, C., Moses, J. E. Copper-catalyzed azide–alkyne cycloaddition: Regioselective synthesis of 1,4,5-trisubstituted 1,2,3-triazoles. *Angew. Chem. Int. Ed. Engl.* **49**, 31-33 (2010).
12. Stuparu, M. C., Khan, A. Thiol-epoxy "click" chemistry: Application in preparation and postpolymerization modification of polymers. *J. Polym. Sci., Part A: Polym. Chem.* **54**, 3057-3070 (2016).
13. Hoyle, C. E., Bowman, C. N. Thiol–ene click chemistry. *Angew. Chem. Int. Ed. Engl.* **49**, 1540-1573 (2010).
14. Ulrich, S., Boturyn, D., Marra, A., Renaudet, O., Dumy, P. Oxime ligation: A chemoselective click-type reaction for accessing multifunctional biomolecular constructs. *Chem. Eur. J.* **20**, 34-41 (2014).
15. Rashidian, M., Mahmoodi, M. M., Shah, R., Dozier, J. K., Wagner, C. R., Distefano, M. D. A highly efficient catalyst for oxime ligation and hydrazone–oxime exchange suitable for bioconjugation. *Bioconjugate Chem.* **24**, 333-342 (2013).
16. Collins, J., Xiao, Z., Mullner, M., Connal, L. A. The emergence of oxime click chemistry and its utility in polymer science. *Polym. Chem.* **7**, 3812-3826 (2016).
17. Dirksen, A., Dirksen, S., Hackeng, T. M., Dawson, P. E. Nucleophilic catalysis of hydrazone formation and transimination: Implications for dynamic covalent chemistry. *J. Am. Chem. Soc.* **128**, 15602-15603 (2006).

18. Crisalli, P., Kool, E. T. Water-soluble organocatalysts for hydrazone and oxime formation. *J. Org. Chem.* **78**, 1184-1189 (2013).
19. Larsen, D., Pittelkow, M., Karmakar, S., Kool, E. T. New organocatalyst scaffolds with high activity in promoting hydrazone and oxime formation at neutral ph. *Org. Lett.* **17**, 274-277 (2015).
20. Kölmel, D. K., Kool, E. T. Oximes and hydrazones in bioconjugation: Mechanism and catalysis. *Chem. Rev.* **117**, 10358-10376 (2017).
21. Lin, F., Yu, J., Tang, W., Zheng, J., Defante, A., Guo, K., Wesdemiotis, C., Becker, M. L. Peptide-functionalized oxime hydrogels with tunable mechanical properties and gelation behavior. *Biomacromolecules* **14**, 3749-3758 (2013).
22. McKinnon, D. D., Domaille, D. W., Cha, J. N., Anseth, K. S. Bis-aliphatic hydrazone-linked hydrogels form most rapidly at physiological ph: Identifying the origin of hydrogel properties with small molecule kinetic studies. *Chem. Mat.* **26**, 2382-2387 (2014).
23. Nair, D. P., Podgórski, M., Chatani, S., Gong, T., Xi, W., Fenoli, C. R., Bowman, C. N. The thiol-michael addition click reaction: A powerful and widely used tool in materials chemistry. *Chem. Mat.* **26**, 724-744 (2014).
24. Zhang, X., Xi, W., Wang, C., Podgórski, M., Bowman, C. N. Visible-light-initiated thiol-michael addition polymerizations with coumarin-based photobase generators: Another photoclick reaction strategy. *ACS Macro Lett.* **5**, 229-233 (2016).
25. van Bommel, K. J. C., van der Pol C., Muizebelt I., Friggeri A., Heeres A., Meetsma A., Feringa B. L., van Esch, J. H. Responsive cyclohexane-based low-molecular-weight hydrogelators with modular architecture. *Angew. Chem. Int. Ed. Engl.* **43**, 1663-1667 (2004).
26. Boekhoven, J., Poolman, J. M., Maity, C., Li, F., van der Mee, L., Minkenberg, C. B., Mendes, E., van Esch, J. H., Eelkema, R. Catalytic control over supramolecular gel formation. *Nat. Chem.* **5**, 433–437 (2013).
27. Blanco, V., Leigh, D. A., Marcos, V. Artificial switchable catalysts. *Chem. Soc. Rev.* **44**, 5341-5370 (2015).
28. Stoll, R. S., Hecht, S. Artificial light-gated catalyst systems. *Angew. Chem. Int. Ed. Engl.* **49**, 5054-5075 (2010).
29. Bléger, D., Hecht, S. Visible-light-activated molecular switches. *Angew. Chem. Int. Ed. Engl.* **54**, 11338-11349 (2015).
30. van Dijk L., Tilby, M. J., Szpera, R., Smith, O. A., Bunce, H. A. P., Fletcher, S. P. Molecular machines for catalysis. *Nat. Rev. Chem.* **2**, 0117 (2018).
31. Würthner, F., Rebek, J. Light-switchable catalysis in synthetic receptors. *Angew. Chem.* **34**, 446-448 (1995).
32. Cacciapaglia, R., Di Stefano, S., Mandolini, L. The bis-barium complex of a butterfly crown ether as a phototunable supramolecular catalyst. *J. Am. Chem. Soc.* **125**, 2224-2227 (2003).
33. Imahori, T., Yamaguchi, R., Kurihara, S. Azobenzene-tethered bis(trityl alcohol) as a photoswitchable cooperative acid catalyst for morita–baylis–hillman reactions. *Chem. Eur. J.* **18**, 10802-10807 (2012).

34. Samanta, M., Siva Rama Krishna, V., Bandyopadhyay, S. A photoresponsive glycosidase mimic. *Chem. Commun.* **50**, 10577-10579 (2014).
35. Ueno, A., Takahashi, K., Osa, T. Photoregulation of catalytic activity of [small beta]-cyclodextrin by an azo inhibitor. *J. Chem. Soc., Chem. Commun.*, 837-838 (1980).
36. Neri, S., Garcia, Martin, S., Pezzato, C., Prins, L. J. Photoswitchable catalysis by a nanozyme mediated by a light-sensitive cofactor. *J. Am. Chem. Soc.* **139**, 1794-1797 (2017).
37. Sud, D., Norsten, T. B., Branda, N. R. Photoswitching of stereoselectivity in catalysis using a copper dithienylethene complex. *Angew. Chem. Int. Ed. Engl.* **44**, 2019-2021 (2005).
38. Wang, J., Feringa, B. L. Dynamic control of chiral space in a catalytic asymmetric reaction using a molecular motor. *Science* **331**, 1429-1432 (2011).
39. Neilson, B. M., Bielawski, C. W. Photoswitchable organocatalysis: Using light to modulate the catalytic activities of n-heterocyclic carbenes. *J. Am. Chem. Soc.* **134**, 12693-12699 (2012).
40. Shirai, M., Tsunooka, M. Photoacid and photobase generators: Chemistry and applications to polymeric materials. *Prog. Polym. Sci.* **21**, 1-45 (1996).
41. Shi, Z., Peng, P., Strohecker, D., Liao, Y. Long-lived photoacid based upon a photochromic reaction. *J. Am. Chem. Soc.* **133**, 14699-14703 (2011).
42. Maity, C., Hendriksen, W. E., van Esch, J. H., Eelkema, R. Spatial structuring of a supramolecular hydrogel by using a visible-light triggered catalyst. *Angew. Chem. Int. Ed. Engl.* **54**, 998-1001 (2015).
43. Beswick, J., Blanco, V., De Bo, G., Leigh, D. A., Lewandowska U., Lewandowski B., Mishiro K. Selecting reactions and reactants using a switchable rotaxane organocatalyst with two different active sites. *Chem. Sci.* **6**, 140-143 (2015).
44. McGuirk, C. M., Mendez-Arroyo, J., d'Aquino, A. I., Stern, C. L., Liu, Y., Mirkin, C. A. A concerted two-prong approach to the in situ allosteric regulation of bifunctional catalysis. *Chem. Sci.* **7**, 6674-6683 (2016).
45. Gaikwad, S., Goswami, A., De, S., Schmittel, M. A metalloregulated four-state nanoswitch controls two-step sequential catalysis in an eleven-component system. *Angew. Chem. Int. Ed. Engl.* **55**, 10512-10517 (2016).
46. Roth, M. E., Green, O., Gnaim, S., Shabat, D. Dendritic, oligomeric, and polymeric self-immolative molecular amplification. *Chem Rev* **116**, 1309-1352 (2016).
47. Peterson, G. I., Larsen M. B., Boydston A. J. Controlled depolymerization: Stimuli-responsive self-immolative polymers. *Macromolecules* **45**, 7317-7328 (2012).
48. Baker, M. S., Phillips, S. T. A two-component small molecule system for activity-based detection and signal amplification: Application to the visual detection of threshold levels of pd(ii). *J. Am. Chem. Soc.* **133**, 5170-5173 (2011).
49. Sella, E., Shabat, D. Dendritic chain reaction. *J. Am. Chem. Soc.* **131**, 9934-9936 (2009).
50. Goggins, S., Marsh, B. J., Lubben, A. T., Frost, C. G. Signal transduction and amplification through enzyme-triggered ligand release and accelerated catalysis. *Chem. Sci.* **6**, 4978-4985 (2015).
51. Alouane, A., Labruère, R., Le Saux, T., Schmidt, F., Jullien, L. Self-immolative spacers: Kinetic aspects, structure–property relationships, and applications. *Angew. Chem. Int. Ed. Engl.*, **54**, 7492-7509 (2015).

52. Staben, L. R.*, et al.* Targeted drug delivery through the traceless release of tertiary and heteroaryl amines from antibody–drug conjugates. *Nat. Chem.* **8**, 1112-1119, (2016).
53. Mock, W. L., Irra, T. A., Wepsiec, J. P., Manimaran, T. L. Cycloaddition induced by cucurbituril. A case of pauling principle catalysis. *J. Org. Chem.* **48**, 3619-3620 (1983).
54. Quan, M. L. C., Cram, D. J. Constrictive binding of large guests by a hemicarcerand containing four portals. *J. Am. Chem. Soc.* **113**, 2754-2755 (1991).
55. Roach, P., Warmuth, R. The room-temperature stabilization of bicyclo[2.2.2]oct-1-ene and bicyclo[3.2.1]oct-1-ene. *Angew. Chem. Int. Ed. Engl.* **42**, 3039-3042 (2003).
56. Horng, Y.-C., Huang, P.-S., Hsieh, C.-C., Kuo, C.-H., Kuo, T.-S. Selective encapsulation of volatile and reactive methyl iodide. *Chem. Commun.* **48**, 8844-8846 (2012).
57. Gao, C.-Y., Zhao, L., Wang, M.-X. Stabilization of a reactive polynuclear silver carbide cluster through the encapsulation within a supramolecular cage. *J. Am. Chem. Soc.* **134**, 824-827 (2012).
58. Zhang, Q., Tiefenbacher, K. Terpene cyclization catalysed inside a self-assembled cavity. *Nat. Chem.* **7**, 197 (2015).
59. Deraedt, C., Astruc, D. Supramolecular nanoreactors for catalysis. *Coord. Chem. Rev.* **324**, 106-122 (2016).
60. Breiner, B., Clegg, J. K., Nitschke, J. R. Reactivity modulation in container molecules. *Chem. Sci.* **2**, 51-56 (2011).
61. Ahmedova, A.*, et al.* M2l4 coordination capsules with tunable anticancer activity upon guest encapsulation. *Dalton Trans.* **45**, 13214-13221 (2016).
62. Assaf, K. I., Nau, W. M. Cucurbiturils: From synthesis to high-affinity binding and catalysis. *Chem. Soc. Rev.* **44**, 394-418 (2015).
63. Barrow, S. J., Kasera, S., Rowland, M. J., del Barrio, J., Scherman, O. A. Cucurbituril-based molecular recognition. *Chem. Rev.* **115**, 12320-12406 (2015).
64. Eelkema, R., Maeda, K., Odell, B., Anderson, H. L. Radical cation stabilization in a cucurbituril oligoaniline rotaxane. *J. Am. Chem. Soc.* **129**, 12384-12385 (2007).
65. Berbeci, L. S., Wang, W., Kaifer, A. E. Drastically decreased reactivity of thiols and disulfides complexed by cucurbit[6]uril. *Org. Lett.* **10**, 3721-3724 (2008).
66. Ren, H., Huang, Z., Yang, H., Xu, H., Zhang, X. Controlling the reactivity of the se□se bond by the supramolecular chemistry of cucurbituril. *ChemPhysChem* **16**, 523-527 (2015).
67. Barooah, N., Pemberton, B. C., Sivaguru, J. Manipulating photochemical reactivity of coumarins within cucurbituril nanocavities. *Org. Lett.* **10**, 3339-3342 (2008).
68. Wang, R., Yuan, L., Macartney, D. H. Cucurbit[7]uril mediates the stereoselective [4+4] photodimerization of 2-aminopyridine hydrochloride in aqueous solution. *J. Org. Chem.* **71**, 1237-1239 (2006).
69. Jon, S. Y., Ko, Y. H., Park, S. H., Kim, H.-J., Kim, K. A facile, stereoselective [2 + 2] photoreaction mediated by cucurbit[8]uril. *Chem. Commun.*, 1938-1939 (2001).
70. Pemberton, B. C., Raghunathan, R., Volla, S., Sivaguru, J. From containers to catalysts: Supramolecular catalysis within cucurbiturils. *Chem. Eur. J.* **18**, 12178-12190 (2012).

71. Pemberton, B. C., Barooah, N., Srivatsava, D. K., Sivaguru, J. Supramolecular photocatalysis by confinement-photodimerization of coumarins within cucurbit[8]urils. *Chem. Commun.* **46**, 225-227 (2010).

72. Klöck, C., Dsouza, R. N., Nau, W. M. Cucurbituril-mediated supramolecular acid catalysis. *Org. Lett.* **11**, 2595-2598 (2009).

73. Lu, X., Masson, E. Silver-promoted desilylation catalyzed by ortho- and allosteric cucurbiturils. *Org. Lett.* **12**, 2310-2313 (2010).

74. Palma, A., Artelsmair, M., Wu, G., Lu, X., Barrow, S. J., Uddin, N., Rosta, E., Masson, E., Scherman, O. A. Cucurbit[7]uril as a supramolecular artificial enzyme for diels–alder reactions. *Angew. Chem. Int. Ed. Engl.* **56**, 15688-15692 (2017).

75. Liu, L. Controlled release from cucurbituril. *J. Incl. Phenom. Macrocycl. Chem.* **87**, 1-12 (2017).

76. Tian, F., Jiao, D., Biedermann, F., Scherman, O. A. Orthogonal switching of a single supramolecular complex. *Nat. Commun.* **3**, 1207 (2012).

77. Vazquez, J., Romero, M. A., Dsouza, R. N., Pischel, U. Phototriggered release of amine from a cucurbituril macrocycle. *Chem. Commun.* **52**, 6245-6248 (2016).

78. Romero, M. A., Basílio, N., Moro, A. J., Domingues, M., González-Delgado, J. A., Arteaga, J. F., Pischel, U. Photocaged competitor guests: A general approach toward light-activated cargo release from cucurbiturils. *Chem. Eur. J.* **23**, 13105-13111 (2017).

79. Tonga, G. Y*., et al.* Supramolecular regulation of bioorthogonal catalysis in cells using nanoparticle-embedded transition metal catalysts. *Nat. Chem.* **7**, 597-603 (2015).

80. Gupta, A., Das, R., Yesilbag Tonga, G., Mizuhara, T., Rotello, V. M. Charge-switchable nanozymes for bioorthogonal imaging of biofilm-associated infections. *ACS Nano* **12**, 89-94 (2018).

81. Zhou, X., Su, X., Pathak, P., Vik, R., Vinciguerra, B., Isaacs, L., Jayawickramarajah, J. Host–guest tethered DNA transducer: Atp fueled release of a protein inhibitor from cucurbit[7]uril. *J. Am. Chem. Soc.* **139**, 13916-13921 (2017).

82. Ong, W., Kaifer, A. E. Salt effects on the apparent stability of the cucurbit[7]uril−methyl viologen inclusion complex. *J. Org. Chem.* **69**, 1383-1385 (2004).

Chapter 2

Chemical signal activation of an organocatalyst enables control over soft material formation

Abstract

Cells can react to their environment by changing the activity of enzymes in response to specific chemical signals. Artificial catalysts capable of being activated by chemical signals are rare, but of interest for creating autonomously responsive materials. We present an organocatalyst that is activated by a chemical signal, enabling temporal control over reaction rates and the formation of materials. Using self-immolative chemistry, we design a deactivated aniline organocatalyst that is activated by the chemical signal hydrogen peroxide and catalyses hydrazone formation. Upon activation of the catalyst, the rate of hydrazone formation increases 10-fold almost instantly. The responsive organocatalyst enables temporal control over the formation of gels featuring hydrazone bonds. The generic design should enable the use of a large range of triggers and organocatalysts, and appears a promising method for the introduction of signal response in materials, constituting a first step towards achieving communication between artificial chemical systems.

This chapter is published as:

Trausel, F., Maity, C., Poolman, J.M., Kouwenberg, D.S.J., Versluis, F., van Esch, J.H., Eelkema, R. Chemical signal activation of an organocatalyst enables control over soft material formation, *Nature Commun*. **8**, 879 (2017).

2.1 Introduction

Control over enzymatic activity is at the basis of cellular communication and the regulation of a wide range of biological processes. Enzymes are often activated in a covalent manner by (de-)phosphorylation, for example in cell signalling. Allosteric enzymes, such as haemoglobin, are hindered or stimulated by non-covalent interactions with a regulatory molecule.[1,2] Such rudimentary forms of communication and regulation are almost entirely absent in artificial materials, but could lead to the development of soft materials capable of autonomously responding to changes in their environment. Although enzymes are typically very efficient catalysts, the type of reactions they catalyse and their operating conditions are limited. An artificial catalyst that is activated by a chemical signal opens possibilities for autonomous spatial and temporal control over systems at a molecular and supramolecular level. Only a few examples of synthetic catalysts with addressable activity exist, predominantly controlled using light as a signal.[3-7] Catalysts whose activity is controlled using a chemical signal are nearly absent from the literature[8-11] and often suffer from complex design and synthesis as well as a very specific operating mechanism.

Here, we present proof of principle of an organocatalyst that is activated by a chemical signal. This concept provides a generic design to enable autonomous response to biologically and mechanically relevant signals from the environment. The signal responsive catalyst is designed as a self-immolative molecule[12-15] which fragments upon reaction with a specific chemical signal to release an active catalyst. We synthesize a protected aniline (pro-aniline **1**) that liberates the organocatalyst aniline **2** upon reaction with the chemical signal H_2O_2. Aniline is a nucleophilic catalyst for hydrazone formation and exchange[16-18], a reaction frequently used in soft[19] and dynamic covalent materials.[20] H_2O_2 is released by the enzymatic oxidation of many different disease related biomarkers such as glucose, lactose, sarcosine, uric acid, choline and acetylcholine, making it a highly relevant biological signal.[21-23] Furthermore, strained polymers have been shown to generate H_2O_2 in the presence of water, making H_2O_2 an interesting mechanically generated chemical signal.[24] Activating pro-aniline **1** with H_2O_2 as a chemical signal leads to an almost instant 10-fold increase in rate of hydrazone formation. Additionally, using the pro-catalyst in gels

featuring hydrazone bonds enables control over material formation, creating materials that can respond to a specific chemical signal.

2.2 Results and discussion

Activation of the catalyst

The pro-catalyst pro-aniline **1** is activated by the chemical signal H_2O_2 and catalyses hydrazone formation (Fig. 2.1a, b).

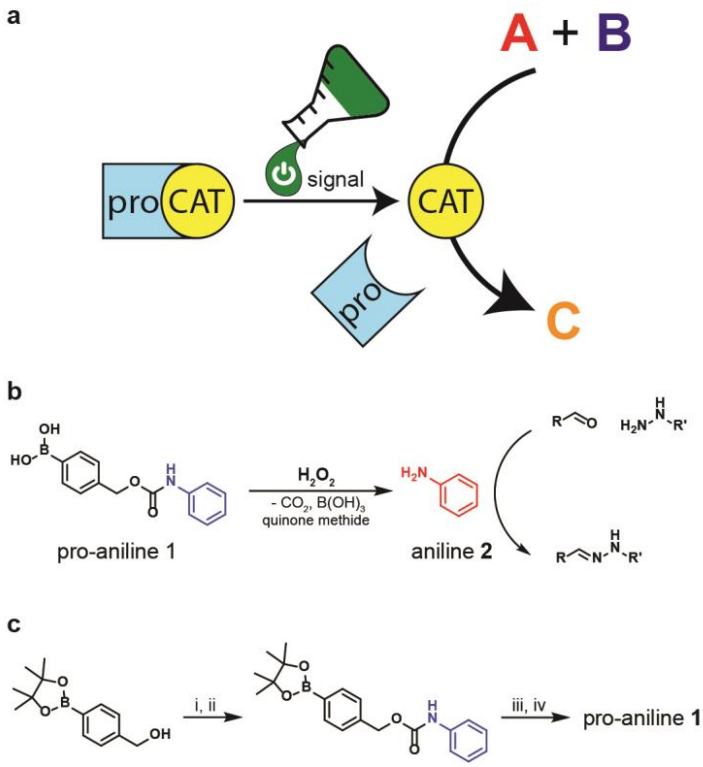

Figure 2.1: Design and synthesis of the protected catalyst. (**a**) Schematic representation of the activation of a protected catalyst and subsequent catalysis of a chemical reaction. (**b**) The pro-catalyst pro-aniline **1** and the chemical signal H_2O_2 react to release the organocatalyst aniline **2** which catalyzes hydrazone formation between an aldehyde and a hydrazide. (**c**) Synthetic route for the synthesis of pro-aniline **1**, i) K_2CO_3, triphosgene, 0 °C – room temperature, ii) aniline **2**, $NaHCO_3$, tetrahydrofuran, 0 °C – room temperature, iii) $NaIO_4$, ammonium acetate, room temperature, iv) 1 M aqueous HCl. Total yield over two steps is 64%.

Pro-aniline **1** was synthesized in only two steps in good yields (Fig. 2.1c). We confirmed the release of aniline **2** from pro-aniline **1** (72 mM) upon reaction with H_2O_2 (18 equivalents) using GC/MS (gas chromatography/mass spectrometry), showing that **1** fragments completely to release **2** (Supplementary Fig. 2.1).

We analysed the kinetics of aniline **2** release using UV/vis spectroscopy (Supplementary Fig. 2.2a, b). The time scale for the liberation of **2** from **1** (0.5 mM) depends on the amount of H_2O_2 added, taking 5 minutes using 50 equivalents of H_2O_2, and 15 minutes using 10 equivalents. In the absence of the H_2O_2 signal, pro-aniline **1** is stable in solution for over 15 hours (Supplementary Fig. 2.2c, d).

We investigated the catalytic activity of pro-aniline **1** upon activation, by comparing the rates of hydrazone formation in a model reaction (Fig. 2.2a).[25,26] Aldehyde **4** (0.5 mM) reacts with hydrazide **3** (0.1 mM) to form hydrazone **5** in a buffered medium (100 mM phosphate buffer pH 7.4) with 20% dimethylformamide (DMF) (Fig. 2.2b). This reaction is catalysed by aniline **2** (0.5 mM), giving a 19-fold increase in reaction rate with respect to the uncatalyzed reaction. Unactivated pro-aniline **1** (0.5 mM) does not influence the reaction rate of hydrazone formation.

Addition of H_2O_2 (2.5 mM) to pro-aniline **1** (0.5 mM) gives a relative reaction rate of 10, indicating efficient activation of the organocatalyst (Fig. 2.2b, Table 2.1). H_2O_2 alone (2.5 mM) does not increase the reaction rate of hydrazone formation (Supplementary Fig. 2.3a,b). Furthermore, the pH was monitored during the reaction with pro-aniline **1** and H_2O_2: the pH remained stable at a value of 8. As our solvent system alone (100 mM phosphate buffer with 20% DMF) gives a pH of 8, we conclude that the reactions were sufficiently buffered.

After activation of pro-aniline **1**, the reaction rate is lower than when using native aniline **2**. In an attempt to explain this apparent loss of catalytic activity, we investigated the influence of H_2O_2 and of boric acid on the activity of aniline **2**, but did not observe a lower rate (Supplementary Fig. 2.3c,d).

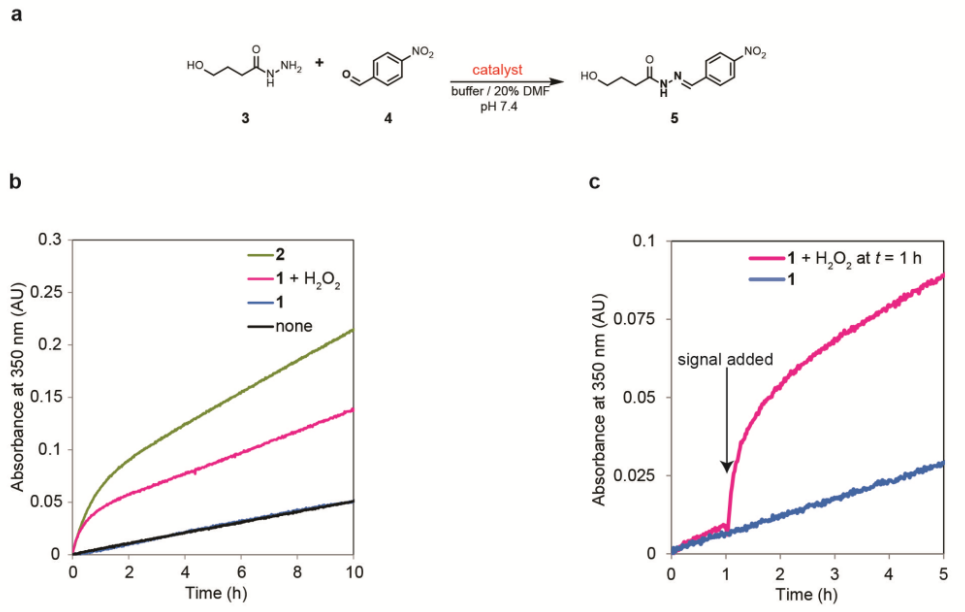

Figure 2.2: Control over the rate of hydrazone formation by activation of the catalyst. (**a**) Model hydrazone formation reaction, yielding the UV active probe **5**. Reaction conditions: 0.1 mM hydrazide **3**, 0.5 mM aldehyde **4**, 0.5 mM pro-aniline **1**, 0.5 mM aniline **2**, 2.5 mM (5 equivalents) H_2O_2 in 20% dimethylformamide (DMF) in phosphate buffer (100 mM, pH 7.4). All experiments were carried out at 25 °C. The 20% DMF was used to ensure that **1** was completely dissolved. The rate of formation of **5** is 10 times higher when using H_2O_2-activated pro-aniline **1** than for unactivated pro-aniline **1**. (**b**) Formation of **5** over time, without catalyst (black line), in the presence of aniline **2** (green line), in the presence of unactivated pro-aniline **1** (blue line) and in the presence of activated pro-aniline **1** with 5 equivalents of H_2O_2 (magenta line). (**c**) The rate of formation of **5** can be controlled during the process by adding a chemical signal (5 equivalents of H_2O_2 here after 1 hour), liberating the catalyst. Reaction with pro-aniline **1** and subsequent addition of H_2O_2 (magenta line), reaction with unactivated pro-aniline **1** (blue dashed line). After addition of the chemical signal an immediate response was observed: the reaction rate increased 9-fold.

Although we confirmed complete conversion of pro-aniline **1** after addition of more than 1 equivalent of H_2O_2 and we were able to detect aniline **2** after an overnight hydrazone reaction in the presence of a substoichiometric amount of pro-aniline **1** + H_2O_2 (Supplementary Fig. 2.4), it might be the case that a small amount of aniline **2** is degraded over time.

Table 2.1: Activation of the catalyst determines the initial rate of hydrazone formation. Pseudo-first-order reaction rate constants (k_1) for hydrazone formation were determined by following the absorbance of **5** in UV/vis spectroscopy. The errors are the standard error of mean (the standard deviation divided by the square root of the number of measurements).

Catalyst system	k_1 (10^{-6} s^{-1})	k_{rel}
none	6.1 ± 0.1	1.0
H_2O_2	6.0 ± 0.3	1.0
1	5.6 ± 0.7	0.9
1 + H_2O_2	60 ± 8	10
2	113 ± 5	19

Importantly, using our signal responsive catalyst, we should be able to elicit a change in reaction rate at any given time during the process. To show this, pro-aniline **1** (0.5 mM) and reactants **3** (0.1 mM) and **4** (0.5 mM) were dissolved in buffer and mixed. Upon addition of the signal H_2O_2 after 1 hour, we observed an immediate 9-fold increase in the reaction rate (Fig. 2.2c). The rapid and significant increase of reaction rate when exposed to a chemical signal shows that the activation of a pro-catalyst enables an instant and autonomous response to a chemical change in the environment.

Control over gel formation by activation of the catalyst

As a first application of the signal responsive catalyst, we chose to couple the formation of a hydrazone polymer gel material[27] to a chemical signal. We synthesized an alternating polyethylene glycol/benzaldehyde copolymer using mesylated polyethylene glycol (molecular weight 5.4–6.6 kg mol^{-1}) and 3,4-dihydroxybenzaldehyde. A polydisperse polymer **6** ($M_w \sim 1 \cdot 10^5$ g mol^{-1}) featuring benzaldehyde groups was obtained (Fig. 2.3a).
Hydrazone formation between polymer aldehyde **6** and trishydrazide **7** is catalysed by aniline **2** and leads, under the right conditions, to the formation of transparent polymer gels (Fig. 2.3a, c). Using the signal induced activation of pro-aniline **1** we are able to control the rate of gel formation, the moment of gel formation (temporal control), and the mechanical properties of the obtained gels. An inverted tube test was used to investigate the influence of catalyst activation on gel formation.

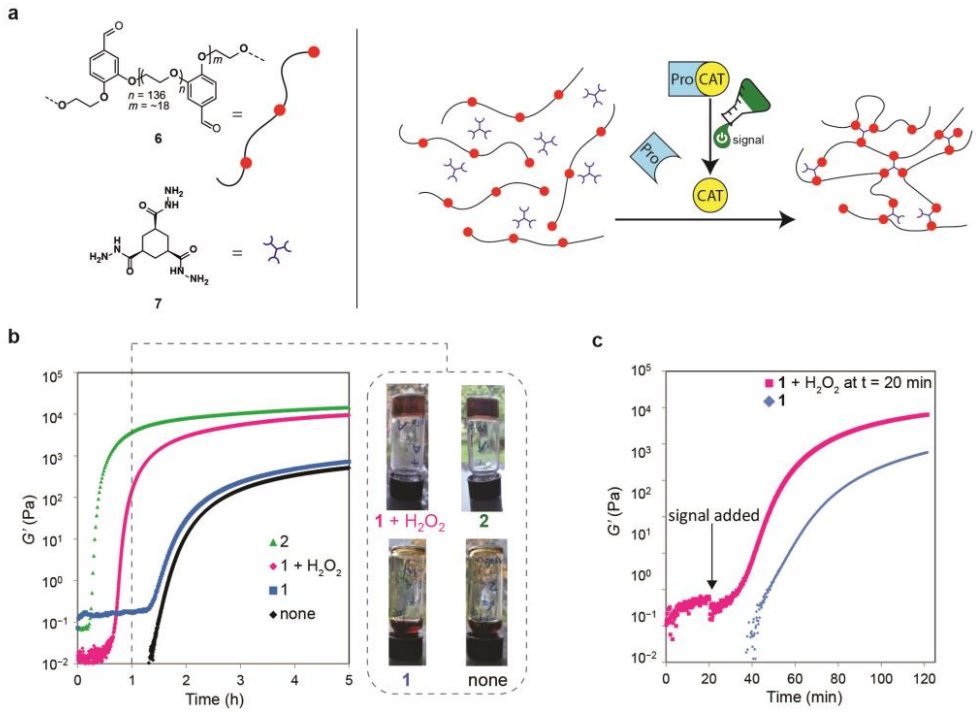

Figure 2.3: Polymer gel formation controlled by the activation of pro-aniline **1**. (**a**) The formation of a hydrazone polymer gel: aldehyde **6** and hydrazide **7** react to form a cross-linked hydrazone polymer gel. (**b**) The storage modulus *G'* measured with oscillatory rheology during gel formation at 25 °C (10 mM hydrazide **7**, 136 mg mL^{-1} aldehyde **6** in 20% dimethylformamide (DMF) in 100 mM phosphate buffer, pH 6.0) for the uncatalyzed gel (black line), the gel with 10 mM pro-aniline **1** (blue line), the gel with 10 mM pro-aniline **1** and 10 equivalents H_2O_2 (magenta line) and the gel with 10 mM aniline **2** (green line). The gelation rate with activated pro-aniline **1** is comparable to the gelation rate with aniline **2**. Without activation of the pro-aniline **1**, the gelation rate is comparable to the gelation rate of the uncatalyzed reaction. After 1 hour of gelation time, the mixtures with aniline **2** or activated pro-aniline **1** have gelled, whereas the mixtures without catalyst or with unactivated pro-aniline **1** have not gelled yet. We performed the gelation experiment in vials using the same conditions as we used for rheology and took a photograph after 1 hour of reaction time. Top left: pro-aniline **1** (10 mM) and H_2O_2 (100 mM), top right: aniline **2** (10 mM), bottom left: pro-aniline **1** (10 mM) and bottom right: without catalyst. (**c**) The gelation rate can be controlled during the process by adding a chemical signal (here after 20 minutes), liberating the catalyst. The storage modulus *G'* measured with oscillatory rheology for the aldehyde **6**/hydrazide **7** (10 mM) mixture with 10 mM pro-aniline **1** (blue line) and the mixture with pro-aniline **1** when 10 equivalents of H_2O_2 was added after 20 min (magenta line). Addition of the chemical signal induces a significant increase in gelation rate.

The gel tests presented here were performed using 136 mg mL^{-1} polymer aldehyde **6**, 10 mM hydrazide **7** and 10 mM catalyst in 20% DMF in aqueous buffer (100 mM phosphate buffer pH 7.4) in 4 mL vials. The hydrazide **7** and aldehyde **6** mixtures with either aniline **2** or pro-aniline **1** activated with H_2O_2 (10 equivalents) form gels within 1 hour (Fig. 2.3b). In contrast, for the mixtures with unactivated pro-aniline **1** or without catalyst, gelation takes 2 hours.

We performed oscillatory rheology to quantify the rate of gel formation under influence of the catalyst and to investigate the mechanical properties of the formed materials (Fig. 2.3b). The gel prepared with unactivated pro-aniline **1** is comparable in stiffness and formation time to the uncatalyzed gel, whereas the gel prepared with pro-aniline **1** and H_2O_2 (10 equivalents) is comparable to the gel formed using aniline **2** as a catalyst. After 6 hours of gelation time the catalysed gels show elastic moduli (*G'*) that are 1.5 times higher than the *G'* values we measured for the uncatalyzed gels, which indicates that the gel stiffness is controlled by catalysis.[19, 28] The difference in time scale of gel formation is especially apparent in rheology, as the cross-over for *G'* and *G''* (the gel point) for the catalysed gels is observed after 30 min, whereas this cross-over takes place after almost 2 hours for uncatalyzed gels (Supplementary Fig. 2.5a). Thus, activation of the catalyst by the chemical signal influences the gel formation rate as well as the gel stiffness.

With the signal responsive catalyst, we can now attempt to control the moment of material formation using a chemical signal. In the rheometer, we added a chemical signal to a solution of **6** and **7** containing pro-aniline **1**, 20 minutes after mixing all components (Fig. 2.3c). We observed a significant increase in the rate of gel formation shortly after addition of the chemical signal. A control experiment lacking the added signal showed a delayed and smaller increase of the elastic modulus. Importantly, these observations show that our system allows for temporal control over reaction rates and material formation.

Control over supramolecular gel formation by activation of the catalyst

To investigate the scope of our signal responsive catalyst, we also used pro-aniline **1** to control the formation of a supramolecular trishydrazone hydrogel described previously by our group,[19,29] featuring trishydrazide **7** (16 mM) and aldehyde **8** (96 mM) (Fig. 2.4a). Using either aniline **2** (10 mM), or pro-aniline **1** (10 mM) with H_2O_2 (10 equivalents), the supramolecular gels forms overnight. In contrast, without catalyst or with unactivated pro-aniline **1**, no gels are obtained (Fig. 2.4b). The activated pro-aniline can thus be used to control the formation rate and properties of polymer gels as well as supramolecular gels featuring hydrazone bonds.

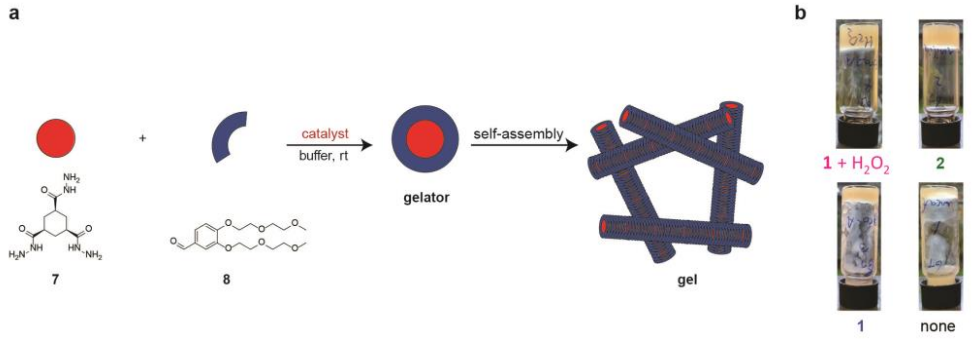

Figure 2.4: Supramolecular gel formation controlled by the activation of pro-aniline **1**. To demonstrate the versatility of the pro-aniline system, we used the pro-aniline **1** to control the formation of a supramolecular gel.[18] (**a**) Schematic representation of the two water-soluble building blocks aldehyde **8** and hydrazide **7** that react by hydrazone formation in the presence of a catalyst to form a gelator which stacks into fibers and forms a gel. (**b**) We performed a gelation test for the supramolecular gel in vials. Photographs of gelation samples taken after 15 h of reaction time for the mixture (16 mM hydrazide **7** and 96 mM aldehyde **8** in 20% methanol in phosphate buffer, 100 mM, pH 6.0) with, top left: pro-aniline **1** (10 mM) and H_2O_2 (100 mM), top right: aniline **2** (10 mM), bottom left: unactivated pro-aniline **1** (10 mM), bottom right: without catalyst. The mixtures with aniline **2** or pro-aniline **1** with H_2O_2 formed gels after 15 h, whereas the mixture without catalyst or with unactivated pro-aniline **1** did not form gels, although the viscosity of the mixtures was increased after 15 h.

2.3 Conclusions

In summary, we report a deactivated organocatalyst that is activated by a chemical signal. The pro-aniline **1** was synthesized in only two steps in good yields. Activating the pro-aniline **1** organocatalyst with H_2O_2 as a chemical signal increases the rate of hydrazone formation 10-fold almost instantly. We obtained control over gel formation for a polymer gel and for a supramolecular gel, both featuring hydrazone bonds. For the polymer gel, we controlled the moment of gelation: addition of the chemical signal to the unactivated pro-aniline **1** catalyst at an arbitrary moment after mixing all gelation components leads to a significant increase in the rate of gel formation. This shows that it is possible to control the moment of material formation in response to a chemical signal. As self-immolative trigger groups allow response to a wide range of signals[12], we have aimed to develop a generic method for the design of activatable catalysts. Furthermore, since self-immolative molecules can be used to incorporate more than one molecule of interest, the design can be used for signal amplification.[12] We are currently working on several organocatalysts that are responsive to a range of specific chemical signals. With the current results, we have developed a promising method for the introduction of signal response in molecular materials, constituting a first step towards achieving communication between artificial chemical systems.

2.4 References

1. Traut, T. *Allosteric Regulatory Enzymes*. New York: Springer (2010).
2. Hunter, T. Protein kinases and phosphatases: The Yin and Yang of protein phosphorylation and signaling. *Cell* **80,** 225-236 (1995).
3. Stoll, R. S. *et al.* Photoswitchable catalysts: correlating structure and conformational dynamics with reactivity by a combined experimental and computational approach. *J. Am. Chem. Soc.* **131,** 357-367 (2009).
4. Vlatkovic, M., Bernardi, L., Otten, E., Feringa, B. L. Dual stereocontrol over the Henry reaction using a light- and heat-triggered organocatalyst. *Chem. Commun.* **50,** 7773-7775 (2014).
5. Neilson, B. M., Bielawski, C. W. Photoswitchable NHC-promoted ring-opening polymerizations. *Chem. Commun.* **49,** 5453-5455 (2013).
6. Xi, W., Krieger, M., Kloxin, C. J., Bowman, C. N. A new photoclick reaction strategy: photo-induced catalysis of the thiol-Michael addition via a caged primary amine. *Chem. Commun.* **49,** 4504-4506 (2013).
7. Maity, C., Hendriksen, W. E., van Esch, J. H., Eelkema, R. Spatial structuring of a supramolecular hydrogel by using a visible-light triggered catalyst. *Angew. Chem. Int. Ed.* **54,** 998-1001 (2015).
8. Blanco, V., Leigh, D. A., Marcos, V. Artificial switchable catalysts. *Chem. Soc. Rev.* **44,** 5341-5370 (2015).
9. McGuirk, C. M., Mendez-Arroyo, J., Lifschitz, A. M., Mirkin, C. A. Allosteric regulation of supramolecular oligomerization and catalytic activity via coordination-based control of competitive hydrogen-bonding events. *J. Am. Chem. Soc.* **136,** 16594-16601 (2014).
10. Hu, L., Lu, C-H., Willner, I. Switchable catalytic DNA catenanes. *Nano Lett.* **15,** 2099-2103 (2015).
11. Tonga, G. Y. *et al.* Supramolecular regulation of bioorthogonal catalysis in cells using nanoparticle-embedded transition metal catalysts. *Nature Chem.* **7,** 597-603 (2015).
12. Roth, M. E., Green, O., Gnaim, S., Shabat, D. Dendritic, oligomeric, and polymeric self-immolative molecular amplification. *Chem. Rev.* **116,** 1309-1352 (2016).
13. Brooks, A. D., Mohapatra, H., Phillips, S. T. Design, synthesis, and characterization of small-molecule reagents that cooperatively provide dual readouts for triaging and, when necessary, quantifying point-of-need enzyme assays. *J. Org. Chem.* **80,** 10437-10445 (2015).
14. Alouane, A., Labruère, R., Le Saux, T., Schmidt, F., Jullien, L. Self-immolative spacers: kinetic aspects, structure–property relationships, and applications. *Angew. Chem. Int. Ed.* **54,** 7492-7509 (2015).
15. Peterson, G. I., Larsen, M. B., Boydston, A. J. Controlled depolymerization: stimuli-responsive self-immolative polymers. *Macromolecules* **45,** 7317-7328 (2012).
16. Dirksen, A., Dirksen, S., Hackeng, T. M., Dawson, P. E. Nucleophilic catalysis of hydrazone formation and transimination: Implications for dynamic covalent chemistry. *J. Am. Chem. Soc.* **128,** 15602-15603 (2006).

17. Bhat, V. T., *et al.*Nucleophilic catalysis of acylhydrazone equilibration for protein-directed dynamic covalent chemistry. *Nature Chem.* **2,** 490-497 (2010).
18. Larsen, D., Pittelkow, M., Karmakar, S., Kool, E. T. New organocatalyst scaffolds with high activity in promoting hydrazone and oxime formation at neutral pH. *Org. Lett.* **17,** 274-277 (2015).
19. Boekhoven, J., *et al.*Catalytic control over supramolecular gel formation. *Nature Chem.* **5,** 433–437 (2013).
20. McKinnon, D. D., Domaille, D. W., Cha, J. N., Anseth, K. S. Bis-aliphatic hydrazone-linked hydrogels form most rapidly at physiological pH: identifying the origin of hydrogel properties with small molecule kinetic studies. *Chem. Mat.* **26,** 2382-2387 (2014).
21. Ikeda, M. *et al.* Installing logic-gate responses to a variety of biological substances in supramolecular hydrogel–enzyme hybrids. *Nature Chem.* **6,** 511-518 (2014).
22. Alberti, K. G. M. M., Zimmet, P. Z. Definition, diagnosis and classification of diabetes mellitus and its complications. Part 1: diagnosis and classification of diabetes mellitus. Provisional report of a WHO Consultation. *Diabet. Med.* **15,** 539-553 (1998).
23. Sreekumar, A. *et al.* Metabolomic profiles delineate potential role for sarcosine in prostate cancer progression. *Nature* **457,** 910-914 (2009).
24. Baytekin, H. T., Baytekin, B., Grzybowski, B. A. Mechanoradicals created in "polymeric sponges" drive reactions in aqueous media. *Angew. Chem. Int. Ed.* **51,** 3596-3600 (2012).
25. Crisalli, P., Kool, E. T. Water-soluble organocatalysts for hydrazone and oxime formation. *J. Org. Chem.* **78,** 1184-1189 (2013).
26. Versluis, F., *et al.* Negatively charged lipid membranes catalyze supramolecular hydrogel formation. *J. Am. Chem. Soc.* **138,** 8670-8673 (2016).
27. White, S. R., *et al.*Restoration of large damage volumes in polymers. *Science* **344,** 620-623 (2014).
28. Lin, F. *et al.* Peptide-functionalized oxime hydrogels with tunable mechanical properties and gelation behavior. *Biomacromolecules* **14,** 3749-3758 (2013).
29. Trausel, F., *et al.* Catalysis of supramolecular hydrogelation. *Acc. Chem. Res.* **49,** 1440-1447 (2016).
30. Poolman, J. M., *et al.*Variable gelation time and stiffness of low-molecular-weight hydrogels through catalytic control over self-assembly. *Nat. Protoc.* **9,** 977-988 (2014).

2.5 Supplementary information

Supplementary Figures

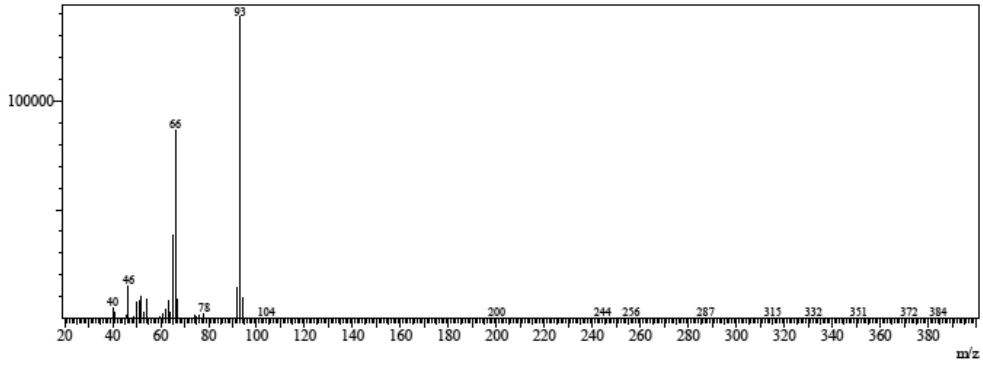

Supplementary Figure S2.1: GC/MS spectrum taken after the reaction of pro-aniline **1** with 18 equivalents of H_2O_2. Conditions: 5 mg, 18 µmol pro-aniline **1** in 0.25 mL ethyl acetate, H_2O_2 (18 equivalents, 25.4 µL in 0.25 mL deionized water), stirred for 1 h at room temperature. The reaction mixture was quenched with a saturated sodium thiosulfate solution and the organic layer was used for analysis in GC/MS. Only aniline **2** was detected in the reaction mixture, MS (GC/MS) m/z: 93 $[M]^{+\bullet}$, 66 $[C_5H_6]^{+\bullet}$ (expected m/z = 93.06, 66.05), retention time: 11 min.

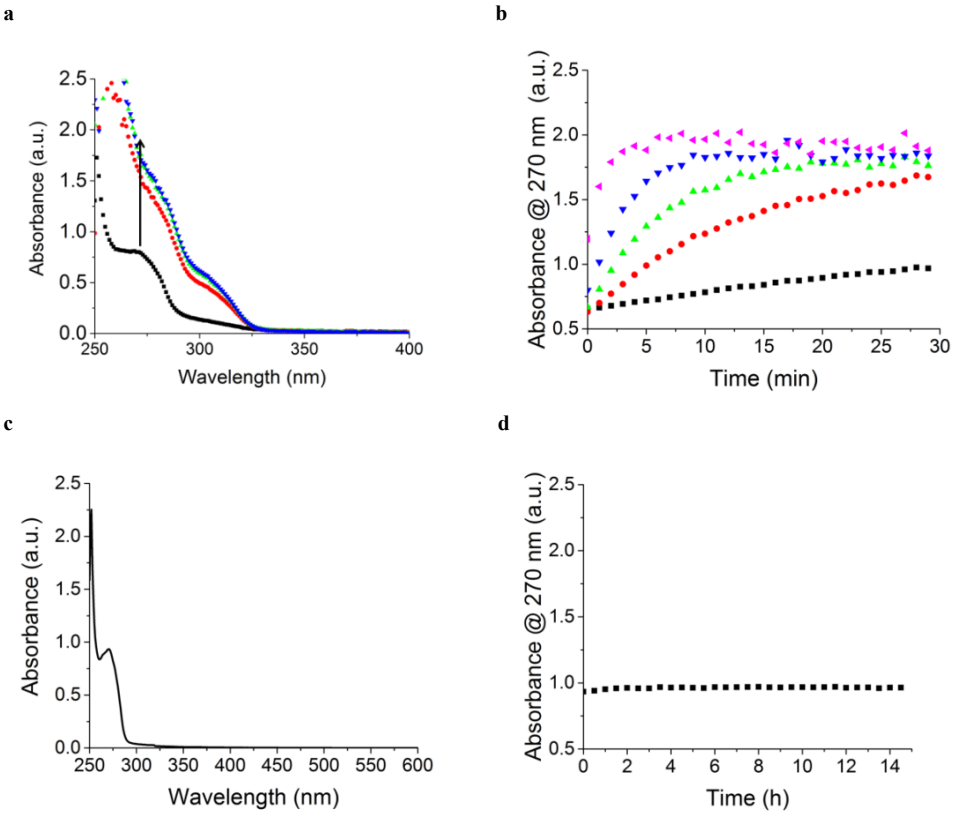

Supplementary Figure S2.2: The self-immolative reaction of pro-aniline **1** (0.5 mM) with H_2O_2 (9 mM) in 20% DMF in phosphate buffer (100 mM, pH 7.4) followed in UV/vis spectroscopy. (**a**) UV/vis absorption spectra of pro-aniline **1** after addition of H_2O_2, spectrum at t = 0 min (black), spectrum at t = 5 min (red), spectrum at t = 10 min (green), spectrum at t = 15 min (blue). (**b**) The increase of absorption at 270 nm after addition of H_2O_2 to a solution of **1**, 1 equivalent of H_2O_2 (black), 5 equivalents (red), 10 equivalents (green), 18 equivalents (blue), 50 equivalents (pink). (**c**) The UV/vis absorption spectrum of pro-aniline **1**. (**d**) Without H_2O_2 the absorption spectrum of pro-aniline **1** does not change in 15 h.

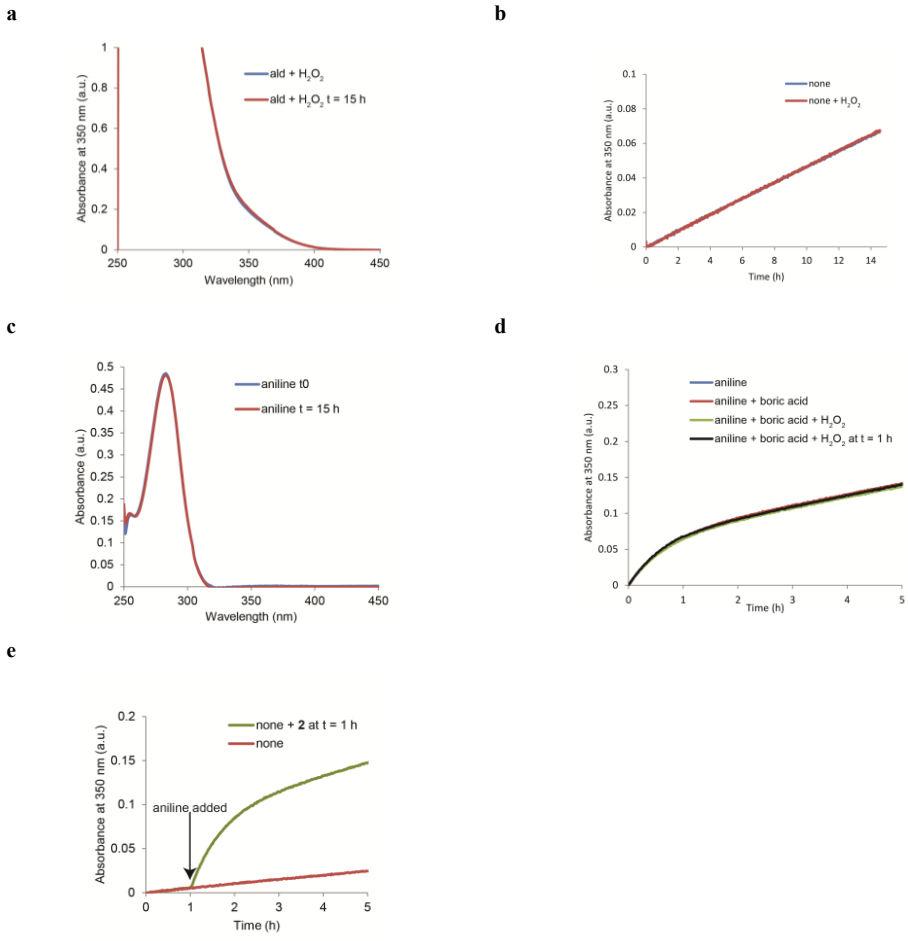

Supplementary Figure S2.3: (**a**) UV/vis absorbance spectrum measured for aldehyde **4** (0.5 mM) with H_2O_2 at t = 0 h and at t = 15 h, the compound remains stable. (**b**) Absorbance at 350 nm of hydrazone **5** formation followed in UV/vis spectroscopy (conditions: hydrazide **3** (0.1 mM), aldehyde **4** (0.5 mM), 20% DMF in 100 mM phosphate buffer pH 7.4) without catalyst (blue line), with H_2O_2 (2.5 mM, red line). H_2O_2 has no influence on the reaction rate. (**c**) UV/vis absorbance spectrum measured for aniline **2** (0.5 mM) at t = 0 h and at t = 15 h, the compound remains stable. (**d**) Absorbance at 350 nm of hydrazone **5** formation followed in UV/vis spectroscopy (conditions: hydrazide **3** (0.1 mM), aldehyde **4** (0.5 mM), 20% DMF in 100 mM phosphate buffer pH 7.4) with aniline **2** (0.5 mM, blue line), with aniline **2** + boric acid (0.5 mM, red line), with aniline **2** + boric acid + H_2O_2 (2.5 mM, green line), with aniline **2** + boric acid + H_2O_2 at t = 1 h (2.5 mM, black line. Boric acid has no influence on the catalytic activity of aniline **2**, with and without H_2O_2. (**e**) Absorbance at 350 nm of hydrazone **5** formation followed in UV/vis spectroscopy (conditions: hydrazide **3** (0.1 mM), aldehyde **4** (0.5 mM), 20% DMF in 100 mM phosphate buffer pH 7.4) without catalyst (red line), aniline **2** was added after 1 hour (green line, 2.5 mM. For more blank experiments, see Supplementary Table 1.

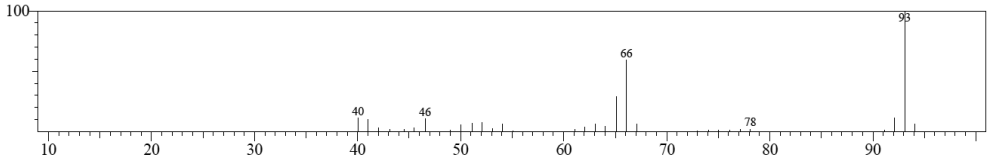

Supplementary Figure S2.4: GC/MS spectrum taken after 65 h of reaction time of hydrazide **3** with aldehyde **4** in the presence of pro-aniline **1** and H_2O_2. Conditions: hydrazide **3** (20 mM), aldehyde **4** (20 mM), pro-aniline **1** (10 mM), H_2O_2 (11 mM) in 20% DMF in 100 mM phosphate buffer pH 7.4. The reaction mixture was extracted after 65 h of reaction time with dichloromethane. The organic layer was evaporated and re-dissolved in ethyl acetate for GC/MS analysis. Aniline **2** was detected in the extract of the reaction mixture, MS (GC/MS) m/z: 93 $[M]^{+\bullet}$, 66 $[C_5H_6]^{+\bullet}$ (expected m/z = 93.06, 66.05), retention time: 11 min.

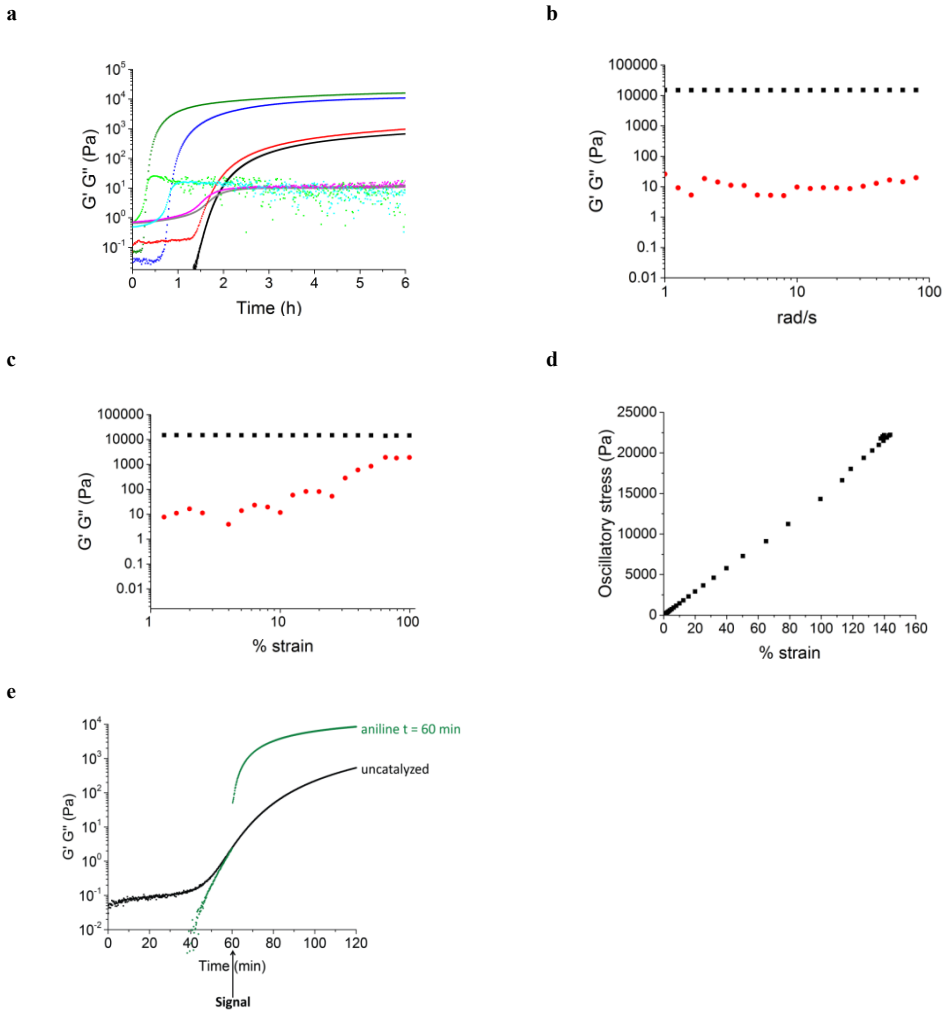

Supplementary Figure S2.5: Rheological data of the polymer gel. Total volume of the gels is 0.6 mL. Composition of the gels: 140 mg/mL polymer aldehyde **6**, 10 mM aniline **2** or 10 mM pro-aniline **1**, 10 mM hydrazide **7**, 20% DMF in 100 mM phosphate buffer pH 6.0. (**a**) Time sweep, *G'* and *G''* measured during the formation of the gel, uncatalyzed *G'* (black), uncatalyzed *G''* (grey), aniline **2** *G'* (green), aniline **2** *G''* (light green), pro-aniline **1** *G'* (red), pro-aniline **1** *G''* (pink), pro-aniline **1** + H_2O_2 (blue), pro-aniline **1** + H_2O_2 (light blue). (**b**) Frequency sweep of polymer gel formed with aniline **2** (10 mM) *G'* (black), *G''* (red). (**c**) Strain sweep of polymer gel formed with aniline **2** (10 mM), *G'* (black), *G''* (red). (**d**) Stress/strain curve of polymer gel formed with aniline **2** (10 mM) *G'* (black), *G''* (red). (**e**) Time sweep, *G'* and *G''* measured during the formation of the gel (total volume 1 mL), aniline **2** is added after 60 minutes, uncatalyzed (black), catalysed and aniline **2** (50 µL, 200 mM) added at *t* = 60 min (green).

a **b**

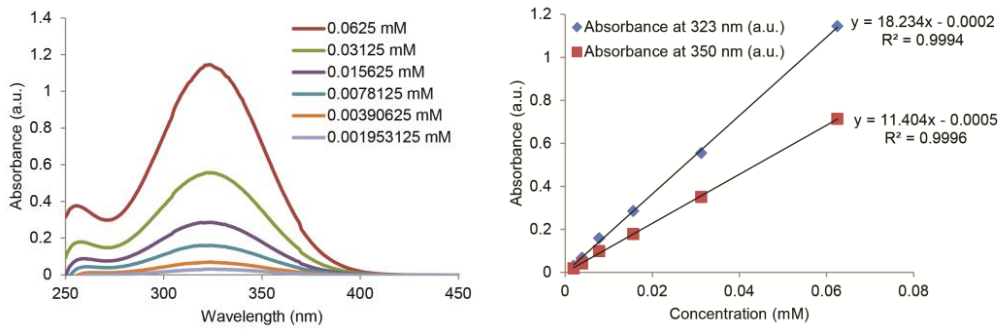

Supplementary Figure S2.6: (**a-b**) Calibration line of hydrazone **5** measured in 20% DMF in phosphate buffer (100 mM, pH 7.4). The extinction coefficient of hydrazone **5** under these conditions at the absorbance maximum of 323 nm is $2.1 \pm 0.13 \cdot 10^4$ M^{-1} s^{-1}. The extinction coefficient at 350 nm is $1.3 \pm 0.087 \cdot 10^4$ M^{-1} s^{-1}. The errors are the standard error of mean (the standard deviation divided by the square root of the number of measurements).

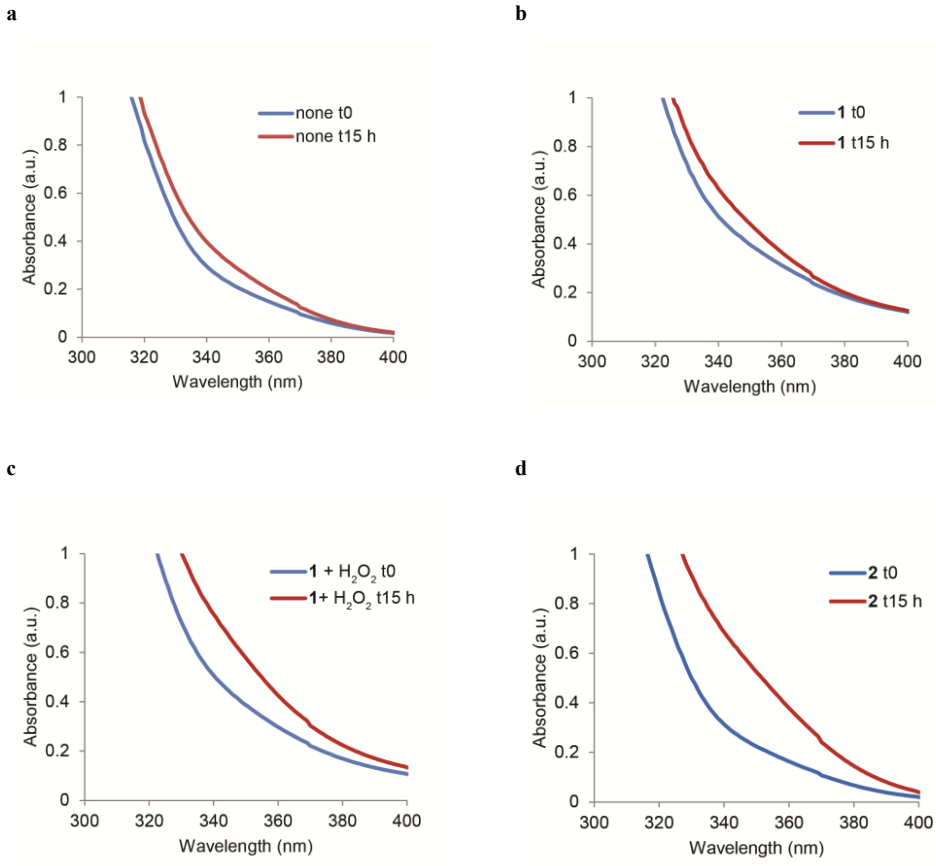

Supplementary Figure S2.7: UV/vis spectra of the reaction mixture of hydrazone formation at t = 0 h (blue lines) and at t = 15 h (red lines). (**a**) Uncatalyzed reaction, (**b**) reaction in presence of pro-aniline **1**, (**c**) reaction in presence of pro-aniline **1** and H_2O_2, (**d**) reaction in the presence of aniline **2**. Reaction conditions: 0.1 mM hydrazide **3**, 0.5 mM aldehyde **4** in 20% DMF in phosphate buffer (100 mM, pH 7.4) without catalyst, in the presence of either unactivated pro-aniline **1** (0.5 mM), or activated pro-aniline **1** (0.5 mM) with 5 equivalents of H_2O_2 (2.5 mM) or aniline **2** (0.5 mM).

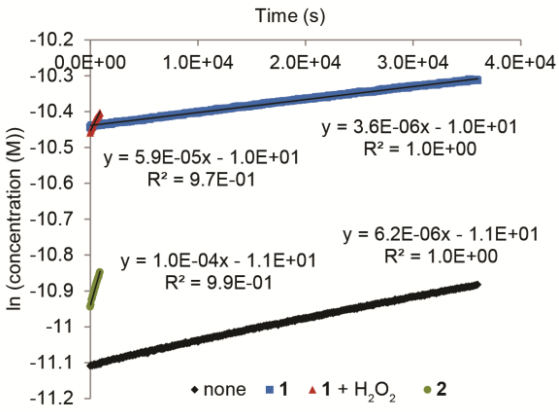

Supplementary Figure S2.8: Plots of ln (concentration (M)) versus time (s) result in linear graphs, the slope represents the pseudo-first-order rate constant with unit s^{-1}, without catalyst (black), with pro-aniline **1** (blue), with pro-aniline **1** + H_2O_2 (red) and with aniline **2** (green). Concentrations were obtained using the extinction coefficient of the product at 350 nm ($1.3 \pm 0.087 \cdot 10^4$ M^{-1} s^{-1}). The errors are the standard error of mean (the standard deviation divided by the square root of the number of measurements). Reaction conditions: 0.1 mM hydrazide **3**, 0.5 mM aldehyde **4** in 20% DMF in phosphate buffer (100 mM, pH 7.4) without catalyst, in the presence of either unactivated pro-aniline **1** (0.5 mM), or activated pro-aniline **1** (0.5 mM) with 5 equivalents of H_2O_2 (2.5 mM) or aniline **2** (0.5 mM).

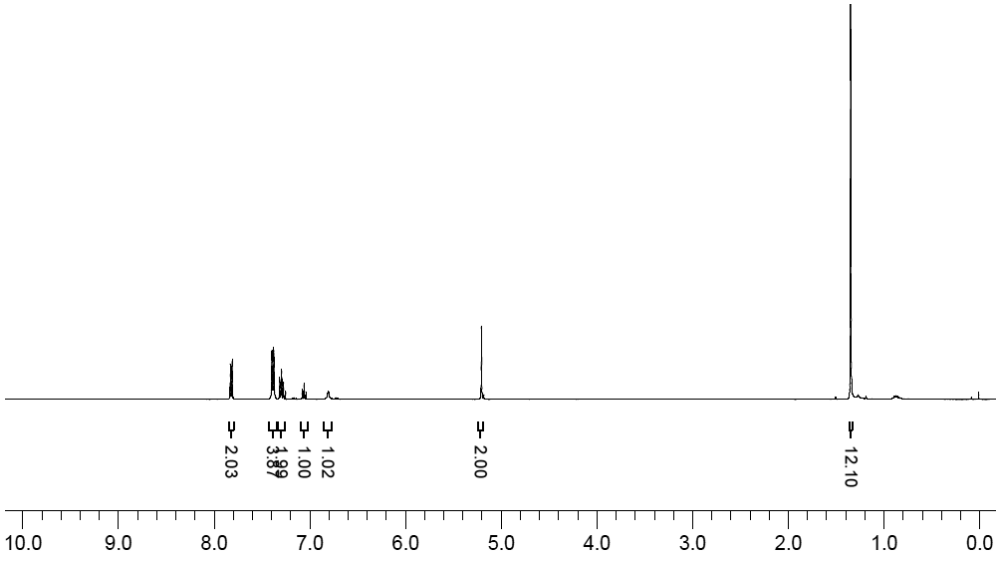

Supplementary Figure S2.9: ^{1}H NMR spectrum of pro-aniline boronate ester **S1** in $CDCl_3$.

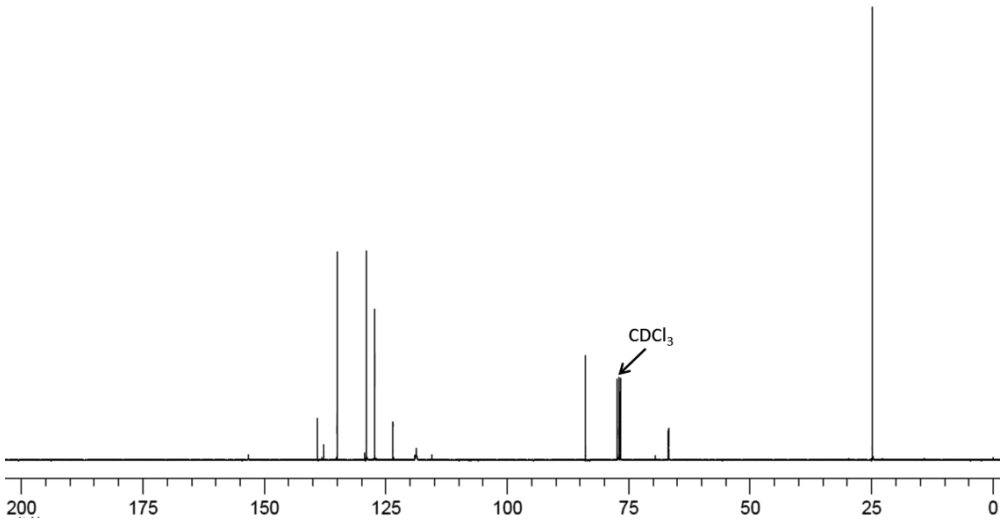

Supplementary Figure S2.10: ^{13}C NMR spectrum of pro-aniline boronate ester **S1** in $CDCl_3$.

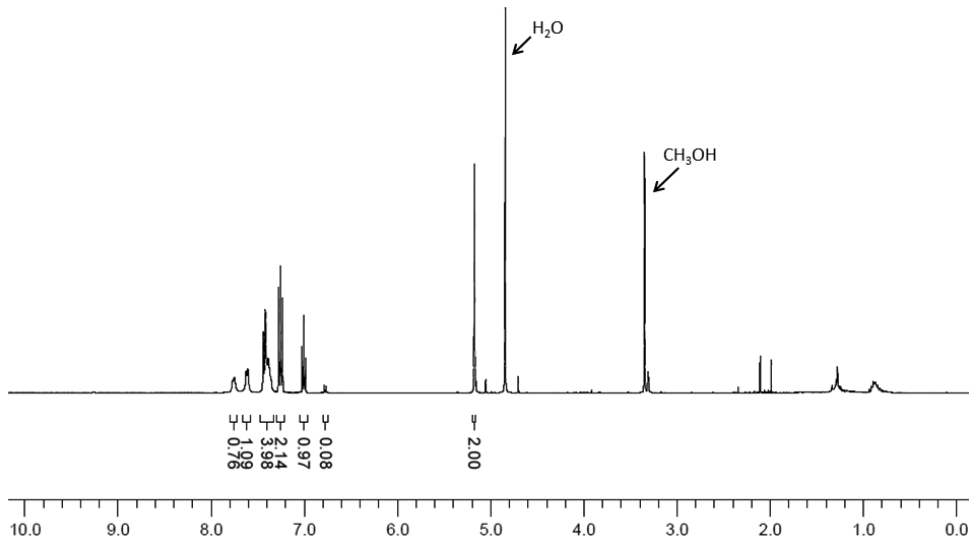

Supplementary Figure S2.11: ^{1}H NMR spectrum of pro-aniline **1** in CD_3OD.

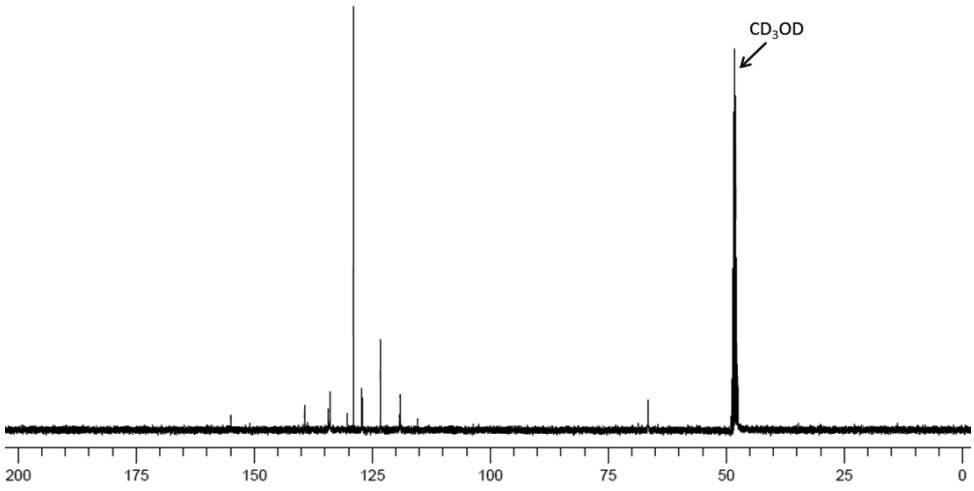

Supplementary Figure S2.12: ^{13}C NMR spectrum of pro-aniline **1** in CD_3OD.

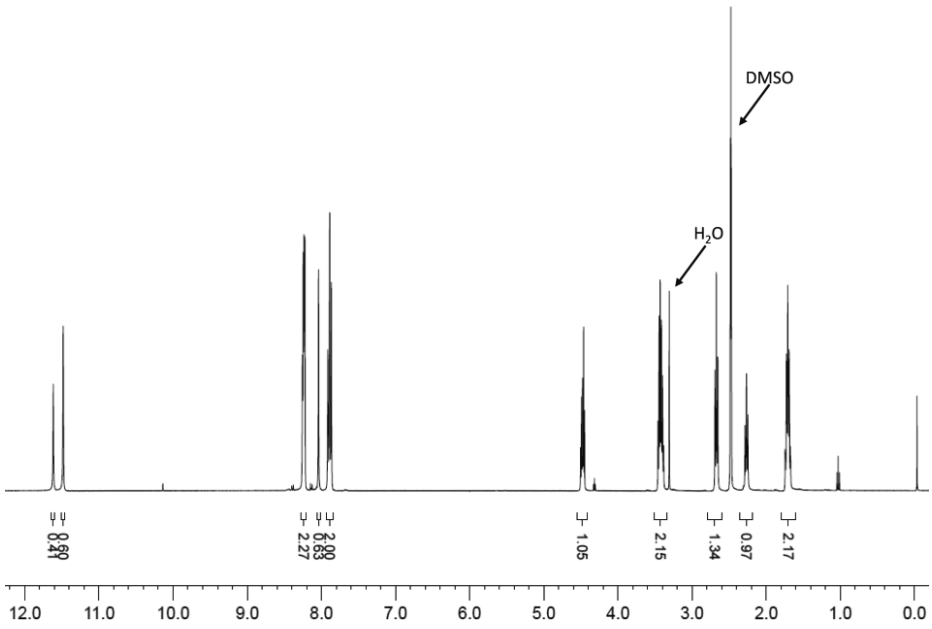

Supplementary Figure S2.13: ^{1}H NMR spectrum of hydrazone **5** in DMSO-d6.

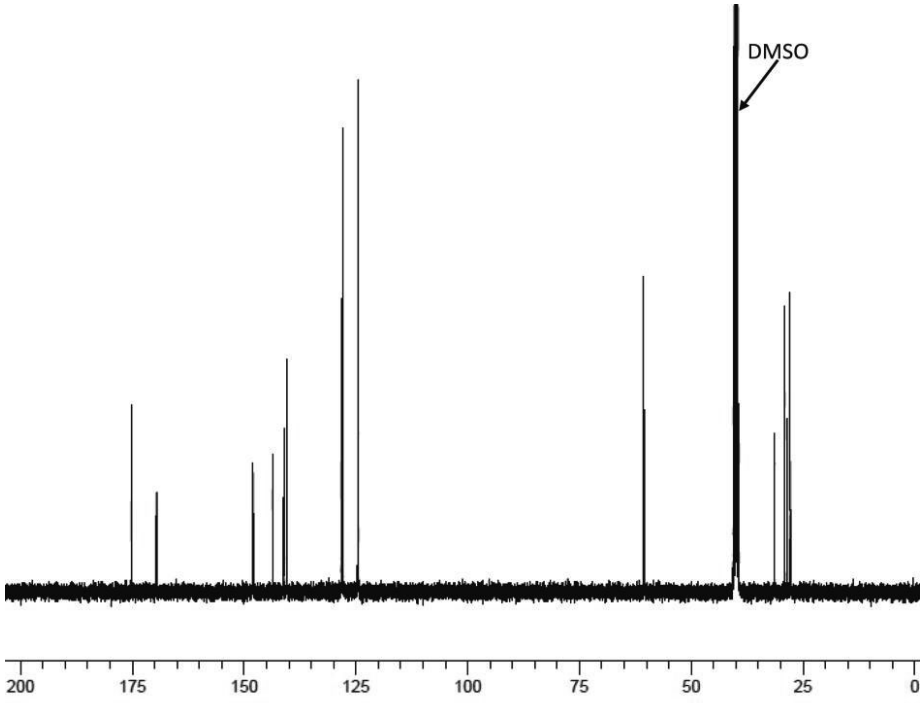

Supplementary Figure S2.14: ^{13}C NMR spectrum of hydrazone **5** in DMSO-d6.

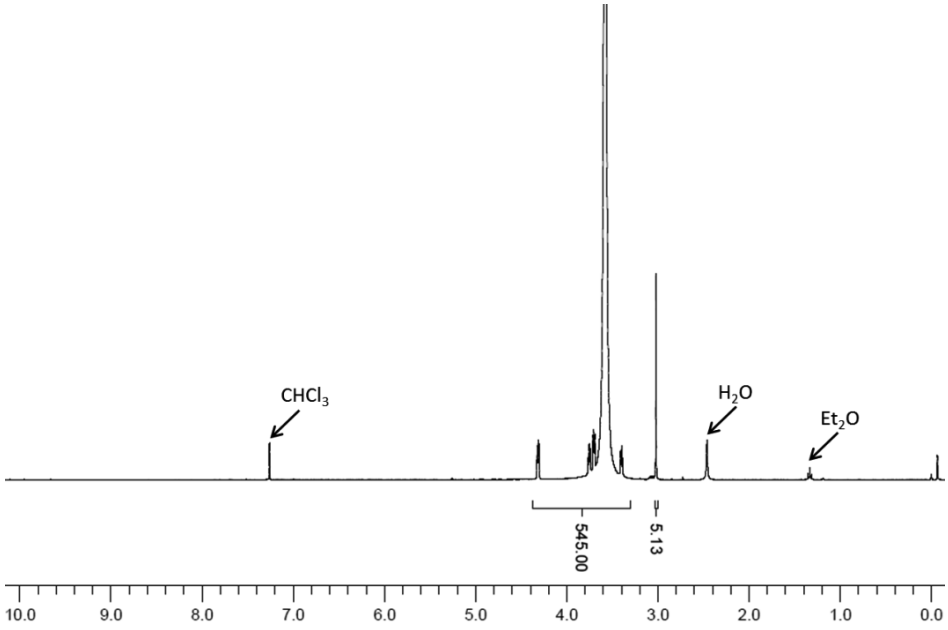

Supplementary Figure S2.15: ^{1}H NMR spectrum of PEG-mesylate **S2** in $CDCl_3$.

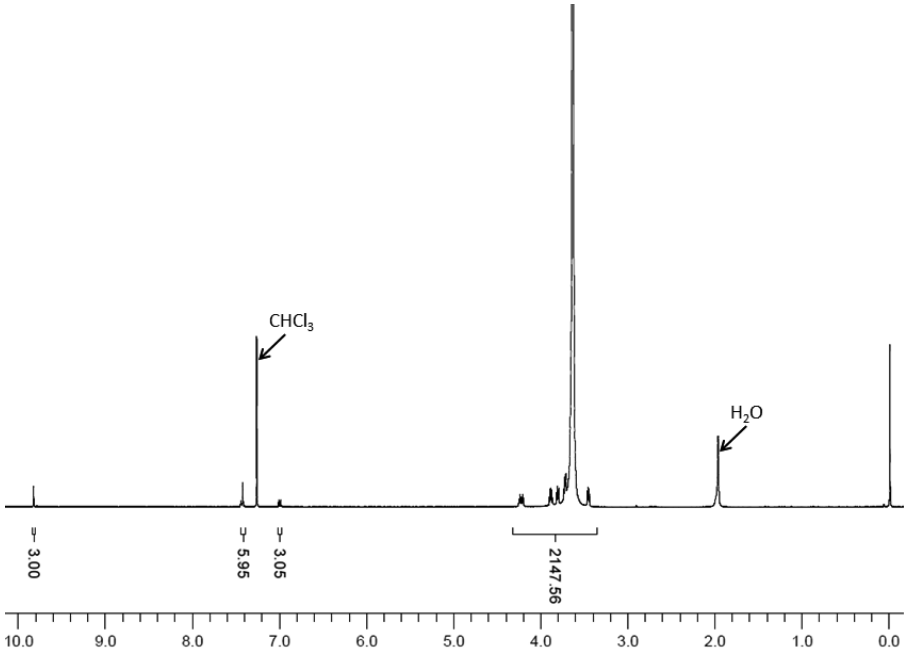

Supplementary Figure S2.16: ^{1}H NMR spectrum of PEG-aldehyde **6** in $CDCl_3$.

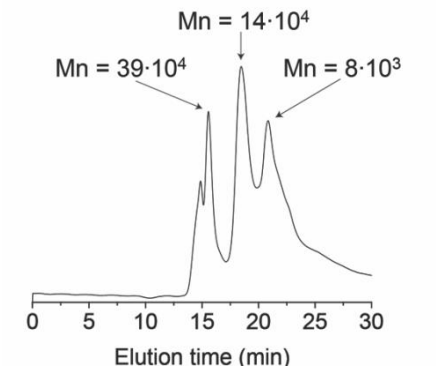

Supplementary Figure S2.17: Gel permeation chromatogram of PEG-aldehyde **6** (10 mg/mL in water).

Supplementary Tables

Supplementary Table S2.1: Overview of control experiments performed for the catalytic activity of hydrazone **5** formation. In all cases, the absorbance at 350 nm was followed during the reaction and spectra between 250 – 450 nm were taken at the start and at the end of the reaction.

#	Hydrazide **3**	Aldehyde **4**	Pro-aniline **1**	H_2O_2	Aniline **2**	Boric acid	Results
1	x						stable for 15 h
2	x			x			no reaction 15 h
3	x		x				no reaction 15 h
4	x		x	x			no reaction 15 h
5	x				x		no reaction 15 h
6	x	x		x			same as uncatalyzed reaction
7	x	x		x	x		same as reaction with aniline **2**
8	x	x	x		x		same as reaction with aniline **2**
9	x	x	x	x	x		proportional increase in reaction rate
10		x					no change in absorbance, stable 15 h
11		x		x			no reaction 15 h
12		x	x				no reaction 15 h
13		x	x	x			no reaction 15 h
14		x			x		iminium formation negligible at 350 nm
15				x	x		stable for 15 h
16			x				stable for 15 h
17			x	x			no change in absorbance at 350 nm
18	x	x			x	x	same as reaction with aniline **2**
19	x	x		x	x	x	same as reaction with aniline **2**

Supplementary Table S2.2: Pseudo-first-order reaction rates for hydrazone formation were determined by following the absorbance of hydrazone **5** in UV/vis spectroscopy. The rate constants were determined by plotting the natural logarithm of the concentration (M) over time (s), in which the obtained slope is equal to the first-order rate constant of hydrazone **5** formation.

Catalyst system	**Slope·10^6**	**k_1 (10^{-6} s^{-1})**	**k_{rel}**
none	6.1 ± 0.1	6.1 ± 0.1	1.0
H_2O_2	6.0 ± 0.3	6.0 ± 0.3	1.0
1	5.6 ± 0.7	5.6 ± 0.7	0.9
1 + H_2O_2	60 ± 8	60 ± 8	10
2	113 ± 5	113 ± 5	19

Supplementary Methods

Instrumentation and characterization

NMR spectra were recorded on an Agilent-400 MR DD2 (400 MHz for ^{1}H and 100.5 MHz for ^{13}C) at 298 K using residual protonated solvent signals as internal standard (^{1}H: $\delta(CHCl_3)$ = 7.26 ppm, $\delta(CH_3OH)$ = 3.31 ppm, and ^{13}C: $\delta(CHCl_3)$ = 77.16 ppm, $\delta(CH_3OH)$ = 49.00 ppm). TLC was performed on Merck Silica Gel 60 F254 TLC plates with a fluorescent indicator with a 254 nm excitation wavelength and compounds were visualized under UV light of 254 nm wavelength. GC/MS was performed with a Shimadzu QP-2010S GCMS. LCMS-MS was performed on a Shimadzu Liquid Chromatograph Mass Spectrometer 2010, LC-8A pump with a diode array detector SPD-M20. The column used was the Xbridge Shield RP 18.5 µm (4.6 x 150 mm). UV/Vis spectroscopic measurements were performed on an Analytik Jena Specord 250 spectrophotometer; quartz cuvettes with a path length of 1 cm were used. Oscillatory experiments were performed using an AR G2 rheometer from TA Instruments in a strain-controlled mode; the rheometer was equipped with a steel plate-and-plate geometry of diameter 40 mm and a water trap. The temperature of the plates was controlled at 25 ± 0.2 °C. Measurements were performed at a frequency of 1 Hz while applying 1% strain. GPC was performed using a Shimadzu Prominence GPC system equipped with 2x PL aquagel-OH MIXED H columns (Agilent, 8 µm, 300 × 7.5 mm) and refractive index detector (RID).

Materials

All compounds and solvents were used without further purification. The technical solvents were purchased from VWR and the reagent grade solvents were purchased from Sigma Aldrich. 4-(Hydroxymethyl)benzeneboronic acid pinacol ester and 4-hydroxybutyric acid hydrazide were purchased from Alfa Aesar. Triphosgene, sodium periodate, PEG-6000, trimethylamine, palladium on activated charcoal, hydrazine hydrate (64%), trimesic acid, diethylene glycol monomethyl ether and 3,4-dihydroxybenzaldehyde were purchased from Sigma Aldrich. Aniline **2**, 4-nitrobenzaldehyde, acetic acid, methanesulfonyl chloride, *p*-toluenesulfonic acid monohydrate and *p*-toluenesulfonyl chloride were purchased from Acros. 3,4-Dihydroxybenzaldehyde was purchased from AK Scientific. Special safety precautions should be taken for the reaction with triphosgene as this compound can release

highly toxic phosgene gas. Triphosgene should be handled in a closed fume hood at all times, while wearing protective gloves and glasses. We also offer an alternative synthetic route to pro-aniline **1** that avoids the use of triphosgene[1]. Hydrogen gas is highly flammable; DMF, aniline **2**, hydrazine hydrate and diethylene glycol monomethyl ether are suspected carcinogens, hydrogen peroxide is corrosive: these compounds should be handled with care.

Synthetic procedures

For the synthesis of *cis,cis*-cyclohexane-1,3,5-tricarbohydrazide **7** and 3,4-bis(2-(2-methoxyethoxy)ethoxy)benzaldehyde **8** we refer to procedures described in the literature.[30] Detailed procedures for the synthesis of pro-aniline **1**, hydrazone **5** and PEG-aldehyde copolymer **6** are described in the Supplementary Methods, NMR and GPC spectra are shown in Supplementary Figures 2.9-2.17.

Investigation of the release of aniline 2 from pro-aniline 1

The self-immolative reaction of pro-aniline **1** with H_2O_2 was investigated with thin layer chromatography (TLC), gas chromatography/mass spectroscopy (GC/MS) and UV/vis spectroscopy. TLC: pro-aniline **1** (4.8 mg, 13.6 μmol) was dissolved in acetonitrile (0.5 mL) and a solution of H_2O_2 in deionized water (18 equivalents, 0.245 mM, 0.5 mL) was added. TLCs (eluent = 1:1 petroleum ether : ethyl acetate) were taken at t = 0, 1, 5, 10, 15 and 20 minutes. The reaction mixture and aniline **2** were run on the TLC plate for comparison. After 10 minutes all starting compound had disappeared, replaced by aniline **2** and side products. GC/MS: pro-aniline **1** (5 mg, 18 μmol) was dissolved in 0.25 mL ethyl acetate. H_2O_2 (18 equivalents, 25.4 μL in 0.25 mL deionized water) was added and after the mixture was allowed to stir for 1 hour at room temperature, the reaction was quenched with a saturated sodium thiosulfate solution. The organic layer of the reaction mixture was analysed by GC/MS: after the reaction the product peak had disappeared and aniline **2** (m/z 93) was detected in the reaction mixture (Supplementary Fig. 2.1). UV/vis: the self-immolative reaction of pro-aniline **1** followed in UV/vis was performed in a 20% DMF in phosphate buffer (100 mM, pH 7.4) solution, using 0.5 mM concentration of pro-aniline **1** and 18 equivalents of H_2O_2 (Supplementary Fig. 2.2a, b)). The self-immolative reaction is complete when the increase of absorption reaches a plateau. The stability measurement of

pro-aniline **1** overnight was performed using the same conditions of pro-aniline **1** (0.5 mM) in a mixture of 20% DMF in buffer. Without H_2O_2 pro-aniline **1** is stable for over 15 hours (i.e., does not release aniline **2**, Supplementary Fig. 2.2c, d).

Investigation of the catalytic activity of pro-aniline 1 after activation

A calibration line was measured for hydrazone product **5** in 20% DMF in phosphate buffer (100 mM, pH 7.4). The extinction coefficient of hydrazone **5** at 350 nm under these conditions is $1.3 \pm 0.087 \cdot 10^4$ M^{-1} cm^{-1} (Supplementary Fig. 2.6). The hydrazone reaction (Fig. 2.2a) was performed in 20% DMF in a 100 mM phosphate buffer pH 7.4, containing 0.5 mM of 4-nitrobenzaldehyde **4**, 0.5 mM of catalyst, 0.1 mM of 4-hydroxybutyric acid hydrazide **3** and 2.5 mM of H_2O_2. The quartz cuvettes contained a total reaction volume of 2 mL. The stock solutions of the reagents were added as follows: aldehyde **4** solution (10 mM in DMF), phosphate buffer, DMF, catalyst solution (10 mM in DMF), the hydrazide **3** solution (2 mM in buffer). The cuvettes were closed using Teflon caps and thoroughly mixed by converting the cuvette upside down 4 times. The spectra of the starting reaction mixtures were measured (reference measurement, 250 – 450 nm, 10 nm s^{-1}). The product peak at 350 nm was followed using a 6-sample holder (standard absorption measurement, slow time scan, measuring wavelength 350 nm, scan every 60 s, Fig. 2.2b, c). At the end of the measurement, single scans were measured again using the same settings as for the starting reaction mixtures (Supplementary Fig. 2.7). The pH was monitored for the reaction with pro-aniline **1** (0.5 mM) and H_2O_2 (2.5 mM), every 10 minutes for the first 2 h and once after 18 h. At all times a pH of 8.0 was measured. As the phosphate buffer (100 mM, pH 7.4) with 20% DMF alone also gives a pH of 8.0, this indicates that the pH did not change during the reaction. We ensured that no side reactions occurred (Supplementary Table 1). Addition of aniline **2** to the uncatalyzed reaction after 1 h of reaction time gave a similar response in reaction rate as addition of H_2O_2 to the reaction with pro-aniline **1** (Supplementary Fig. 2.3e). The pseudo-first-order rate constants were determined by converting the absorbance measured during the reactions to concentration using the extinction coefficient of the product and by fitting the natural logarithm of the concentration (M) over time (s). The graph was fitted using linear regression in Origin Pro 2015 to yield the pseudo-first-order reaction rate constant. For the uncatalyzed reaction and the reaction with pro-aniline **1**, the first 10 h of the reaction were taken to determine the

rates. For the reaction in the presence of activated pro-aniline **1** and for the reaction catalysed by aniline **2**, the first 15 minutes were used to determine the rate (Supplementary Fig. 2.8, Supplementary Table 2). In order to ensure that aniline **2** was not used up during the reaction, we performed a 65 h reaction of hydrazide **3** with aldehyde **4** in the presence of 0.5 equivalents of pro-aniline **1** with H_2O_2 and analysed the reaction mixture afterwards with GC/MS. We were able to detect aniline **2** (m/z 93) in the reaction mixture. Conditions: hydrazide **3** (20 mM), aldehyde **4** (20 mM), pro-aniline **1** (10 mM), H_2O_2 (1.1 mM) in 20% DMF in 100 mM phosphate buffer pH 7.4. The reaction mixture was extracted after 65 h of reaction time with dichloromethane. The organic layer was evaporated and re-dissolved in ethyl acetate for GC/MS analysis. Aniline **2** was detected in the reaction mixture, MS (GC/MS) m/z: 93 [M], 66 $[C_5H_6]^{+\bullet}$ (expected m/z = 93.06), retention time: 11 min.

Rheology of the polymer gel

The storage and loss moduli *G′* and *G″* were followed in time during the formation of the gel, using a rheometer (Supplementary Fig. 2.5a). Total volume of the gels is 0.6 mL. Composition of the gels: 140 mg/mL polymer aldehyde **6**, 10 mM aniline **2** or 10 mM pro-aniline **1**, 10 mM hydrazide **7**, 20% DMF in 100 mM phosphate buffer pH 6.0. First, the polymer aldehyde **6** (84 mg) was weighed out in the shell vial, then we added buffer, the catalyst solution (120 µL of 50 mM stock solution in DMF) or 120 µL DMF, the H_2O_2 solution (120 µL of 500 mM stock solution in buffer, 10 equivalents) and last, the hydrazide **7** solution (150 µL of 40 mM stock solution in buffer). The mixture was vortexed and poured directly on the rheometer plate. The rheometer plate was rotated slowly when it was lowered to ensure equal spreading of the sample. The *G'* and *G''* were measured while the gel formed on the plate. When no significant change in the moduli was observed anymore, the measurement was stopped. The frequency dependence of the gels was measured (Supplementary Fig. 2.5b): none of the gels showed frequency dependency in the frequency range that was used (0.01 – 100 Hz). A strain sweep was measured additionally; a strain higher than 100% could usually not be applied, as the gel gave too much resistance to the rheometer (Supplementary Fig. 2.5c). At increasing strain, the oscillatory stress increases linearly (Supplementary Fig. 2.5d). The rheology experiments where the chemical signal was added during the measurement, a gel volume of 1 mL was used. After mixing the stock solutions of polymer aldehyde **6**, hydrazide **7** and pro-aniline **1**, we poured the

mixture on the rheometer plate and allowed gelation while measuring rheology. After 20 minutes the measurement was stopped, the top rheometer plate was raised and H_2O_2 (50 µL, 2 M, 10 equivalents) was added (Fig. 2.3c). We also performed an experiment where we let the uncatalyzed gel form and added aniline **2** (50 µL, 200 mM) after 60 minutes (Supplementary Fig. 2.5e).

Inverted tube test supramolecular gel

Aldehyde **8**, hydrazide **7** and catalyst solutions were mixed in 4 mL vials and left over night. The next day, the vials were turned upside down. When the content of the vial would stay at the bottom of the vial for at least 5 minutes and was able to sustain its own weight, we assumed a gel had formed. Gelation conditions: 16 mM *cis,cis*-cyclohexane-1,3,5-tricarbohydrazide **7**, 96 mM 3,4-bis(2-(2-methoxyethoxy)ethoxy)benzaldehyde **8**, 10 mM catalyst, 100 mM H_2O_2, solvent 20% methanol in phosphate buffer (100 mM, pH 6.0). Sample size = 1 mL. The gelation took place over night at room temperature (Fig. 2.4a,b).

Synthesis

Synthesis of pro-aniline 1

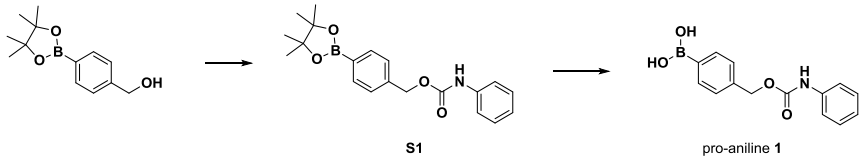

Scheme S2.1: Synthetic route to form pro-aniline **1**.

The 4-(4,4,5,5-tetramethyl-1,3,2-dioxaborolan-2-yl)benzyl phenylcarbamate (boronate ester derivative of pro-aniline **S1**) was synthesized using procedures described in the literature.[2, 3] The 4-(hydroxymethyl)phenylboronic acid pinacol ester was functionalized with triphosgene to form the chloroformate derivative. The boronate ester chloroformate was coupled to aniline **2** in the presence of a base ($NaHCO_3$). The boronic acid derivative pro-aniline **1** was obtained via elimination of pinacol using sodium periodate. Pro-aniline **1** can also be synthesized via the Curtius rearrangement of 4-formyl benzoic acid with diphenylphosphoryl azide and reaction with 4-(hydroxymethyl)phenylboronic acid pinacol ester and subsequent removal of the pinacol group.[1]

4-(4,4,5,5-Tetramethyl-1,3,2-dioxaborolan-2-yl)benzyl phenylcarbamate (S1)

First, K_2CO_3 (4.35 g, 31.5 mmol) was flame dried in a round-bottom flask. It was cooled in an ice bath and triphosgene (2.07 g, 7.0 mmol) in toluene was added. After stirring for 0.5 h at 0 °C, 4-(hydroxymethyl)phenylboronic acid pinacol ester (0.82 g, 3.5 mmol) in toluene was added. The mixture was allowed to reach ambient temperature and stirred overnight. After completion of the reaction, the reaction mixture was diluted with $CHCl_3$ and filtered through celite. The filtrate was washed with water, brine and dried over $MgSO_4$. Concentration under reduced pressure provided the chloroformate derivative which was used without further purification. To a stirred solution of aniline **2** (0.2 mL, 2.2 mmol) in THF at 0 °C $NaHCO_3$ was added (0.23 g, 2.7 mmol), followed by addition of the chloroformate derivative. After 1 h, the reaction mixture was allowed to reach ambient temperature, followed by addition of water to quench the reaction. The mixture was extracted with ethyl acetate (3x). The combined organic layers were dried over $MgSO_4$ and concentrated under reduced pressure to provide the desired compound (0.71 g, 90%). **^{1}H NMR** (Supplementary Figure 2.9) (400 MHz, $CDCl_3$): δ = 7.83 (d, *J* = 7.9 Hz, 2H, Ar-*H*), 7.40 (d, *J* = 7.9 Hz, 4H, Ar-*H*), 7.30 (t, *J* = 7.5 Hz, 2H, Ar-*H*), 7.06 (t, *J* = 7.4 Hz, 1H, Ar-*H*), 6.81 (s, 1H, -N*H*-), 5.21 (s, 2H, -CH_2-), 1.35 (s, 12H, CH_3). **^{13}C NMR** (Supplementary Figure 2.10) (100 MHz, $CDCl_3$): δ = 153.3 (-*C*OO-), 139.1 (C_{Ar}), 137.7 (C_{Ar}), 135.0 (C_{Ar}), 129.0 (C_{Ar}), 127.3 (C_{Ar}), 123.5 (C_{Ar}), 118.7 (C_{Ar}), 83.9 (-*C*Me_2-), 66.8 (-*C*H_2-), 24.8 (-*C*H_3). **Mp**: 113 – 115 °C. **MS** (GC/MS) m/z: 353 [M] (expected m/z = 353.2).

(4-(((Phenylcarbamoyl)oxy)methyl)phenyl)boronic acid (pro-aniline 1)

4-(4,4,5,5-tetramethyl-1,3,2-dioxaborolan-2-yl)benzyl phenylcarbamate **S1** (0.71 g, 2.0 mmol) was dissolved in acetone. $NaIO_4$ (3.42 g, 16.0 mmol) and ammonium acetate (1.23 g, 16.0 mmol) in water were added and the mixture was stirred overnight at room temperature. After completion of the reaction, the reaction mixture was acidified with 1M aqueous HCl and concentrated under reduced pressure. The crude substance was diluted with ethyl acetate and the mixture was washed with water, brine and dried over $MgSO_4$. Concentration under reduced pressure provided the desired compound as a light brown powder (0.45 g, 71%). **^{1}H NMR** (Supplementary Figure 2.11) (400 MHz, CD_3OD): δ = 7.75 (d, *J* = 7.3 Hz, 1H, Ar-*H*), 7.61 (d, *J* = 7.6 Hz, 1H, Ar-*H*), 7.42 – 7.34 (m, 4H, Ar-*H*), 7.26 – 7.21 (m, 2H, Ar-*H*), 7.01 – 6.97 (m, 1H, Ar-*H*), 5.17 (s, 2H, -CH_2-). **^{13}C NMR**

(Supplementary Figure 2.12) (100 MHz, CD_3OD): δ = 155.9 (-*C*OO-), 140.3 (C_{Ar}), 135.2 (C_{Ar}), 134.9 (C_{Ar}), 131.2 (C_{Ar}), 129.9 (C_{Ar}),128.1 (C_{Ar}), 128.0 (C_{Ar}), 124.2 (C_{Ar}), 120.0 (C_{Ar}), 67.5 (-*C*H_2-). **Mp**: 189 – 190 °C. **MS** (ESI Neg.) m/z: 270.0 [$(M-H)^-$] (expected m/z = 271.1).

Synthesis 4-hydroxy-N'-(4-nitrobenzylidene)butanehydrazide hydrazone (5)

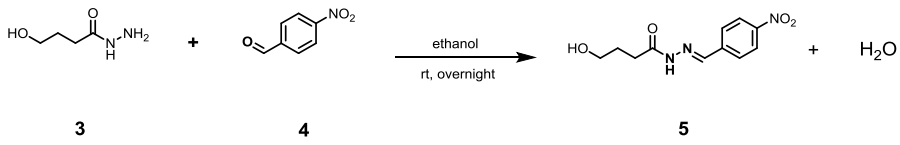

3 **4** **5**

Scheme S2.2: Synthetic route to form hydrazone **5**.

4-hydroxy-N'-(4-nitrobenzylidene)butanehydrazide was synthesized using a procedure reported in the literature.[4] 4-nitrobenzaldehyde **4** (129 mg, 0.855 mmol) and 4-hydroxybutyric acid hydrazide **3** (100 mg, 0.846 mmol) were dissolved in absolute ethanol (3 mL). A drop of acetic acid was added after which a yellow precipitate formed immediately and the reaction mixture was stirred at room temperature overnight. The precipitate was collected by filtration, washed with ethanol and dried in a vacuum oven at 40 °C to yield a fluffy yellow powder. Yield: 0.19 g, 0.75 mmol, 89%: a mixture of the *cis*- and *trans*-isomers. **^{1}H NMR** (Supplementary Figure 2.13) (400 MHz, DMSO-d6): δ = 11.62 (s, 1H, N-*H*), 11.48 (s, 1H, N-*H*), 8.23 (m, 2H, Ar-*H*), 8.04 (s, 1H, *C*-H) 7.89 (t, *J* = 8.9 Hz, 2H, Ar-*H*), 4.46 (m, 1H, O-*H*), 3.43 (m, 2H, -CH_2-), 2.67 (t, *J* = 7.5 Hz, 2H, -CH_2-), 2.27 (t, *J* = 7.5 Hz, 2H, -CH_2-), 1.71 (q, *J* = 6.6 Hz, 2H, -CH_2-). **^{13}C NMR** (Supplementary Figure 2.14) (100 MHz, DMSO-d6): δ = 175.2 (-*C*O-), 169.6 (*C*-NO_2), 148.0 (C_{Ar}), 141.3 (C_{Ar}), 140.4 (C_{Ar}), 128.2(C_{Ar}), 124.5(C_{Ar}), 60.7 (-*C*H_2-), 31.4(-*C*H_2-), 29.1(-*C*H_2-), 28.6(-*C*H_2-), 27.9(-*C*H_2-). **Mp**: 225-226 °C. **MS** (LC/MS, ESI neg.) m/z: 250 [$(M-H)^-$], (LC/MS, ESI pos.) m/z: 274 [$(M+Na)^+$], (expected m/z = 251.1).

Synthesis of PEG-aldehyde copolymer (6)

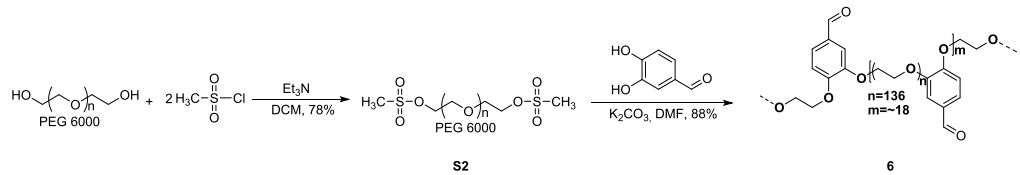

S2 **6**

Scheme S2.3: Synthetic route to form PEG-aldehyde copolymer **6**.

After functionalizing PEG-6000 with mesylchloride, the substitution reaction with 3,4-hydroxybenzaldehyde yielded the polydisperse PEG-aldehyde copolymer **6**.

Synthesis PEG-mesylate (S2)

PEG-6000 (molecular weight 5400 – 6600 g/mol) (50 g, 8.33 mmol) was dissolved in dry dichloromethane (300 mL), dry triethylamine (11.6 mL, 83.3 mmol) was added and the mixture was cooled on ice and brought under an argon atmosphere. Methanesulfonyl chloride (6.5 mL, 83.3 mmol) was added dropwise and the reaction mixture was stirred for 5 days at room temperature. Deionized water (200 mL) was added and the reaction was stirred vigorously. The water layer was extracted with dichloromethane (4 x 150 mL). The combined organic layers were dried over magnesium sulfate, filtered and most of the solvent was removed under reduced pressure. The concentrated reaction mixture was precipitated out in diethyl ether (1.5 L) using a dropping funnel. The obtained powder was again dissolved in dichloromethane and precipitated out in diethyl ether (1.5 L) to obtain the PEG mesylate **S2** as a white powder (39 g, 6.3 mmol, 78% yield, 86% modification). The modification rate was determined by comparing the NMR peak of the mesyl group on the PEG-mesylate **S2** with the bulk peak of the PEG. PEG-6000 has on average 136 PEG-units per molecule; each PEG-unit has 4 protons, so the integral of the bulk PEG should be 545. The resulting integral of the mesylate peak is 5.13 whereas for 100% modification, the mesylate groups should give an integral of 6, so the modification rate is 5.13/6 is 86%. **^{1}H NMR** (Supplementary Figure 2.15) (400 MHz, CD_3OD): δ = 4.30 – 3.36 (m, 543H, bulk PEG-*H*), 3.00 (s, 6H, -CH_3).

Synthesis of PEG-aldehyde copolymer (6)

The PEG-mesylate **S2** (25 g, 4.1 mmol) was dissolved in dry DMF (250 mL) and the solution was bubbled through with argon. Oven dried K_2CO_3 (4.5 g, 32.5 mmol) and 3,4-dihydroxybenzaldehyde (0.843 g, 6.09 mmol) were added. The reaction mixture was stirred at 130 °C for 5 days. The reaction mixture was cooled down to room temperature. Deionized water (100 mL) was added and the reaction mixture was stirred for 30 minutes. An aqueous HCl solution (100 mL, 1 M) was added and the reaction mixture was extracted with dichloromethane (4 x 100 mL) and washed with deionized water (150 mL). The mixture was dried over Na_2SO_4 and filtered. Most of the solvent was removed under reduced pressure and the concentrated product was precipitated out in diethyl ether (1.5 L). The obtained product was dissolved in dichloromethane (150 mL) and precipitated out again in diethyl ether (1.5 L) to yield a light brown fluffy powder (22 g, 88%). **^{1}H NMR** (Supplementary Figure 2.16) (400 MHz, CD_3OD): δ = 9.82 (s, 3H, C*H*O), 7.45 (s, 6H, Ar-*H*), 7.01 (d, J = 8.0 Hz, 3H, Ar-*H*), 4.25 – 3.44 (m, 2148H, bulk PEG-*H*). GPC: 10 µL of 10 mg/mL polymers solutions were injected and eluted with milliQ water at 1 mL/min and 40 °C for 30 minutes (Supplementary Figure 2.17). Weighted average $M_n = 97 \cdot 10^3$ g/mol, weighted average $M_w = 109 \cdot 10^3$ g/mol, weighted average $M_z = 121 \cdot 10^3$ g/mol, PDI over all peaks = 9. These observations were confirmed in a DOSY experiment where we found a diffusion constant of $0.07 \cdot 10^{-10}$ $m^2 \cdot s^{-1}$, which corresponds to polyethylene glycol with a molecular weight of $100 \cdot 10^3$ g/mol.

Synthesis of *cis*,*cis*-cyclohexane-1,3,5-tricarbohydrazide (7)

For a detailed procedure we refer to a protocol reported earlier in our group.[5] Trimesic acid (50.0 g, 238 mmol) and 10% palladium on activated charcoal (1.27 g, 11.9 mmol) were suspended in deionized water (300 mL) in a mechanically stirred Parr autoclave with a 1-liter volume. The autoclave was flushed with nitrogen gas. Hydrogen gas was added to the autoclave. The pressure was increased to 50 bar and the temperature to 150 °C. After complete conversion was confirmed by NMR, the reaction mixture was filtered through a sintered funnel, concentrated under reduced pressure and dried in a vacuum oven to obtain a mixture of *cis*,*cis*- and *cis*,*trans*-isomers of 1,3,5-cyclohexanetricarboxylic acid. The obtained acid (37.2 g, 172 mmol) was dissolved in methanol (1 L). *p*-Toluenesulfonic acid monohydrate (1.48 g, 8.61 mmol, 5 ml%) was added to the solution and the reaction was

stirred at 80 °C for 36 h. After NMR confirmed complete conversion of the starting compound, trimethylamine (10 mL) was added and the reaction mixture was concentrated under reduced pressure. Diethyl ether (1 L) was added and the reaction mixture was washed with water (1 L) and brine (1 L), dried with magnesium sulfate, filtered and concentrated under reduced pressure. Crystallization of the crude product in petroleum ether yielded the *cis*,*cis*-trimethylcyclohexane-1,3,5-tricarboxylate as colourless crystals. This carboxylate (40.2 g, 156 mmol) was dissolved in methanol (600 mL), hydrazine hydrate (141 mL, 64% in water) was added and the reaction mixture was stirred for 3 h at room temperature. The reaction mixture was concentrated under reduced pressure to obtain the *cis*,*cis*-cyclohexane-1,3,5-tricarbohydrazide **7** as a white powder (39.7 g, 154 mmol, 70% yield in two steps). **^{1}H NMR** (400 MHz, DMSO-d6) δ = 8.98 (s, 3H), 4.17 (bs, 6H), 2.11 (t, *J* = 11.8, 3H), 1.57 (d, *J* = 11.7, 3H), 1.45 (q, *J* = 12.6, 3H).

Synthesis of 3,4-bis(2-(2-methoxyethoxy)ethoxy)benzaldehyde (8)

For a detailed procedure we refer to a protocol reported earlier in our group.[5] Diethylene glycol monomethyl ether (100 g, 832 mmol) was dissolved in tetrahydrofuran (THF) (500 mL) and triethylamine (168 g, 1.66 mol, 231 mL) was added. The reaction mixture was cooled to 0 °C and a solution of *p*-toluenesulfonyl chloride (132 g, 694 mmol) in THF (200 mL) was added dropwise (60 min). The reaction mixture was stirred overnight at room temperature after which most of the solvent was removed under reduced pressure. The crude product was dissolved in dichloromethane (DCM) (800 mL), washed with deionized water (1 L) and extracted with DCM (3 x 500 mL). The combined organic layers were washed with brine (200 mL), dried over magnesium sulfate, filtered and concentrated under reduced pressure to obtain the tosylate product as a pale yellow oil that crystallized out as a light yellow solid (181 g, 660 mmol, 95%). The 2-(2-methoxyethoxy)ethyl tosylate (40.0 g, 146 mmol) was dissolved in dry DMF (200 mL), oven dried potassium carbonate (40.3 g, 292 mmol) was added and the reaction was brought under an argon atmosphere. 3,4-Hydroxybenzaldehyde (9.16 g, 66.3 mmol) was added and the reaction was stirred overnight at 90 °C under an argon atmosphere. The reaction mixture was cooled to room temperature, 1 M HCl (200 mL) was added and the mixture was extracted with ethyl acetate (4 x 250 mL). The combined organic layers were washed with a saturated sodium bicarbonate solution (5 x 200 mL) and brine (5 x 200 mL), dried over magnesium sulfate,

filtered and concentrated under reduced pressure to yield the product as a yellow oil (21.3 g, 62.1 mmol, 94%). **^{1}H NMR** (400 MHz, $CDCl_3$) δ = 9.82 (s, 1H), 7.42 (m, 2H), 6.98 (d, *J* = 11.6, 1H), 4.19–4.27 (m, 4H), 3.89 (t, *J* = 6.8, 2H), 3.88 (t, *J* = 6.4, 2H), 3.70–3.75 (m, 4H), 3.53–3.58 (m, 4H), 3.37 (s, 6H).

Determination pseudo-first-order rates hydrazone formation 5

Pseudo-first-order conditions were obtained by using a 5 times excess of aldehyde **4** (0.5 mM) with respect to hydrazide **3** (0.1 mM) during the reactions.

The integrated rate law for first-order reactions is:

$$[P] = [\mathrm{P}]_0 \cdot e^{k_1 \cdot t} \quad \text{(eq. 2.1)}$$

$$\ln[P] = \ln[P]_0 + k_1 \cdot t \quad \text{(eq. 2.2)}$$

$$[P] = \frac{A}{\varepsilon_{350} \cdot l} \quad \text{(eq. 2.3)}$$

In which $[P]$ is the concentration of hydrazone **5**, determined by dividing the absorbance measured at 350 nm during the reaction with the extinction coefficient of hydrazone **5** at 350 nm. k_1 is the first-order rate constant (s^{-1}). A is the absorbance at 350 nm measured during the reaction. ε_{350} is the extinction coefficient of hydrazone product **5** at 350 nm. Plotting ln[P] versus the time (s) gives the first order rate constant. The graphs were fitted using linear regression in Origin Pro 2015. For the uncatalyzed reaction and the reaction with pro-aniline **1**, the first 10 h of the reaction were taken to determine the reaction rate constants. For the reaction in the presence of activated pro-aniline **1** and for the reaction catalysed by aniline **2**, the first 15 minutes were used to determine the reaction rate constant (Supplementary Fig. 2.8).

UV/vis hydrazone formation blank experiments

After activation of pro-aniline **1**, the reaction rate of hydrazone formation was lower than when using native aniline **2**. In an attempt to explain this loss of catalytic activity we investigated the influence of H_2O_2 and of boric acid to aniline **2**, but could not find any loss in catalytic activity (Supplementary Fig. 2.3c, d). Reaction conditions: 0.1 mM hydrazide **3**, 0.5 mM aldehyde **4**, 0.5 mM boric acid, 2.5 mM H_2O_2, 0.5 mM aniline **2** in 20% DMF in phosphate buffer (100 mM, pH 7.4). Even though we confirmed complete conversion of pro-aniline **1** after addition of more than 1 equivalent of H_2O_2 and we detected aniline **2**

after an overnight hydrazone reaction in the presence of pro-aniline **1** and H_2O_2 (Supplementary Fig. 2.4), it might be the case that some aniline **2** is lost or degraded in the process. Furthermore, the pH was monitored for the reaction with pro-aniline **1** (0.5 mM) and H_2O_2 (2.5 mM), every 10 minutes for the first 2 h and once after 18 h. No pH change was observed during the reaction: the pH remained stable at a pH of 8.0. The solvent system itself, 20% DMF in phosphate buffer (100 mM, pH 7.4) gives a pH of 8.0, which indicates that the phosphate buffer concentration is sufficient to buffer the reaction mixtures.

Supplementary References

1. Nuñez, S. A., Yeung, K., Fox, N. S., Phillips, S. T. A structurally simple self-immolative reagent that provides three distinct, simultaneous responses per detection event. *J. Org. Chem.* **76,** 10099-10113 (2011).
2. Wipf, P., Maciejewski, J. P. Titanocene(III)-catalyzed formation of indolines and azaindolines. *Org. Lett.* **10,** 4383-4386 (2008).
3. Chung, C., Srikun, D., Lim, C. S., Chang, C. J., Cho, B. R. A two-photon fluorescent probe for ratiometric imaging of hydrogen peroxide in live tissue. *Chem. Commun.* **47,** 9618-9620 (2011).
4. Popiołek, Ł., Biernasiuk, A., Malm, A. Synthesis and antimicrobial activity of new 1,3-thiazolidin-4-one derivatives obtained from carboxylic acid hydrazides, *Phosphorus, Sulfur, Silicon Relat. Elem.* **190,** 251-260 (2015).
5. Poolman, J. M. *et al.* Variable gelation time and stiffness of low-molecular-weight hydrogels through catalytic control over self-assembly. *Nat. Protoc.* **9,** 977-988 (2014).

Chapter 3
Selective activation of organocatalysts by specific signals

Reminiscent of signal transduction in biological systems, artificial catalysts whose activity can be controlled by physical or chemical signals would be of high interest in the design of chemical systems that can respond to their environment. Self-immolative chemistry offers a generic method for the development of catalysts that can be activated by different signals. To demonstrate the versatility of that concept, we synthesized organocatalysts that can be activated by three different signals and that can be used to control two different reactions. In this way the organocatalyst proline is designed as a pro-catalyst that is activated either by the chemical signal H_2O_2, by light or by the enzyme penicillin acylase. The pro-catalysts were used to exert temporal control over the rate of an aldol reaction and a Michael reaction.

This chapter is published as:

Maity, C.,[#] Trausel, F.,[#] Eelkema, R. Selective activation of organocatalysts by specific signals, *Chem. Sci.*, **9**, 5999-6005 (2018).

[#]Equal contributions.

3.1 Introduction

In nature, cells communicate and respond to signals from their environment by changing the activity of enzymes.[1,2] Artificial catalysts that can be activated by different signals are scarce and would be of high interest to design systems that can respond to the environment. Some catalysts that can be activated by signals have been reported.[3] Many of these catalysts use light as a signal.[4-7] Only a small number of catalysts that can be activated by chemical signals are found in the literature.[3,8–10] Many of these catalysts suffer from complex syntheses and a lack of generic design. A versatile tool to design catalysts that can respond to different signals is self-immolative chemistry.[11–13] A self-immolative molecule contains a signal-labile functional group. When this group reacts with the signal, the molecule fragments and releases a molecule of interest, in our case a catalyst. Recently we reported an organocatalyst that can be activated by a chemical signal and that controls the formation of a polymer or a self-assembled material.[14]

Here we report a general strategy to design organocatalysts that can be selectively activated in response to a specific signal. To demonstrate the versatility of the design we report how to render an organocatalyst responsive to three different signals and that it can be used to control the rates of two different reactions. Specifically, we synthesized three different protected proline catalysts that can be activated by three different signals (Fig. 3.1): PP-**1** is activated by the chemical signal H_2O_2, PP-**2** is activated by light and PP-**3** is activated via catalytic hydrolysis by the enzyme Penicillin Acylase (PA). When the pro-prolines are activated by the relevant signal, the catalyst proline P-**4** is released. In addition, we used the pro-prolines to catalyse an aldol reaction between a ketone and an aldehyde and a Michael reaction between an nitro-olefin and an aliphatic aldehyde. The strategy constitutes a versatile method for the development of a wide range of pro-catalysts to control a large variety of reactions.

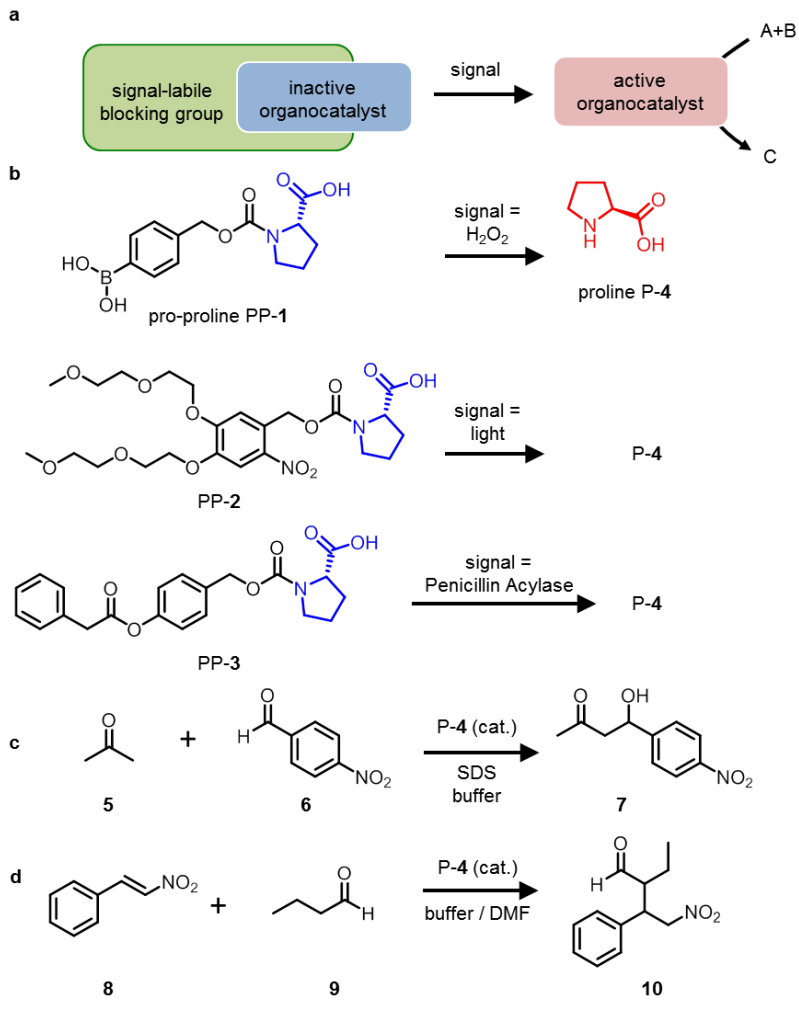

Figure 3.1: A generic design for a pro-catalyst that can be activated by a signal to catalyse a reaction. (**a**) Schematic representation of the protected organocatalyst that is activated by the signal and then catalyses a reaction. (**b**) The pro-proline PP-**1** is activated by the chemical signal H_2O_2 and releases the organocatalyst proline P-**4**. PP-**2** is activated by light and releases P-**4**. PP-**3** is activated by the enzyme Penicillin Acylase (PA) and releases P-**4**. (**c**) The aldol reaction between acetone **5** and an 4-nitrobenzaldehyde **6** is catalysed by P-**4**. (**d**) The Michael reaction between *trans*-β-nitrostyrene **8** and butanal **9** is catalysed by P-**4**.

3.2 Results and discussion

Catalyst design

The general strategy to design an organocatalyst that can be activated by a signal to control a catalytic target reaction, is based on the following considerations (Fig. 3.1a):

1) The catalytic centre of the organocatalyst should allow protection with a self-immolative moiety: organocatalysts which have a primary or secondary amine or an alcohol as a catalytic centre are promising candidates.
2) It should be possible to activate the catalyst in less than 30 minutes (depending on the timescale of the reaction) under the same conditions as are required for the catalytic target reaction. To enable the facile release of the catalyst it may be important to include a carbamate or carbonate group.[11]
3) All reagents, the catalyst and the pro-catalyst should be soluble in the same solvent and the solvent should be compatible with the signal and the self-immolative reaction.
4) The signal that activates the catalyst should not lead to a different outcome of the catalytic target reaction.
5) The pro-catalyst should be stable under the conditions used in the catalytic target reaction and should not release the catalyst without being triggered by a specific signal.
6) The catalytic target reaction should be susceptible to catalysis (show at least a 2-fold increase in reaction rate upon addition or activation of the catalyst) under the operating conditions.

Based on these guidelines we recently designed an organocatalyst that can be activated by a chemical signal and that controls the formation of a polymer or supramolecular network material.[14] There, hydrazone bond formation[15-17] was catalysed by a signal-responsive aniline pro-catalyst.

In the current work, we want to demonstrate the versatility of the design. We chose proline as an organocatalyst for two reasons. Firstly, proline is a simple organocatalyst with a catalytic centre that can easily be modified. Secondly, proline is a nucleophilic catalyst used for many different reactions.[18] We decided to protect proline with three different self-

immolative groups that react to three different signals (Fig. 3.1b). PP-**1** is protected with a boronic acid self-immolative group that is oxidatively cleaved by hydrogen peroxide. Hydrogen peroxide is a relevant disease related biomarker as it is generated during oxidative stress by the oxidation of enzyme substrates such as glucose.[19–21] PP-**2** contains a light-sensitive group that is cleaved upon irradiation. To extend the scope of our design to biological systems we designed PP-**3**: the hydrolysis of the ester group in PP-**3** to induce the self-immolative reaction is catalysed by the enzyme Penicillin Acylase (PA).

Synthesis of the catalysts

The pro-prolines were synthesized via chloroformate intermediates in two steps (Fig. 3.2). The total yield over all steps for PP-**1** is 74%, for PP-**2** it is 45% and PP-**3** it is 48% (see SI for more information).

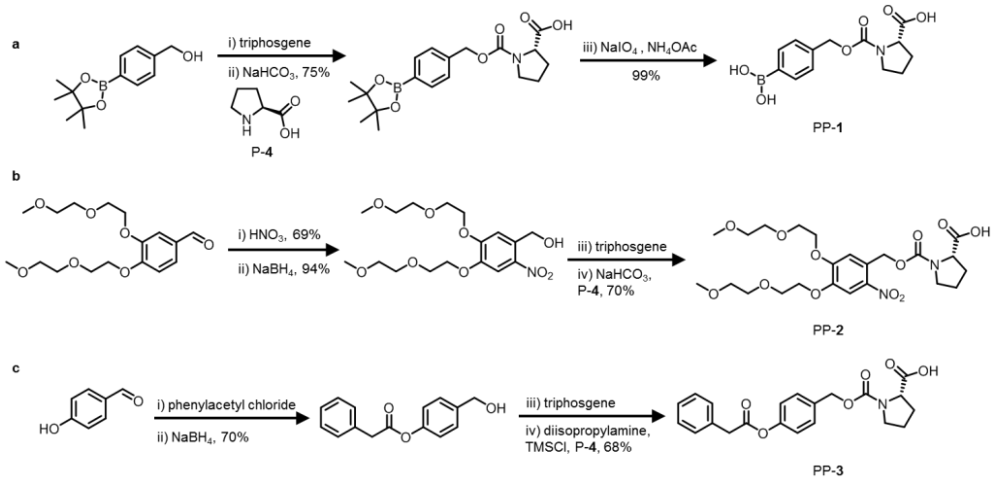

Figure 3.2: Synthetic route to form pro-prolines PP-**1**, PP-**2** and PP-**3**. (**a**) Synthesis of PP-**1**, reaction conditions: i) Na_2CO_3, triphosgene, toluene, 0 °C – room temperature, 6 h. ii) $NaHCO_3$, proline P-**4**, water , 0 °C – room temperature, overnight, iii) $NaIO_4$, NH_4OAc, water / acetone (2:1 v/v). (**b**) Synthesis of PP-**2**, reaction conditions: i) HNO_3 (70% in water), 0 – 20 °C, 2 h, ii) $NaBH_4$, methanol, 1 h, room temperature, iii) K_2CO_3, triphosgene, toluene, 0 °C – room temperature, 6 h, iv) $NaHCO_3$, P-**4**, water, 0 °C – room temperature, overnight. (**c**) Synthesis of PP-**3**, reaction conditions: i) phenylacetyl chloride, triethylamine, tetrahydrofuran, 0 °C – room temperature, overnight, ii) $NaBH_4$, 2-propanol, 1 h, room temperature, iii) K_2CO_3, triphosgene, toluene, 0 °C – room temperature, 6 h, iv) trimethylsilylchloride (TMSCl), diisopropylamine, dichloromethane, 0 °C – room temperature, 4 h.

By incorporating a carbamate group in the design we took into account design guideline 2. The synthetic route is generic: it enables the protection of a large range of organocatalysts and the use of a variety of self-immolative protecting groups to allow response to different signals.

Activation of the catalysts

We tested whether the pro-prolines would release proline when the relevant signal was applied and whether this conversion was complete (see SI for more information). To PP-**1** (50 mg) in methanol (2 mL) we added H_2O_2 (1 mL, 30%). After 10 min, thin layer chromatography showed complete conversion of PP-**1**. The reaction mixture was concentrated under reduced pressure, diluted with ethyl acetate and washed with sodium sulfite (sat., aq). The obtained solution was concentrated under reduced pressure and analysed by ^{1}H NMR spectroscopy and mass spectrometry to confirm complete conversion of PP-**1** and the formation of proline P-**4**. When we followed the activation of PP-**1** (10 mM in 20% dimethylformamide-d_7 in 10 mM sodium phosphate buffer of pH 8.0) in NMR, we found that 10 equivalents of H_2O_2 are sufficient to convert PP-**1** completely into P-**4** in within 10 minutes. We noticed that although the boronic acid group is efficiently removed in up to 80% organic solvent, for the release of proline, 70 - 80% buffer is necessary to decrease the activation time (from 2 hours in 50% buffer to 10 minutes in 80% buffer). To investigate the activation of PP-**2** we irradiated PP-**2** (50 mg) in methanol (2 mL) in a 4 mL vial with light for 30 minutes using a Nikon Intensilight C-HGFI lamp (130 W mercury lamp with 100% light intensity, 320 – 600 nm). The activation of PP-**2** was analysed by UV/vis spectroscopy, ^{1}H-NMR spectroscopy and mass spectrometry and confirmed complete conversion and release of P-**4**. To activate PP-**3** we added a solution of PA (5.5 mg, 98U) in sodium phosphate buffer (100 mM, pH 7.4) to a solution of PP-**3** (0.5 mg) in acetone (10 μL). After stirring for 10 minutes we concentrated the reaction mixture, added chloroform and filtered. The solution was concentrated under reduced pressure and analysed by ^{1}H NMR and mass spectroscopy and confirmed complete conversion of PP-**3** and release of P-**4**. In short, all pro-prolines were converted completely into proline within 30 minutes, thereby keeping with guideline 2. The design of the pro-catalysts thus enables efficient signal triggered release of the catalyst.

Using the pro-catalysts to control reaction kinetics

We investigated whether we could use the pro-prolines to control reaction kinetics. We focussed on two reactions that obey guidelines 3-6 reasonably well: an aldol reaction between a ketone and an aldehyde (Fig. 3.1c) and a Michael reaction between an nitro-olefin and an aldehyde (Fig. 3.1d).

Control over the aldol reaction

We chose the proline-catalysed aldol reaction between acetone **5** and 4-nitrobenzaldehyde **6**. For the activation of both PP-**1** and PP-**3** an aqueous environment is necessary. As reported in the literature, proline catalysis of aldol reactions is typically severely hindered by water. Still, in buffered media with the help of the surfactant sodium dodecyl sulfate (SDS), the reaction is accelerated by proline P-**4**.[22] Proline acts as a nucleophilic catalyst by forming an enamine intermediate with acetone.[23] The aldol reaction was followed using ^{1}H-NMR spectroscopy, reaction conditions: 4-nitrobenzaldehyde **6** (10 mM), PP-**1** (2 mM) in 20% acetone **5** in sodium phosphate buffer (100 mM, pH 7.4) with 10% D_2O and SDS (1 mM) as an additive[22] (Fig. 3.3 and Table 3.1).

Without catalyst the aldol product **7** is still formed, it reaches 65% conversion in 48 h. The native catalyst P-**4** (2 mM) induces a 4.2-fold increase in reaction rate and reaches 99% conversion in 48 h: this indicates that the aldol reaction is indeed catalysed by P-**4**. The reactions in the presence of unactivated PP-**1**, PP-**2** and PP-**3** (2 mM) show the same reaction rate as the uncatalysed reaction and reach a 65% conversion as well after 48 h. Without activation the pro-catalysts thus do not show any catalytic activity. Addition of H_2O_2 (2 mM, 1 equivalent to PP-**1**) to the reaction with PP-**1** (2 mM) induces a 2.6-fold increase in reaction rate and the reaction reaches 93% conversion in 48 h. This indicates an efficient activation of the catalyst. H_2O_2 alone does not have any influence on the reaction rate. It is important not to use an excess of H_2O_2 with respect to PP-**1** to prevent oxidation of nitro-benzaldehyde (see supplementary information). Irradiating the reaction mixture containing PP-**2** (2 mM) leads to a 2.3-fold increase of reaction rate and a conversion of 93% after 48h, another demonstration of efficient catalyst activation. Light-irradiation in the absence of PP-**2** does not have any influence on the reaction rate. Addition of PA (5.5 mg, 98 U) to a reaction mixture containing PP-**3** (2 mM) leads to a 2.7-fold increase in reaction rate and a conversion of 97% after 48h. These results indicate efficient activation

of pro-catalysts when the relevant signal is applied. Additionally, we applied 'wrong' signals to check whether each pro-catalyst is selectively activated by a specific signal. Irradiation of the reaction mixture with PP-**1** or PP-**3** did not result in any increase in reaction rate. To the reaction mixture with PP-**2** we added H_2O_2 as a 'wrong' signal, and again, we did not observe an increase in reaction rate. These results demonstrate that the pro-catalysts are specific in their response, keeping with guideline 5. Altogether, the pro-catalyst-aldol system adheres to the guidelines reasonably well, however, because of the relatively large background reaction rate for aldol reactions,[24] response to catalyst activation is only modest.

Importantly, addition of the signal at any given time during the reaction should lead to a change in reaction rate at that particular moment. To investigate this, we followed the reaction with PP-**1** (2 mM) and added H_2O_2 (2 mM) after 22 hours (Fig. 3.3). The reaction rate increased 1.6-fold. This result demonstrates an autonomous response to a chemical change in the environment. The increase in reaction rate is lower than when the signal was added at the beginning of the reaction: this can be explained because a large part of the 4-nitrobenzaldehyde **6** has already been consumed and lower concentrations of reagents that are part of the rate equation lead to lower reaction rates. Similarly, when we followed the reaction with PP-**2** (2 mM) and irradiated with light after 22 h we found a 1.5-fold increase in reaction rate. Furthermore, addition of PA (5.5 mg, 98U) after 22 h to the reaction containing PP-**3** led to a 1.4-fold increase in reaction rate. The pro-catalysts thus allow temporal response to signals from the environment.

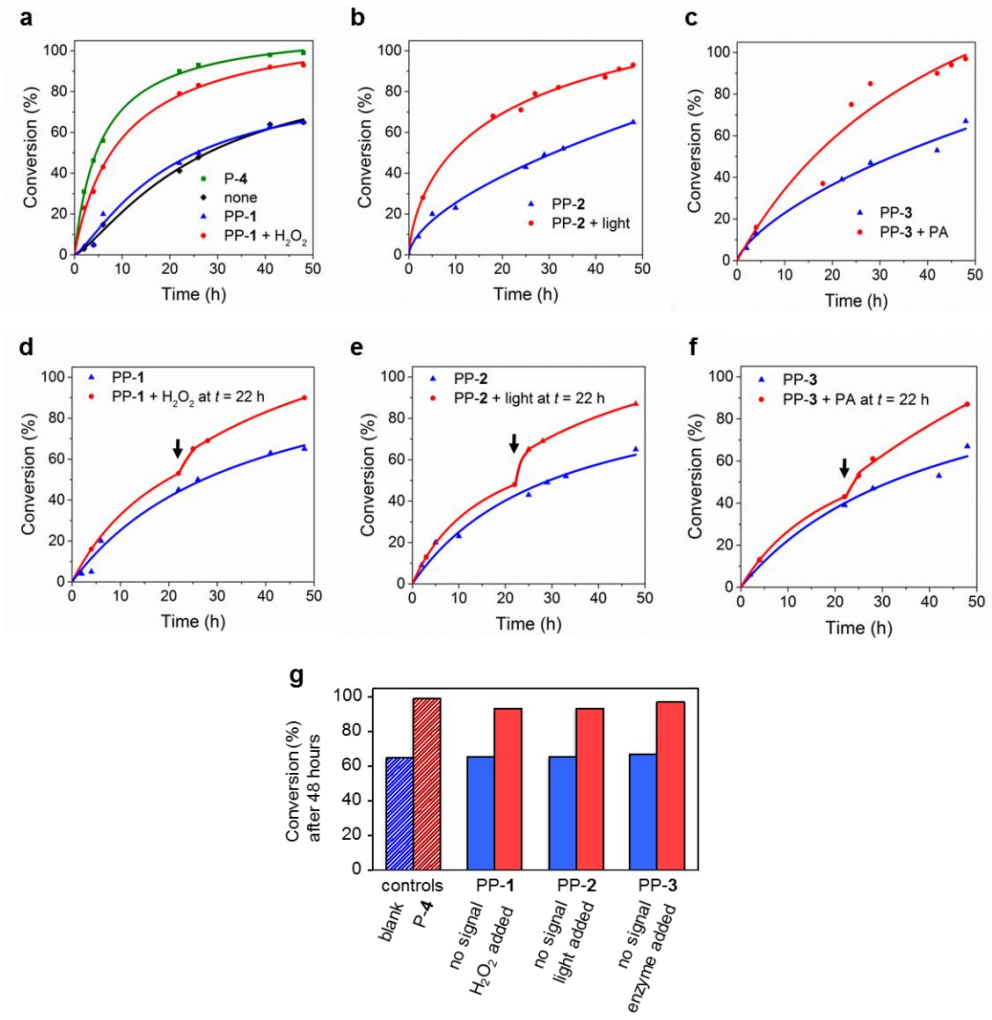

Figure 3.3: Kinetic analysis of the aldol reaction between 4-nitrobenzaldehyde **6** and acetone **5**. Conditions: 10 mM 4-nitrobenzaldehyde **6**, 20 volume % acetone **5**, 2 mM (20 mol%) PP-**1**, 2 mM (1 eq.) H_2O_2 in sodium phosphate buffer (100 mM, pH 7.4) with 10 v% D_2O and 1 mM sodium dodecyl sulfate (SDS). (**a**) Conversion of the aldol product followed with NMR spectroscopy in the presence of P-**4** (green), without catalyst (black), PP-**1** without activation (blue), PP-**1** and H_2O_2 (red). (**b**) Conversion of the aldol reaction in the presence of PP-**2** without activation (blue) and in the presence of PP-2 after irradiation with light (red). (**c**) Conversion of the aldol reaction in the presence of PP-**3** without activation (blue) and in the presence of PP-**3** after addition of penicillin acylase (PA) (red). (**d**) Conversion of the aldol reaction in the presence of PP-**1** (blue), the signal H_2O_2 was added after 22 h (red). (**e**) Conversion of the aldol reaction in the presence of PP-**2** (blue), after 22 h, the reaction mixture was irradiated with light (red). (**f**) Aldol reaction in the presence of PP-**3** (blue), after 22 h, penicillin acylase (PA) was added (red). (**g**) Conversion to the aldol product after 48 hours, in the absence or presence of the appropriate signal. In (d–f) the arrow indicates the moment of signal addition.

Table 3.1: Second order reaction rate constants for the aldol reaction between 4-nitrobenzaldehyde **6** and acetone **5**. Reaction conditions: 4-nitrobenzaldehyde **6** (10 mM), proline (2 mM) or pro-proline (2 mM) in 20% acetone **5** in sodium phosphate buffer (100 mM, pH 7.4) with 10% D_2O and sodium dodecyl sulfate (1 mM) as an additive.k_2 is the second order reaction rate constant, $k_{rel} = k_{cat} / k_{uncatalysed}$.

Catalyst system	k_2 (M^{-1} s^{-1})	k_{rel}
None	2.4×10^{-6}	1.0
P-**4**	1.0×10^{-5}	4.2
PP-**1** + H_2O_2	6.2×10^{-6}	2.6
PP-**1**	2.4×10^{-6}	1.0
PP-**1** + light	2.4×10^{-6}	1.0
PP-**2** + light	5.5×10^{-6}	2.3
PP-**2**	2.3×10^{-6}	1.0
PP-**2** + H_2O_2	2.4×10^{-6}	1.0
PP-**3** + PA	6.6×10^{-6}	2.7
PP-**3**	2.2×10^{-6}	0.9
PP-**3** + light	2.3×10^{-6}	0.9

Control over the Michael reaction

To demonstrate the versatility of the responsive catalyst system, we also used PP-1 to control the rate of a Michael reaction between trans-β-nitrostyrene **8** and butanal **9** (Fig. 3.4). Proline acts as a nucleophilic catalyst in the Michael reaction by forming an enamine intermediate with the aldehyde.[25, 26] Even though the reaction is commonly performed in organic solvents, the organocatalyzed Michael reaction is known to proceed in water.[27] Reaction conditions: 10 mM *trans*-β-nitrostyrene **8**, 100 mM butanal **9**, 10 mM P-**4** or PP-**1**, 100 mM (10 eq) H_2O_2 in phosphate buffer (10 mM, pH 8.0) + dimethyl formamide-d_7 (DMF-d_7). DMF-d_7 (20% v/v) was used to ensure solubility of the product. An advantage of the Michael reaction is the complete lack of back ground reaction: without catalyst the reaction does not show any detectable conversion. Addition of the native catalyst P-**4** (10 mM) increases the reaction rate constant to 7.7×10^{-3} M^{-1} s^{-1}. This indicates that the Michael reaction is catalysed by P-**4**: in fact for the reaction to proceed on a reasonable timescale, it requires a catalyst. The reaction in the presence of PP-**1** (10 mM) without the chemical signal does not show any conversion. The reaction with PP-**1** (10 mM) and H_2O_2 (10 equivalents, 100 mM) proceeds with a rate constant of 2.0×10^{-4} M^{-1} s^{-1}. These results indicate that the catalyst is efficiently activated. The rate for the reaction with PP-**1** and

H_2O_2 is considerably lower than the rate for the reaction with P-**4**. This decrease in reaction rate can partially be explained by the use of H_2O_2: the Michael reaction in the presence of P-**4** and H_2O_2 has a lower rate constant (9.3 × 10-4 M^{-1} s^{-1}) than the reaction with only P-**4** (7.7 × 10^{-3} M^{-1} s^{-1}). Analysis of the reaction mixture by NMR spectroscopy reveals that the *trans*-β-nitrostyrene **8** degrades slowly in the presence of H_2O_2. This negative influence of the signal H_2O_2 on the reaction is in conflict with guideline 3. The rate constant for the Michael reaction in the presence of PP-**1** and H_2O_2 is even lower: because we confirmed with NMR measurements that PP-**1** is completely converted during the reaction, a reason for the decrease in reaction rate might be that more *trans*-β-nitrostyrene **8** is degraded in the time (10 min) that it takes to activate the PP-**1**. Importantly, because of the complete lack of background reaction we should be able to use our responsive catalyst to switch the system from 'off' (no conversion) to 'on' (the reaction proceeds). Indeed, the reaction (or lack thereof) was followed for 1 hour, after which H_2O_2 (100 mM) was added: this resulted in an immediate response and again a reaction rate constant of 2.0 × 10^{-4} M^{-1} s^{-1}. All in all, the pro-catalyst can be used to design a system that can autonomously switch on when a specific chemical signal is detected (Table 2).

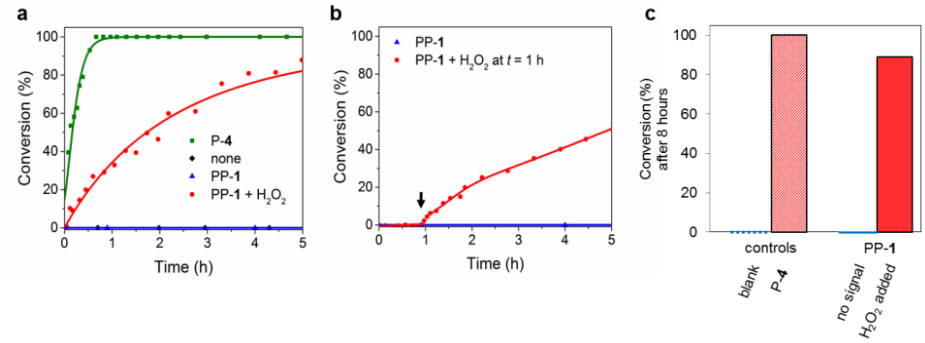

Figure 3.4: Kinetic analysis of the Michael reaction between *trans*-β-nitrostyrene **8** and butanal **9**. Reaction conditions: 10 mM *trans*-β-nitrostyrene **8**, 100 mM butanal **9**, 10mM PP-1, 100 mM (10 eq.) H_2O_2 in phosphate buffer (10 mM, pH 8.0) + dimethyl formamide-d_7 (DMF-d_7). (**a**) Conversion to the Michael product **10** followed with NMR spectroscopy, reaction with PP-**4** (10 mM, blue), without catalyst (black, overlapping with blue), with P-**4** (10 mM, green) and with PP-**1** (10 mM) and H_2O_2 (100 mM, red). (**b**) Conversion to the Michael product **10** followed with ^{1}H-NMR spectroscopy, reaction with PP-**1** (10 mM, blue) and the reaction with PP-**1** (10 mM) where H_2O_2 (100 mM) was added after 1 hour (red). The arrow indicates the moment of signal addition. (**c**) Conversion (%) after 8 hours of reaction time, without signal (blue), with signal (red). With P-**4** the reaction reaches >99% conversion in 8 h and with PP-**1** and the H_2O_2 the reaction reaches 89% conversion. Without catalyst or signal, there is no conversion.

Table 3.2: Second order reaction rate constants for the Michael reaction between *trans*-β-nitrostyrene **8** and butanal **9**. Reaction conditions: 10 mM *trans*-β-nitrostyrene **8**, 100 mM butanal **9**, 10 mM PP-**1**, 100 mM (10 eq) H_2O_2 in phosphate buffer (10 mM, pH 8.0) + dimethyl formamide-d_7 (DMF-d_7). k_2 is the second order reaction rate constant.

Catalyst system	k_2 (M^{-1} s^{-1})
None	0
PP-**1**	0
H_2O_2	0
P-**4**	7.7×10^{-3}
PP-**1** + H_2O_2	2.0×10^{-4}
P-**4** + H_2O_2	9.3×10^{-4}

3.3 Conclusions

In summary, we demonstrate a versatile design for the development of responsive catalysts that can be selectively activated by various signals. The generic design allows for a straightforward synthesis for the blocking of catalysts with a variety of self-immolative groups. The self-immolative design enables efficient activation of the pro-catalysts with a reasonable amount of signal. We demonstrated an application of our catalyst design by synthesizing three examples of blocked proline catalysts, of which one can be activated by H_2O_2 (PP-**1**), the second by light (PP-**2**) and the third by the enzyme penicillin acylase (PP-**3**). PP-**1**, PP-**2** and PP-**3** were used to control the rate of an aldol reaction: activation of the pro-catalyst showed the same increase in rate as when the native catalyst was added. The pro-catalysts could also be activated efficiently during the reaction, allowing temporal control over the reaction rate. The versatility of the pro-catalyst system was made more apparent as we additionally used PP-**1** to control a Michael reaction. This reaction does not show any conversion without active catalyst. Activation of PP-**1** enables the reaction to proceed, even though the reaction rate is lower than when the native proline catalyst is used. The reaction can be initialized at any moment in a mixture of the starting materials for the Michael reaction with PP-**1** and leads to an immediate response in reaction rate. The pro-catalysts can thus autonomously respond to signals from the environment. A next step in responsive catalysis would be autonomous or controlled deactivation of the activated catalyst, to allow for transient signal amplification. We are currently working on a system

to gain reversible control over catalyst activity. We envision that our design for organocatalysts that can be selectively activated by specific signals may be applied to create systems and materials that can respond to their environment, as the next step towards communication between artificial chemical systems.

3.4 References

1. Whitehead, E. The regulation of enzyme activity and allosteric transition. *Prog. Biophys. Mol. Biol.* **21**, 321-397 (1970).
2. Traut, T. *Allosteric regulatory enzymes*. Springer (2008).
3. Blanco, V., Leigh, D. A., Marcos, V. Artificial switchable catalysts. *Chem. Soc. Rev.* **44**, 5341-5370 (2015).
4. Stoll, R. S., Hecht, S. Artificial light-gated catalyst systems. *Angew. Chem. Int. Ed. Engl.* **49**, 5054-5075 (2010).
5. Neri, S., Garcia Martin, S., Pezzato, C., Prins, L. J. Photoswitchable catalysis by a nanozyme mediated by a light-sensitive cofactor. *J. Am. Chem. Soc.* **139**, 1794-1797 (2017).
6. Zhao, H.*, et al.* Reversible trapping and reaction acceleration within dynamically self-assembling nanoflasks. *Nature Nanotechnology* **11**, 82 (2015).
7. Maity, C., Hendriksen, W. E., van Esch, J. H., Eelkema, R. Spatial structuring of a supramolecular hydrogel by using a visible-light triggered catalyst. *Angew. Chem. Int. Ed. Engl.* **54**, 998-1001 (2015).
8. Gianneschi, N. C., Bertin, P. A., Nguyen, S. T., Mirkin, C. A., Zakharov, L. N., Rheingold, A. L. A supramolecular approach to an allosteric catalyst. *J. Am. Chem. Soc.* **125**, 10508-10509 (2003).
9. Kovbasyuk, L., Krämer, R. Allosteric supramolecular receptors and catalysts. *Chem. Rev.* **104**, 3161-3188 (2004).
10. Mendez-Arroyo, J., Barroso-Flores, J., Lifschitz, A. M., Sarjeant, A. A., Stern, C. L., Mirkin, C. A. A multi-state, allosterically-regulated molecular receptor with switchable selectivity. *J. Am. Chem. Soc.* **136**, 10340-10348 (2014).
11. Alouane, A., Labruère, R., Le Saux, T., Schmidt, F., Jullien, L. Self-immolative spacers: Kinetic aspects, structure–property relationships, and applications. *Angew. Chem. Int. Ed. Engl.* **54**, 7492-7509 (2015).
12. Peterson, G. I., Larsen, M. B., Boydston, A. J. Controlled depolymerization: Stimuli-responsive self-immolative polymers. *Macromolecules* **45**, 7317-7328 (2012).
13. Roth, M. E., Green, O., Gnaim, S., Shabat, D. Dendritic, oligomeric, and polymeric self-immolative molecular amplification. *Chem Rev* **116**, 1309-1352 (2016).
14. Trausel, F., Maity, C., Poolman, J. M., Kouwenberg, D. S. J., Versluis, F., van Esch, J. H., Eelkema, R. Chemical signal activation of an organocatalyst enables control over soft material formation. *Nat. Commun.* **8**, 879 (2017).

15. Kölmel, D. K., Kool, E. T. Oximes and hydrazones in bioconjugation: Mechanism and catalysis. *Chem. Rev.* **117**, 10358-10376 (2017).
16. Trausel, F., Fan, B., van Rossum, S. A. P., van Esch, J. H., Eelkema, R. Aniline catalysed hydrazone formation reactions show a large variation in reaction rates and catalytic effects. *Adv. Synth. Catal.*, (2018).
17. Trausel, F., Versluis, F., Maity, C., Poolman, J. M., Lovrak, M., van Esch, J. H., Eelkema, R. Catalysis of supramolecular hydrogelation. *Acc. Chem. Res.* **49**, 1440-1447 (2016).
18. List, B. Proline-catalyzed asymmetric reactions. *Tetrahedron* **58**, 5573-5590 (2002).
19. Ikeda, M., Tanida, T., Yoshii, T., Kurotani, K., Onogi, S., Urayama, K., Hamachi, I. Installing logic-gate responses to a variety of biological substances in supramolecular hydrogel–enzyme hybrids. *Nat. Chem.* **6**, 511-518 (2014).
20. Alberti, K. G. M. M., Zimmet, P. Z. Definition, diagnosis and classification of diabetes mellitus and its complications. Part 1: Diagnosis and classification of diabetes mellitus. Provisional report of a who consultation. *Diabet. Med.* **15**, 539-553 (1998).
21. Sreekumar, A.*, et al.* Metabolomic profiles delineate potential role for sarcosine in prostate cancer progression. *Nature* **457**, 910-914 (2009).
22. Cordova, A., Notz, W., Barbas, Iii C. F. Direct organocatalytic aldol reactions in buffered aqueous media. *Chem. Commun.*, 3024-3025 (2002).
23. List, B., Lerner, R. A., Barbas, C. F. Proline-catalyzed direct asymmetric aldol reactions. *J. Am. Chem. Soc.* **122**, 2395-2396 (2000).
24. Zhang, X., Houk, K. N. Acid/base catalysis by pure water: The aldol reaction. *J. Org. Chem.* **70**, 9712-9716 (2005).
25. List, B., Pojarliev, P., Martin, H. J. Efficient proline-catalyzed michael additions of unmodified ketones to nitro olefins. *Org. Lett.* **3**, 2423-2425 (2001).
26. Yang, H., Wong, M. W. (s)-proline-catalyzed nitro-michael reactions: Towards a better understanding of the catalytic mechanism and enantioselectivity. *Org. Biomol. Chem.* **10**, 3229-3235 (2012).
27. Zheng, Z., Perkins, B. L., Ni, B. Diarylprolinol silyl ether salts as new, efficient, water-soluble, and recyclable organocatalysts for the asymmetric michael addition on water. *J. Am. Chem. Soc.* **132**, 50-51 (2010).

3.5 Supplementary information

General methods

Starting materials were commercially available and used as received unless stated otherwise. **TLC** was performed on Merck Silica Gel 60 F254 TLC plates with a fluorescent indicator with a 254 nm excitation wavelength. Compounds were visualized under UV light at 254 nm. **NMR** spectra were recorded on a Bruker Avance-400 spectrometer (399.90 MHz for ^{1}H and 100.56 MHz for ^{13}C) at 298 K using residual protonated solvent signals as internal standard (^{1}H: $\delta(CHCl_3)$ = 7.26 ppm, $\delta((CH_3)_2SO)$ = 2.50 ppm, $\delta(CH_3OH)$ = 3.31 ppm, $\delta(D_2O)$ = 4.79 ppm, and ^{13}C: $\delta(CHCl_3)$ = 77.16 ppm, $\delta((CH_3)_2SO)$ = 39.52 ppm, $\delta(CH_3OH)$ = 49.00 ppm, D_2O was referenced to internal dioxane, 67.19 ppm. NMR spectra were processed by Mnova NMR software (mestrelab research). **HPLC-MS** analysis was performed on a Shimadzu Liquid Chromatograph Mass Spectrometer, LCMS-2010, LC-8A pump with a diode array detector SPD-M20. The column used was the Xbridge Shield RP 18.5µm (4.6x150mm). **UV-Vis** spectroscopic measurements were performed on an Analytik Jena Specord 250 spectrophotometer.

Synthesis of pro-prolines

Synthesis of PP-1:

PP-**1** was obtained by reaction between the boronate ester chloroformate derivative and proline and subsequent removal of the pinacol ester (Scheme S3.1).

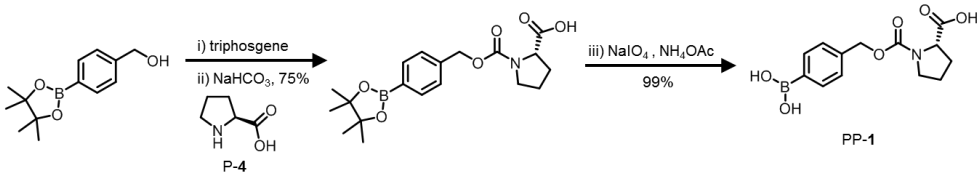

Scheme S3.1: Synthetic pathway for the preparation of PP-**1**.

1-(((4-(4,4,5,5-Tetramethyl-1,3,2-dioxaborolan-2-yl)benzyl)oxy)carbonyl)pyrrolidine-2-carboxylic acid (boronate-ester derivative):

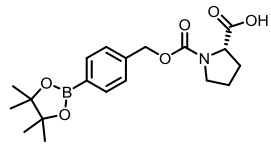

4-(4,4,5,5-Tetramethyl-1,3,2-dioxaborolan-2-yl)benzylchloroformate was synthesized adopting the literature procedure.[1] To a stirred solution of proline (0.48 g, 4.2 mmol)

and $NaHCO_3$ (0.88 g, 10.5 mmol) in water (10.0 mL) was added 4-(4,4,5,5-tetramethyl-1,3,2-dioxaborolan-2-yl)benzylchloroformate (1.03 g, 1.0 mmol) dropwise at 0 °C. The mixture was allowed to reach ambient temperature and was stirred overnight. After that, the reaction mixture was quenched with 1M HCl solution and diluted with ethyl acetate. The organic layer was washed with water, brine and dried over $MgSO_4$. Concentration under reduced pressure provided the desired compound as a sticky solid (0.98 g, 75 %). **^{1}H NMR** (400 MHz, $CDCl_3$): δ = 7.74–7.67 (m, 2H, Ar-*H*), 7.30-7.22 (m, 2H, Ar-*H*), 5.15-5.04 (m, 2H, Ar-CH_2), 5.21 (s, 2H, -CH_2-), 4.36-4.29 (m, 1H, -C*H*(CO_2H)), 3.55-3.36 (m, 2H, -CO_2NCH_2-), 2.20-1.98 (m, 2H, -CH_2-), 1.90-1.77 (m, 2H, -CH_2-), 1.26-1.24 (d, 12H, -CH_3). **^{13}C NMR** (100 MHz, $CDCl_3$): δ = 176.3 & 175.9 (-*C*O_2H-), 155.1 & 154.3 (-*C*O_2-), 139.3 & 139.2 (C_{Ar}), 134.7 & 134.6 (C_{Ar}), 126.8 (C_{Ar}), 126.4 (C_{Ar}), 83.6 & 83.5 (-*C*Me_2-), 67.0 & 66.8 (Ar-*C*H_2-), 58.9 & 58.4 (-*C*H(CO_2H)), 46.7 & 46.3 (-CO_2N*C*H_2-), 30.6 & 29.5 (-*C*H_2-), 24.6 (-*C*H_3), 24.0 & 23.2 (-*C*H_2-). Two signals are due to the presence of two rotational isomers, which is well known for carbamate rotamers.[2, 3] **MS** (ESI neg) m/z: 374.2 [(M-H)$^+$] (expected m/z = 374.19).

PP-1:

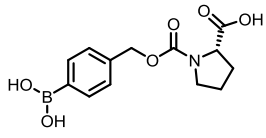

Boronate-ester derivative (0.61 g, 1.6 mmol) was dissolved in acetone (10.0 mL). To that, $NaIO_4$ (2.10 g, 9.8 mmol) and NH_4OAc (0.76 g, 9.8 mmol) in water (20.0 mL) were added and the mixture was stirred at room temperature. After completion of the reaction, it was acidified with 1M HCl and concentrated under reduced pressure. The crude product was diluted with ethyl acetate and the mixture was washed with water, brine and dried over $MgSO_4$. Concentration under reduced pressure provided the desired compound as a yellow-brown solid (0.48 g, 99 %). **^{1}H NMR** (400 MHz, DMSO-D_6): δ = 7.67 (bs, 2H, Ar-*H*), 7.35-7.29 (m, 2H, Ar-*H*), 5.13-5.08 (m, 2H, ArCH_2), 4.36-4.30 (m, 1H, -C*H*-CO_2H), 3.58-3.44 (m, 2H, -CO_2NCH_2-), 2.34-2.23 & 2.07-2.00 (m, 2H, -CH_2-), 1.96-1.88 (m, 2H, -CH_2-). **^{13}C NMR** (100 MHz, CD_3OD): δ = 174.0 & 173.7 (-*C*O_2H), 154.0 & 153.7 (-*C*O_2N-), 139.0 & 138.7 (C_{Ar}), 134.2 & 134.1 (C_{Ar}), 126.4 (C_{Ar}), 126.0 (C_{Ar}), 67.0 & 66.8 (Ar-*C*H_2-), 58.9 & 58.4 (-*C*H(CO_2H)), 46.8 & 46.2 (-CO_2N*C*H_2-), 30.5 & 29.4 (-*C*H_2-), 23.9 & 23.0 (-*C*H_2-). Two signals are due to the presence of two rotational

isomers, which is well known for carbamate rotamers.[2] **MS** (ESI Neg.) m/z: 292.0 [(M-H)$^+$] (expected m/z = 292.11).

Synthesis of PP-2:

PP-**2** was synthesized (Scheme S3.2) by the reaction of proline and corresponding chloroformate derivative which was obtained from 4,5-bis(2-(2-methoxyethoxy)ethoxy)-2-nitrophenyl methanol by the treatment with phosgene. 4,5-Bis(2-(2-methoxyethoxy)ethoxy)-2-nitrophenyl methanol was obtained from 3,4-bis(2-(2-methoxyethoxy)ethoxy)benzaldehyde[4] via nitration with HNO_3, followed by $NaBH_4$ reduction of the aldehyde group to an alcohol functional group.

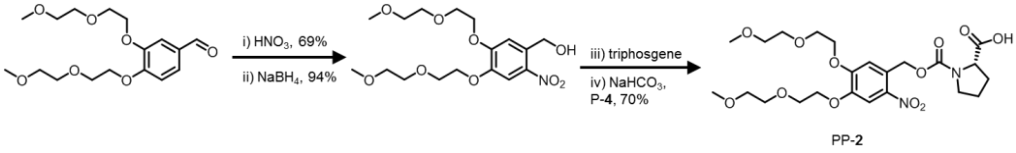

Scheme S3.2: Synthetic pathway for the preparation of PP-**2**.

4,5-Bis(2-(2-methoxyethoxy)ethoxy)-2-nitrobenzaldehyde:

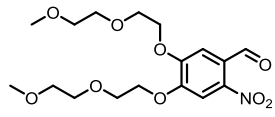

3,4-Bis(2-(2-methoxyethoxy)ethoxy)benzaldehyde (1.03 g, 3.0 mmol) was added while stirring to a chilled nitric acid solution (70 %, 3.0 mL) at 0 °C. The mixture was then allowed to reach ambient temperature. After completion of the reaction, it was diluted with water and extracted with ethyl acetate. The organic layer was washed with water, brine and dried over $MgSO_4$. Concentration under reduced pressure provided the desired compound as a yellow oil (0.80 g, 69 %). **^{1}H NMR** (400 MHz, DMSO-D_6): δ = 10.41 (s, 1H, -C*H*O), 7.68 (s, 1H, Ar-*H*), 7.45 (s, 1H, Ar-*H*), 4.33-4.29 (m, 4H, ArOC*H*$_2$CH$_2$-), 3.93-3.90 (m, 4H, ArOCH$_2$C*H*$_2$-), 3.73-3.71 (m, 4H, -OC*H*$_2$CH$_2$OCH$_3$), 3.56-3.54 (m, 4H, -OCH$_2$C*H*$_2$OCH$_3$), 3.37 (s, 6H, -OC*H*$_3$). **^{13}C NMR** (100 MHz, $CDCl_3$): δ = 187.6 (-*C*HO), 152.9 (2xC_{Ar}), 152.1 (C_{Ar}), 125.6 (C_{Ar}), 111.4 (C_{Ar}), 109.2 (C_{Ar}), 71.9 (ArO*C*H$_2$CH$_2$O-, for 2 peaks), 71.0 (ArOCH$_2$*C*H$_2$O-), 70.9 (ArOCH$_2$*C*H$_2$O-), 69.5 (-O*C*H$_2$CH$_2$OMe), 69.4 (-O*C*H$_2$CH$_2$OMe), 69.3 (-OCH$_2$*C*H$_2$OMe), 69.2 (-OCH$_2$*C*H$_2$OMe), 59.2 (-O*C*H$_3$, for 2 peaks).

4,5-Bis(2-(2-methoxyethoxy)ethoxy)-2-nitrophenyl)methanol:

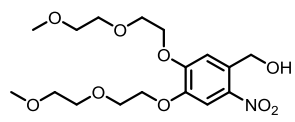

$NaBH_4$ (0.03 g, 0.70 mmol) was added slowly to a solution of 4,5-bis(2-(2-methoxyethoxy)ethoxy)-2-nitrobenzaldehyde (0.54 g, 1.4 mmol) in methanol (8.0 mL). The mixture was stirred at room temperature for 1 h. After completion of the reaction, the mixture was concentrated under reduced pressure, and the residue was partitioned between ethyl acetate and water. After extraction the combined organic layers were washed with brine, dried over $MgSO_4$ and concentrated under reduced pressure. The obtained crude compound was purified by flash column chromatography (silica gel, $CHCl_3$/MeOH 9/1) to obtain the desired compound as a pale yellow oil (0.51 g, 94 %). **^{1}H NMR** (400 MHz, $CDCl_3$): δ = 7.57 (s, 1H, Ar-*H*), 7.19 (s, 1H, Ar-*H*), 4.84 (s, 2H, ArC*H*$_2$), 4.17-4.08 (m, 4H, Ar-OC*H*$_2$CH$_2$-), 3.80-3.78 (t, 4H, Ar-OCH$_2$C*H*$_2$-), 3.65-3.62 (m, 4H, -OC*H*$_2$CH$_2$-OMe), 3.49-3.46 (m, 4H, -OCH$_2$C*H*$_2$-OMe), 3.29 & 3.28 (s, 6H, -OC*H*$_3$). **^{13}C NMR** (100 MHz, $CDCl_3$): δ = 153.4 (*C*$_{Ar}$), 146.6 (*C*$_{Ar}$), 138.7 (*C*$_{Ar}$), 133.5 (*C*$_{Ar}$), 111.4 (*C*$_{Ar}$), 110.1 (*C*$_{Ar}$), 71.6 (ArO*C*H$_2$CH$_2$O-, for 2 peaks), 70.5 (ArOCH$_2$*C*H$_2$O-), 70.4 (ArOCH$_2$*C*H$_2$O-), 69.2 (-O*C*H$_2$CH$_2$OMe, for 2 peaks), 68.9 (-OCH$_2$*C*H$_2$OMe), 68.5 (-OCH$_2$*C*H$_2$OMe), 61.6 (Ar*C*H$_2$-), 58.7 (-O*C*H$_3$), 58.6 (-O*C*H$_3$).

PP-2:

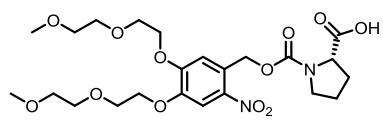

K_2CO_3 (2.49 g, 18.0 mmol) was oven dried in a round-bottom flask. The flask was cooled in an ice bath and triphosgene (1.19 g, 4.0 mM) in toluene (10.0 mL) was added. After stirring for 30 minutes at 0 °C, 4,5-bis(2-(2-methoxyethoxy)ethoxy)-2-nitrophenyl)methanol (0.78 g, 2.0 mmol) in toluene (10.0 mL) was added and stirred at ambient temperature. After completion of the reaction, it was worked-up by diluting with $CHCl_3$, filtering and concentrating under reduced pressure. The obtained chloroformate derivative was used without further purification. To a stirred solution of proline (0.25 g, 2.2 mM) and $NaHCO_3$ (0.23 g, 2.8 mM) in water (10.0 mL), the chloroformate derivative was added dropwise and the reaction mixture was stirred overnight at room temperature. After that, it was quenched with 1M HCl (pH 2) and then it was extracted with ethyl acetate. The organic layer was washed with water, brine and dried over $MgSO_4$. Concentration under reduced pressure provided the desired compound as a

light brown oil (0.74 g, 70 %). **^{1}H NMR** (400 MHz, CD_3OD): δ = 7.80 (s, 1H, Ar-*H*), 7.14 (s, 1H, Ar-*H*), 5.60-5.30 (m, 2H, ArC*H*$_2$), 4.48-4.26 (m, 3H, -C*H*CO_2H & ArOC*H*$_2$-), 4.24-4.21 (m, 2H, ArOC*H*$_2$-), 3.89-3.83 (m, 4H, ArOCH$_2$C*H*$_2$-), 3.72-3.53 (m, 10H, -OC$_2$*H*$_4$-; 8 protons & -CO_2NC*H*$_2$-), 3.34 (bs, 6H, -OC*H*$_3$), 2.38-2.06 (m, 2H, -C*H*$_2$-), 2.01-1.91 (m, 2H, -C*H*$_2$-). **MS** (ESI Neg.) m/z: 529.3 [$(M-H)^+$] (expected 529.21).

Synthesis of PP-3

PP-**3** is a known compound and was synthesized following a reported procedure (Scheme S3.3).[5] The analytical data were in accordance with the literature. A short description: 4-(phenylacetoxy)benzyloxycarbonyl chloride was obtained via acylation of 4-hydroxybenzaldehyde, followed by reduction of the aldehyde group to give the benzyl alcohol, and conversion to the chloroformate. Reaction between the chloroformate and proline gave PP-**3**.

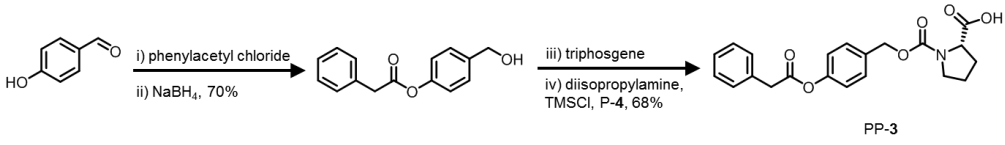

Scheme S3.3: Synthetic pathway for the preparation of **PP-3**.

Synthesis of Michael product 10

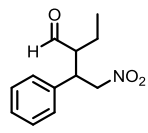

Trans-β-nitrostyrene **8** (200 mg, 1.34 mmol) and *L*-proline (34.5 mg, 0.30 mmol) were dissolved in methanol (2 mL). Butanal **9** (181 µL, 0.145 g, 2.01 mmol) was added and the reaction was stirred overnight until NMR confirmed complete conversion. The reaction mixture was concentrated under reduced pressure and purified using column chromatography (eluent 5% ethyl acetate in petroleum ether) to yield the product as a colourless oil (0.134 g, 0.60 mmol, 45%). The double peaks in the NMR spectrum are due to the presence of two different diastereoisomers in a 1:3 ratio. **^{1}H NMR** (400 MHz, methanol-d4) δ 9.69 (s, 1H), 7.28 (m, 5H), 4.94 (d, 1H, *J* = 5.4), 4.82 (d, 1H, *J* = 4.9), 3.83 (m, 1H), 2.73 (m, 1H), 1.45 (m, 2H), 0.78 (m, 3H). **^{13}C NMR** (100.5 MHz, methanol-d4) δ 205.1, 139.0, 130.0, 79.7, 56.1, 44.0, 21.0, 10.8. **MS** (ESI Neg.) m/z: 220.1 [$(M-H)^-$] (expected m/z = 220.11).

Release of catalyst by the signal:

H_2O_2 triggered proline release:

H_2O_2 (1.0 mL, 30 % aq. H_2O_2 solution, excess) was added to a solution of PP-**1** (0.05 g) in MeOH (2.0 mL). The mixture was stirred for 10 minutes. After completion of the reaction (monitored via TLC analysis), the mixture was concentrated and diluted with ethyl acetate. The organic layer was washed with sodium sulfite, brine and dried over $MgSO_4$. After filtration, the obtained solution was concentrated under reduced pressure and the residue was analyzed by ^{1}H NMR spectroscopy and mass spectroscopy.

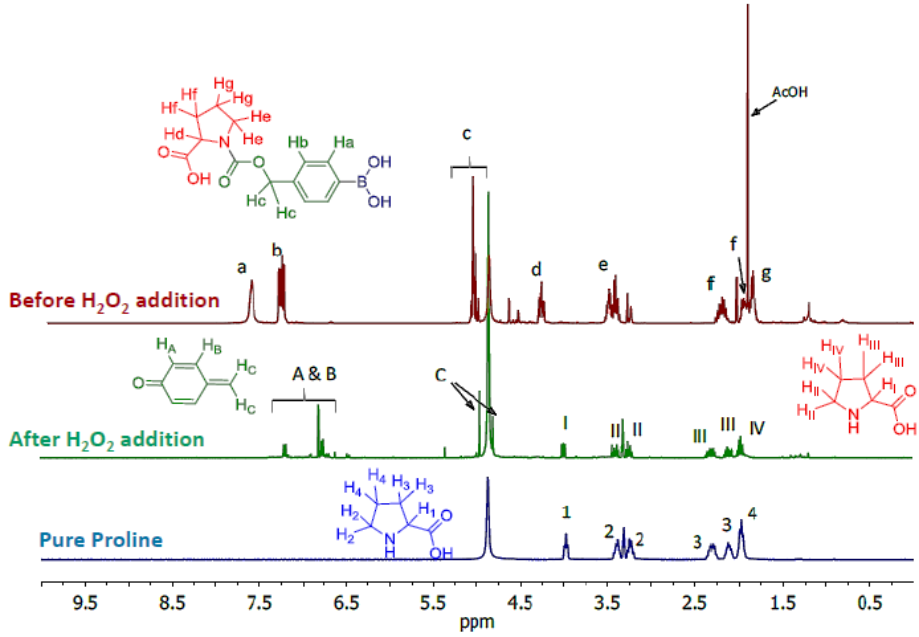

Figure S3.1: ^{1}H NMR analysis of chemical (H_2O_2) trigger proline release from PP-**1** in CD_3OD at 25 °C: PP-**1** before (top in red) and after H_2O_2 treatment (middle in green). The released proline has comparable spectrum as pure proline (bottom in blue).

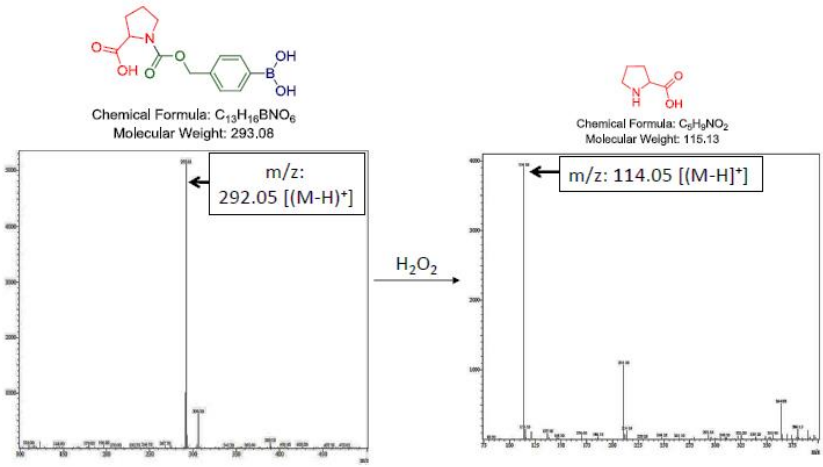

Figure S3.2: Mass spectrometry analysis of chemical (H_2O_2) triggered proline release from PP-**1**: before (left) and after (right) the treatment of H_2O_2.

Light-triggered proline release

Light activation method:

Light signal experiment was performed using an optical fiber illuminator with a Nikon Intensilight C-HGFI lamp (lamp-ultrahigh pressure 130W mercury lamp, with 100 % light intensity). In a typical experiment, a vial containing only a solution of PP-**2** in CD_3OD or a mixture of PP-**2** and precursors for aldol reaction in buffer solution was placed directly in front of the optical fiber aperture and illuminated with light for 30 minutes.

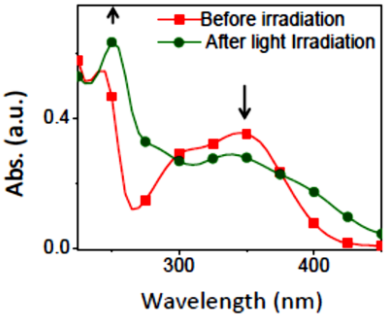

Figure S3.3: UV-Vis absorption spectra of PP-**2** before (red) and after (green) light irradiation.

Light-triggered proline release:

A vial with a solution of PP-**2** (0.05 g) in MeOH (2.0 mL) was placed directly in front of the optical fiber aperture and illuminated with light for 30 minutes. The mixture was then concentrated and the residue was analyzed by ^{1}H NMR spectroscopy and mass spectroscopy.

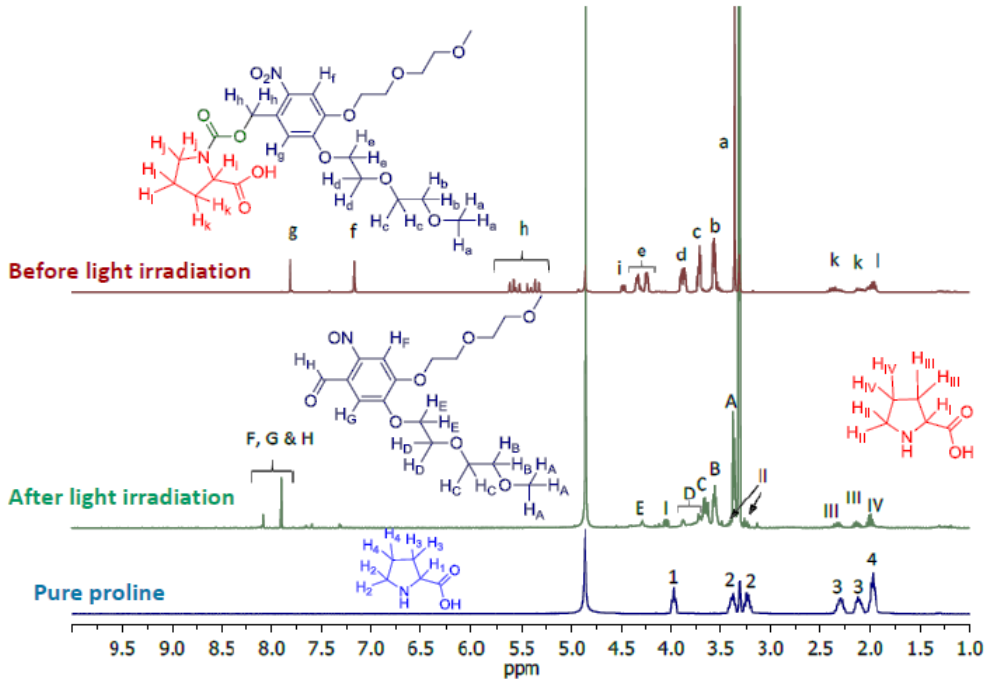

Figure S3.4: ^{1}H NMR analysis of light triggered proline release from PP-**2** in CD_3OD at 25 °C – before (top in red) and after light irradiation (middle in green). The released proline has a comparable spectrum to pure proline (bottom in blue).

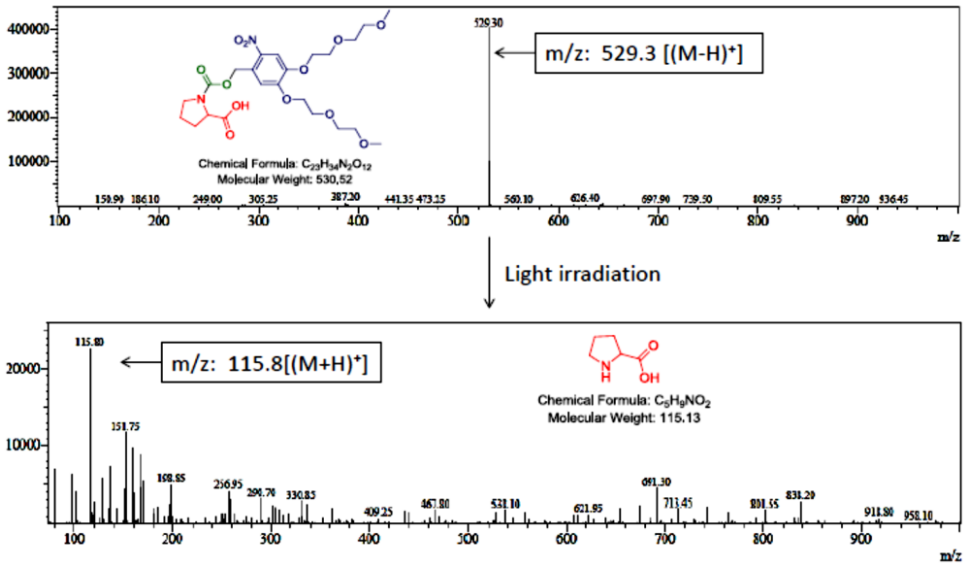

Figure S3.5: Mass spectrometry analysis of proline release from PP-**2**: before (top) and after (bottom) light irradiation.

Enzyme triggered proline release

Penicillin Acylase (5.5 mg, 98 U, Penicillin Acylase from *Escherichia coli*, Sigma Aldrich) in sodium phosphate buffer (100 mM, pH 7.4, 100 µL) was added to a solution of PP-**3** (0.5 mg) in acetone (10 µL) and the mixture was stirred for 10 minute at room temperature. After that, it was concentrated under reduced pressure and diluted with CH_3OH, followed by filtration. After concentration under reduced pressure, the obtained residue was analyzed by ^1H NMR and mass spectrometry.

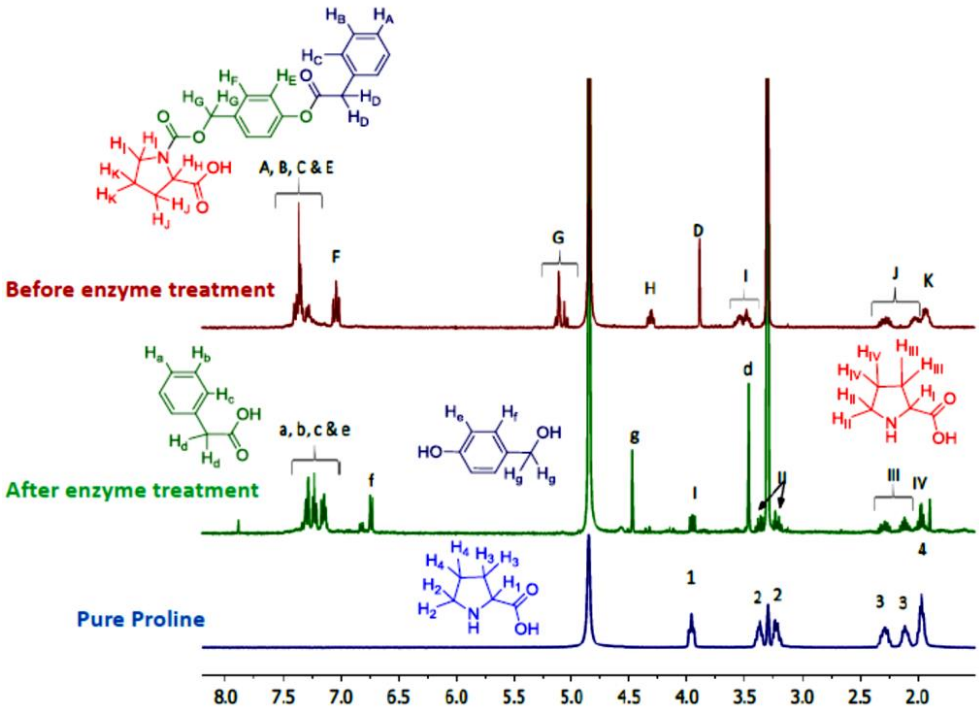

Figure S3.6: ^1H NMR analysis of enzyme (Peniciline Acylase) triggered proline release from PP-**3** in CD_3OD at 25 °C: PP-**3** before (top in red) and after enzyme treatment (middle in green). The released proline has a comparable spectrum to pure proline (bottom in blue).

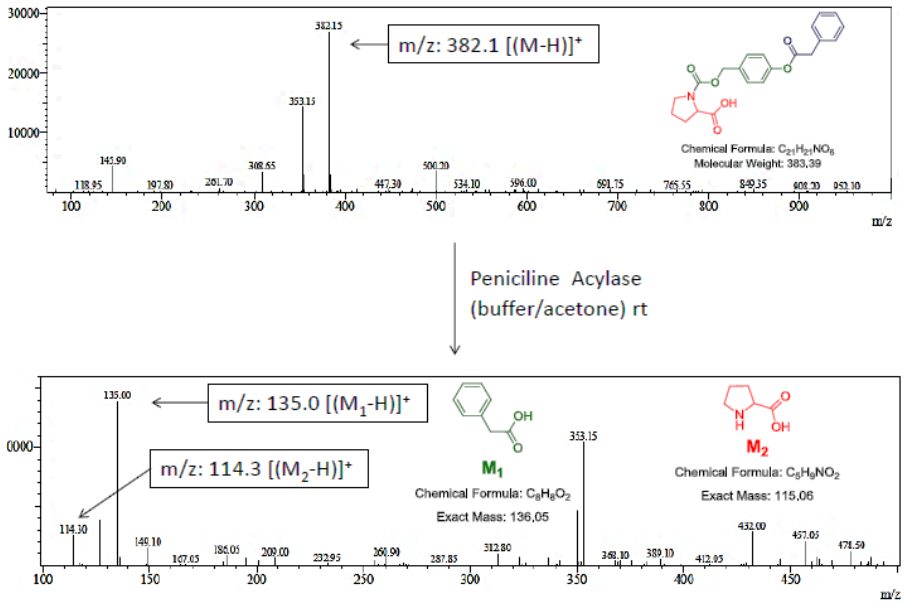

Figure S3.7: Mass spectrometry analysis of enzyme (Penicilin Acylase) triggered proline release from PP-**3**: before (top) and after (bottom) enzyme treatment.

Procedure for the aldol reaction

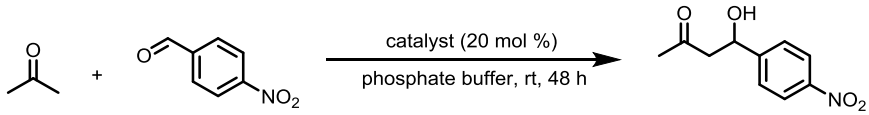

(20 vol %)

Scheme S3.4: General reaction scheme for direct aldol reaction**.**

General procedure to follow the aldol reactions

In a typical experiment, 4-nitrobenzyldehyde **6** (10.0 mmol) was added to the mixture of aqueous solution (480 µL) and acetone **5** (120 µL, 20 vol %) of a total volume of 600 µL. The aqueous solution consist of 430 µL of 100 mM sodium phosphate buffer of pH 7.4 and 50 µL D_2O. Sodium dodecyl sulfate (SDS, 0.1 equivalents) was added as an additive following the reported procedure.[6] The pro-prolines and signals were added to the mixture and in the mixture was transferred to an NMR tube. Conversion of the aldol reaction was determined by ^{1}H NMR analysis. We did not investigate the enantioselectivity of the

reaction. The direct aldol reaction was compared using proline (0.14 mg, 2.0 mmol, 20 mol %) as catalyst.

H_2O_2 triggered aldol reaction:

In an NMR tube, 4-nitrobenzaldehyde **6** (0.9 mg, 10.0 mmol) was added to the mixture of sodium phosphate buffer of pH 7.4 (100 mM, 430 µL), D_2O (50 µL), acetone **5** (120 µL, 20 vol %), SDS (0.2 mg, 1.0 mM) and PP-**1** (0.4 mg, 20 mol %). To this mixture H_2O_2 was added and reaction was followed via analyzing ^{1}H NMR spectra. For the control reactions, PP-**1** (0.4 mg, for inactivated catalysis), PP-**1** (0.4 mg) & light irradiation for 30 minutes (a wrong trigger) or nothing (for background reaction) was used replacing PP-**1** and H_2O_2. A controlled chemical triggered direct aldol reaction was performed when PP-**1** (0.4 mg) was used in the reaction mixture and H_2O_2 (1 eq.) was added after 22 h.

Table S3.1: H_2O_2 triggered proline release from PP-**1** and direct aldol reaction between 4-nitrobenzaldehyde **6** and acetone **5** (pH 7.4, room temperature, 48 h)

Entry	trigger	Compound used for catalysis[a]	Yield (%) of aldol product[b]
1	-	-	65
2	-	PP-**1**	65
3	H_2O_2[C]	PP-**1**	93
4	-	P-**4**	99
5	Light	PP-**1**	67

[a]0.1 equivalent SDS used as an additive, [b]conversion as determined by ^{1}H NMR, [C]1 equivalent H_2O_2 with respect to PP-**1**.

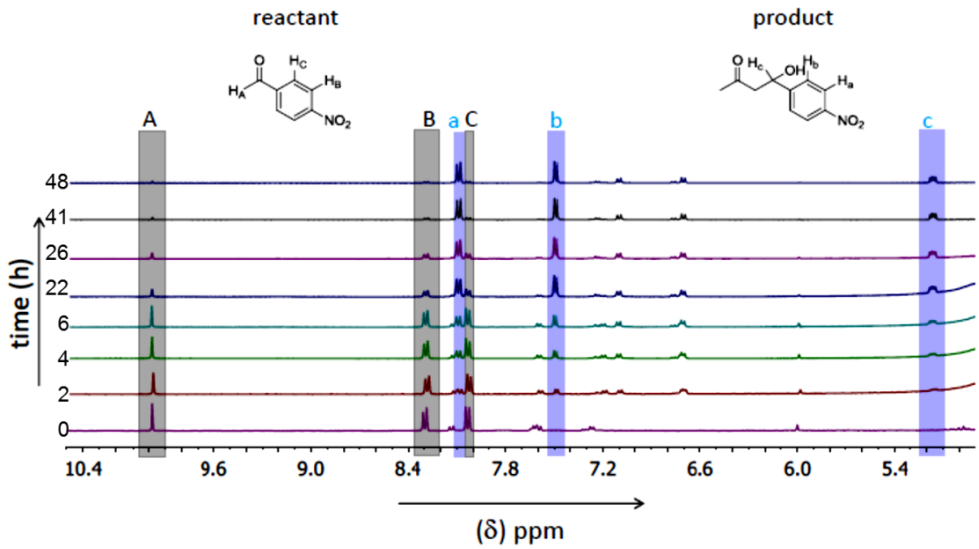

Figure S3.8: ^{1}H NMR (partial) spectral analysis of H_2O_2 (1 eq.) triggered direct aldol reaction in phosphate buffer (100 mM, pH 7.4) at room temperature at different time intervals.

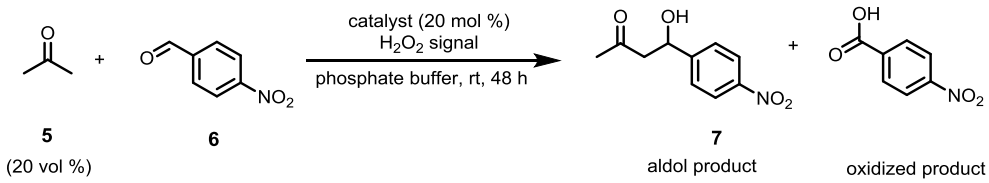

Scheme S3.5: Aldol formation and the oxidation of 4-nitrobenzaldehyde **6**.

Table S3.2: H_2O_2 trigger direct aldol reaction between 4-nitrobenzaldehyde and acetone at room temperature using PP-**1.**

Entry	Equivalence of H_2O_2 with respect to PP-**1**[a]	Yield (%) of aldol product[b]	Yield (%) of oxidized product
1	0	65	0
2	1	93	<1.0
3	2	93	1.5
4	4	92	3.5
5	6	90	5.0
6	40	75	20.0

[a]0.1 equivalent SDS used as an additive, [b]conversion as determined by ^{1}H NMR.

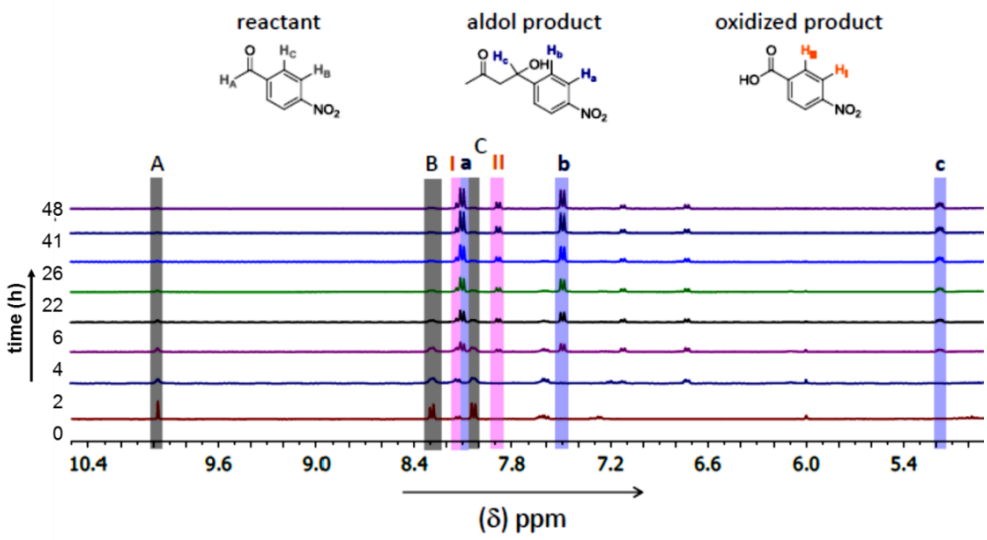

Figure S3.9: Partial ^{1}H NMR spectra of H_2O_2 (40 eq.) triggered direct aldol reaction in phosphate buffer (100 mM, pH 7.4) at room temperature at different time intervals.

Light triggered aldol reaction

In a vial, 4-nitrobenzaldehyde **6** (0.9 mg, 10.0 mmol) was added to the mixture of sodium phosphate buffer of pH 7.4 (100 mM, 430 µL), D_2O (50 µL), acetone **5** (120 µL, 20 vol %), SDS (0.2 mg, 1.0 mmol) and PP-**2** (0.6 mg, 20 mol %). The mixture was then placed directly in front of the optical fiber aperture and illuminated with light. After that the mixture was transferred to an NMR tube and the aldol reaction was followed via analyzing ^{1}H NMR spectra. For control reactions, PP-**2** (0.6 mg, 20 mol %, for inactivated catalysis), PP-**2** (0.6 mg) and H_2O_2 (a wrong trigger) or nothing (for background reaction) was added replacing PP-**2** and light illumination. A controlled light triggered aldol reaction was performed when PP-**2** was added to the reaction mixture and after 22 h light was irradiated and aldol reaction was monitored via ^{1}H NMR spectroscopy.

Table S3.3: Direct aldol reaction between 4-nitrobenzaldehyde **6** and acetone **5** at room temperature after (pH 7.4, 48 h, room temperature)

Entry	Compound used for catalysis[a]	Trigger	Yield (%) of aldol product[b]
1	-	-	65
2	PP-**2**	-	65
3	PP-**2**	Light	93
4	P-**4**	-	99
5	PP-**2**	H_2O_2	67

[a]0.1 equivalent SDS used as an additive, [b]conversion as determined by ^{1}H NMR.

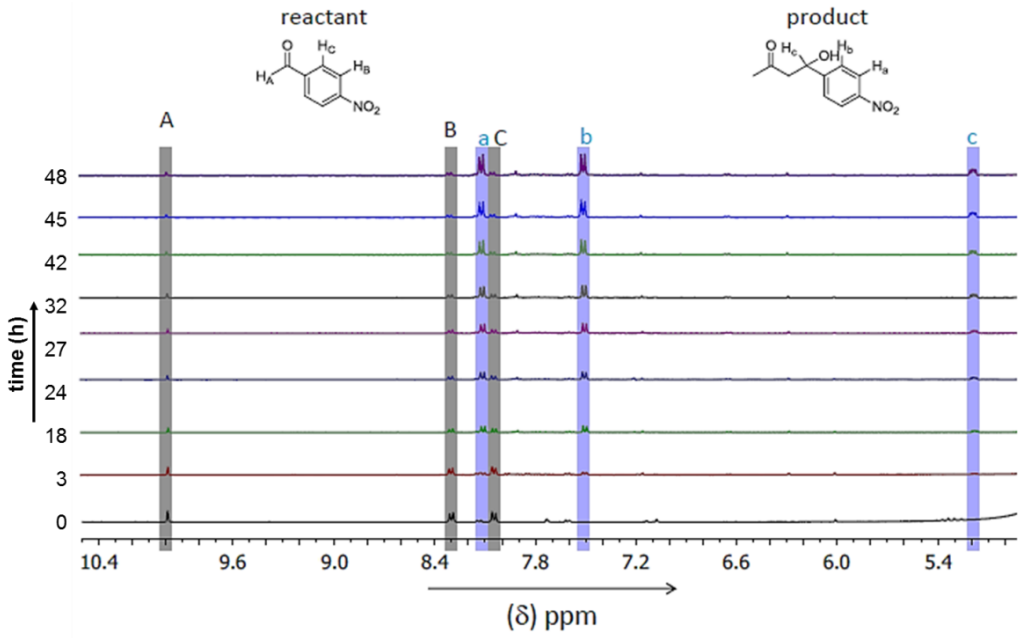

Figure S3.10: ^{1}H NMR (partial) spectral analysis of light triggered direct aldol reaction using PP-**2** in phosphate buffer (100 mM, pH 7.4) at room temperature at different time intervals.

Enzyme triggered aldol reaction

In an NMR tube, 4-nitrobenzaldehyde **6** (0.9 mg, 10.0 mmol) was added to the mixture of phosphate buffer of pH 7.4 (100 mM, 330 μL), D_2O (50 μL), acetone **5** (120 μL, 20 vol %), SDS (0.2 mg, 1.0 mmol) and PP-**3** (0.5 mg, 20 mol %). To this mixture Penicillin Acylase (5.5 mg, 98 U, Penicillin Acylase from *Escherichia coli*, Sigma Aldrich) in phosphate buffer (100 μL) was added and reaction was followed via analyzing ^{1}H NMR spectra. For control reaction, PP-**3** (0.5 mg, 20 mol %, for inactivated catalysis) or PP-**3** (0.5 mg) & light irradiation for 30 minutes (a wrong trigger) was employed. A controlled enzyme triggered aldol reaction was performed when PP-**3** (0.5 mg) was used and after 22h Penicillin Acylase enzyme (5.5 mg) was added to the reaction mixture.

Table S3.4: Direct aldol reaction between 4-nitrobenzaldehyde and acetone at room temperature (pH 7.4, 48 h, room temperature)

Entry	Compound used for catalysis[a]	Trigger	Yield (%) of aldol product[b]
1	None (background)	-	65
2	PP-**3**	-	67
3	PP-**3**	Penicillin Acylase	97
4	P-**4**	-	99
5	PP-**3**	Light	66

[a]0.1 equivalent SDS used as an additive, [b]conversion as determined by ^{1}H NMR.

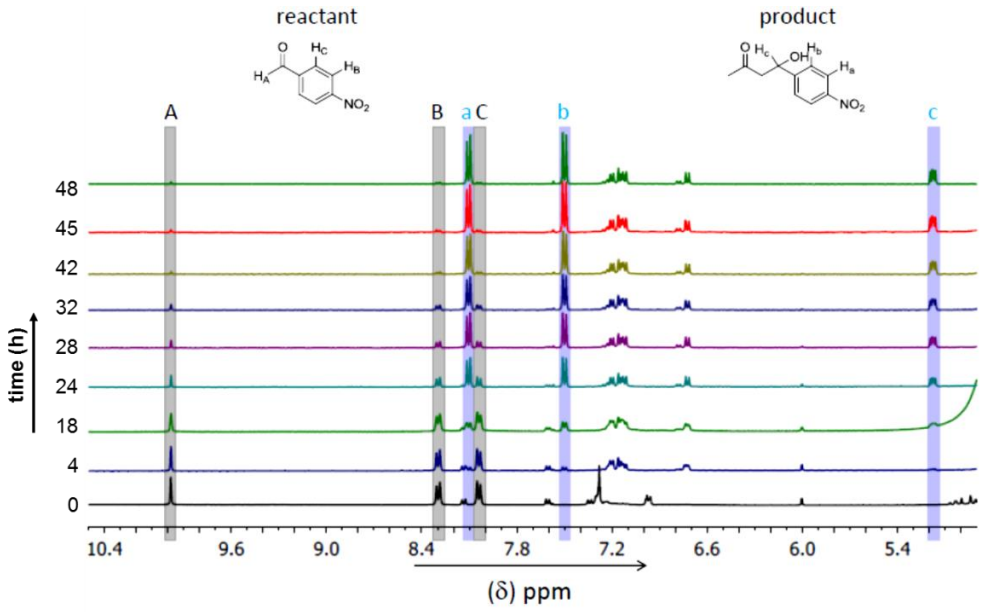

Figure S3.11: ^{1}H NMR (partial) spectral analysis of enzyme triggered direct aldol reaction using PP-**3** in phosphate buffer (100 mM, pH 7.4) at room temperature in different time interval.

Michael reaction

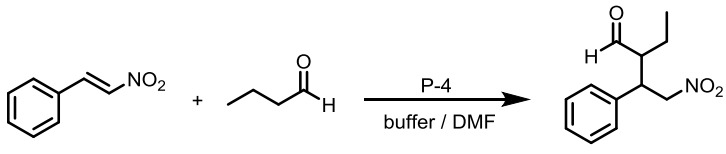

8 **9** **10**

Scheme S3.6: Michael reaction between *trans*-β-nitrostyrene **8** and butanal **9**.

H_2O_2 triggered Michael reaction:

The Michael reaction was performed in 20% DMF-d7 in a sodium phosphate buffer (10 mM, pH 8.0), containing *trans*-β-nitrostyrene **8** (10 mM), butanal **9** (100 mM), PP-**1** (10 mM) or P-**4** (10 mM), or H_2O_2 (100 mM). The NMR tube contained a total solvent volume of 0.6 mL. The stock solutions were added as follows: *trans*-β-nitrostyrene **8** solution (100 mM in DMF-d7), DMF-d7, PP-**1** (100 mM in DMF-d7), P-**4** (100 mM in buffer), buffer. H_2O_2 (6.1 µL, 30%) and butanal **9** (5.4 µL, 99%) were added at the last possible moment before the NMR measurement started.

Table S3.5: H_2O_2 triggered proline release from PP-**1** and Michael reaction between *trans*-β-nitrostyrene **8** and butanal **9** (20% DMF-d7 in 10 mM sodium phosphate buffer pH 8.0).

Catalyst system	***Yield (%) of Michael product after 8 h of reaction***
None	0
PP-**1**	0
H_2O_2	0
P-**4**	100
PP-**1** + H_2O_2	89
P-**4** + H_2O_2	72

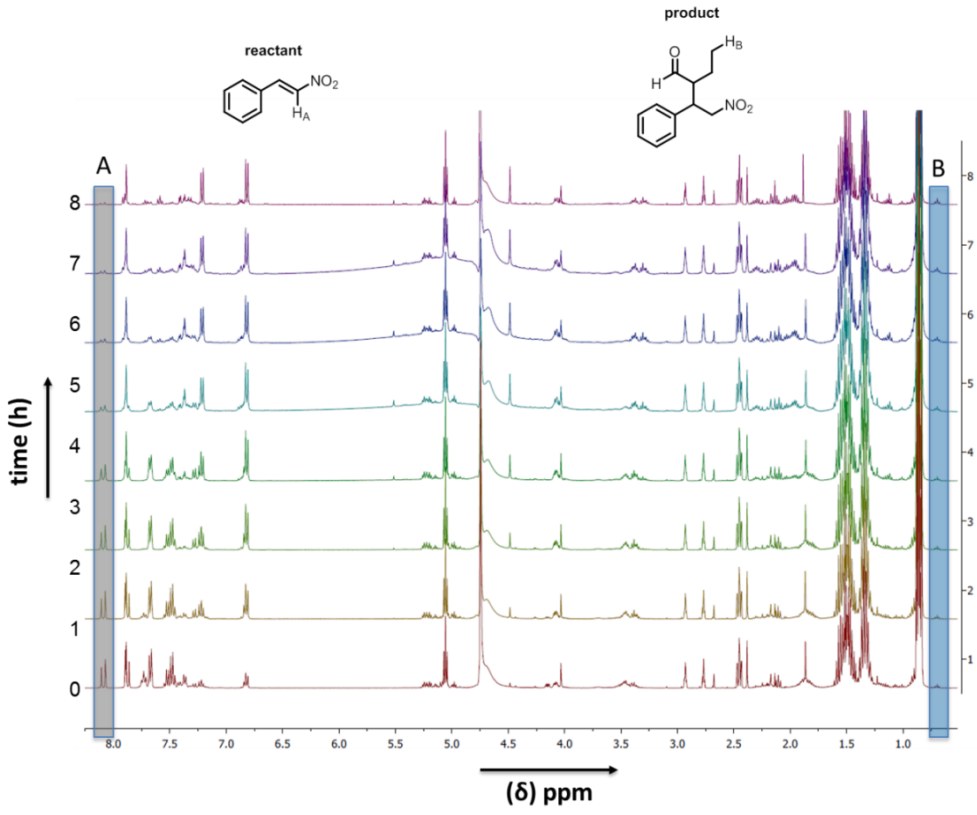

Figure S3.12: ^{1}H NMR (partial) spectral analysis of H_2O_2 (10 eq.) Michael reaction between *trans*-β-nitrostyrene **8** and butanal **9** (20% DMF-d7 in 10 mM sodium phosphate buffer pH 8.0) at 25 °C.

Reaction kinetics

General procedure

The aldol reaction and the Michael reaction are both second order reactions. The reactions were performed at pseudo-first order conditions with one of the reagents in excess. Concentrations used in the aldol reaction: 2.72 M acetone, 0.01 M 4-nitrobenzaldehyde. Concentrations used in the Michael reaction: 100 mM butanal, 10 mM *trans*-β-nitrostyrene.

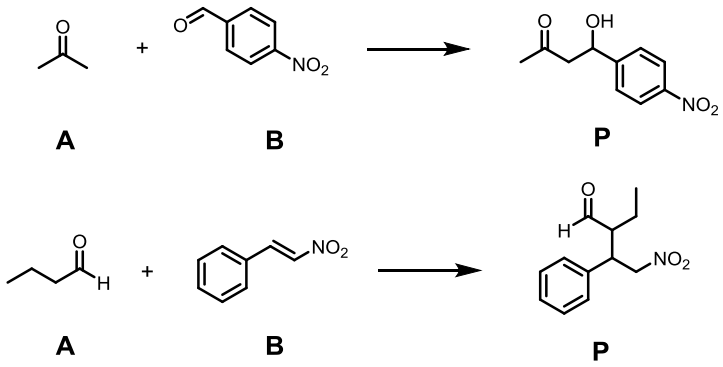

Start, t = 0	$[A]_0$	$[B]_0$	0
At t = t	$[A]_t = [A]_0 - [P]_t$	$[B]_t = [B]_0 - [P]_t$	$[P]_t$

Scheme S3.7: The aldol reaction between acetone **5** and 4-nitrobenzaldehyde **6** and the Michael reaction between *trans*-β-nitrostyrene **8** and butanal **9**.

Here, [A] is the concentration of the reagent used in excess: acetone in the aldol reaction and the concentration of butanal in the Michael reaction. [B] is the concentration of 4-nitrobenzaldehyde in the aldol reaction and *trans*-β-nitrostyrene in the Michael reaction. [P] is the aldol product in the aldol reaction and the Michael product in the Michael reaction.

The 2nd order reaction rate equation (assuming 1st order in both A and B) can be written as:

$$\text{Rate} = -k[A]_t[B]_t \quad \text{(eq. S3.1)}$$

For $[A]_0 \neq [B]_0$, the integrated second order rate law can be written as:

$$\ln([A]_t/[A]_0) - \ln([B]_t/[B]_0) = k([A]_0-[B]_0)t \quad \text{(eq. S3.2)}$$

Because a large excess of A (acetone and butanal) was used in the reaction, it can be assumed that:

$$[A]_0 >>]B]_0,\ [A]_t/[A]_0 \approx 1 \text{ and } [A]_0-[B]_0 \approx [A]_0 \quad \text{(eq. S3.3)}$$

The rate law can be written as:

$[B]_t/[B]_0 = \exp(-k[A]_0t)$ (eq. S3.4)

Rearranging $[B]_t = [B]_0 - [P]_t$ to $[B]_0 = [B]_t + [P]_t$ and replacing $[B]_0$ at the rate law, it can be rewritten as:

$[B]_t/([B]_t + [P]_t) = \exp(-k[A]_0t)$ (eq. S3.5)

This is rearranged to:

$$\ln\left\{1-\frac{[P]_t}{([B]_t + [P]_t)}\right\} = -k[A]_0t \quad \text{(eq. S3.6)}$$

where, $[B]_t$ is the concentration of *trans*-β-nitrostyrene in the Michael reaction and 4-nitrobenzaldehyde in the aldol reaction. $[P]_t$ is the concentration of the Michael product and the aldol product at every specified time obtained from ^{1}H NMR spectral analysis. $[A]_0$ is the initial concentration of acetone in the aldol reaction and the initial concentration of butanal in the Michael reaction. $[B]_0$ is the initial concentration of 4-nitrobenzaldehyde in the aldol reaction and the initial concentration *trans*-β-nitrostyrene in the Michael reaction. A line was obtained via plotting $\ln\left\{1-\frac{[P]_t}{([B]_t + [P]_t)}\right\}$ vs t and it was fitted to the y = mx line in Origin to obtain the rate constants of the pseudo-first order reactions.

Reaction kinetics of the aldol reaction

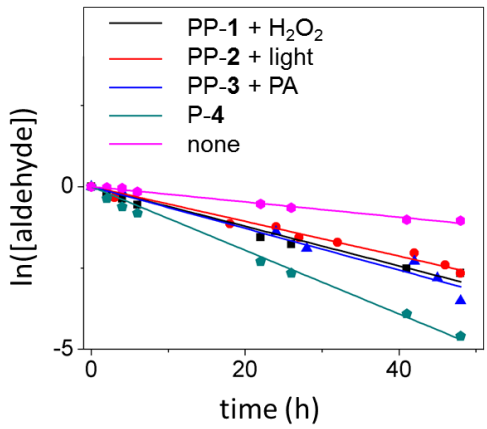

Figure S3.13: Signal triggered proline release and subsequent catalysis of an aldol reaction between 4-nitrobenzaldehyde **6** and acetone **5** in aqueous buffer media (100 mM, pH 7.4), where [aldehyde] = $\ln\left\{1-\frac{[P]_t}{([B]_t + [P]_t)}\right\}$. Signal triggered aldol reaction was compared with proline catalysed aldol reaction and background reaction.

For the delayed activation procedure, aldol product was formed due to the combination of uncatalyzed (background) reaction and proline catalyzed reaction (after signal addition). Therefore two lines were obtained via plotting $\ln\left\{1-\frac{[P]_t}{([B]_t+[P]_t)}\right\}$ vs t and it was fitted to the equation if x<22h, $y = m_1x$, else $y = m_2x$ in Origin to obtain the rate constants for delayed activation procedure.

Table S3.6: Direct aldol reaction between 4-nitrobenzaldehyde and acetone (pH 7.4, 48 h, room temperature) using pro-prolines, whereas they were activated with the signal after 22 h (delayed activation) with calculated second order rate constant.

Pro-proline+ signal	Rate constant ($M^{-1}s^{-1}$) before signal added	Rate constant ($M^{-1}s^{-1}$) after signal added
PP-**1** + H_2O_2	$2.76x10^{-6}$	$4.53\ x10^{-6}$
PP-**2** + Light	$2.83x10^{-6}$	$4.17\ x10^{-6}$
PP-**3** + *Penicillin Acylase*	$2.75\ x10^{-6}$	$3.78\ x10^{-6}$

Rate constant before the signal was employed corresponds to the background reaction and after the signal was employed, the reaction was catalyzed by released proline. Slower reaction rates for the delayed activation procedure compared to when the signal is used at the beginning is due to lower concentrations of the reagents after 22 h.

Reaction kinetics of the Michael reaction

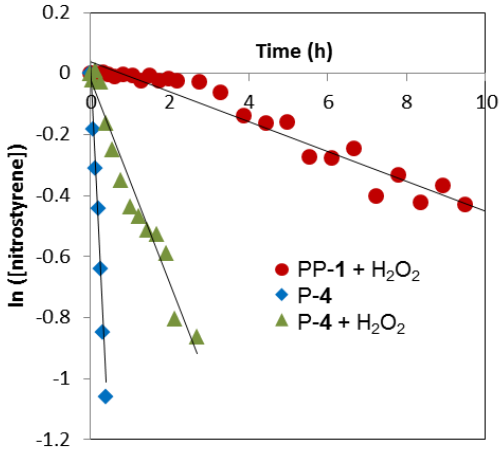

Figure S3.14: H_2O_2 triggered proline release and subsequent catalysis of Michael reaction between trans-β-nitrostyrene **8** and butanal **9** (20% DMF-d7 in 10 mM sodium phosphate buffer pH 8.0) at 25 °C, where $[nitrostyrene] = \ln\left\{1-\frac{[P]_t}{([B]_t + [P]_t)}\right\}$.

NMR spectra

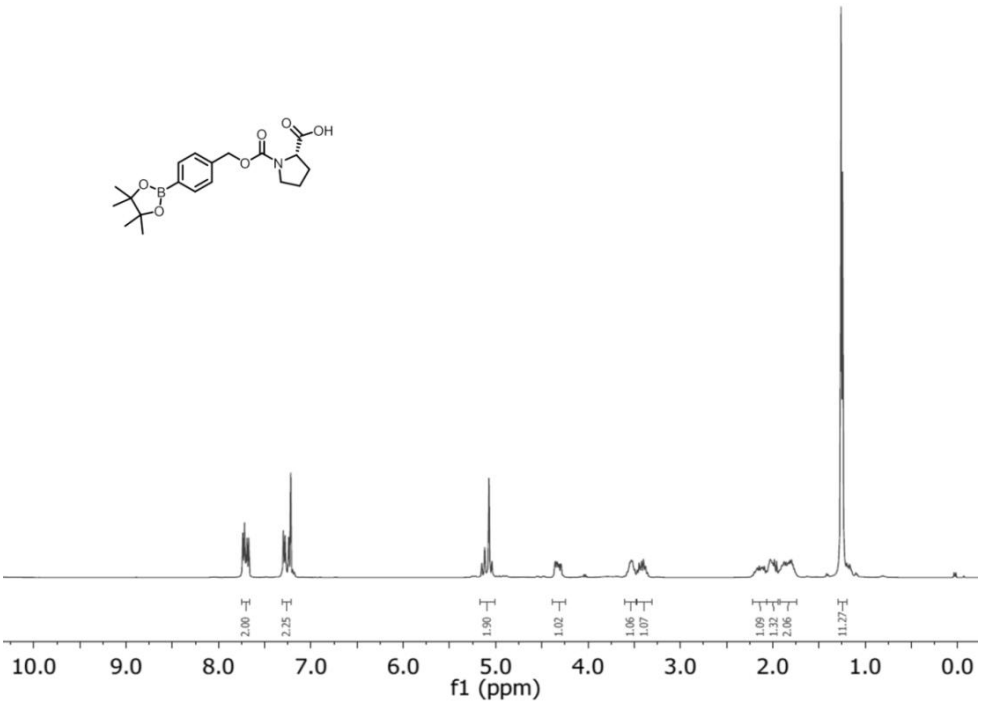

Figure **S3.15**: ^{1}H NMR spectrum of boronate-ester derivative in $CDCl_3$ at 25 °C.

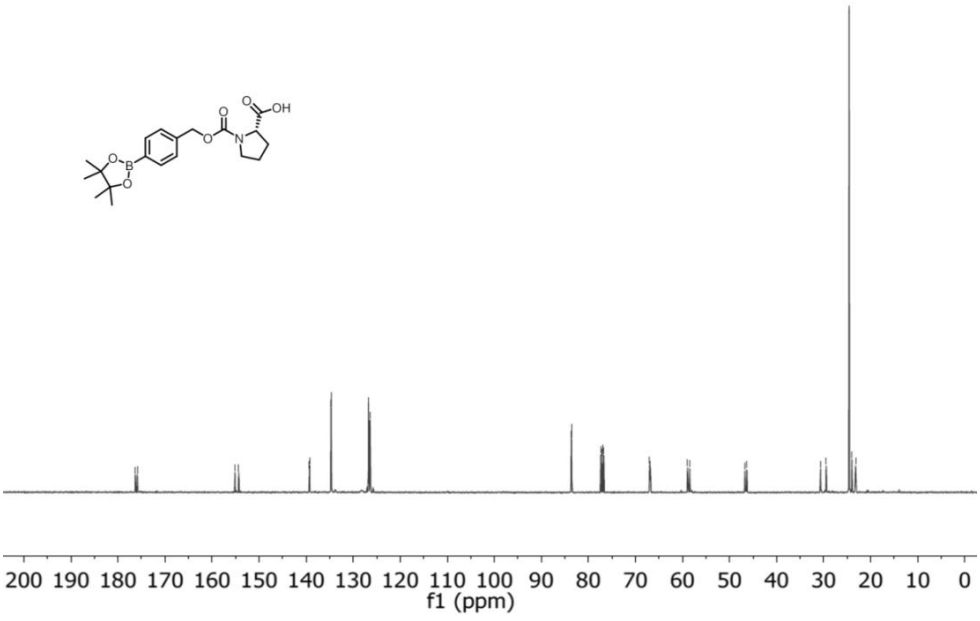

Figure **S3.16**: ^{13}C NMR spectrum of boronate-ester derivative in $CDCl_3$ at 25 °C.

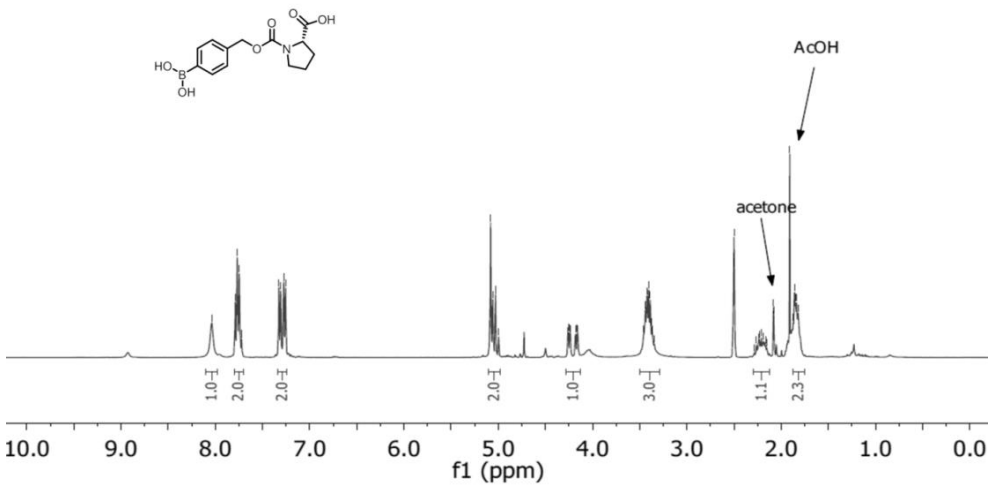

Figure **S3.17**: ^{1}H NMR spectrum of PP-**1** in DMSO-d6 at 25 °C.

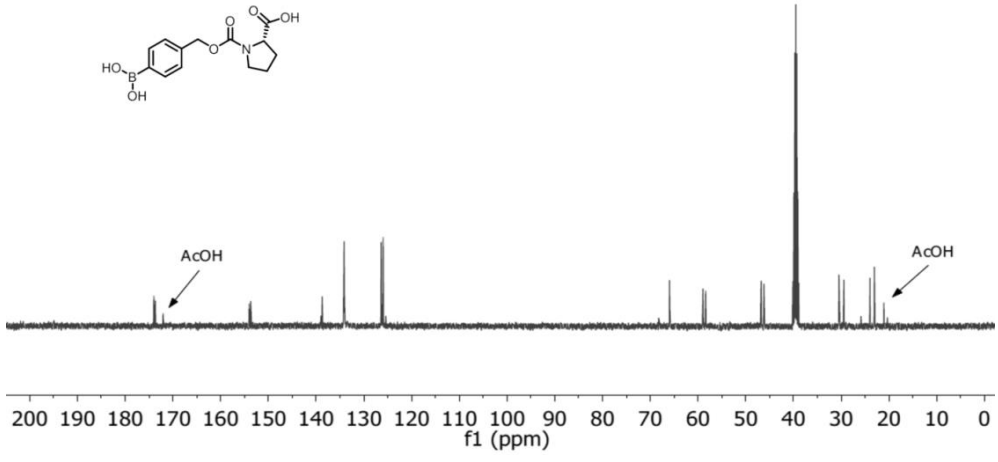

Figure **S3.18**: ^{13}C NMR spectrum of PP-**1** in DMSO-D_6 at 25 °C.

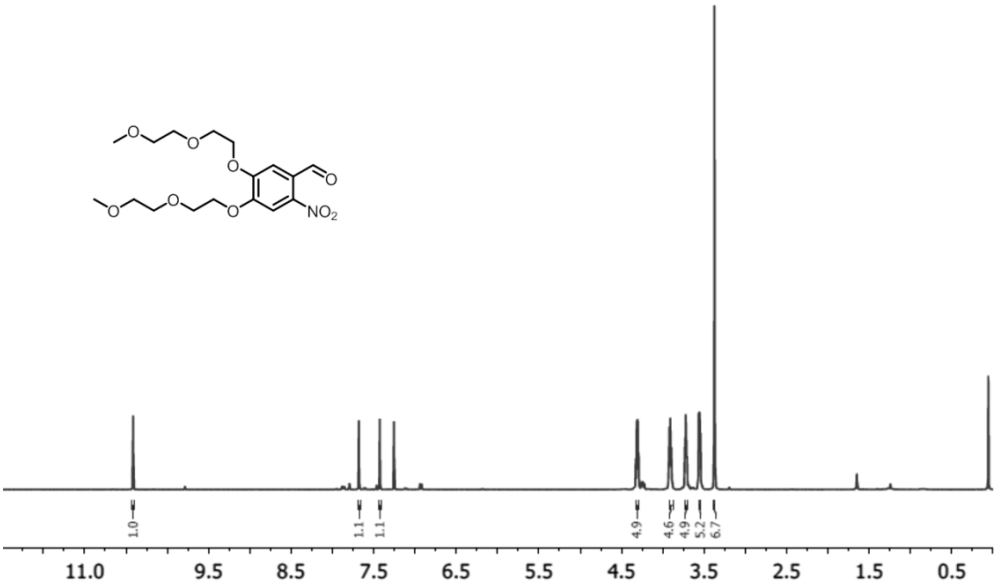

Figure **S3.19**: ^{1}H NMR spectrum of 4,5-bis(2-(2-methoxyethoxy)ethoxy)-2-nitrobenzaldehyde in $CDCl_3$ at 25 °C.

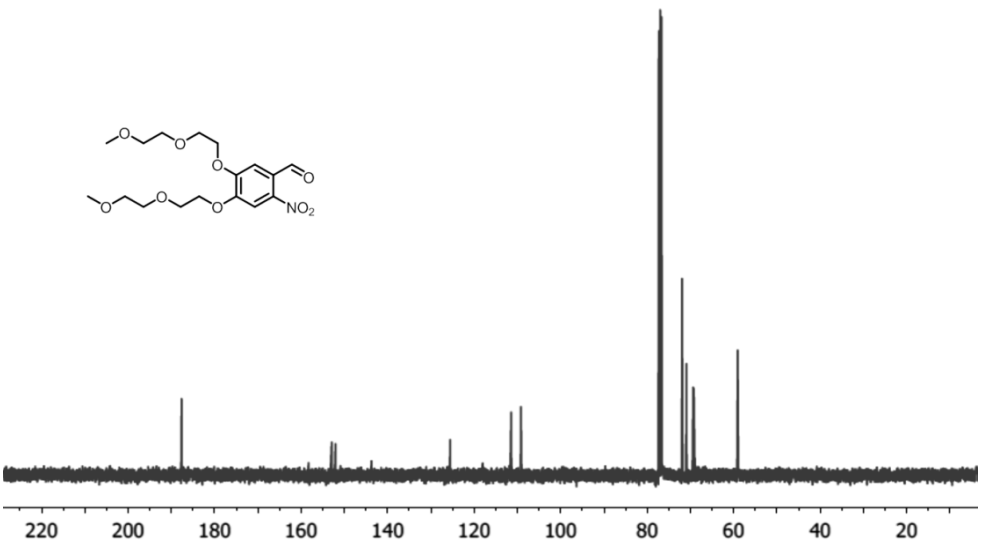

Figure **S3.20**: ^{13}C NMR spectrum of 4,5-bis(2-(2-methoxyethoxy)ethoxy)-2-nitrobenzaldehyde in CDCl3 at 25 °C.

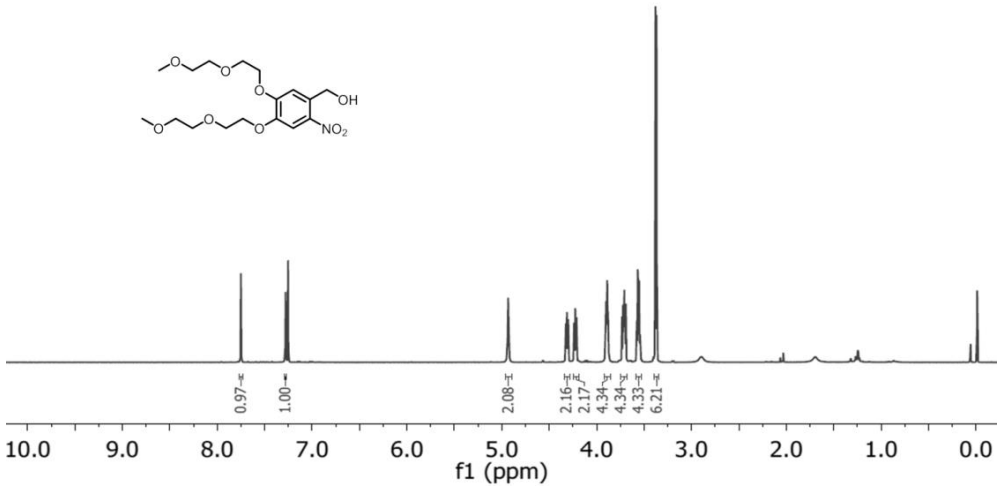

Figure **S3.21**: ^{1}H NMR spectrum of 4,5-bis(2-(2-methoxyethoxy)ethoxy)-2-nitrophenyl)methanol in $CDCl_3$ at 25 °C.

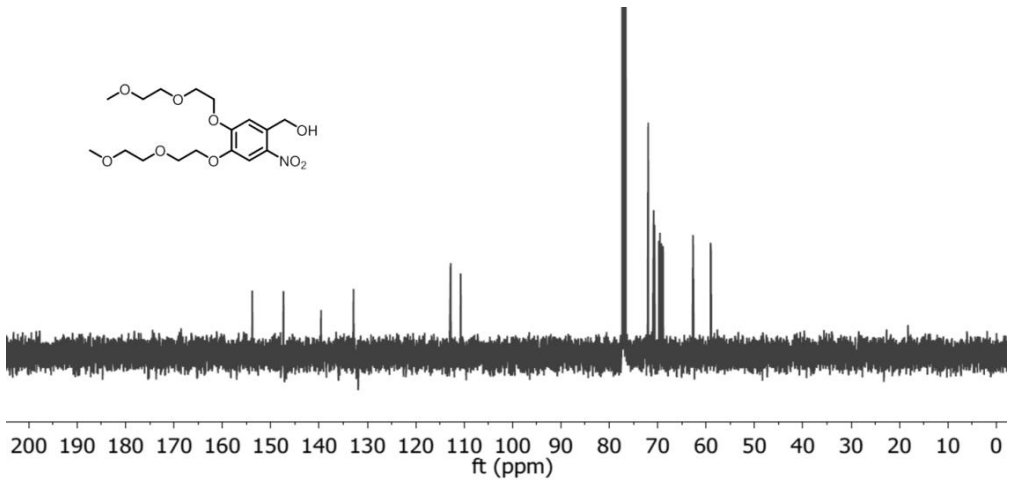

Figure **S3.22**: ^{13}C NMR spectrum of 4,5-bis(2-(2-methoxyethoxy)ethoxy)-2-nitrophenyl)methanol in $CDCl_3$ at 25 °C.

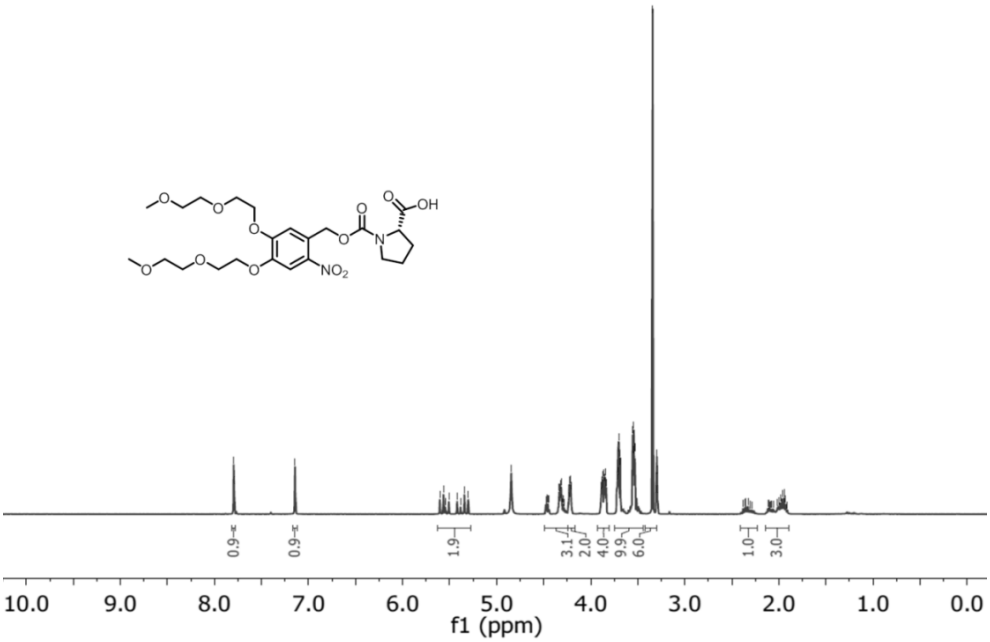

Figure **S3.23**: ^{1}H NMR spectrum of PP-**2** in CD_3OD at 25 °C.

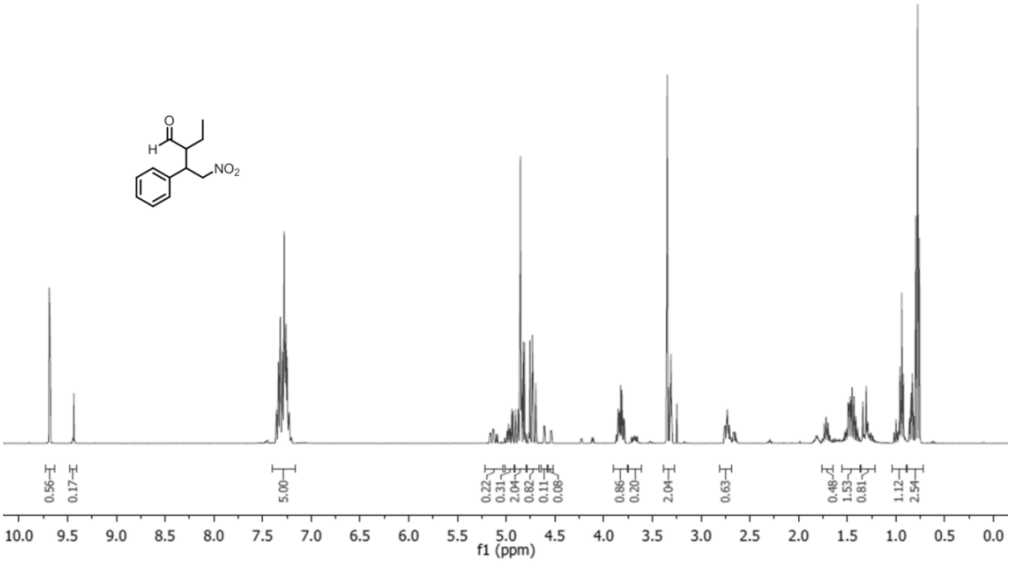

Figure S3.24: ^{1}H NMR spectrum of the Michael product **10** in CD_3OD.

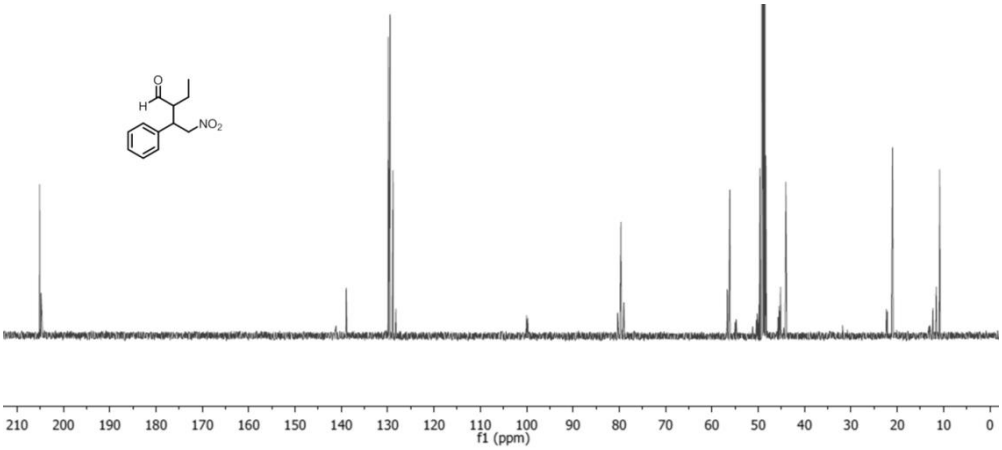

Figure S3.25: ^{13}C NMR spectrum of the Michael product **10** in CD_3OD.

Supplementary references

1. Chung, C., Srikun, D., Lim, C. S., Chang, C. J., Cho, B. R. A two-photon fluorescent probe for ratiometric imaging of hydrogen peroxide in live tissue. *Chem. Commun.* **47**, 9618-9620 (2011).
2. Takeuchi, Y., Yamada, A., Suzuki, T., Koizumi, T. Synthetic studies towards proline amide isosteres, potentially useful molecules for biological investigations. *Tetrahedron* **52**, 225-232 (1996).
3. Aitken, R. A., Karodia, N., Massil, T., Young, R. J. Flash vacuum pyrolysis of stabilised phosphorus ylides. Part 17.1 preparation of aliphatic amino acid derived [gamma]-alkoxycarbonylamino-[small beta]-oxo ylides and pyrolysis to give [small alpha],[small beta]-acetylenic [gamma]-amino acid and gaba analogues. *J. Chem. Soc., Perkin Trans. 1*, 533-541 (2002).
4. Poolman, J. M., Boekhoven, J., Besselink, A., Olive, A. G. L., van Esch, J. H., Eelkema, R. Variable gelation time and stiffness of low-molecular-weight hydrogels through catalytic control over self-assembly. *Nat. Protoc.* **9**, 977-988 (2014).
5. Machauer, R., Waldmann, H. Synthesis of lipidated enos peptides by combining enzymatic, noble metal- and acid-mediated protecting group techniques with solid phase peptide synthesis and fragment condensation in solution. *Chem. Eur. J.* **7**, 2940-2956 (2001).
6. Cordova, A., Notz, W., Barbas, III, C. F. Direct organocatalytic aldol reactions in buffered aqueous media. *Chem. Commun.*, 3024-3025 (2002).

Chapter 4
Reversible control over catalytic activity through host-guest chemistry

Control over the activity of catalysts is crucial to sustain living systems, as shown by allosteric enzyme regulation and G-protein coupled receptor signalling. Yet, such dynamic control is currently out of reach for artificial chemical systems. Here, inspired by responsive biocatalytic systems, we present a host-guest system to control the activity of synthetic organocatalysts. While molecular encapsulation is known to affect the reactivity of guest molecules, we here apply it to reversibly change the activity of organocatalysts. Using cucurbit[7]uril (CB[7]) we are able to decrease the catalytic activity of one organocatalyst whereas we induce an increase in activity of another catalyst. Addition of a stronger binding signal molecule liberates the catalysts and restores the catalytic activity to the original value. We can reversibly switch catalyst activity at any moment by addition of either host or competitive binder molecule. Adjusting the ratio of catalyst and CB[7] enables precise and predictable control over the rate of chemical bond formation, supported by experimental data and a kinetic model. Overall, molecular encapsulation proves a promising tool to control catalytic activity, constituting an important step towards signal response in artificial chemical systems.

This chapter is submitted as:

Trausel, F., van Rossum, S.A.P., Gerlings, H.H.P.J., Lovrak, M., van der Helm, M.P., Brevé, T., van Esch, J. H., Eelkema, R. *Reversible ontrol over catalyst activity by host-guest chemistry.*

4.1 Introduction

Central to living systems is the reversible activation of enzymes. There, small molecules (i.e. enzyme inhibitors, activators or signalling molecules) trigger enzyme (de)activation by non-covalent interactions, as is observed for allosteric enzyme regulation and G-protein coupled receptors.[1, 2] While these regulatory processes are an integral part of biocatalytic pathways, analogous man-made systems are rare and the activity of most artificial catalysts cannot be altered. At the same time, the focus in chemistry has shifted in recent years from purely static to dynamic systems engineering, starting with supramolecular chemistry 50 years ago.[3] Particularly, since the 90's molecular encapsulation has been exploited to change the reactivity of guest molecules.[4] As such, host-guest chemistry is used to stabilize guest-molecules to increase their lifetime and to enable safe handling of explosive or toxic compounds.[5, 6, 7] Other applications include supramolecular catalysis[8] and tuning the anti-cancer activity of drugs.[9]

A very popular family of supramolecular containers are cucurbiturils, which are generally non-toxic host molecules that bind strongly to a wide variety of guests in aqueous environments. Cucurbit[7]uril, a cyclic glycoluril heptamer that binds strongly to small neutral and cationic compounds, is commercially available and relatively soluble in water.[10, 11, 12] Cucurbituril (CB) binding can influence the reactivity of guests, changing oxidation potentials,[13, 14] decreasing chemical reactivity,[15, 16] or manipulating product distribution and stability,[17, 18] amongst many others. Building on the ability to drastically change the reactivity of certain guest molecules, we hypothesized that CB supramolecular encapsulation could also be used to change catalytic activity.

The use of host-guest chemistry to influence catalytic activity is of high interest because it would enable precise, reversible and responsive control over reaction rates by adjusting the amount of available host. Still, only few examples have been reported so far,[19, 20, 21, 22] including supramolecular catalysis with CB itself.[23, 24] Moreover, the effect of the host on the catalytic activity of the catalyst can be reversed by addition of a stronger binding guest that leads to release of the catalyst, creating a highly tuneable and responsive system.

Here we report a host-guest system in which we can reversibly change the catalytic activity of organocatalysts. Specifically, we designed a host-guest system of cucurbit[7]uril (CB[7])

that controls the catalytic activity of two different organocatalysts for hydrazone formation (Fig. 4.1). In this proof-of-concept, we focused on the reaction rate control of hydrazone formation, since this is a widely applied conjugation reaction, which takes place in aqueous buffer and is accelerated by a variety of organocatalysts.[25, 26]

4.2 Results

Choice of catalytic host-guest system

Based on the high binding affinity of CB[7] for positively charged small aromatic compounds, we found two organocatalysts for hydrazone formation that bind strongly to CB[7]: catalyst **1** (aniline) with a binding constant of $(1.85 \pm 0.156) \cdot 10^5$ M^{-1} and catalyst **2** (a benzimidazole-amine) with $(2.28 \pm 0.035) \cdot 10^5$ M^{-1} (Table 4.1). Accordingly, using 0.42 mM of CB[7] with 0.4 mM of either catalyst **1** or **2**, 99% of the catalysts is bound under the operating conditions. The amantadine·HCl super guest **3** has a binding constant to CB[7] of $(4.23 \pm 1.00) \cdot 10^{12}$ M^{-1}, which is seven orders of magnitudes higher (binding constant taken from the literature)[10] compared with catalyst **1** and **2**, meaning that **3** can thus effectively replace the catalysts by competitive binding. Furthermore, the reaction starting materials and product should not interfere with the catalytic host-guest system. Hence, aldehyde **4** and hydrazide **5** and the resulting hydrazone product **6** were chosen, as their binding constants to CB[7] are found to be negligible (Table 4.1).

a

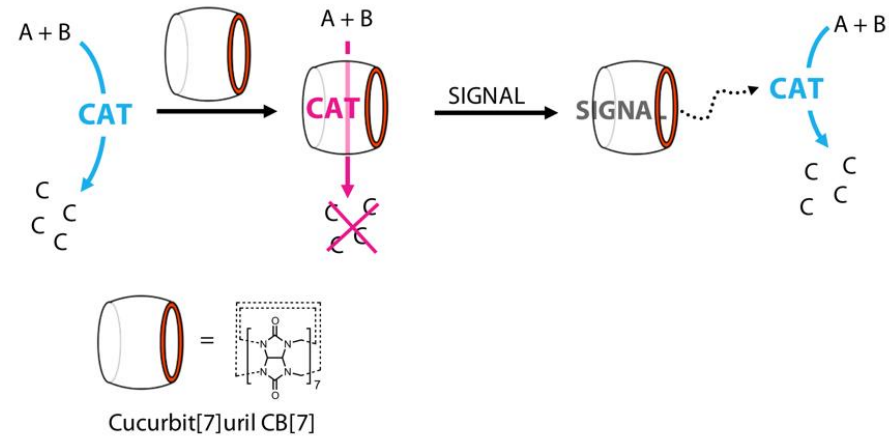

b

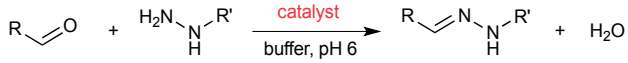

Figure 4.1: Using host-guest chemistry to control the activity of catalysts. (**a**) Schematic representation of cucurbit[7]uril (CB[7]) binding to the organocatalyst (cat), hindering its catalytic activity. Addition of the stronger binding signal leads to the release of the catalyst and restores its catalytic activity. (**b**) The hydrazone formation reaction between an aldehyde and hydrazide is catalysed by organocatalysts, such as catalysts **1** and **2** (Table 4.1).

Table 4.1: Binding constants measured by Isothermal Titration Calorimetry (ITC) of organocatalysts and reagents for hydrazone formation with CB[7] in 10 mM sodium phosphate buffer pH 6.0, 25 °C.

Compound	K_a (M^{-1})
 catalyst **1**	$(1.85 \pm 0.16) \cdot 10^5$
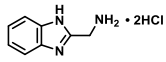 catalyst **2**	$(2.28 \pm 0.04) \cdot 10^5$
 super guest **3**	$(4.23 \pm 1.00) \cdot 10^{12}$*
 aldehyde **4**	<10
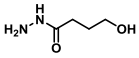 hydrazide **5**	<10
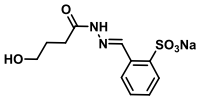 hydrazone product **6**	<10

*This value was taken from the literature.[10]

Control over catalyst activity

We investigated the influence of CB[7] on the activity of the catalysts by following the rate of a hydrazone reaction and comparing the reaction rate constants of the different systems (Table 4.2). Aldehyde **4** (0.4 mM) and hydrazide **5** (0.04 mM) react to form hydrazone **6** in aqueous buffer (10 mM sodium phosphate buffer pH 6.0) (Fig. 4.2a) and this reaction can be catalysed by catalyst **1** (Fig. 4.2b) or **2** (Fig. 4.2c). All reaction rate constants for the different systems were fitted with second-order rate equations (eq. 4.4, experimental section). As is apparent from Table 4.2, catalyst **1** (0.4 mM) increases the reaction rate 13-fold with respect to the uncatalysed reaction. A blank reaction with CB[7] (0.42 mM) alone increases the reaction rate 1.9-fold with respect to the uncatalysed reaction: this result indicates that the macrocycle shows a small catalytic activity towards the hydrazone reaction, even though the reagents and the product do not bind.[27] In contrast, addition of CB[7] (0.42 mM) to the reaction system with catalyst **1** (0.4 mM) gives a relative rate of 3.7: the host molecule decreases the reaction rate by a factor 3.5, thus effectively blocking

the catalytic activity of catalyst **1**. On top of that, hydrazone formation in the presence of CB[7] (0.42 mM), catalyst **1** (0.4 mM) and super guest **3** (0.8 mM) gives a relative reaction rate of 15: this shows that the super guest effectively replaces the catalyst by competitive binding with CB[7], restoring the catalytic activity of catalyst **1**. Noteworthy, the reaction rate in the presence of CB[7], catalyst **1** and super guest **3** is slightly higher than the reaction rate with only catalyst **1**. A reason might be that the catalytic activity of CB[7] adds up to the catalytic activity of catalyst **1**, leading to a higher reaction rate. Super guest **3** (0.8 mM) alone does not show any catalytic activity, while the reaction in the presence of CB[7] (0.42 mM) and super guest **3** (0.8 mM) gives a relative reaction rate of 1.3: when a guest occupies the cavity of CB[7] it does not reduce its catalytic activity completely. Compared to catalyst **1**, catalyst **2**[26] (0.4 mM) increases the reaction rate by 2.5-fold: the catalyst is less active than catalyst **1**. Surprisingly, the reaction in the presence of catalyst **2** (0.4 mM) and CB[7] (0.42 mM) gives a relative reaction rate of 7.5 which is 3-fold higher than the reaction rate with only catalyst **2**. Thus, whereas CB[7] encapsulation decreased the catalytic activity of catalyst **1**, it shows an opposite effect for catalyst **2** by increasing its activity. The origins of the increase in catalytic activity for catalyst **2** upon binding to CB[7] remain unclear. Next, addition of super guest **3** (0.8 mM) to the reaction with catalyst **2** (0.4 mM) and CB[7] (0.42 mM) gives a relative reaction rate of 2.3, restoring the catalytic activity of catalyst **2** to its original value. In essence, supramolecular encapsulation thus changes the catalytic activity of organocatalysts, which can be restored by competitive binding with another guest.

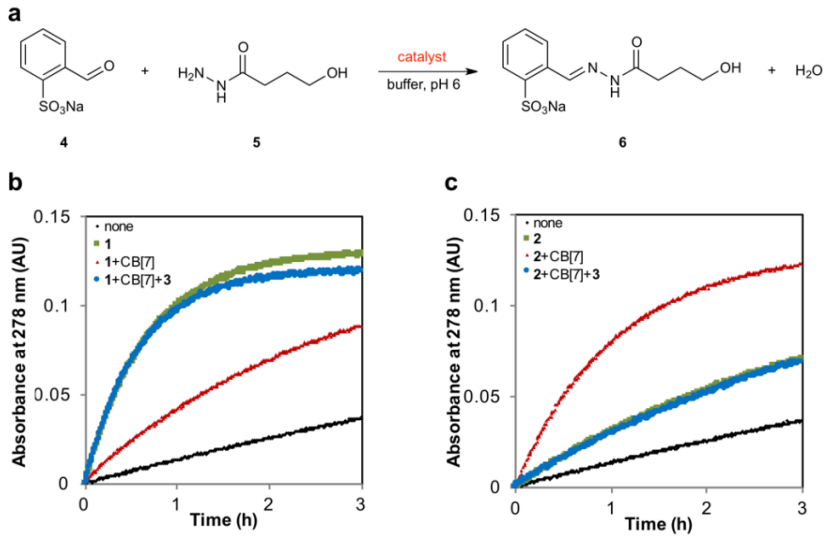

Figure 4.2: Using cucurbit[7]uril (CB[7]) to control hydrazone formation. Conditions: 0.4 mM aldehyde **4**, 0.040 M hydrazide **5**, 0.4 mM catalyst **1**, 0.4 mM catalyst **2**, 0.42 mM CB[7], 0.8 mM super guest **3** in 10 mM phosphate buffer pH 6.0, 25 °C. (**a**) Aldehyde **4** and hydrazide **5** react to form hydrazone **6**. (**b**) Absorbance of hydrazone product **6** followed over time without catalyst (black), with catalyst **1** (green), with catalyst **1** + CB[7] (red) and with catalyst **1** + CB[7] + super guest **3** (blue). (**c**) Absorbance of hydrazone product **6** followed over time without catalyst (black), with catalyst **2** (green), with catalyst **2** + CB[7] (red) and with catalyst **2** + CB[7] + super guest **3** (blue).

Table 4.2: Second order rate constants for the formation of hydrazone **6**. Conditions: 0.4 mM aldehyde **4**, 0.040 M hydrazide **5**, 0.4 mM catalyst **1**, 0.4 mM catalyst **2**, 0.42 mM CB[7], 0.8 mM super guest **3** in 10 mM sodium phosphate buffer pH 6.0, 25 °C. k_{rel} is the ratio of the rate constant of the reaction in the presence of catalyst, host and/or guest, and the rate constant of the uncatalysed reaction: $k_{rel} = k_{cat}/ k_{uncat}$.

Catalyst system	k **(M^{-1} s^{-1})**	k_{rel}
none	0.075 ± 0.002	1.0
CB[7]	0.14 ± 0.01	1.9
cat **1**	0.96 ± 0.03	13
cat **1** + CB[7]	0.28 ± 0.01	3.7
cat **1** + CB[7] + **3**	1.2 ± 0.03	15
3	0.073 ± 0.001	1.0
3 + CB[7]	0.095 ± 0.001	1.3
cat **2**	0.19 ± 0.01	2.5
cat **2** + CB[7]	0.57 ± 0.08	7.5
cat **2** + CB[7] + **3**	0.17 ± 0.004	2.3

In-situ control over catalytic activity

Based on our findings, we hypothesized that we should be able to change the reaction rate at any given time during the process, by adding CB[7] or by releasing the catalyst with super guest **3**. To do so, we determined the second-order reaction rate constants (in M^{-1} s^{-1}) using the Guggenheim time-lag method[28, 29, 30] before and after addition of CB[7] and super guest **3** respectively (Fig. 4.3a – b). Following the reaction with catalyst **1** (0.4 mM), and adding CB[7] (0.42 mM) after 10 minutes, we immediately observed a decrease in reaction rate (Fig. 4.3a). This result demonstrates that the host molecule very rapidly changes the activity of the catalyst upon binding. When after 20 minutes super guest **3** (0.8 mM) was added to the reaction with catalyst **1** (0.4 mM) and CB[7] (0.42 mM), the reaction rate increased again to the original value. Overall, the host CB[7] can thus be used to switch off catalyst **1**, and when super guest **3** is added, it switches the system back on again.

In contrast, catalyst **2** responds in a complete opposite way to encapsulation and release experiments. When CB[7] (0.42 mM) was added after 10 minutes of reaction time with catalyst **2** (0.4 mM), the reaction rate increased (Fig. 4.3b). Addition of super guest **3** (0.8 mM) immediately decreased the reaction rate again to the original value. CB[7] thus activates catalyst **2** and super guest **3** switches the system off again. Summarizing, addition of CB[7] or super guest **3** induces an immediate change in reaction rate: the system thus responds efficiently to chemical changes in the environment.

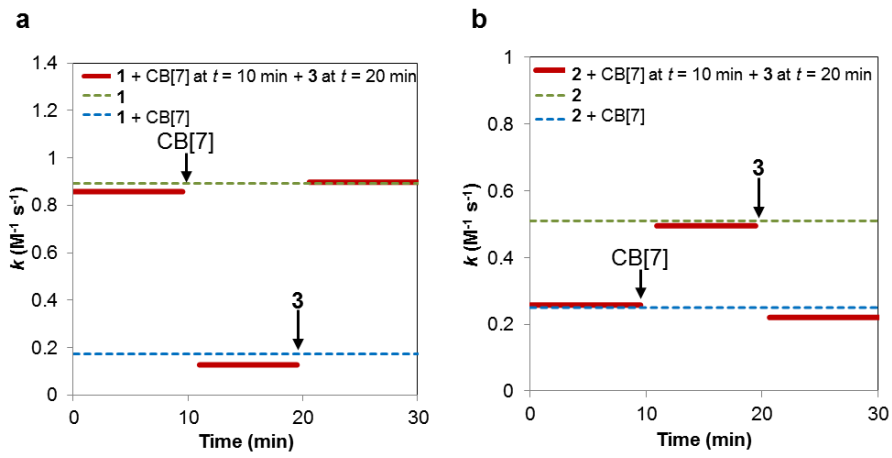

Figure 4.3: Using cucurbit[7]uril (CB[7]) to control hydrazone formation by reversibly binding to the catalyst. Conditions: 0.4 mM aldehyde **4**, 0.040 M hydrazide **5**, 0.4 mM catalyst **1**, 0.4 mM catalyst **2**, 0.42 mM CB[7], 0.8 mM super guest **3** in 10 mM phosphate buffer pH 6.0, 25 °C. The second-order reaction rate constants (M^{-1} s^{-1}) were determined using the Guggenheim time lag method.[28, 29] (a) The second-order reaction rate constant (M^{-1} s^{-1}) with catalyst **1**, CB[7] (0.42 mM) is added after 10 min and super guest **3** (0.8 mM) is added after 20 min (red line). For comparison, the second-order rate constant with catalyst **1** (green line) and the second-order rate constant with catalyst **1** and CB[7] (blue line). (b) The second-order reaction rate constant (M^{-1} s^{-1}) with catalyst **2**, CB[7] (0.42 mM) is added after 10 min and super guest **3** (0.8 mM) is added after 20 min (red line). For comparison, the second-order rate constant with catalyst **1** (green line) and the second-order rate constant with catalyst **1** and CB[7] (blue line).

Precise reaction rate control and predictive kinetic modelling

With the CB[7] responsive catalyst systems in hand, we wondered whether we could control the rate of hydrazone formation precisely by varying the ratio of [catalyst] versus [CB[7]]. We followed the reactions with different concentrations of catalyst **1**, catalyst **2** and CB[7] and determined the reaction rates constants experimentally (Figure 4.4, black dots). Additionally, we developed a kinetic model to predict the reaction rate constants (Figure 4.4, red lines). In the kinetic model we assumed that hydrazone formation occurred without catalyst (k_1), via organocatalysis (k_2), catalysed by CB[7] (k_3) and catalysed by the catalyst⊂CB[7] complex (k_4) (eq. 4.1, for more information see Supplementary Methods). We quantified how well the model fits the experimental values by determining the coefficients of determination R^2.[31]

$$k_{total} = k_1 + k_2 \cdot [cat] + k_3 \cdot [CB7] + k_4 \cdot [cat \subset CB7] \quad \text{(eq. 4.1)}$$

In Fig. 4.4a we kept the concentration of CB[7] (0.42 mM) constant and varied the concentration of catalyst **1**. When [**1**] > [CB[7]] the reaction rate increases linearly until at the highest concentration of catalyst **1** that was used (1.8 mM) the reaction rate is 25-fold higher than without catalyst **1**. The reaction rates are predicted well by the kinetic model of equation 1 with an R^2 value of 0.987. In Fig. 4.4b we kept the concentration of catalyst **1** (0.4 mM) constant and varied the concentration of CB[7]. The reaction rates decreased linearly with increasing CB[7] concentrations until the concentration of CB[7] exceeds the catalyst concentration: then the reaction rates level off and even increase slightly again. The model predicts the experimental data in Fig. 4.4b with an R^2 value of 0.971. The increase of the reaction rate at higher concentrations of CB[7] is caused by the catalytic activity of CB[7] itself. The kinetic model of equation 1 predicts the reactions rates well, indicating that the reaction rate constants are a linear combination of all processes taking place and thus CB[7] complexation allows for precise control over catalytic activity.

In Fig. 4.4c we kept the concentration of CB[7] (0.42 mM) constant and varied the concentration of catalyst **2**. With increasing concentration of catalyst **2** the reaction rates increase dramatically until, at a concentration of catalyst **2** of 1.8 mM, the reaction rate is 39-fold higher than without catalyst **2**. When we apply a similar model as for catalyst **1** using equation 1, model-eq. 4.1 shows a trend that is very different from the experimental data, with an R^2 value of -0.325. In Fig. 4.4d the concentration of catalyst **2** (0.4 mM) was kept constant and the concentration of CB[7] was varied. When the concentration of CB[7] is increased, the reaction rate increases exponentially. The kinetic model-eq. 4.1 cannot explain the exponential increase in reaction rate, with an R^2 value of 0.300. Even though the model predicts that the **2**⊂CB[7] complex has a higher catalytic activity than CB[7] and catalyst **2** separately, adding more CB[7] should only increase the reaction rate by the small catalytic activity of CB[7] itself, whereas the data show that the reaction rate increases drastically. Looking at the speciation, when [CB[7]] is held constant and we increase [**2**], $[CB[7]_{free}]$ goes to zero, while [**2**⊂CB[7] complex] reaches a plateau and [cat $\mathbf{2}_{free}$] keeps increasing linearly. The same accounts for the experiment where we keep [**2**] constant: when we increase [CB[7]], [cat $\mathbf{2}_{free}$] goes to zero, [**2**⊂CB[7] complex] reaches a plateau, but $[CB[7]_{free}]$ keeps increasing linearly. An explanation for the disproportionally large increase in reaction rates might be the existence of a synergistic effect between CB[7],

catalyst **2** and the **2**⊂CB[7] complex that leads to a higher catalytic activity than all species separately. In an attempt to incorporate this synergistic effect into the kinetic model, we extended our existing model with two extra rate constants: k_5 for CB[7] with the **2**⊂CB[7]-complex and k_6 for catalyst **2** with the **2**⊂CB[7]-complex (equation 2). In equation 2 we assume that the reaction rate increases linearly with an increasing concentration of the CB[7] in combination with the **2**⊂CB[7]-complex and that an increasing concentration of catalyst **2** with the **2**⊂CB[7]-complex also has a linear influence on the reaction rate.

$$k_{total} = k_1 + k_2 \cdot [cat] + k_3 \cdot [CB7] + k_4 \cdot [cat \subset CB7] + k_5 \cdot [CB7] \cdot [cat \subset CB7] + k_6 \cdot [cat] \cdot [cat \subset CB7] \quad \text{(eq. 4.2)}$$

Using the extended model-eq. 4.2 (green lines) we can predict the reaction rate constants for hydrazone formation with different concentrations of catalyst **2** and CB[7] better, with an R^2 value of 0.647. Model-eq. 4.2 predicts the reaction rates in Fig. 4.4d, where we increase the concentration of CB[7], with an R^2 value of 0.945 rather well, but in Fig. 4.4c, where the concentration of catalyst **2** is increased, the model still underestimates the reaction rates. These results might indicate that the increase of [**2**] to the reaction with the **2**⊂CB[7]-complex has a second-order influence on the reaction rate. To adjust for this second-order influence of catalyst **2**, we formulated equation 4.3.

$$k_{total} = k_1 + k_2 \cdot [cat] + k_3 \cdot [CB7] + k_4 \cdot [cat \subset CB7] + k_5 \cdot [CB7] \cdot [cat \subset CB7] + k_6 \cdot [cat]^2 \cdot [cat \subset CB7] \quad \text{(eq. 4.3)}$$

With model-eq. 4.3 the prediction of the reaction rates in both Fig. 4.4c and 4.4d is in much better agreement with the experimental data with R^2 values of respectively 0.855 and 0.997, which suggests that there is indeed a synergistic effect and a second-order influence of catalyst **2**.

In short we can control the reaction rates with high accuracy by only adjusting the CB[7] to catalyst ratio. For catalyst **1** we can predict the reaction rate for every ratio of catalyst and CB[7] with the kinetic model of equation 1 based on a linear relationship. However, for catalyst **2** we had to incorporate a quadratic dependence and take into account a synergistic effect that increases the catalytic activities, along model 3. In the future, it would be highly interesting to investigate this synergistic effect in more detail to establish the limits, utility and mechanism of this effect and to find out if other organocatalysts also show this behaviour.

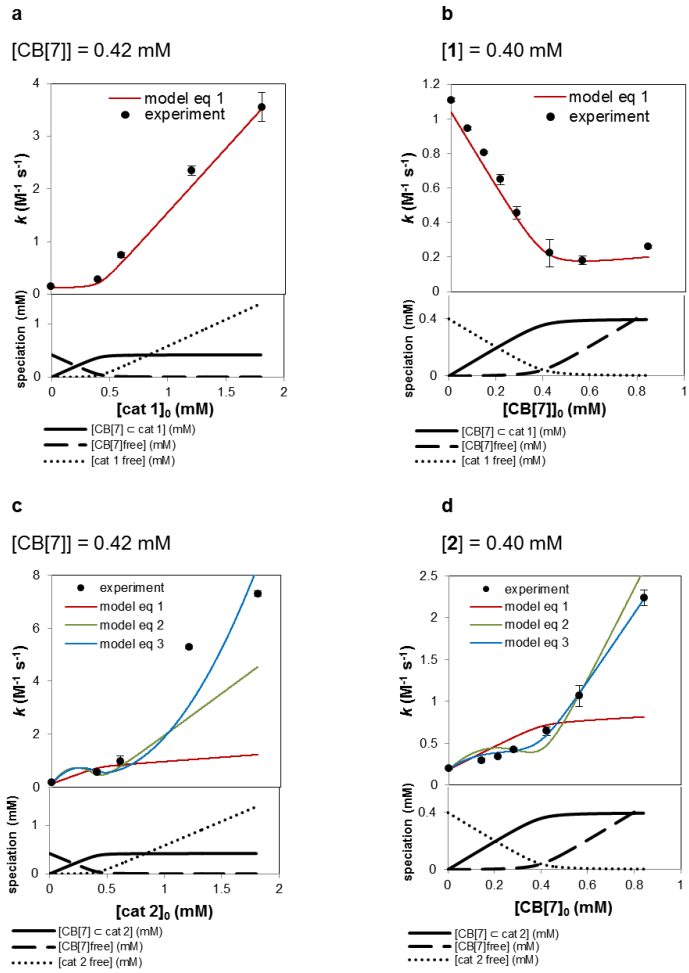

Figure 4.4: The rate of hydrazone formation can be controlled precisely by adjusting the ratio of CB[7] and catalyst. Conditions: 0.4 mM aldehyde **3**, 0.040 M hydrazide **4**, 0.4 mM catalyst **1**, 0.4 mM catalyst **2**, 0.42 mM CB[7] in 10 mM sodium phosphate buffer pH 6.0, 25 °C. Experimentally determined second-order rate constants (black dots), model-eq. 4.1 (red lines), model-eq. 4.2 (green lines), model-eq. 4.3 (blue lines). (**a**) The concentration of CB[7] is kept constant at 0.42 mM whereas the concentration of **1** is varied between 0 – 1.8 mM, R^2 between experimental data and model is 0.987. (**b**) The concentration of **1** is kept constant at 0.4 mM whereas the concentration of CB[7] is varied between 0 – 0.84 mM, R^2 between experimental data and model is 0.971. (**c**) The concentration of CB[7] is kept constant at 0.42 mM whereas the concentration of **2** is varied between 0 – 1.8 mM, R^2 between experimental data and model eq. 4.1 is -0.325, R^2 between experimental data and model eq. 4.2 is 0.647, R^2 between experimental data and model eq. 4.3 is 0.855. (**d**) The concentration of **2** is kept constant at 0.4 mM whereas the concentration of CB[7] is varied between 0 – 0.84 mM, R^2 between experimental data and model eq. 4.1 is 0.300, R^2 between experimental data and model eq. 4.2 is 0.945, R^2 between experimental data and model eq. 4.3 is 0.997.

4.3 Conclusions

In this work, we show that supramolecular encapsulation of organocatalysts with CB[7] is a powerful tool to reversibly change catalytic activity. Addition of a stoichiometric amount of CB[7] to catalyst **1** leads to an immediate 3.5-fold decrease and for catalyst **2** in a 3-fold increase in the rate of hydrazone formation. On top of that, by adjusting the ratio of catalyst and CB[7] we can precisely control the rate of hydrazone formation. Encapsulation and release experiments demonstrated that CB[7] hosts can be used to switch the catalytic activity of **1** off and addition of a stronger binding guest **3** restores the reaction rate back to the original value. Conversely, CB[7] increases the activity of catalyst **2** and addition of the stronger binding guest **3** switches the system off again. Additionally, the experimental data were supported by a kinetic model that accurately predicts the rate of hydrazone formation for different CB[7] and catalyst **1** concentrations. A linear kinetic model was, however, unable to predict hydrazone formation rates with catalyst **2** and CB[7]. Here, a non-linear quadratic model suggests a synergistic effect between CB[7], catalyst **2** and the **2**⊂CB[7]-complex to account for the disproportionally high increase in reaction rate.

From a future perspective, CB[7], having the advantageous property to bind strongly to a wide variety of compounds, as well as water-solubility and non-toxicity, is a promising candidate to control the activity of many other (organo)catalysts by applying different signals. Likewise, similar principles likely apply to many other hosts. For example, using CB[7], we are currently developing a mechanically-responsive system to modulate catalytic activity. Altogether, we designed a chemical signal responsive system where reversible CB[7] encapsulation enables tuneable control over organocatalytic activity, which proves a generic method for the control of catalyst activity. This responsive catalyst system is a step forward in the development of man-made systems that respond to chemical changes in the environment, as ubiquitously present in nature.

4.4 References

1. Monod, J., Changeux, J.-P., Jacob, F. Allosteric proteins and cellular control systems. *J. Mol. Biol.* **6**, 306-329 (1963).
2. Cornish-Bowden, A. Understanding allosteric and cooperative interactions in enzymes. *FEBS J.* **281**, 621-632 (2014).
3. Pedersen, C. J. Cyclic polyethers and their complexes with metal salts. *J. Am. Chem. Soc.* **89**, 2495-2496 (1967).
4. Quan, M. L. C., Cram, D. J. Constrictive binding of large guests by a hemicarcerand containing four portals. *J. Am. Chem. Soc.* **113**, 2754-2755 (1991).
5. Nishimura, N., Yoza, K., Kobayashi, K. Guest-encapsulation properties of a self-assembled capsule by dynamic boronic ester bonds. *J. Am. Chem. Soc.* **132**, 777-790 (2010).
6. Horng, Y.-C., Huang, P.-S., Hsieh, C.-C., Kuo, C.-H., Kuo, T.-S. Selective encapsulation of volatile and reactive methyl iodide. *Chem. Commun.* **48**, 8844-8846 (2012).
7. Galán, A., Gil-Ramírez, G., Ballester, P. Kinetic stabilization of n,n-dimethyl-2-propyn-1-amine n-oxide by encapsulation. *Org. Lett.* **15**, 4976-4979 (2013).
8. Zhang, Q., Tiefenbacher, K. Terpene cyclization catalysed inside a self-assembled cavity. *Nat. Chem.* **7**, 197 (2015).
9. Ahmedova, A*., et al.* M2l4 coordination capsules with tunable anticancer activity upon guest encapsulation. *Dalton Trans.* **45**, 13214-13221 (2016).
10. Liu, S., Ruspic, C., Mukhopadhyay, P., Chakrabarti, S., Zavalij, P. Y., Isaacs, L. The cucurbit[n]uril family: Prime components for self-sorting systems. *J. Am. Chem. Soc.* **127**, 15959-15967 (2005).
11. Isaacs, L. Cucurbit[n]urils: From mechanism to structure and function. *Chem. Commun.*, 619-629 (2009).
12. Barrow, S. J., Kasera, S., Rowland, M. J., del Barrio, J., Scherman, O. A. Cucurbituril-based molecular recognition. *Chem. Rev.* **115**, 12320-12406 (2015).
13. Eelkema, R., Maeda, K., Odell, B., Anderson, H. L. Radical cation stabilization in a cucurbituril oligoaniline rotaxane. *J. Am. Chem. Soc.* **129**, 12384-12385 (2007).
14. Liu, Y., Shi, J., Chen, Y., Ke, C. F. A polymeric pseudorotaxane constructed from cucurbituril and aniline, and stabilization of its radical cation. *Angew. Chem. Int. Ed. Engl.* **47**, 7293-7296 (2008).
15. Berbeci, L. S., Wang, W., Kaifer, A. E. Drastically decreased reactivity of thiols and disulfides complexed by cucurbit[6]uril. *Org. Lett.* **10**, 3721-3724 (2008).
16. Ren, H., Huang, Z., Yang, H., Xu, H., Zhang, X. Controlling the reactivity of the Se-Se bond by the supramolecular chemistry of cucurbituril. *ChemPhysChem* **16**, 523-527 (2015).
17. Barooah, N., Pemberton, B. C., Sivaguru, J. Manipulating photochemical reactivity of coumarins within cucurbituril nanocavities. *Org. Lett.* **10**, 3339-3342 (2008).
18. Choi, S., Park, S. H., Ziganshina, A. Y., Ko, Y. H., Lee, J. W., Kim, K. A stable cis-stilbene derivative encapsulated in cucurbit[7]uril. *Chem. Commun.*, 2176-2177 (2003).

19. Tonga, G. Y.*, et al.* Supramolecular regulation of bioorthogonal catalysis in cells using nanoparticle-embedded transition metal catalysts. *Nat. Chem.* **7**, 597-603 (2015).
20. Gupta, A., Das, R., Yesilbag Tonga, G., Mizuhara, T., Rotello, V. M. Charge-switchable nanozymes for bioorthogonal imaging of biofilm-associated infections. *ACS Nano* **12**, 89-94 (2018).
21. Aleman Garcia, M. A., Hu, Y., Willner, I. Switchable supramolecular catalysis using DNA-templated scaffolds. *Chem. Commun.* **52**, 2153-2156 (2016).
22. Beswick, J., Blanco, V., De Bo, G., Leigh, D. A., Lewandowska, U., Lewandowski, B., Mishiro, K. Selecting reactions and reactants using a switchable rotaxane organocatalyst with two different active sites. *Chem. Sci.* **6**, 140-143 (2015).
23. Klöck, C., Dsouza, R. N., Nau, W. M. Cucurbituril-mediated supramolecular acid catalysis. *Org. Lett.* **11**, 2595-2598 (2009).
24. Pemberton, B. C., Raghunathan, R., Volla, S., Sivaguru, J. From containers to catalysts: Supramolecular catalysis within cucurbiturils. *Chem. Eur. J.* **18**, 12178-12190 (2012).
25. Crisalli, P., Kool, E. T. Water-soluble organocatalysts for hydrazone and oxime formation. *J. Org. Chem.* **78**, 1184-1189 (2013).
26. Larsen, D., Pittelkow, M., Karmakar, S., Kool, E. T. New organocatalyst scaffolds with high activity in promoting hydrazone and oxime formation at neutral ph. *Org. Lett.* **17**, 274-277 (2015).
27. Palma, A., Artelsmair, M., Wu, G., Lu, X., Barrow, S. J., Uddin, N., Rosta, E., Masson, E., Scherman, O. A. Cucurbit[7]uril as a supramolecular artificial enzyme for diels–alder reactions. *Angew. Chem. Int. Ed. Engl.* **56**, 15688-15692 (2017).
28. Guggenheim, E. A. Xlvi. On the determination of the velocity constant of a unimolecular reaction. *Philos. Mag.* **2**, 538-543 (1926).
29. Hemalatha, M. R. K., Noorbatcha, I. An undergraduate physical chemistry experiment on the analysis of first-order kinetic data. *J. Chem. Educ.* **74**, 972 (1997).
30. Trausel, F., Fan, B., van Rossum, S. A. P.., van Esch J. H., Eelkema, R. Aniline catalysed hydrazone formation reactions show a large variation in reaction rates and catalytic effects. *Adv. Synth. Catal.*, (2018).
31. Magee, L. R2 measures based on wald and likelihood ratio joint significance tests. *Am. Stat.* **44**, 250-253 (1990).

4.5 Supplementary information

Experimental details

General information

NMR spectra were recorded on an Agilent-400 MR DD2 (400 MHz for ^{1}H and 100.5 MHz for ^{13}C) at 298 K using residual protonated solvent signals as internal standard (D_2O: ^{1}H δ = 4.79, ^{13}C in D_2O was referenced to internal dioxane, δ = 67.19). UV/Vis spectroscopic measurements were performed on an Analytik Jena Specord 250 spectrophotometer; quartz cuvettes with a path length of 0.2 cm were used. Measurements were carried at a controlled temperature of 25 °C. Isothermal titration calorimetry (ITC) measurements were carried out at 25 °C using a MicroCal VP-ITC. Kinetic modelling was done using Matlab 2016.

Materials

All compounds and solvents were used without further purification. The technical solvents were purchased from VWR and the reagent grade solvents were purchased from Sigma Aldrich. Aniline **1** and catalyst **2** were purchased from Sigma Aldrich. Aldehyde **3** was purchased from Honeywell Fluka Fischer Scientific. Hydrazide **4** was purchased from Alfa Aesar. Cucurbit[7]uril was purchased from Strem Chemicals Inc., based on the kinetic model and ITC measurements we estimated that it contained 30 wt% hydration water ($C_{42}H_{42}N_{28}O_{14} \cdot xH_2O$ (x = 28)).

Synthesis of hydrazone 6

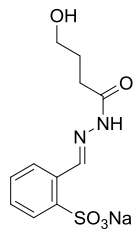

6

Aldehyde **4** (200 mg, 0.961 mmol) was added to a solution of hydrazide **5** (114 mg, 0.961 mmol) in absolute ethanol (6 mL). Glacial acetic acid (3 drops) was added and the reaction mixture was stirred overnight at room temperature, until complete conversion of the aldehyde was confirmed by NMR. The solvent was evaporated under reduced pressure to afford the pure hydrazone **6** product as a white powder (235 g, 0.763 mmol, 79.4%). Extra splitting of the peaks in the NMR spectrum is due to cis and trans isomers. **^{1}H NMR** (400 MHz, D_2O) δ 8.95 (s, 1H), 8.14 (d, 2H, *J* = 7.5

Hz), 7.96 (d, 2H, J = 7.7 Hz), 7.63 (m, 2H), 3.66 (t, 2H, J = 6.5 Hz), 2.46 (t, 2H, J = 7.5 Hz), 1.92 (m, 2H). **^{13}C NMR** (100.5 MHz, D_2O) δ 173.7, 148.2, 142.1, 132.4, 130.9, 130.8, 128.0, 127.6, 61.4, 31.2, 28.1. **MS** (ESI Neg.) m/z: 285.0 [$(M\text{-}Na^{+})^{-}$] (expected m/z = 285.05). **Extinction coefficient** in phosphate buffer (10 mM, pH 6.0): (2.03 ± 0.003) 10^4 M^{-1} cm^{-1} at 287 nm.

UV/vis measurements of hydrazone reactions

Extinction coefficient of hydrazone 6

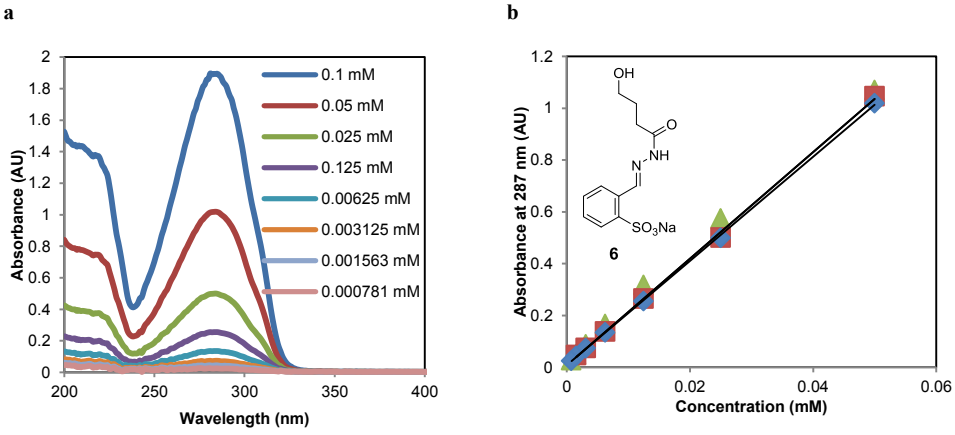

Figure S4.1: Extinction coefficient for hydrazone **6** at 287 nm: (2.03 ± 0.003) 10^4 M^{-1} cm^{-1}, error is the standard error of the mean (n = 3). (**a**) UV/vis spectra of hydrazone **6** at different concentrations. (**b**) Absorbance at 287 nm of hydrazone **6** at different concentrations, the experimental data of 3 experiments are shown.

Fitting second-order reaction rates

The second-order reaction rate constants were determined by fitting the relative absorbance (At – A0) over time with the following equation:

$$A = \frac{A_{max} \cdot e^{([H]_0 - [B]_0) \cdot kt} - A_{max}}{\frac{[H]_0}{[B]_0} \cdot e^{([H]_0 - [B]_0) \cdot kt} - 1} \qquad \text{(eq. S4.1)}^{1}$$

$[H]_0$ = concentration of hydrazide **3** at t = 0, $[B]_0$ = concentration of aldehyde **4** at t = 0, A_{max} = the maximum absorbance (when all **3** is converted), k is the second order reaction rate constant (M^{-1} s^{-1}).

a

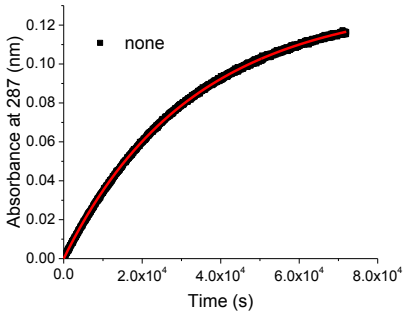
none
Absorbance at 287 (nm)
Time (s)
0.00
0.02
0.04
0.06
0.08
0.10
0.12
0.0
2.0x10^4
4.0x10^4
6.0x10^4
8.0x10^4

b

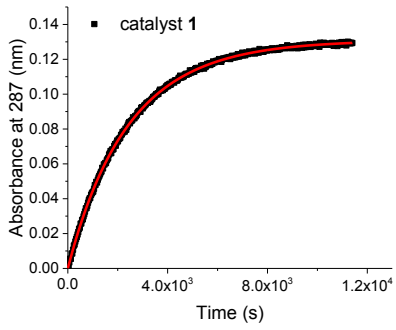
catalyst 1
Absorbance at 287 (nm)
Time (s)
0.00
0.02
0.04
0.06
0.08
0.10
0.12
0.14
0.0
4.0x10^3
8.0x10^3
1.2x10^4

c

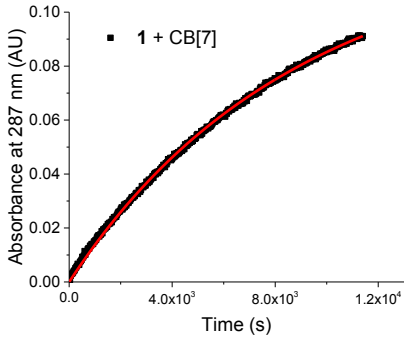
1 + CB[7]
Absorbance at 287 nm (AU)
Time (s)
0.00
0.02
0.04
0.06
0.08
0.10
0.0
4.0x10^3
8.0x10^3
1.2x10^4

d

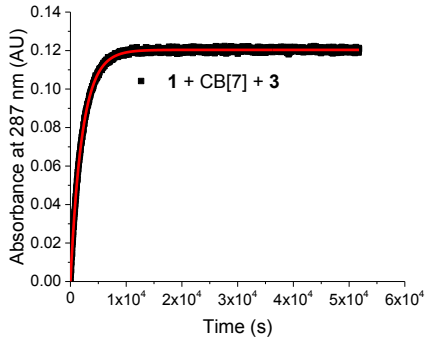
1 + CB[7] + 3
Absorbance at 287 nm (AU)
Time (s)
0.00
0.02
0.04
0.06
0.08
0.10
0.12
0.14
0
1x10^4
2x10^4
3x10^4
4x10^4
5x10^4
6x10^4

e

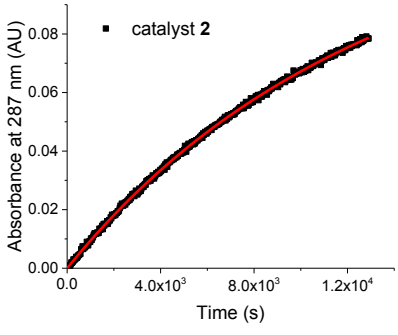
catalyst 2
Absorbance at 287 nm (AU)
Time (s)
0.00
0.02
0.04
0.06
0.08
0.0
4.0x10^3
8.0x10^3
1.2x10^4

f

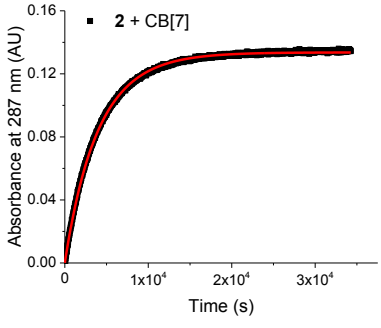
2 + CB[7]
Absorbance at 287 nm (AU)
Time (s)
0.00
0.04
0.08
0.12
0.16
0
1x10^4
2x10^4
3x10^4

g

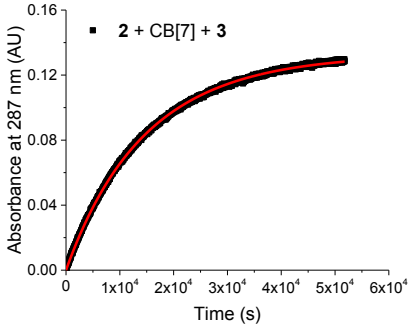

Figure S4.2: Fits of relative absorbance followed at 287 nm of the hydrazone reactions. Experimental data: black squares, fit: red lines. Reaction conditions: 0.4 mM aldehyde **4**, 0.040 M hydrazide **5**, 0.4 mM catalyst **1**, 0.4 mM catalyst **2**, 0.42 mM CB[7], 0.8 mM super guest **3** in 10 mM phosphate buffer pH 6.0, 25 °C. (**a**) Uncatalysed reaction, (**b**) reaction with catalyst **1**, (**c**) reaction with CB[7] + **1**, (**d**) reaction with **1** + CB[7] + **3**, (**e**) reaction with catalyst **2**, (**f**) reaction with **2** + CB[7], (**g**) reaction with **2** + CB[7] + **3**.

Isothermal titration calorimetry results

General procedure: a solution of catalyst **1**, catalyst **2** or super guest **3** (10 mM) was titrated to the CB[7] (0.35 mM) solution at 25 °C. The first titration point of each ITC measurement was omitted. Binding constants are fitted with Microcal LLC ITC Origin 7 software.

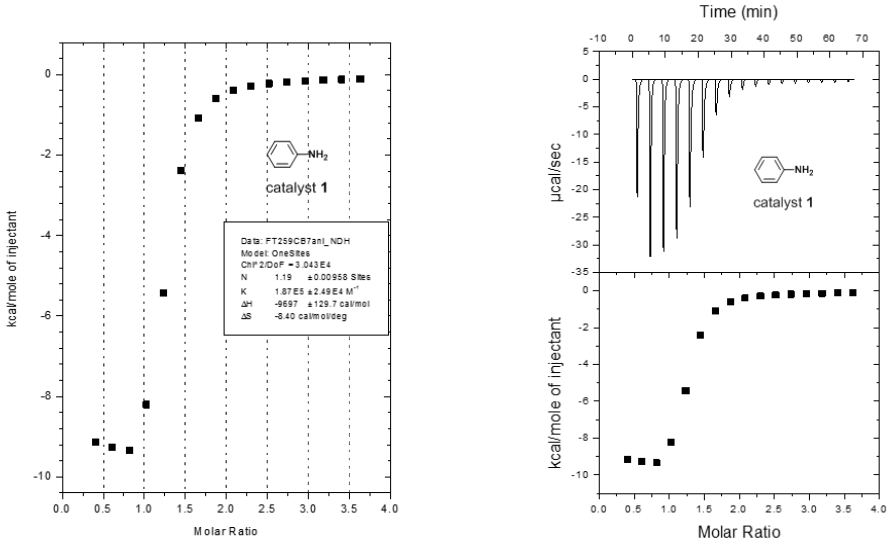

Figure S4.3: ITC measurements for catalyst **1**. Found K_a (1.85 ± 0.16) · 10^5 M^{-1}, error is the standard error of the mean, n = 3.

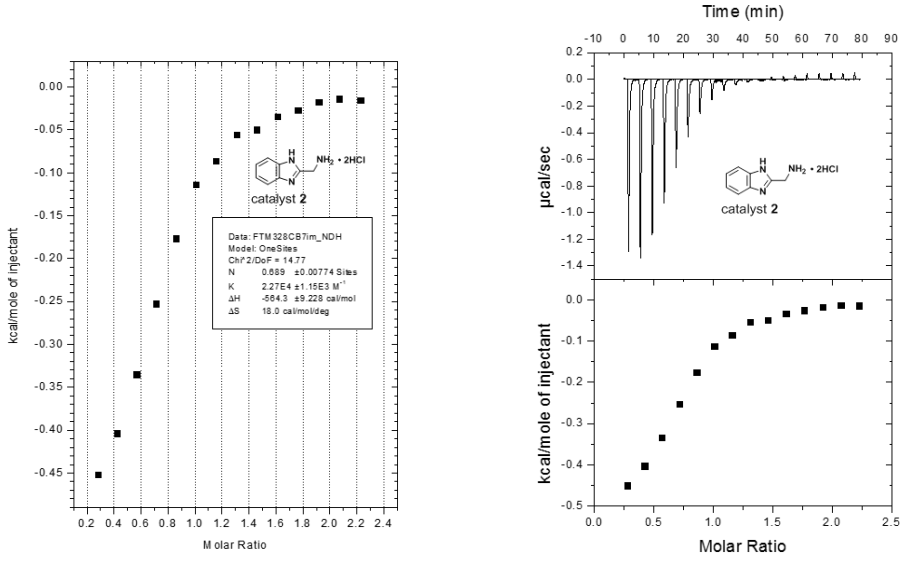

Figure S4.4: ITC measurements for catalyst **2**. Found K_a (2.28 ± 0.04) · 10^5 M^{-1}, error is the standard error of the mean, n = 3.

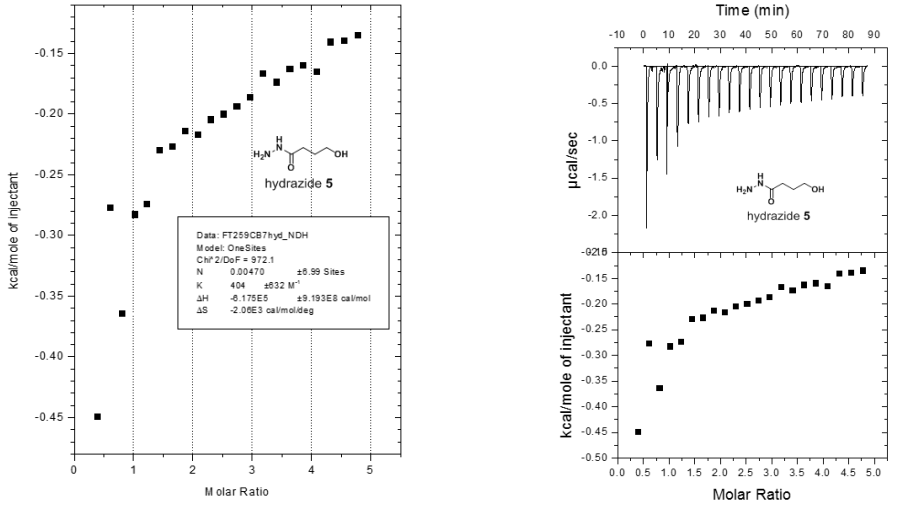

Figure S4.5: ITC measurements for hydrazide **5**. The binding constant was too low to determine.

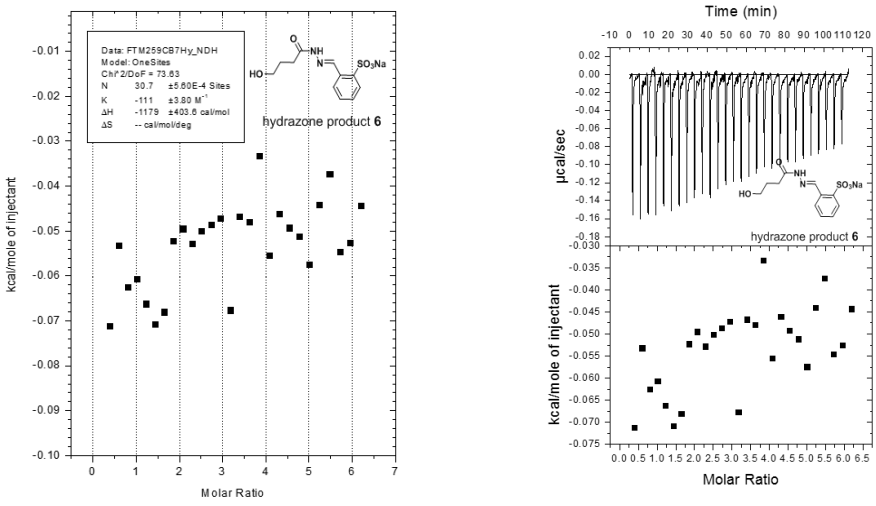

Figure S4.6: ITC measurements for hydrazide **5**. The binding constant was too low to determine.

The binding constant of aldehyde **4** was determined with a titration experiment using UV/vis spectroscopy, because the ITC was temporarily unavailable. We used to following equation to find the binding constant:

$$A = \{\varepsilon_G \cdot b + \frac{\varepsilon_{HG} \cdot b \cdot K \cdot [H]_t}{1+0.5 \cdot \{-(1-K \cdot [G]_t + K \cdot [H]_t) + \sqrt{(1-K \cdot [G]_t + [H]_t)^2 + 4 \cdot K \cdot [G]_t}\}}\} \times \frac{-1 \cdot (1-K \cdot [G]_t + K \cdot [H]_t) + \sqrt{(1-K \cdot [G]_t + K \cdot [H]_t)^2 + 4 \cdot K \cdot [G]_t}}{2 \cdot K} \quad \text{(eq. S4.2)}^2$$

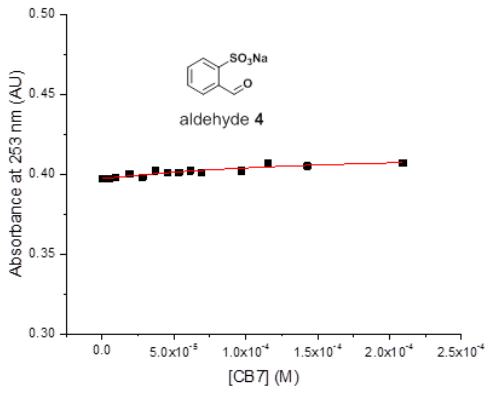

Parameter	Value	Standard error
K_a (M^{-1})	7963.928	7373.09
eHG	9411.579	164.9886
eG	9023.305	17.83858
b	1	0
Gt	4.40E-05	0

Figure S4.7: UV/vis titration measurement to determine the binding constant of aldehyde **4** with CB[7]. The binding constant was too low to determine.

Kinetic model

Explanation kinetic model

We assumed that the hydrazone reaction between hydrazide **4** and aldehyde **5** to form hydrazone **6** is first order in each reactant. We took into account the catalytic influence of the catalyst, of CB[7] and of the catalyst⊂CB[7]-complex. Therefore we proposed the following rate equations for the reactions with catalyst and CB[7]:

$$\frac{d[A]}{dt} = -k_1[A][H] - k_2[A][H][cat] - k_3[A][H][CB7] - k_4[A][H][cat \subset \text{CB7}] \quad \text{(eq. S4.3)}$$

$$\frac{d[H]}{dt} = -k_1[A][H] - k_2[A][H][cat] - k_3[A][H][CB7] - k_4[A][H][cat \subset \text{CB7}] \quad \text{(eq. S4.4)}$$

$$\frac{d[P]}{dt} = k_1[A][H] + k_2[A][H][cat] + k_3[A][H][CB7] + k_4[A][H][cat \subset \text{CB7}] \quad \text{(eq. S4.5)}$$

Here, $\frac{d[P]}{dt}$ is the formation of hydrazone product **6** over time, $[A]$ is the concentration of aldehyde **4**, $[H]$ is the concentration of hydrazide **5**, $[cat]$ is the concentration catalyst **1** or catalyst **2** free in solution (not bound to CB[7]), $[CB7]$ is the concentration CB[7] free in solution (not bound to the catalyst) and $[cat \subset \text{CB7}]$ is the concentration of the catalyst⊂CB[7]-complex, which was determined using the binding constant of the catalyst with CB[7], k_1 is the rate constant of the uncatalysed reaction, k_2 the rate constant for the reaction catalysed by catalyst **1** or catalyst **2**, k_3 is the rate constant for the reaction catalysed by CB[7] and k_4 is the rate constant for the reaction catalysed by the catalyst⊂CB[7]-complex.

The equilibrium concentrations of CB[7], catalyst and the catalyst⊂CB[7]-complex were calculated using the initial, change, equilibrium Table S4.1.

Table S4.1: Initial, change, equilibrium table to calculate the concentration of CB[7] free in solution, catalyst free in solution and catalyst⊂CB[7]-complex.

	[CB[7]]	**[cat]**	**[cat ⊂ CB[7]]**
Initial	a	b	0
Change	−x	−x	x
Equilibrium	a−x	b−x	x

$$K_a = \frac{[cat \subset \mathrm{CB7}]}{[CB7][cat]} \quad \text{(eq. S4.6)}$$

we substituted (4) with the results from table S4.1: $c = \frac{x}{(a-x)(b-x)}$ (eq. S4.7)

Here, a = $CB[7]_0$ (concentration of CB[7] that was added to the reaction mixture), b = cat_0 (concentration of catalyst **1** or **2** that was added to the reaction mixture), c = K_a (binding constant of catalyst **1** ($(1.85 \pm 0.156) \cdot 10^5$ M^{-1}) or **2** ($(2.28 \pm 0.035) \cdot 10^5$ M^{-1}) to CB[7], x = [catalyst⊂CB[7]].

Solving (6) for x gives the concentration of [catalyst⊂CB[7]]:

$$[cat \subset \mathrm{CB7}] = \frac{a \cdot c + b \cdot c + 1 - \sqrt{a^2 \cdot c^2 - 2 \cdot a \cdot b \cdot c^2 + b^2 \cdot c^2 + 2 \cdot a \cdot c + 2 \cdot b \cdot c + 1}}{2 \cdot c} \quad \text{(eq. S4.8)}$$

$$[CB7] = CB7_0 - cat \subset \mathrm{CB7} \quad \text{(eq. S4.9)}$$

$$[cat] = cat_0 - cat \subset \mathrm{CB7} \quad \text{(eq. S4.10)}$$

Here $[CB7]$ is again the concentration CB[7] free in solution (not bound to the catalyst), $[cat]$ is the concentration of catalyst free in solution (not bound to CB[7]).

Because we followed the reaction by measuring the absorbance of the reaction mixture over time, we had to calculate the concentrations of the product using the following equation:

$$[P] = \frac{A - \varepsilon_A \cdot l \cdot [A]_0 - \varepsilon_{cat} \cdot l \cdot [cat]}{\varepsilon_P \cdot l - \varepsilon_A \cdot l} \quad \text{(eq. S4.11)}$$

Here, $[P]$ is the concentration product, A is the absorbance of the reaction mixture, ε_A is the extinction coefficient at the rate analysis wavelength of 287 nm of aldehyde **4** (1423.6 (± 5.5) M^{-1} cm^{-1}), ε_{cat} is the extinction coefficient of the catalyst (for catalyst **1** 1081.5 (± 50)

M^{-1} cm^{-1} and for catalyst **2** 314.0 (± 9.2) M^{-1} cm^{-1}), ε_P is the extinction coefficient of hydrazone **6** (20296 (±301) M^{-1} cm^{-1}), l is the path length (0.2 cm).

We found k_1 using the uncatalysed hydrazone reaction and performing a least-square error analysis in Matlab to find the best fit for k_1. Similarly, k_2 was found by fitting the reaction in the presence of catalyst, k_3 was found using the reaction in the presence of CB[7] and k_4 was found for the reactions with CB[7] and catalyst.

Results for catalyst 1

a

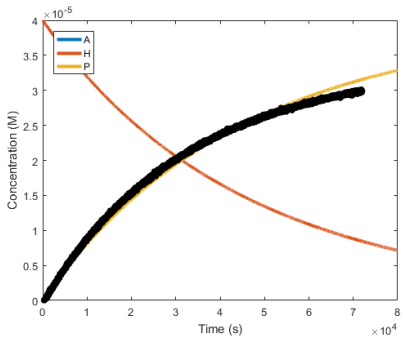

b

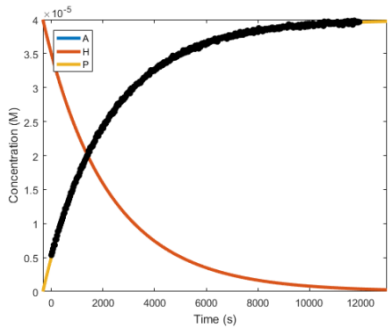

c

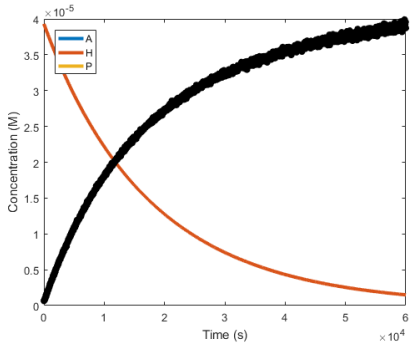

d

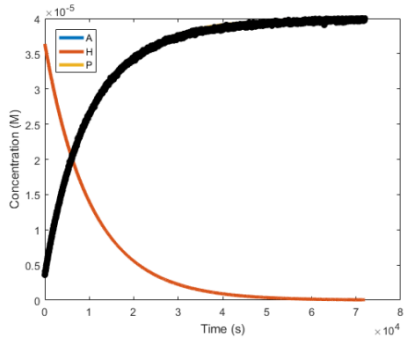

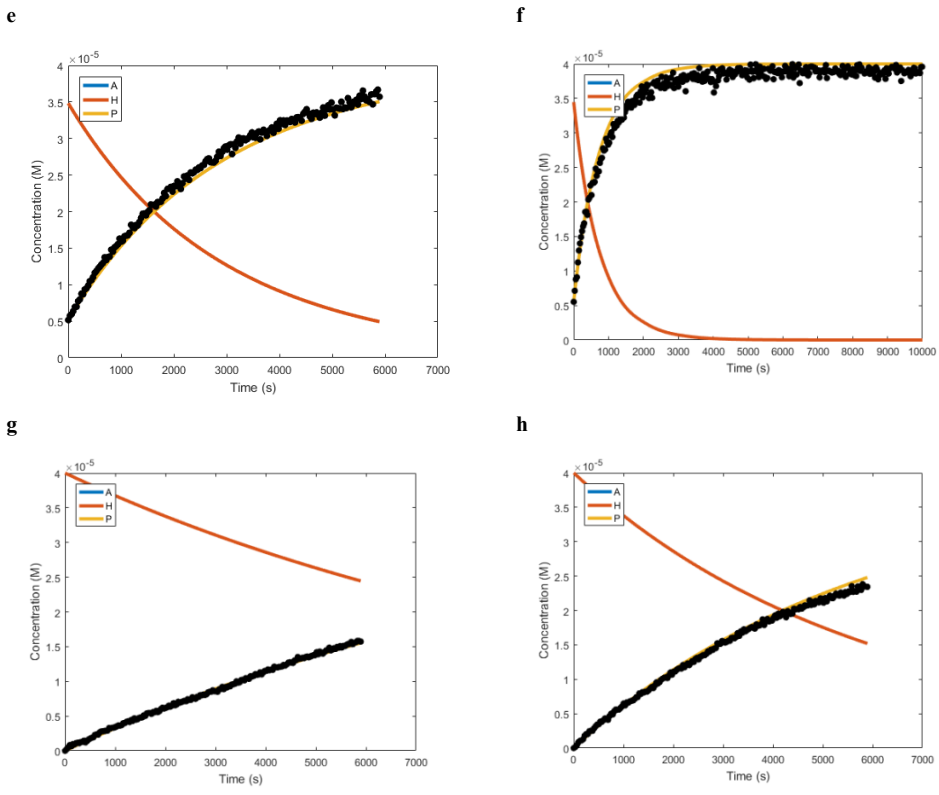

Figure S4.8: Best fits found with a least square error fit with Matlab for the concentration profiles of the formation of hydrazone **6** (black dots) compared with the kinetic model (product **6**: yellow line, aldehyde **4**: blue line (not visible because of the scale), hydrazide **5**: red line). Reaction conditions: 0.4 mM aldehyde **4**, 0.040 M hydrazide **5** in 10 mM phosphate buffer pH 6.0, 25 °C. (**a**) Uncatalysed reaction, (**b**) reaction with catalyst **1**, (**c**) reaction with CB[7], (**d**) reaction used to fit k_4 with CB[7] (0.84 mM) and catalyst **1** (0.4 mM), (**e**) with CB[7] (0.07 mM) and catalyst **1** (0.4 mM), (**f**) with CB[7] (0.42 mM) and catalyst **1** (1.8 mM), (**g**) with CB[7] (0.42 mM) and catalyst **1** (0.4 mM), (**h**) with CB[7] (0.28 mM) and catalyst **1** (0.4 mM).

Table S4.2: Partial reaction rate constants found with least-square error optimization fits in Matlab for catalyst **1**.

Catalyst system	**Rate constant**	**Best fit for**
None	k_1	0.0568 M^{-1} s^{-1}
Catalyst **1**	k_2	2.46 · 10^3 M^{-2} s^{-1}
CB[7]	k_3	150 M^{-2} s^{-1}
[**1**⊂CB[7]]	k_4	166 M^{-2} s^{-1}

The resulting values that were found for k_1, k_2, k_3 and k_4 were used to calculate the total reaction rate constants:

$$k_{total} = k_1 + k_2 \cdot [cat] + k_3 \cdot [CB7] + k_4 \cdot [cat \subset \mathrm{CB7}] \quad \text{(eq. 4.1)}$$

How well the model fits the experimental values was quantified by determining the coefficient of determination R^2.[3] When [CB[7]] is kept constant, the model fits the experimental data with an R^2 of 0.987. When [**2**] is kept constant, the model fits the experimental data with an R^2 of 0.971. These high values (close to unity) show that the model predicts the experimental data accurately.

a

[CB[7]] = 0.42 mM

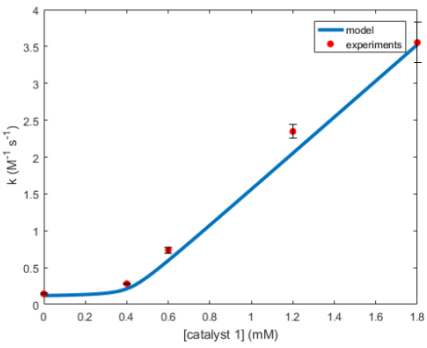

b

[**1**] = 0.4 mM

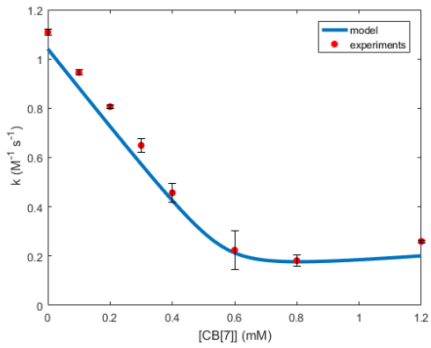

c

[CB[7]] = 0.42 mM

[**1**] = 0.4 mM

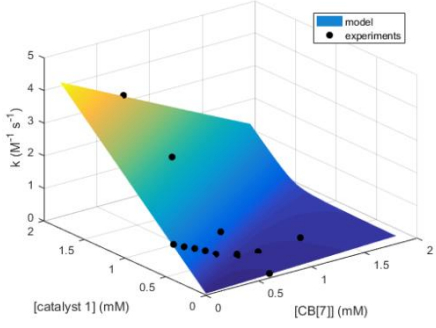

Figure S4.9: Kinetic model defined by eq. 4.1 fits total reaction rate constants for different concentrations of CB[7] and catalyst **1**. (a) 0.42 mM CB[7], 0 – 1.8 mM catalyst **1**, the model fits the experimental values with an R^2 of 0.987. (**b**) 0.4 mM catalyst **1**, 0 – 0.84 mM CB[7], the model fits the experimental values with an R^2 of 0.971. (**c**) 0 – 1.8 mM catalyst **1**, 0 – 0.84 mM CB[7].

Results for catalyst 2

For catalyst **2** we were not able to find a k_4 that can fit the reaction for different ratios of catalyst **2** and CB[7].

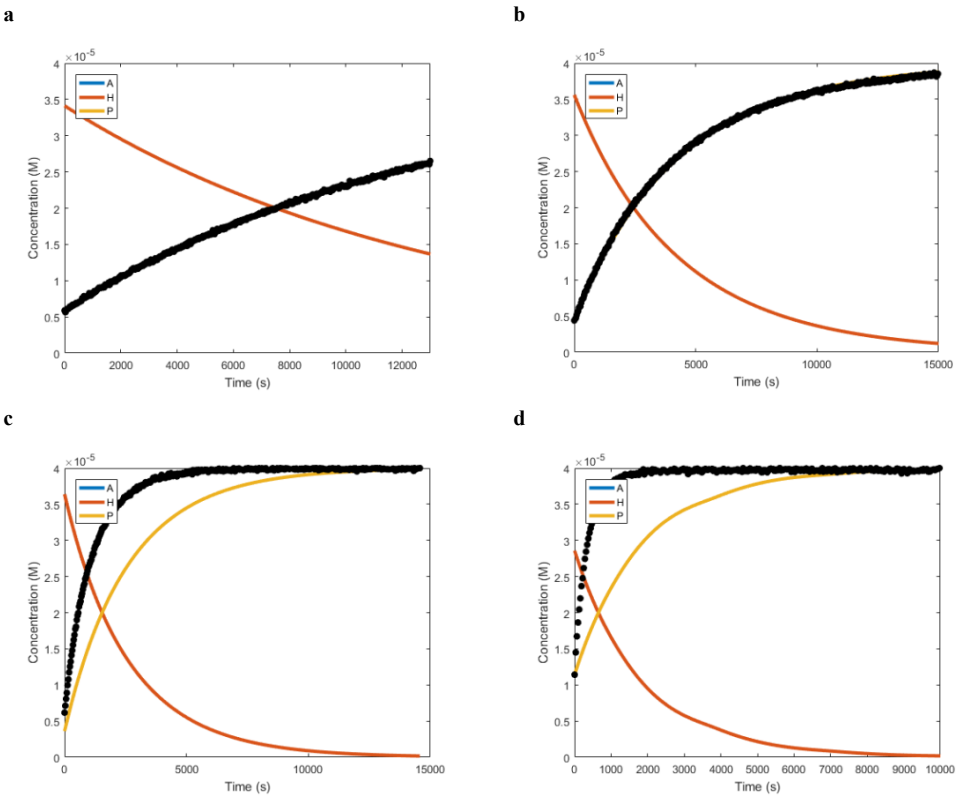

Figure S4.10: Best fits found with a least square error fit with Matlab for the concentration profiles of the formation of hydrazone **6** (black dots) compared with the kinetic model (product **6**: yellow line, aldehyde **4**: blue line (not visible because of the scale), hydrazide **5**: red line). Reaction conditions: 0.4 mM aldehyde **4**, 0.040 M hydrazide **5** in 10 mM phosphate buffer pH 6.0, 25 °C. (**a**) reaction with catalyst **2**, (**b**) reaction used to fit k_4 with CB[7] (0.42 mM) and catalyst **2** (0.4 mM), (**c**) reaction with CB[7] (0.84 mM) and catalyst **2** (0.4 mM), (**d**) reaction with CB[7] (0.42 mM) and catalyst **2** (1.8 mM).

Table S4.3: Partial reaction rate constants found with least-square error optimization fits in Matlab for catalyst **2**.

Catalyst system	Rate constant	Best fit for
None	k_1	0.0568 M^{-1} s^{-1}
Catalyst **2**	k_2	318 M^{-2} s^{-1}
CB[7]	k_3	150 M^{-2} s^{-1}
[**2**⊂CB[7]]	k_4	$1.52 \cdot 10^3$ M^{-2} s^{-1}*

*This value is only valid when we use 0.42 mM CB[7] and 0.4 mM [**2**]

The resulting values that were found for k_1, k_2, k_3 and k_4 were again used to calculate the total reaction rate constants:

$$k_{total} = k_1 + k_2 \cdot [cat] + k_3 \cdot [CB7] + k_4 \cdot [cat \subset \mathrm{CB7}] \quad \text{(eq. 4.1)}$$

When [CB[7]] is kept constant, the model fits the experimental data with an R^2 of -0.325. When [**2**] is kept constant, the model fits the experimental data with an R^2 of 0.300. This shows that the model does not describe the experimental data.

a

[CB[7]] = 0.42 mM

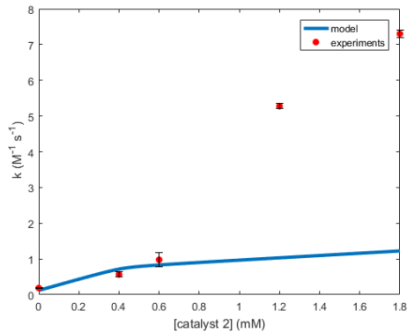

b

[**2**] = 0.40 mM

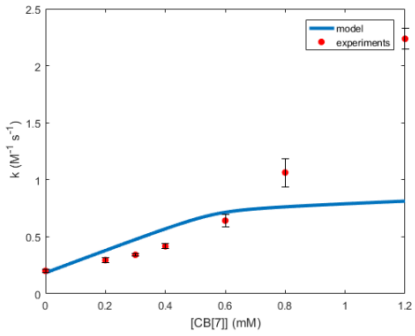

c

[CB[7]] = 0.42 mM

[**2**] = 0.4 mM

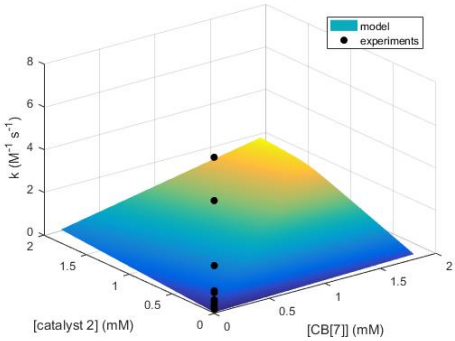

Figure S4.11: Kinetic model model defined by eq. 4.1 fits total reaction rate constants for different concentrations of CB[7] and catalyst **2**. (a) 0.42 mM CB[7], 0 – 1.8 mM catalyst **2**, the model fits the experimental values with an R^2 of -0.325. (**b**) 0.4 mM catalyst **2**, 0 – 0.84 mM CB[7], the model fits the experimental values with an R^2 of 0.300. (**c**) 0 – 1.8 mM catalyst **2**, 0 – 0.84 mM CB[7].

To take the synergistic effect of CB[7] with the **2**⊂CB[7]-complex and of catalyst **2** with the **2**⊂CB[7]-complex into account we added k_5 and k_6 and we determined k_5 and k_6 by a least-square error fit to both sets of experimental data: 1) the rate constants with respect to the concentration of CB[7], with [**2**] is 0.4 mM and 2) the rate constants with respect to the concentration of [**2**], with [CB[7]] is 0.42 mM.

$$k_{total} = k_1 + k_2 \cdot [cat] + k_3 \cdot [CB7] + k_4 \cdot [cat \subset \mathrm{CB7}] + k_5 \cdot [CB7] \cdot [cat \subset \mathrm{CB7}] + k_6 \cdot [cat] \cdot [cat \subset \mathrm{CB7}] \quad \text{(eq. 4.2)}$$

When [CB[7]] is kept constant, the model fits the experimental data with an R^2 of 0.647. When [**2**] is kept constant, the model fits the experimental data with an R^2 of 0.945. This shows that the model of eq. 4.2 predicts the experimental data when [**2**] is kept constant reasonably well. When [CB[7]] is kept constant the model does not describe the experimental data.

a

[CB[7]] = 0.42 mM

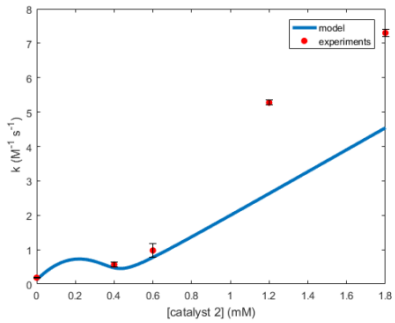

b

[**2**] = 0.40 mM

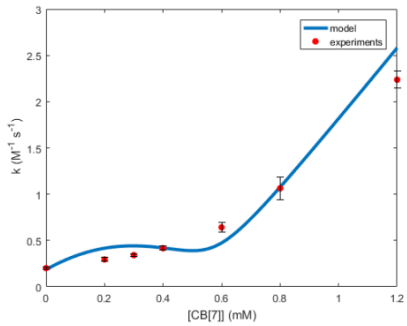

c

[CB[7]] = 0.42 mM

[**2**] = 0.40 mM

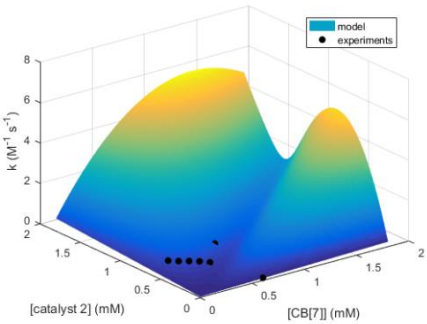

Figure S4.12: Kinetic model defined by eq. 4.2 fits total reaction rate constants for different concentrations of CB[7] and catalyst **2**. (a) 0.42 mM CB[7], 0 – 1.8 mM catalyst **2**, the model fits the experimental values with an R^2 of 0.647. (**b**) 0.4 mM catalyst **2**, 0 – 0.84 mM CB[7], the model fits the experimental values with an R^2 of 0.945. (**c**) 0 – 1.8 mM catalyst **2**, 0 – 0.84 mM CB[7].

Table S4.4: Partial reaction rate constants found with least-square error optimization fits in Matlab for catalyst **2**.

Catalyst system	Rate constant	Best fit for
None	k_1	0.0568 M^{-1} s^{-1}
Catalyst **2**	k_2	318 M^{-2} s^{-1}
CB[7]	k_3	150 M^{-2} s^{-1}
2⊂CB[7]-complex	k_4	172 M^{-2} s^{-1}
2⊂CB[7]-complex + CB[7]	k_5	$1.35 \cdot 10^7$ M^{-3} s^{-1}
2⊂CB[7]-complex + catalyst **2**	k_6	$6.86 \cdot 10^6$ M^{-3} s^{-1}

The model fits the rate constants we find with varying [CB[7]] and keeping [**2**] constant at 0.4 mM, much better. However, it still underestimates the rate constants found with varying [**2**] and keeping [CB[7]] constant at 0.42 mM. To take this nonlinear effect of [**2**] into account we proposed the following equation to calculate the rate constants:

$$k_{total} = k_1 + k_2 \cdot [cat] + k_3 \cdot [CB7] + k_4 \cdot [cat \subset \mathrm{CB7}] + k_5 \cdot [CB7] \cdot [cat \subset \mathrm{CB7}] + k_6 \cdot [cat]^2 \cdot [cat \subset \mathrm{CB7}] \quad \text{(eq. 4.3)}$$

When [CB[7]] is kept constant, the model fits the experimental data with an R^2 of 0.855. When [**2**] is kept constant, the model fits the experimental data with an R^2 of 0.997. Model-eq. 4.3 thus gives the best fit for the reaction rates with different concentrations of CB7] and [**2**].

a

[CB[7]] = 0.42 mM

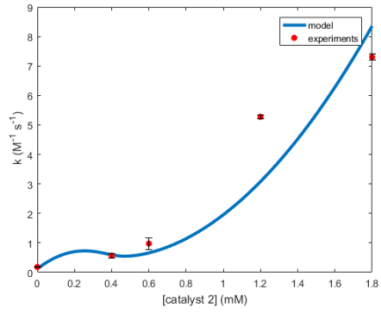

b

[**2**] = 0.40 mM

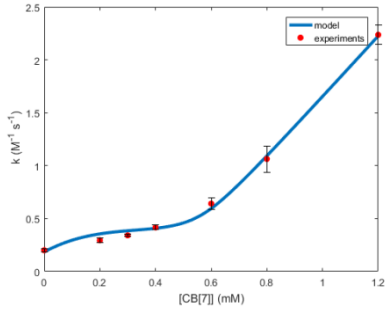

c

[CB[7]] = 0.42 mM

[**2**] = 0.40 mM

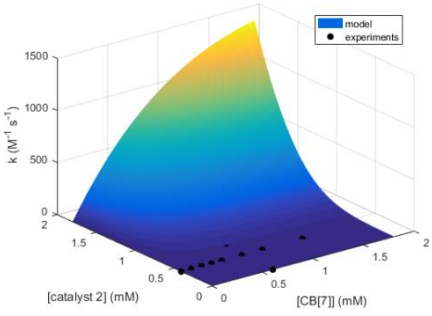

Figure S4.13: Kinetic model defined by eq. 4.3 fits total reaction rate constants for different concentrations of CB[7] and catalyst **2**. (a) 0.42 mM CB[7], 0 – 1.8 mM catalyst **2**, the model fits the experimental values with an R^2 of 0.855. (**b**) 0.4 mM catalyst **2**, 0 – 0.84 mM CB[7], the model fits the experimental values with an R^2 of 0.997. (**c**) 0 – 1.8 mM catalyst **2**, 0 – 0.84 mM CB[7].

Table S4.5: Partial reaction rate constants found with least-square error optimization fits in Matlab for catalyst **2**.

Catalyst system	**Rate constant**	**Best fit for**
None	k_1	0.0568 M^{-1} s^{-1}
Catalyst **2**	k_2	318 M^{-2} s^{-1}
CB[7]	k_3	150 M^{-2} s^{-1}
2⊂CB[7]-complex	k_4	893 M^{-2} s^{-1}
2⊂CB[7]-complex + CB[7]	k_5	$9.93 \cdot 10^6$ M^{-3} s^{-1}
2⊂CB[7]-complex + catalyst **2**	k_6	$9.36 \cdot 10^9$ M^{-4} s^{-1}

NMR spectra of hydrazone 6

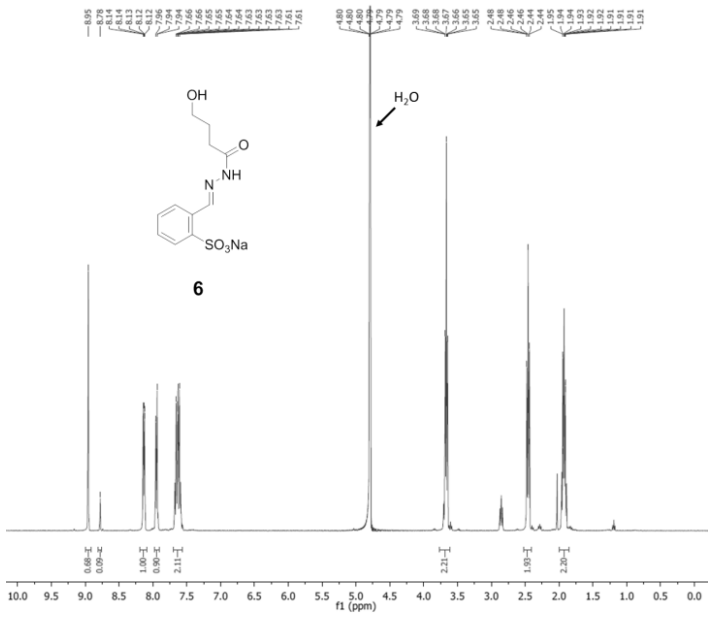

Figure S4.14: ^{1}H NMR Hydrazone **6** in D_2O.

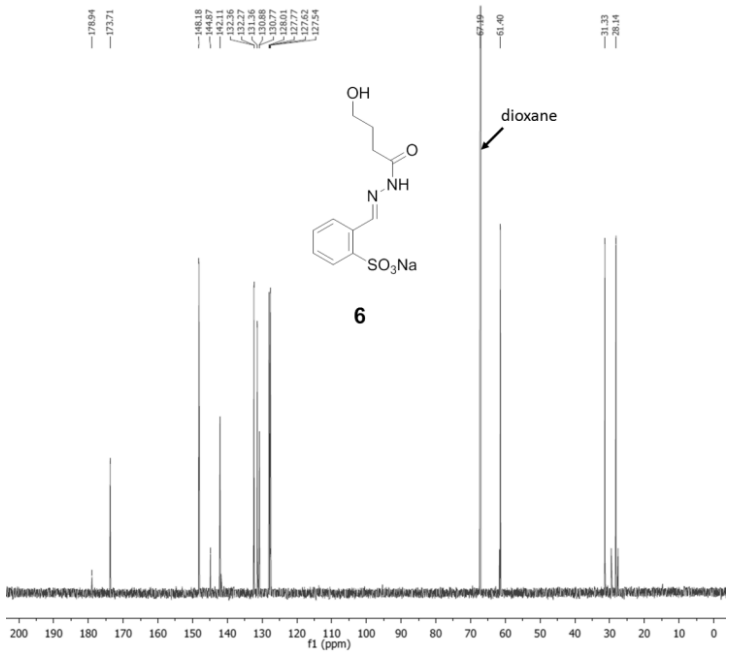

Figure S4.15: ^{13}C NMR Hydrazone **6** in D_2O.

Supplementary references

1. Larsen, D., Pittelkow, M., Karmakar, S., Kool, E. T. New organocatalyst scaffolds with high activity in promoting hydrazone and oxime formation at neutral ph. *Org. Lett.* **17**, 274-277 (2015).

2. Hargrove, A. E., Zhong, Z., Sessler, J. L., Anslyn, E. V. Algorithms for the determination of binding constants and enantiomeric excess in complex host : Guest equilibria using optical measurements. *New J. Chem.* **34**, 348-354 (2010).

Chapter 5
Aniline catalysed hydrazone formation reactions show a large variation in reaction rates and catalytic effects

Hydrazone formation reactions from aldehydes and hydrazides have the remarkable qualities that they proceed in water and the kinetics can be controlled by organocatalysis. For these reasons, this class of reactions finds widespread use in biological as well as material settings. We recently reported a protected aniline catalyst for hydrazone formation that can be activated using a chemical signal. In our search to find a suitable hydrazone formation reaction to investigate the activation of this pro-catalyst, we found a wide variety in reaction rates and response to catalysis. Here we report an overview of hydrazone formation reactions, their reaction rates and response to aniline catalysis, their compatibility for kinetic analysis by UV/Vis spectroscopy, and their compatibility with the reaction environment and with the pro-catalyst pro-aniline.

This chapter is published as:

Trausel, F., Fan, B., van Rossum, S.A.P., van Esch, J.H., Eelkema R. Aniline catalysed hydrazone formation reactions show a large variation in reaction rates and catalytic effects. *Adv. Synth. Catal.*, 360, 2571 – 2576, (2018).

5.1 Introduction

Non-biological reactions that proceed in water and can be accelerated by catalysis are uncommon, but of high interest for the design of responsive (bio-)materials and for functionalization of biomolecules.[1-8] Hydrazone formation reactions, between aldehydes and hydrazides, are a convenient class of bioorthogonal copper-free click reactions as they proceed in water.[9-12] Furthermore, because hydrazone formation reactions proceed at ambient conditions and are susceptible to catalysis, hydrazone formation reactions are widely applied in dynamic combinatorial chemistry.[13-16] Hydrazone reactions proceed rapidly at pH 5 or lower, but are unpractically slow at physiological pH.[13, 17] Jencks found that hydrazone formation reactions can be accelerated by nucleophilic catalysis using the organocatalyst aniline at physiological pH (Scheme 5.1a).[18] Kool reported alternative organocatalysts for hydrazone formation that are more efficient and less toxic than aniline.[11, 19, 20] However, the rate of hydrazone formation and response to catalysis depends heavily on the type of hydrazide and aldehyde coupling partners. Overviews reporting reaction rate constants can thus be useful in allowing scientists to choose a suitable hydrazone formation system for their purposes.[12, 21, 22]

Recently we reported a protected aniline catalyst for hydrazone formation (pro-aniline **2**, Scheme 5.1b).[23] Addition of the chemical signal H_2O_2 leads to deprotection of pro-aniline **2** and release of aniline **1** which can then catalyse hydrazone formation. We used **2** to control the formation of hydrogels featuring hydrazone bonds, introducing signal response in soft materials.[24] To find a suitable hydrazone formation reaction to investigate the activation of **2**, we compared a selection of hydrazone formation reactions. Our goal was to find a hydrazone formation reaction that shows a detectable conversion within 15 hours when catalysed by **1** at room temperature in aqueous buffer. To enable a clearly observable signal response, the reaction should show at least a three-fold increase in reaction rate when catalysed by **1**.

Furthermore, the reaction mixture should not show any side reactions with **2** or any other component, which would complicate analysis.

Finally, as we ideally wanted to follow the progress of the reaction by UV/Vis spectroscopy, the starting materials, intermediates and products should be soluble in the reaction medium (aqueous buffer with 20% dimethylformamide as co-solvent) and product

formation should give a detectable change in the UV/Vis spectrum above a wavelength of 250 nm.

Here, we disclose our findings on this topic. We find that the reaction rate constants between different hydrazone formation reactions may vary by orders of magnitude, that aniline **1** only catalyses some of the hydrazone formation reactions that we tested and that some hydrazides degrade in the solvent system or react with pro-aniline **2**. These findings may help the reader to choose a suitable hydrazone formation reaction for his or her experimental purposes.

5.2 Results and discussion

Table 5.1shows the selection of hydrazone reactions for which we investigated the response to aniline catalysis and unwanted reactivity towards **2**. The reaction rates were determined by following the change in absorbance in UV/vis spectroscopy. Pseudo-first -order rate constants were determined by using the Guggenheim time lag method.[25, 26] The graphs were fitted using linear regression. All reactions were carried out using the same conditions: 0.020 mM hydrazide, 0.5 mM aldehyde, 0.5 mM aniline **1** or 0.5 mM pro-aniline **2**, 20% (v/v) DMF (dimethylformamide) in 100 mM sodium phosphate buffer pH 7.4, 25 °C. The concentrations of the reagents were chosen such that all reactions are in the right absorbance window to follow the reaction using UV/vis spectroscopy. We used 20% DMF as a co-solvent to ensure solubility of all reagents, catalysts and products.

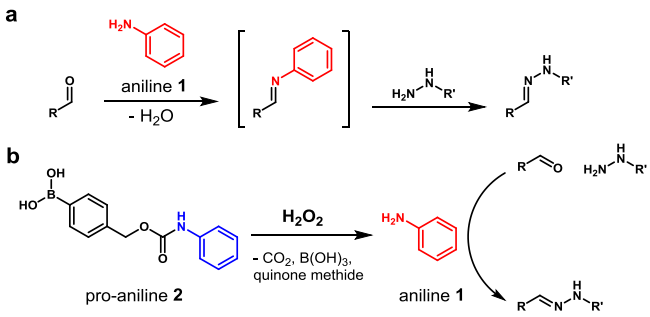

Scheme 5.1. Catalysis of hydrazone formation. (**a**) Hydrazone formation: the reaction between an aldehyde and a hydrazide catalysed by aniline **1**. (**b**) The pro-catalyst pro-aniline **2** and the chemical signal H_2O_2 react to release the organocatalyst aniline **1** which catalyses hydrazone formation between an aldehyde and a hydrazide.[8]

To measure the response on hydrazone formation rate to catalysis by **1** we determined the ratio between the reaction rate constant for the reaction catalysed by **1** and the reaction rate constant of the uncatalysed reaction. We report the wavelength at which we followed each reaction (rate analysis wavelength, Table 5.1). Full range UV/vis spectra of the hydrazone reactions at t0 and t=15 h are shown in Supplementary Fig. 5.1, graphs of the absorbance at the rate analysis wavelength over time are shown in Supplementary Fig. 5.2 and the Guggenheim fits are shown in Supplementary Fig. 5.3.

Reaction 1 is catalysed by **1** but only shows a 1.7-fold increase in reaction rate in the presence of **1**, the difference in rate between the catalysed reaction and the uncatalysed reaction is modest. Reactions 2 and 3 show a more promising response to aniline catalysis: the reaction rate constant of reaction 2 shows a 3.3-fold increase and reaction 3 a 3.7-fold increase in the presence of **1**: the kinetics of these reactions can be controlled by aniline catalysis. Kool found an 11-fold increase of reaction rate for reaction 3 upon addition of **1**, using 1 mM of aldehyde and 1 mM of **1**.[20] The difference for this response to aniline catalysis can be due to the amount of DMF as a co-solvent (Kool used 10% DMF, whereas we used 20% DMF). When testing cross-reactivity with pro-catalyst **2**, the absorbance of a mixture of hydrazide **3** and pro-aniline **2** changes over time, indicating that the two compounds react or form a non-covalent interaction with each other. Therefore, we were unable to use reactions 1-3.

Reaction 4 only shows a 1.1-fold increase in reaction rate with **1**, a value that is barely significant. Reactions 5, 6 and 7 are not catalysed by **1**. The 2nd order rate constants for reactions 4, 5, 6 and 7 were also reported by Kool.[20] He found a very similar response to aniline catalysis for reaction 5, but more convincing responses to aniline catalysis for reactions 4, 6 and 7: the reaction rates increased between 1.8-2.1-fold upon aniline catalysis. Again, this discrepancy with the results of Kool can be due to the difference in amount of DMF that was used as a co-solvent. An explanation for the lack of response to aniline catalysis can be that hydrazide **7** reacts already efficiently with aldehydes without catalysis, and the activation of the aldehydes by aniline in the form of the imine intermediate does not increase the reaction rate.

Table 5.1. Overview of hydrazone formation reactions tested with aniline **1**. Reaction conditions: 0.020 mM hydrazide, 0.5 mM aldehyde and 0.5 mM aniline 1 in 20% DMF in 100 mM sodium phosphate buffer pH 7.4. $k_{1,cat}$ is the pseudo-first-order rate constant of the aniline catalysed reaction, reported with the standard error of the mean (SEM, n≥2). $k_{2\ (app)}$ is de calculated second order rate constant of the aniline catalysed reaction, calculated with $k_{2(app)}=k_{1,cat}/[aldehyde]$. k_{rel} is the ratio of the rate constant of the reaction catalysed by 1 and the rate constant of the uncatalysed reaction ($k_{rel}=k_{cat}/k_{uncat}$). We report the wavelengths at which we followed the hydrazone formation reaction using UV/vis spectroscopy. N.A.: not applicable.

	Hydrazide	Aldehyde	$k_{1,\ cat}$ (s^{-1})	$k_{2\ (app)}$ ($M^{-1}\ s^{-1}$)	k_{rel}	Rate analysis wavelength (nm)
1	 **3**	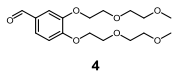 **4**	$(1.8 \pm 0.015) \times 10^{-6}$	$(3.7 \pm 0.033) \times 10^{-3}$	1.7	500
2	 **3**	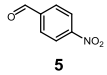 **5**	$(5.0 \pm 2.0) \times 10^{-5}$	$(1.0 \pm 0.39) \times 10^{-1}$	3.3	500
3	 **3**	 **6**	$(6.7 \pm 1.1) \times 10^{-6}$	$(1.3 \pm 0.21) \times 10^{-2}$	3.7	500
4	 **7**	 **8**	$(2.3 \pm 0.016) \times 10^{-4}$	$(4.6 \pm 0.033) \times 10^{-1}$	1.1	350
5	 **7**	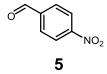 **5**	$(3.2 \pm 0.078) \times 10^{-4}$	$(6.4 \pm 0.16) \times 10^{-1}$	1.0	450
6	 **7**	 **9**	$(4.3 \pm 1.6) \times 10^{-4}$	$(8.6 \pm 3.1) \times 10^{-1}$	1.0	350
7	 **7**	 **10**	$(5.4 \pm 0.57) \times 10^{-4}$	1.1 ± 0.11	1.0	350
8	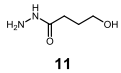 **11**	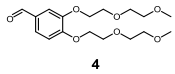 **4**	$(3.7 \pm 0.14) \times 10^{-4}$	$(7.3 \pm 0.28) \times 10^{-1}$	2.6	340
9	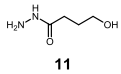 **11**	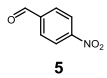 **5**	$(3.1 \pm 0.20) \times 10^{-4}$	$(6.2 \pm 0.40) \times 10^{-1}$	47	330
10	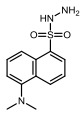 **12**	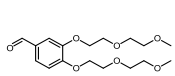 **4**	0	0	N.A.	350

	Hydrazide	Aldehyde	$k_{1,\,cat}$ (s^{-1})	$k_{2\,(app)}$ ($M^{-1}\,s^{-1}$)	k_{rel}	Rate analysis wavelength (nm)
11	 **13**	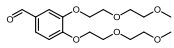 **4**	$(5.2 \pm 0.065) \times 10^{-5}$	$(1.0 \pm 0.013) \times 10^{-1}$	1.2	340
12	 **14**	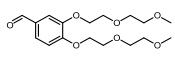 **4**	$(2.1 \pm 0.12) \times 10^{-4}$	$(4.2 \pm 0.24) \times 10^{-1}$	N.A.	340
13	 **14**	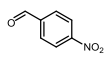 **5**	$(1.8 \pm 0.013) \times 10^{-4}$	$(4.6 \pm 0.033) \times 10^{-1}$	24	340
14	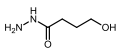 **11**	 **16**	N.A.	N.A.	N.A.	N.A.
15	 **11**	 **8**	5.0×10^{-4}	1.0	N.A.	330
16	 **14**	 **16**	N.A.	N.A.	N.A.	N.A.
17	 **14**	 **8**	2.5×10^{-4}	5.0×10^{-1}	N.A.	330

The reaction rate of reaction 8 increases 2.6-fold when catalysed by **1**. For reactions 10, 14 and 16, there is no detectable change in UV/Vis absorption over the course of 15 hours during both the catalysed and uncatalysed reactions. Reaction 11 only shows a 1.2-fold increase in reaction rate upon addition of **1**. Reactions 12, 15 and 17 are promising reactions: they do not show any conversion within 15 hours without catalyst and with **1** the reactions have considerable rate constants of $(2.1 \pm 0.12) \times 10^{-4}$ s^{-1}, 5.0×10^{-4} $s^{-1}$and 2.5×10^{-4} s^{-1}, respectively. Because the uncatalysed reactions were found to be immeasurably slow, we could not reliably calculate the ratio between the catalysed reaction and uncatalysed reaction rates. A slight disadvantage of these reactions is that the change in absorbance during the reactions is very small, which makes the reactions less reliable to follow. Besides the coupling partners of hydrazides with aromatic aldehydes, we also measured the reaction between hydrazide **14** with the aliphatic aldehyde propanal. Again, there is no detectable change in UV/Vis absorption over the course of 15 hours with or without catalyst **1**. It may be that aliphatic aldehydes are less suited to our analysis method because of their lack of a chromophore.

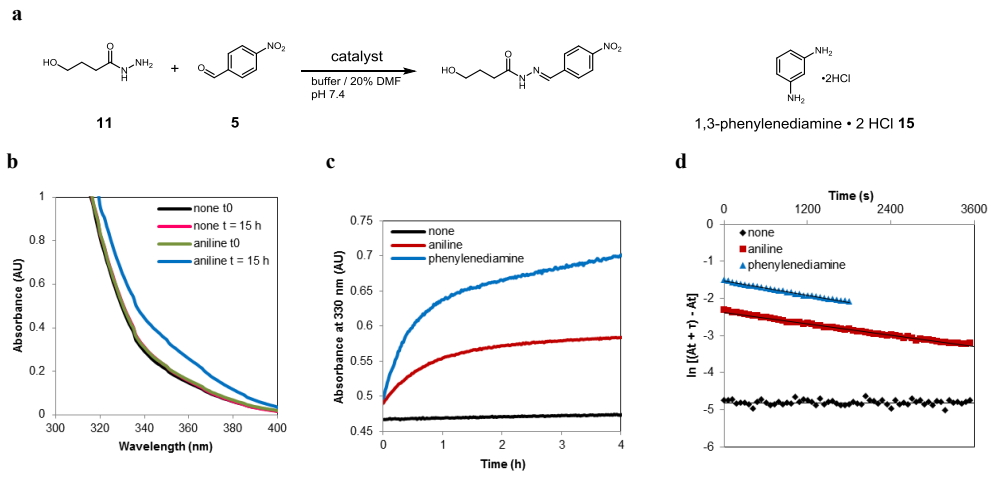

Figure 5.1. The hydrazone formation reaction 9 and response to aniline **1** and 1,3-phenylenediamine ·2HCl **15** catalysis. Reaction conditions: 0.020 mM hydrazide **11**, 0.5 mM aldehyde **5**, 0.5 mM **1** or 0.5 mM **15** catalyst in 20% DMF in 100 mM sodium phosphate buffer pH 7.4 (**a**) Reaction 9 between hydrazide **11** and aldehyde **5**. (**b**) Absorbance spectra of the reaction mixtures for the uncatalysed reaction at t0 (black line) and at t = 15 h (magenta line), for the reaction catalysed by **1** at t0 (green line), at t = 15 h (blue line). (**c**) Hydrazone formation followed over time for the uncatalysed reaction (black), for the reaction catalysed by **1** (red) and for the reaction catalysed by **15** (blue). (**d**) The first-order rate constants were determined by Guggenheim fits, uncatalysed reaction (black), reaction catalysed by **1** (red), reaction catalysed by **15** (blue).

Reaction 13 responds well to aniline catalysis: the reaction rate is increased 24-fold in the presence of **1**. There is a clear change in absorbance during the reaction, making reaction 13 a promising benchmark reaction for aniline catalysis.

With a 47-fold increase in reaction rate in the presence of **1**, reaction 9 shows, apart from reactions 12, 15 and 17, by far the largest increase in reaction rate among the reactions investigated in the current work. Because there is also a clear change in absorbance during the reaction and as we did not find any side reactions with **2** (Supplementary Table 5.2), we chose this reaction as a benchmark reaction for the activation of pro-aniline **2** in the 2017 publication.[23]

We also investigated the activity of the catalyst 1,3-phenylenediamine·2HCl **15** (Fig. 1a, c, d) in reaction 9. Whereas **1** gives a 47-fold increase in reaction rate for reaction 9, catalysis by **15** results in a 74-fold increase in reaction rate (Supplementary Table 5.1), making

catalyst **15** 1.5-times more active than aniline. This result is in agreement with studies from the literature: catalyst **15** was reported by Kool as 2.1-times more active than aniline.[27, 28]

We tested each aldehyde and hydrazide combination for possible side reactions with pro-aniline **2**. None of the aldehydes showed any change in absorbance in the presence of **2**, indicating that the aldehydes do not react with **2**. The absorbance spectrum of hydrazide **3** changes in the presence of **2**, which indicates that the two compounds react or non-covalently bind to each other.

We found that the absorbance spectrum of another nitro-bearing hydrazide, 2,4-dinitrophenylhydrazine (DNPH), also changes in the presence of **2** (Supplementary Fig. 5.4). This might indicate that the nitro-group causes this apparent side reaction. A possible explanation might be that nitro-bearing hydrazides can coordinate or react with the boronic acid group on **2**.[29, 30]

The side reaction of hydrazide **3** with **2** reduced the usefulness of hydrazide **3** under our reaction conditions. However, as long as no compounds similar to pro-aniline **2** are applied, hydrazide **3** may still be a good probe to analyse hydrazone formation.

Furthermore, we studied the stability of the aldehydes and hydrazides in the reaction solvent. The absorbance spectra of the aldehydes and hydrazides **3**, **13** and **14** did not change over a course of 15 h, indicating that the compounds remain stable. In contrast, the absorbance spectra of hydrazide **7** and hydrazide **12** alone changed in the presence of DMF or DMSO (dimethyl sulfoxide), which suggests that these compounds react with the solvents or degrade (Supplementary Fig. 5.5).

Overall it appears that relatively unreactive hydrazides, such as hydrazides **3**, **11**, and **14**, benefit from aniline catalysis. Relative reactive hydrazides, such as hydrazides **7** and **13** react efficiently with the aldehydes without activation by aniline and do not seem to benefit from aniline catalysis.

5.3 Conclusions

In summary, the hydrazone formation reactions we discussed show large variation in reactivity, stability and response to aniline catalysis. Reactions 2, 3, 13 and especially reactions 12, 15, 17 and 9 show a large increase in reaction rate in the presence of aniline **1**. Only a moderate increase in reaction rate in the presence of **1** was found for reactions 1, 4,

8 and 11. Aniline **1** does not show any significant catalytic activity in reactions 5, 6 and 7. Reactions 10, 14, and 16 show no detectable change in absorption, with or without **1**. The organocatalyst **15** is 1.5 times more active in reaction 9, when compared to **1**. Overall, hydrazone formation of NBD-hydrazide **3** and sulfonated benzaldehyde **6** (reaction 3), or acylhydrazide **11** or **14** and *p*-nitrobenzaldehyde **5** or benzaldehyde **8** (reactions 12, 15, 17, 13 and 9) are significantly accelerated by aniline catalysis without observed side reactions, making them useful benchmark reactions to test aniline catalysis or in designing responsive materials where aniline catalysis plays a role.

5.4 References

1. McKinnon, D. D., Domaille, D. W., Cha, J. N., Anseth, K. S. Bis-aliphatic hydrazone-linked hydrogels form most rapidly at physiological ph: Identifying the origin of hydrogel properties with small molecule kinetic studies. *Chem. Mat.* **26**, 2382-2387 (2014).
2. Yang, D., Gustafsson, E., Stimpson, T. C., Esser, A., Pelton, R. H. Hydrazide-derivatized microgels bond to wet, oxidized cellulose giving adhesion without drying or curing. *ACS Appl. Mater. Interfaces* **9**, 21000-21009 (2017).
3. Apostolides, D. E., Sakai, T., Patrickios, C. S. Dynamic covalent star poly(ethylene glycol) model hydrogels: A new platform for mechanically robust, multifunctional materials. *Macromolecules* **50**, 2155-2164 (2017).
4. Boehnke, N., Cam, C., Bat, E., Segura, T., Maynard, H. D. Imine hydrogels with tunable degradability for tissue engineering. *Biomacromolecules* **16**, 2101-2108 (2015).
5. Azagarsamy, M. A., Marozas, I. A., Spaans, S., Anseth, K. S. Photoregulated hydrazone-based hydrogel formation for biochemically patterning 3d cellular microenvironments. *ACS Macro Lett.* **5**, 19-23 (2016).
6. Boekhoven, J., Poolman, J. M., Maity, C., Li, F., van der Mee, L., Minkenberg, C. B., Mendes, E., van Esch, J. H., Eelkema, R. Catalytic control over supramolecular gel formation. *Nat. Chem.* **5**, 433-437 (2013).
7. Poolman, J. M., Boekhoven, J., Besselink, A., Olive, A. G. L., van Esch, J. H., Eelkema, R. Variable gelation time and stiffness of low-molecular-weight hydrogels through catalytic control over self-assembly. *Nat. Protoc.* **9**, 977-988 (2014).
8. Brinkhuis, R. P., de Graaf, F., Hansen, M. B., Visser, T. R., Rutjes, F. P. J. T., van Hest, J. C. M. Dynamically functionalized polymersomes via hydrazone exchange. *Polym. Chem.* **4**, 1345-1350 (2013).

9. Ganguly, T., Kasten, B. B., Bucar, D.-K., MacGillivray, L. R., Berkman, C. E., Benny, P. D. The hydrazide/hydrazone click reaction as a biomolecule labeling strategy for m(co)3 (m = re, 99mtc) radiopharmaceuticals. *Chem. Commun.* **47**, 12846-12848 (2011).
10. McKay, Craig S., Finn, M. G. Click chemistry in complex mixtures: Bioorthogonal bioconjugation. *Chem. Biol.* **21**, 1075-1101 (2014).
11. Crisalli, P., Kool, E. T. Importance of ortho proton donors in catalysis of hydrazone formation. *Org. Lett.* **15**, 1646-1649 (2013).
12. Kool, E. T., Park, D.-H., Crisalli, P. Fast hydrazone reactants: Electronic and acid/base effects strongly influence rate at biological ph. *J. Am. Chem. Soc.* **135**, 17663-17666 (2013).
13. Dirksen, A., Dirksen, S., Hackeng, T. M., Dawson, P. E. Nucleophilic catalysis of hydrazone formation and transimination: Implications for dynamic covalent chemistry. *J. Am. Chem. Soc.* **128**, 15602-15603 (2006).
14. Nguyen, Ivan Huc R. Optimizing the reversibility of hydrazone formation for dynamic combinatorial chemistry. *Chem. Commun.*, 942-943 (2003).
15. Simpson, M. G., Pittelkow, M., Watson, S. P., Sanders, J. K. M. Dynamic combinatorial chemistry with hydrazones: Libraries incorporating heterocyclic and steroidal motifs. *Org. Biomol. Chem.* **8**, 1181-1187 (2010).
16. Cousins, R. L. G., Poulsen, S.-A., Sanders, K. M. J. Dynamic combinatorial libraries of pseudo-peptide hydrazone macrocycles. *Chem. Commun.*, 1575-1576 (1999).
17. Dirksen, A., Dawson, P. E. Rapid oxime and hydrazone ligations with aromatic aldehydes for biomolecular labeling. *Bioconjugate Chem.* **19**, 2543-2548 (2008).
18. Cordes, E. H., Jencks, W. P. Nucleophilic catalysis of semicarbazone formation by anilines. *J. Am. Chem. Soc.* **84**, 826-831 (1962).
19. Crisalli, P., Kool, E. T. Water-soluble organocatalysts for hydrazone and oxime formation. *J. Org. Chem.* **78**, 1184-1189 (2013).
20. Larsen, D., Pittelkow, M., Karmakar, S., Kool, E. T. New organocatalyst scaffolds with high activity in promoting hydrazone and oxime formation at neutral ph. *Org. Lett.* **17**, 274-277 (2015).
21. Kool, E. T., Crisalli, P., Chan, K. M. Fast alpha nucleophiles: Structures that undergo rapid hydrazone/oxime formation at neutral ph. *Org. Lett.* **16**, 1454-1457 (2014).
22. Kölmel, D. K., Kool, E. T. Oximes and hydrazones in bioconjugation: Mechanism and catalysis. *Chem. Rev.* **117**, 10358-10376 (2017).
23. Trausel, F., Maity, C., Poolman, J. M., Kouwenberg, D. S. J., Versluis, F., van Esch, J. H., Eelkema, R. Chemical signal activation of an organocatalyst enables control over soft material formation. *Nat. Commun.* **8**, 879 (2017).
24. Trausel, F., Versluis, F., Maity, C., Poolman, J. M., Lovrak, M., van Esch, J. H., Eelkema, R. Catalysis of supramolecular hydrogelation. *Acc. Chem. Res.* **49**, 1440-1447 (2016).
25. Guggenheim, E. A. Xlvi. On the determination of the velocity constant of a unimolecular reaction. *Philos. Mag.* **2**, 538-543 (1926).
26. Hemalatha, M. R. K., Noorbatcha, I. An undergraduate physical chemistry experiment on the analysis of first-order kinetic data. *J. Chem. Educ.* **74**, 972 (1997).

27. Yuen, L. H., Saxena, N. S., Park, H. S., Weinberg, K., Kool, E. T. Dark hydrazone fluorescence labeling agents enable imaging of cellular aldehydic load. *ACS Chem. Biol.* **11**, 2312-2319 (2016).
28. Rashidian, M., Mahmoodi, M. M., Shah, R., Dozier, J. K., Wagner, C. R., Distefano, M. D. A highly efficient catalyst for oxime ligation and hydrazone–oxime exchange suitable for bioconjugation. *Bioconjugate Chem.* **24**, 333-342 (2013).
29. Nishiyabu, R., Kubo, Y., James, T. D., Fossey, J. S. Boronic acid building blocks: Tools for self-assembly. *Chem. Commun.* **47**, 1124-1150 (2011).
30. Stress, C. J., Schmidt, P. J., Gillingham, D. G. Comparison of boron-assisted oxime and hydrazone formations leads to the discovery of a fluorogenic variant. *Org. Biomol. Chem.* **14**, 5529-5533 (2016).

5.5 Supplementary information

Experimental details

General information

NMR spectra were recorded on an Agilent-400 MR DD2 (400 MHz for ^{1}H and 100.5 MHz for ^{13}C) at 298 K using residual protonated solvent signals as internal standard. UV/Vis spectroscopic measurements were performed on an Analytik Jena Specord 250 spectrophotometer; quartz cuvettes with a path length of 1 cm were used. Measurements were carried out at a controlled temperature of 25 °C.

Materials

All compounds and solvents were used without further purification. The technical solvents were purchased from VWR and the reagent grade solvents were purchased from Sigma Aldrich. Aniline **1**, aldehyde **5**, aldehyde **8**, aldehyde **9**, aldehyde **10**, hydrazide **7**, hydrazide **13** and hydrazide **14** were purchased from Sigma Aldrich. Aldehyde **6** was purchased from Fluka. Hydrazide **11** was purchased from Alfa Aesar. Hydrazide **12** and 1,3-phenylenediamine·2HCl **15** were purchased from TCI Europe. Aldehyde **16** was purchased from Acros Organics.

Synthetic procedures

For the synthesis of pro-aniline **2**, hydrazide **3** and aldehyde **8** we refer to procedures described in the literature.[1-3]

General procedure for the synthesis of hydrazone products

To the hydrazide solution (1.1 eq) in absolute ethanol (2 mL) was added a solution of aldehyde (1 eq, 100 mg) in absolute ethanol (1 mL) and 2 drops of glacial acetic acid. The reaction mixture was stirred for 1 – 3 days at room temperature, until complete conversion of the aldehyde was confirmed by NMR. The solvent was evaporated under reduced pressure to afford the pure hydrazone products. Some hydrazone products were purified further using flash column chromatography. The products were obtained as mixtures of *cis*-

and *trans*-isomers. We labelled the hydrazone products as follows: **H1** is the hydrazone product of reaction 1 (Table 5.1 in the main text), **H2** of reaction 2, **H3** of reaction 3, **H4** of reaction 4, **H5** of reaction 5, **H6** of reaction 6, **H7** of reaction 7, **H8** of reaction 8, **H9** of reaction 9, **H11** of reaction 11, **H12** of reaction 12 and **H13** of reaction 13, **H15** of reaction 15 and **H17** of reaction 17. For the characterisation of hydrazones **H1**[4], **H2**[5], **H4**[6], **H5**[7], **H6**[8], **H7**[9] and **H9**[1] we refer to procedures described in the literature. Characterization data are in accordance with published results.

Characterisation of new compounds

Hydrazone product **H3**

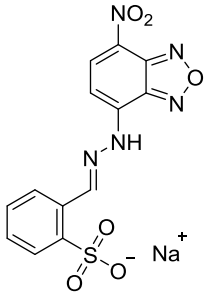

H3

Red powder (169 mg, 0.44 mmol, 85%). Extra peaks are due to a combination of *cis*- and *trans*-isomers and rotamers. **^{1}H NMR** (400 MHz, D_2O) δ 9.49 (s, 2H), 8.49 (s, 1H), 8.30 (d, 2H, J = 9.2 Hz), 8.08 (m, 2H), 7.76 (m, 3H), 7.65 (d, 1H, J = 7.6 Hz), 7.36 (m, 5H), 7.18 (t, 1H, J = 7.4 Hz), 7.09 (t, 1H, J = 7.5 Hz), 6.93 (d, 2H, J = 10.3 Hz), 6.14 (d, 1H, J = 10.2 Hz), 5.78 (d, 2H, J = 10.4 Hz). **^{13}C NMR** (100.5 MHz, D_2O) δ 161.7, 148.5, 147.8, 144.9, 139.2, 133.6, 131.3, 130.0, 128.9, 127.4, 126.4, 124.7, 121.2, 113.6. **MS** (ESI Neg.) m/z: 362.1 [(M-Na^+)$^-$] (expected m/z = 362.0). **Extinction coefficient** in sodium phosphate buffer (10 mM, pH 6.0): (1.1 ± 0.12) × 10^4 M^{-1} cm^{-1} at 487 nm.

Hydrazone product **H8**

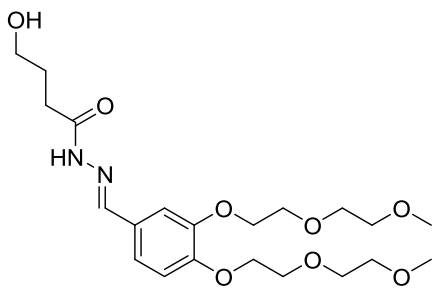

H8

Purified by extraction: dissolved crude product in dichloromethane (10 mL) and washed with deionized water (10 mL), extracted with dichloromethane (3 × 10 mL), washed with brine (15 mL), dried over magnesium sulfate, filtered and removed the solvent. Further purified using flash chromatography, eluent: 5% methanol in acetone. Colourless oil (79.9 mg, 0.18 mmol,

62%). **^{1}H NMR** (400 MHz, CD_3OD): δ = 7.99 (s, 1H), 7.84 (s, 1H), 7.60 (s, 1H), 7.35 (s, 1H), 7.14 (t, 1H, *J* = 8.3 Hz), 6.97 (t, 1H, *J* = 7.9 Hz), 4.17 (m, 4H), 3.84 (m, 4H), 3.70 (m, 4H), 3.62 (m, 2H), 3.55 (m, 4H), 3.35 (s, 6H), 2.81 (t, 1H, *J* = 7.5 Hz), 2.39 (t, 1H, *J* = 7.5 Hz), 1.90 (m, 2H).**^{13}C NMR** (100.5 MHz, CD_3OD): δ 177.3, 172.3, 152.3, 150.5, 149.0, 145.5, 129.2, 128.8, 124.1, 123.1, 114.9, 114.6, 112.9, 112.1, 73.0, 71.6, 70.7, 70.1, 69.9, 69.8, 62.5, 62.1, 59.1, 56.0, 32.0, 30.3, 29.6, 29.5. **MS** (ESI Neg.) m/z: 441.2 $[(M-H)^-]$ (expected m/z = 441.2), (ESI Pos.) m/z: 443.2 $[(M+H)^+]$ (expected m/s = 443.2, (ESI Pos.) m/z: 465.2 $[(M+Na^+)^+]$ (expected m/s = 465.2). **Extinction coefficient** in 20% DMF in sodium phosphate buffer (100 mM, pH 7.4): $(1.7 \pm 0.031) \times 10^4$ M^{-1} cm^{-1} at 314 nm.

Hydrazone product **H11**

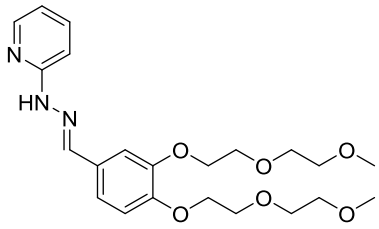

H11

Red oil (100 mg, 0.23 mmol, 79%). **^{1}H NMR** (400 MHz, CD_3OD): δ = 8.05 (d, 1H, *J* = 5.2 Hz), 7.88 (s, 1H), 7.66 (td, 1H, *J* = 8.7, 1.8 Hz), 7.49 (d, 1H, *J* = 2.0 Hz), 7.21 (d, 1H, *J* = 9.5 Hz), 7.16 (dd, 1H, *J* = 8.3, 2.0 Hz), 6.99 (d, 1H, 8.4), 6.78 (td, 1H, *J* = 6.1, 1.0 Hz), 4.22 (t, 2H, *J* = 4.7 Hz), 4.17 (t, 2H, *J* = 4.7 Hz), 3.85 (m, 4H), 3.72 (m, 4H), 3.56 (m, 4H), 3.36 (s, 6H). **^{13}C NMR** (100.5 MHz, CD_3OD): δ = 157.5, 151.4, 150.5, 147.1, 142.3, 140.1, 130.4, 122.5, 116.0, 115.2, 112.5, 109.2, 73.0, 71.6, 70.9, 70.1, 59.1. **MS** (ESI Neg.) m/z: 432.3 $[(M-H)^-]$ (expected m/z = 432.2), (ESI Pos.) m/z: 434.0 $[(M+H)^+]$ (expected m/z = 434.2), m/z: 456.1 $[(M+Na^+)^+]$ (expected m/z = 456.2). **Extinction coefficient** in 20% DMF in sodium phosphate buffer (100 mM, pH 7.4): $(2.2 \pm 0.12) \times 10^4$ M^{-1} cm^{-1} at 336 nm.

Hydrazone product **H12**

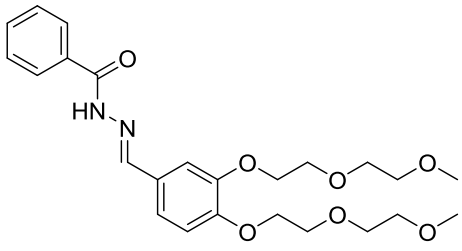

H12

Yellow oil (118 mg, 0.26 mmol, 88%). **^{1}H NMR** (400 MHz, CD_3OD): δ = 8.24 (s, 1H), 7.94 (d, 2H, *J* = 8.2), 7.70 (d, 1H, *J* = 2.0), 7.59 (t, 1H, *J* = 7.3), 7.51 (t, 2H, *J* = 7.4), 7.21 (dd, 1H, *J* = 1.9, *J* = 8.3), 7.01 (d, 1H, *J* = 8.3), 4.24 (t, 2H, *J* = 4.6), 4.19 (t, 2H, *J* = 4.7) 3.87 (m, 4H), 3.72 (m, 4H), 3.57 (m, 4H), 3.36 (s, 6H). **^{13}C NMR** (100.5 MHz, CD_3OD): δ = 165.5, 151.1, 149.2, 132.8, 131.8, 128.3, 127.3, 122.9, 113.2, 110.8, 71.6, 70.2, 69.3, 68.6, 57.7. **MS** (ESI Neg.) m/z: 459.3 $[(M-H)^-]$ (expected m/z = 459.2), (ESI Pos.) m/z: 461.2 $[(M+H)^+]$ (expected m/z = 461.2), m/z: 483.1 $[(M+Na^+)^+]$ (expected m/z = 483.2). Extinction coefficient in 20% DMF in sodium phosphate buffer (100 mM, pH 7.4): (2.5 ± 0.044) × 104 M-1 cm-1 at 322 nm.

Hydrazone product **H15**

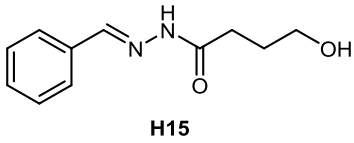

H15

Purified by extraction: dissolved crude product in dichloromethane (10 mL) and washed with deionized water (10 mL), extracted with dichloromethane (3 × 10 mL), washed with brine (15 mL), dried over magnesium sulfate, filtered and removed the solvent. Yellow powder (147 mg, 0.71 mmol, 67%). **^{1}H NMR** (400 MHz, DMSO): δ = 11.35 (s, 2H), 11.21 (s, 3H), 8.15 (s, 2H), 7.97 (s, 3H), 7.66 (m, 10H), 7.41 (m, 15H), 4.49 (s, 5H), 3.45 (q, 10H), 2.66 (t, 6H, J = 7.5), 2.24 (t, 4H, J = 7.5), 1.72 (q, 10H). **^{13}C NMR** (100.5 MHz, DMSO): δ = 174.87, 169.14, 146.07, 142.76, 134.84, 134.79, 130.27, 130.06, 129.24, 129.21, 127.36, 127.04, 60.77, 60.57, 31.36, 29.19, 28.75, 27.99. **MS** (ESI Neg.) m/z: 205.05 [(M-H)-] (expected m/z = 205.11), (ESI Pos.) m/z: 206.90 [(M+H)+] (expected m/z = 207.11). **Extinction coefficient** in 20% DMF in sodium phosphate buffer (100 mM, pH 7.4): 3.49 × 104 M-1 cm-1 at 330 nm.

General procedure to follow a hydrazone reaction in UV/vis spectroscopy.

The hydrazone reactions were performed in 20% (v/v) DMF (dimethylformamide) in a 100 mM sodium phosphate buffer pH 7.4. The quartz cuvettes contained a total reaction volume of 2 mL. All reactions were carried out using the same conditions: 0.020 mM hydrazide, 0.5 mM aldehyde, 0.5 mM aniline **1** or pro-aniline **2**, 20% DMF in 100 mM phosphate buffer pH 7.4, 25 °C. The stock solutions of the reagents were added as follows: aldehyde solution (100 µL, 10 mM in DMF), phosphate buffer, DMF, catalyst solution (100 µL, 10 mM in DMF), the hydrazide solution (100 µL, 0.4 mM in DMF). Stock solutions were made fresh for every reaction and used within 1 h. The cuvettes were closed using Teflon caps and thoroughly mixed by turning the cuvette upside down 4 times. The spectra of the reaction mixtures at t=0 were measured (reference measurement using a cuvette with only solvent as the reference cuvette, 10 nm s^{-1}). The change in absorbance was followed at the rate analysis wavelength using a 6-sample holder (standard absorption measurement, scan every 30 s). At t = 15 h single scans were measured again using the same settings as for the starting reaction mixtures. The pseudo-first-order rate constants were determined using the Guggenheim time lag fit.[10, 11] The graph was fitted using linear regression to yield the pseudo-first-order reaction rate constant.

UV/vis spectra of hydrazone reactions

Absorbance spectra of reaction mixtures

a

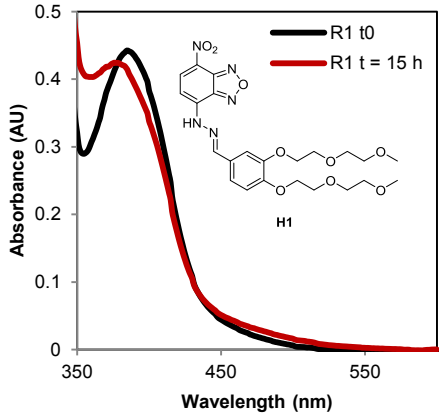

b

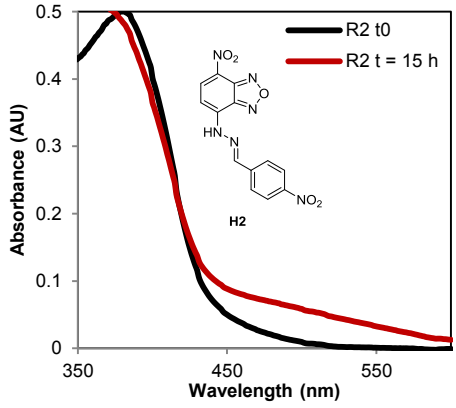

c

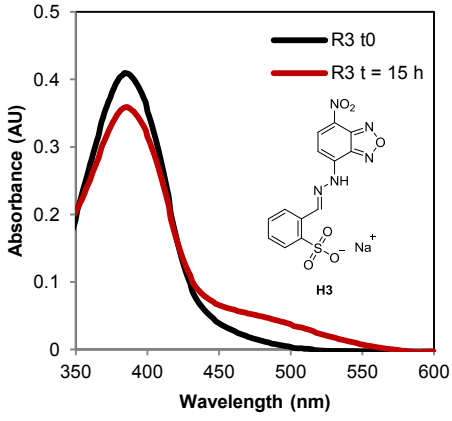

d

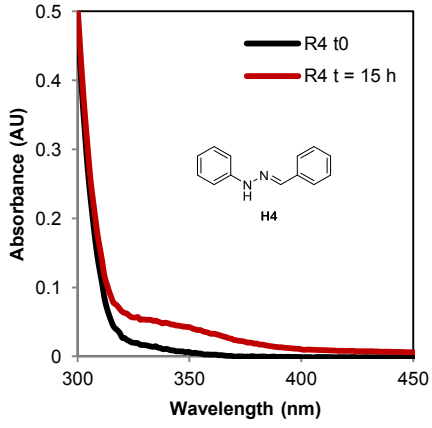

e

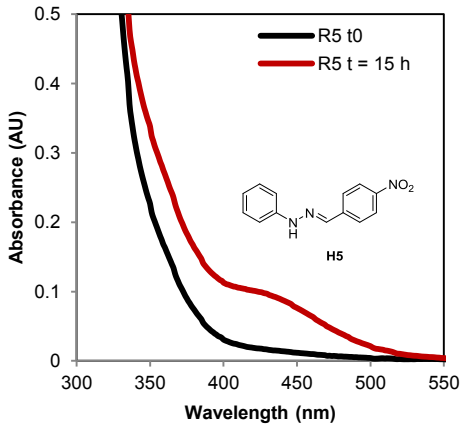
R5 t0
R5 t = 15 h
Absorbance (AU)
Wavelength (nm)
0.5
0.4
0.3
0.2
0.1
0
300
350
400
450
500
550
NO2
H5

f

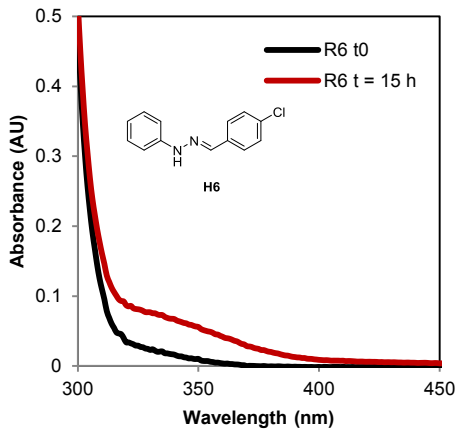
R6 t0
R6 t = 15 h
Absorbance (AU)
Wavelength (nm)
0.5
0.4
0.3
0.2
0.1
0
300
350
400
450
Cl
H6

g

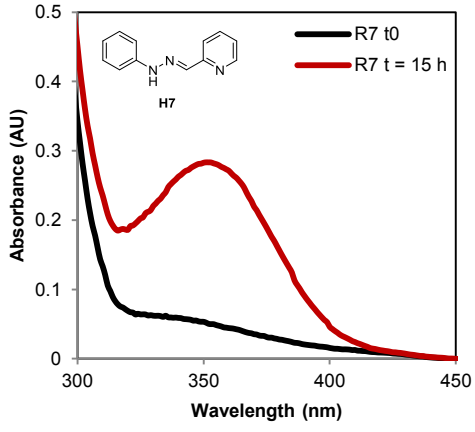
R7 t0
R7 t = 15 h
Absorbance (AU)
Wavelength (nm)
0.5
0.4
0.3
0.2
0.1
0
300
350
400
450
H7

h

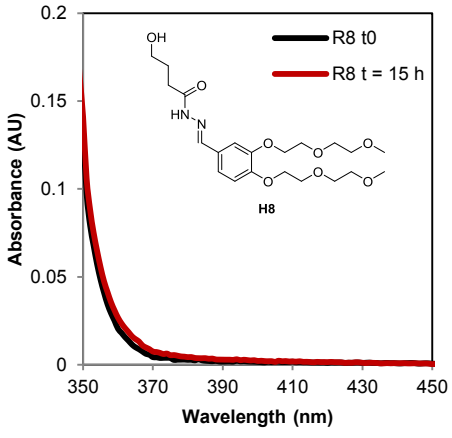
R8 t0
R8 t = 15 h
Absorbance (AU)
Wavelength (nm)
0.2
0.15
0.1
0.05
0
350
370
390
410
430
450
OH
H8

i

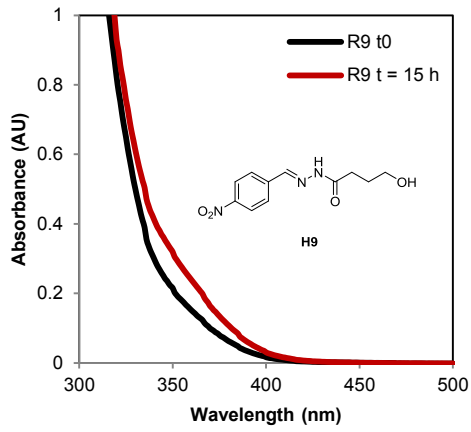
R9 t0
R9 t = 15 h
Absorbance (AU)
Wavelength (nm)
H9

j

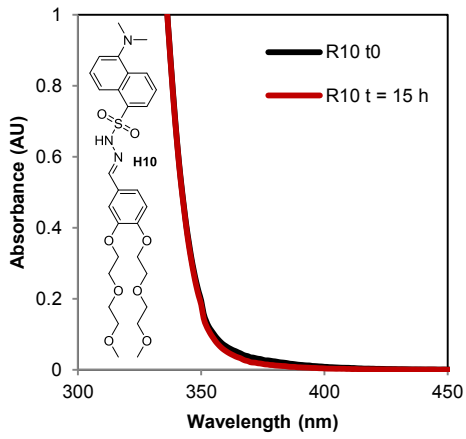
R10 t0
R10 t = 15 h
Absorbance (AU)
Wavelength (nm)
H10

k

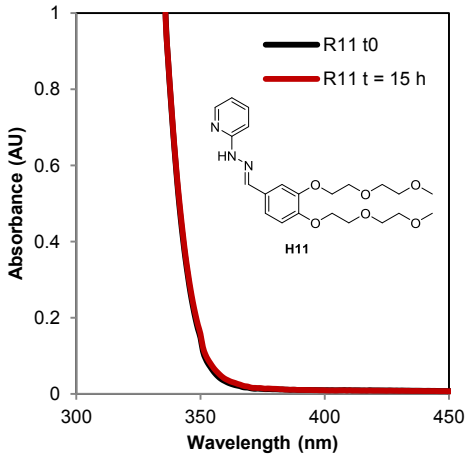
R11 t0
R11 t = 15 h
Absorbance (AU)
Wavelength (nm)
H11

l

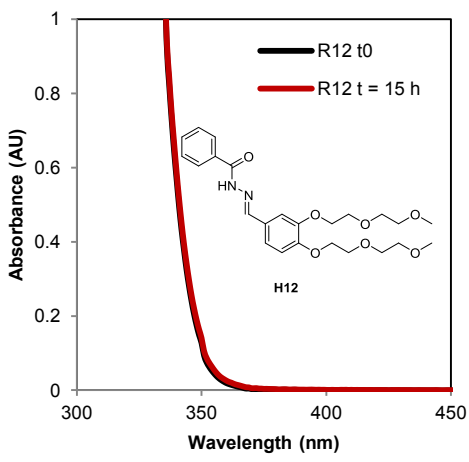
R12 t0
R12 t = 15 h
Absorbance (AU)
Wavelength (nm)
H12

m

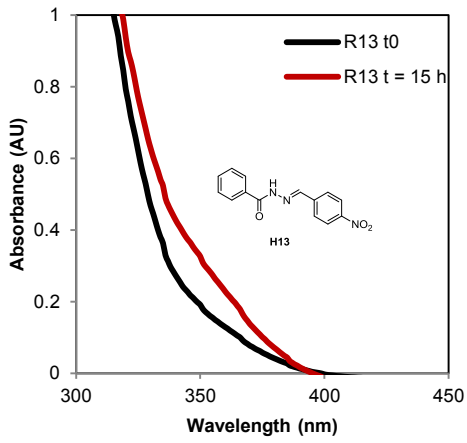
R13 t0
R13 t = 15 h
Absorbance (AU)
Wavelength (nm)
H13

n

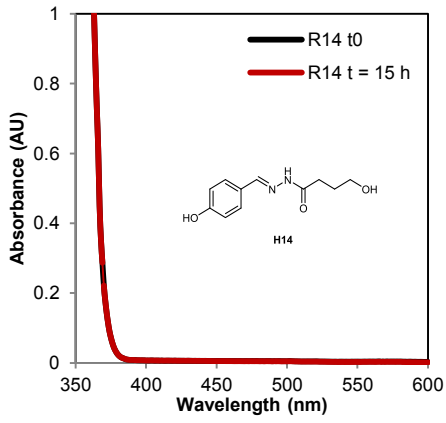
R14 t0
R14 t = 15 h
Absorbance (AU)
Wavelength (nm)
H14

o

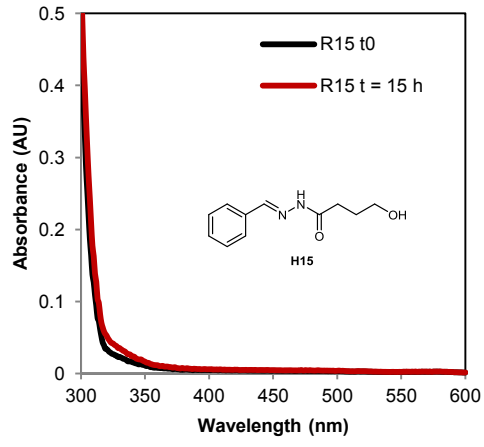
R15 t0
R15 t = 15 h
Absorbance (AU)
Wavelength (nm)
H15

p

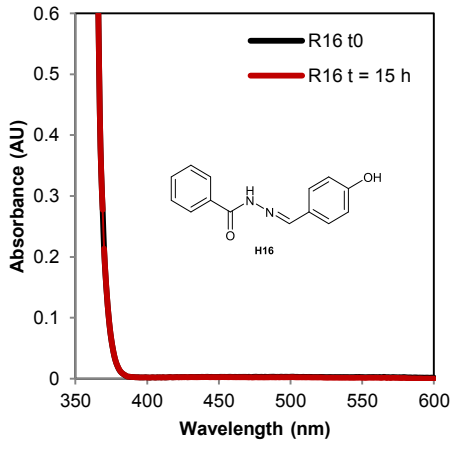
R16 t0
R16 t = 15 h
Absorbance (AU)
Wavelength (nm)
H16

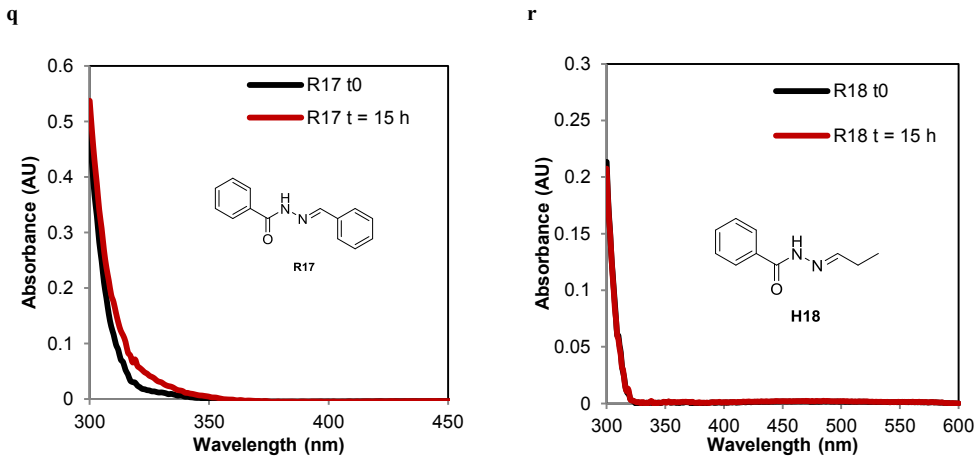

Supplementary Fig. 5.1: Absorbance spectrum of aldehyde and hydrazide mixtures with aniline **1** at t0 (black line) and at t = 15 h (red line). Reaction conditions: 0.020 mM hydrazide, 0.5 mM aldehyde, 0.5 mM aniline **1**, 20% DMF in 100 mM sodium phosphate buffer pH 7.4. R1 means reaction 1 (etc.) from Table 5.1 in the main text. (**a**) Reaction 1 between hydrazide **3** and aldehyde **4**, (**b**) reaction 2 between hydrazide **3** and aldehyde **5**, (**c**) reaction 3 between hydrazide **3** and aldehyde **6**, (**d**) reaction 4 between hydrazide **7** and aldehyde **8**, (**e**) reaction 5 between hydrazide **7** and aldehyde **5**, (**f**) reaction 6 between hydrazide **7** and aldehyde **9**, (**g**) reaction 7 between hydrazide **7** and aldehyde **10**, (**h**) reaction 8 between hydrazide **11** and aldehyde **4**, (**i**) reaction 9 between hydrazide **11** and aldehyde **5**, (**j**) reaction 10 between hydrazide **12** and aldehyde **4** does not take place, (**k**) reaction 11 between hydrazide **13** and aldehyde **4**, (**l**) reaction 12 between hydrazide **14** and aldehyde **4**, (**m**) reaction 13 between hydrazide **14** and aldehyde **5**, (**n**) reaction 14 between hydrazide **11** and aldehyde **16** does not take place, (**o**) reaction 15 between hydrazide **11** and aldehyde **8**, (**p**) reaction 16 between hydrazide **14** and aldehyde **16** does not take place, (**q**) reaction 17 between hydrazide **14** and aldehyde **8,** (**r**) reaction 18 between hydrazide **14** and benzaldehyde **17** does not take place.

Absorbance at rate analysis wavelength of aldehyde and hydrazide mixtures

a

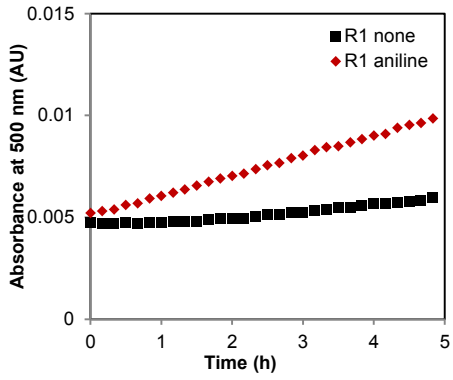

b

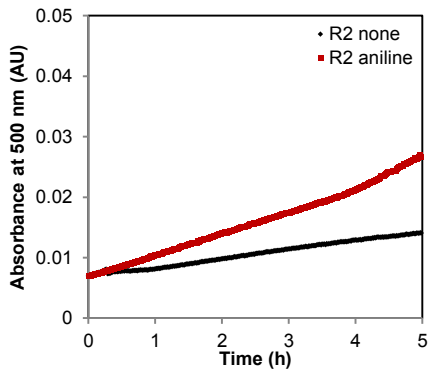

c

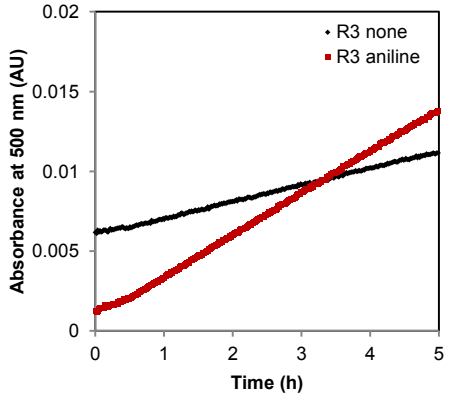

d

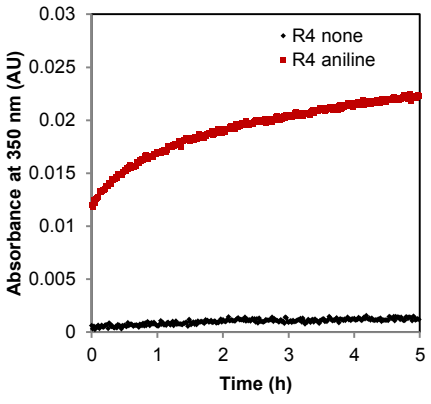

e

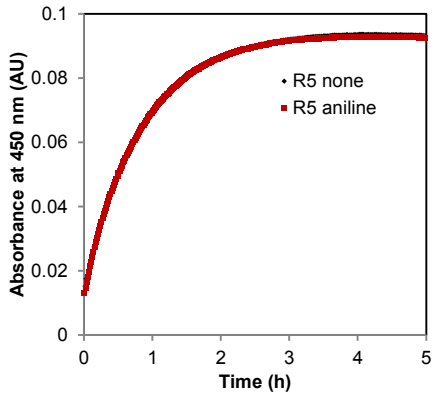
Absorbance at 450 nm (AU)
Time (h)
R5 none
R5 aniline

f

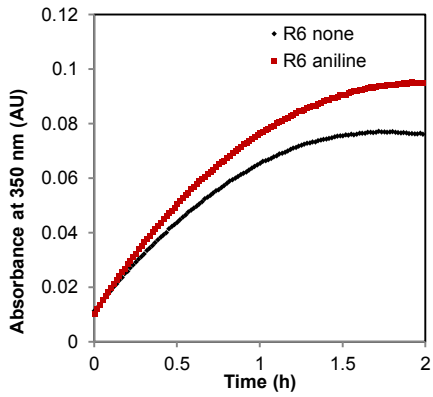
Absorbance at 350 nm (AU)
Time (h)
R6 none
R6 aniline

g

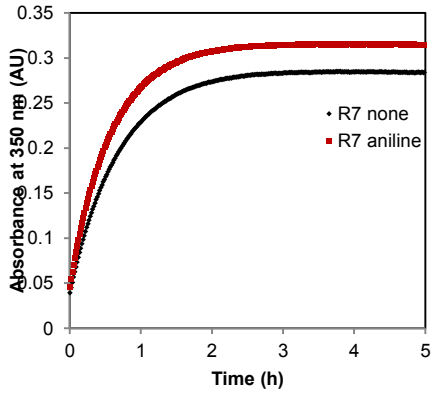
Absorbance at 350 nm (AU)
Time (h)
R7 none
R7 aniline

h

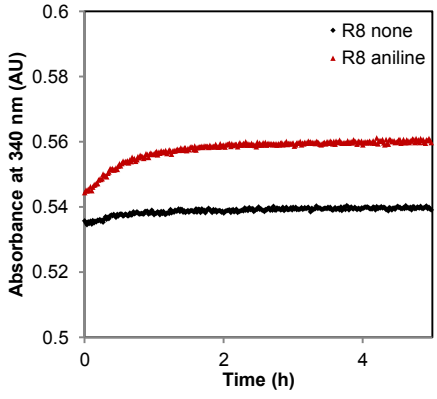
Absorbance at 340 nm (AU)
Time (h)
R8 none
R8 aniline

i

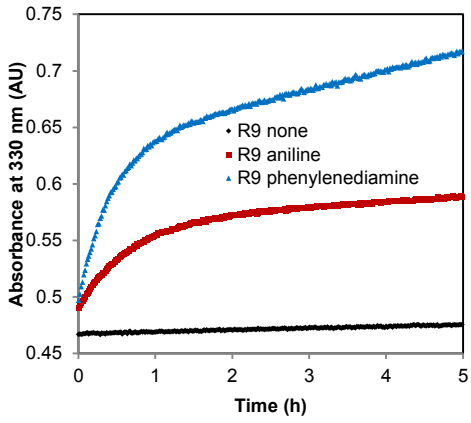
0.75
0.7
0.65
0.6
0.55
0.5
0.45
Absorbance at 330 nm (AU)
0
1
2
3
4
5
Time (h)
R9 none
R9 aniline
R9 phenylenediamine

j

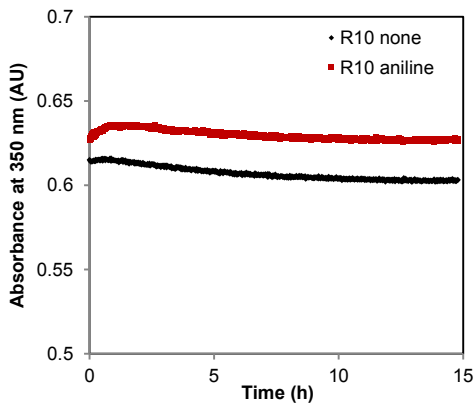
0.7
0.65
0.6
0.55
0.5
Absorbance at 350 nm (AU)
0
5
10
15
Time (h)
R10 none
R10 aniline

k

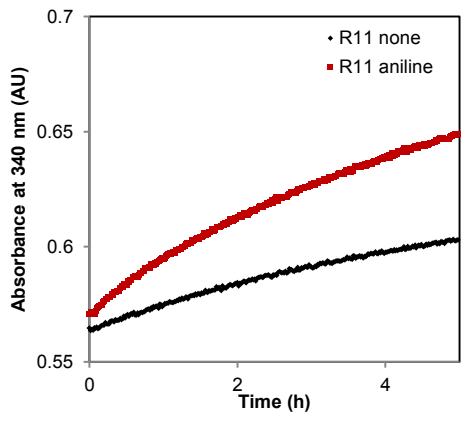
0.7
0.65
0.6
0.55
Absorbance at 340 nm (AU)
0
2
4
Time (h)
R11 none
R11 aniline

l

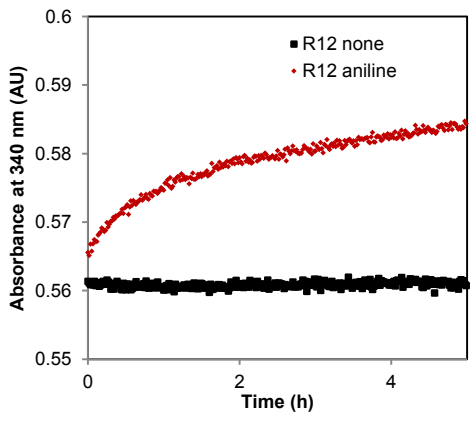
0.6
0.59
0.58
0.57
0.56
0.55
Absorbance at 340 nm (AU)
0
2
4
Time (h)
R12 none
R12 aniline

m

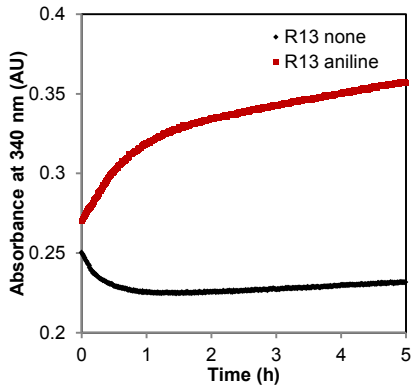
Absorbance at 340 nm (AU)
Time (h)
R13 none
R13 aniline
0.4
0.35
0.3
0.25
0.2
0
1
2
3
4
5

n

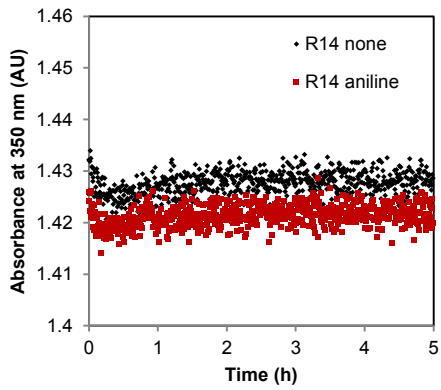
Absorbance at 350 nm (AU)
Time (h)
R14 none
R14 aniline
1.46
1.45
1.44
1.43
1.42
1.41
1.4
0
1
2
3
4
5

o

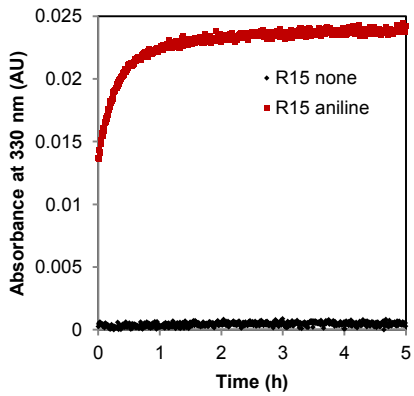
Absorbance at 330 nm (AU)
Time (h)
R15 none
R15 aniline
0.025
0.02
0.015
0.01
0.005
0
0
1
2
3
4
5

p

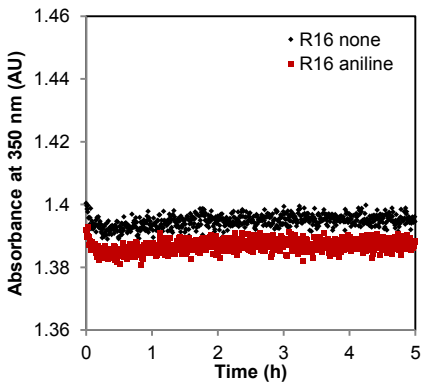
Absorbance at 350 nm (AU)
Time (h)
R16 none
R16 aniline
1.46
1.44
1.42
1.4
1.38
1.36
0
1
2
3
4
5

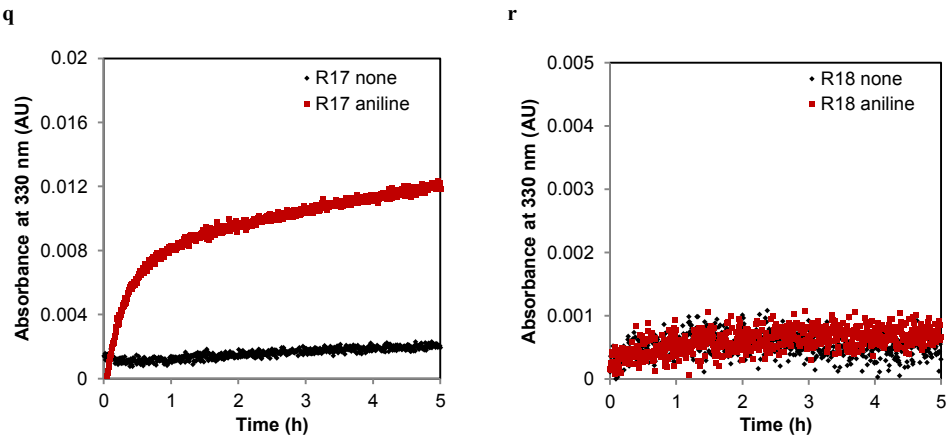

Supplementary Fig. 5.2: Absorbance at rate analysis wavelength of aldehyde and hydrazide mixtures without catalyst (black) and with aniline **1** (red). Reaction conditions: 0.020 mM hydrazide, 0.5 mM aldehyde, 0.5 mM aniline **1** or 0.5 mM 1,3-phenylenediamine · 2 HCl **15** in 20% DMF in 100 mM sodium phosphate buffer pH 7.4. R1 means reaction 1 (etc.) from Table 5.1 in the main text. (**a**) Reaction 1 between hydrazide **3** and aldehyde **4**, (**b**) reaction 2 between hydrazide **3** and aldehyde **5**, (**c**) reaction 3 between hydrazide **3** and aldehyde **6**, (**d**) reaction 4 between hydrazide **7** and aldehyde **8**, (**e**) reaction 5 between hydrazide **7** and aldehyde **5**, (**f**) reaction 6 between hydrazide **7** and aldehyde **9**, (**g**) reaction 7 between hydrazide **7** and aldehyde **10**, (**h**) reaction 8 between hydrazide **11** and aldehyde **4**, (**i**) reaction 9 between hydrazide **11** and aldehyde **5**, (**j**) reaction 10 between hydrazide **12** and aldehyde **4** does not take place, (**k**) reaction 11 between hydrazide **13** and aldehyde **4**, (**l**) reaction 12 between hydrazide **14** and aldehyde **4**, (**m**) reaction 13 between hydrazide **14** and aldehyde **5**, (**m**) reaction 13 between hydrazide **14** and aldehyde **5**, (**n**) reaction 14 between hydrazide **11** and aldehyde **16** does not take place, (**o**) reaction 15 between hydrazide **11** and aldehyde **8**, (**p**) reaction 16 between hydrazide **14** and aldehyde **16** does not take place, (**q**) reaction 17 between hydrazide **14** and aldehyde **8**, (**r**) reaction 18 between hydrazide **14** and benzaldehyde **8** does not take place.

Guggenheim fits of the reactions

a

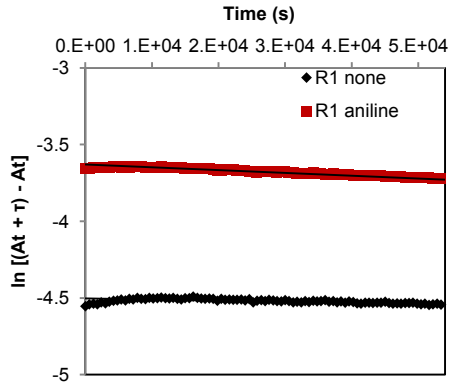

b

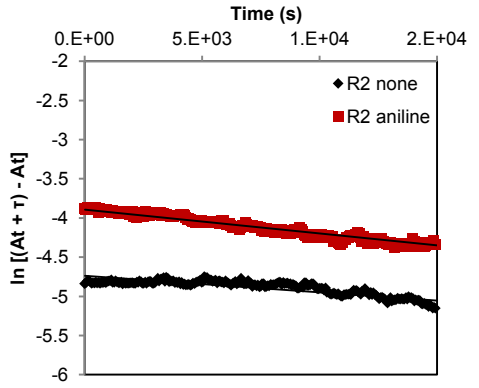

c

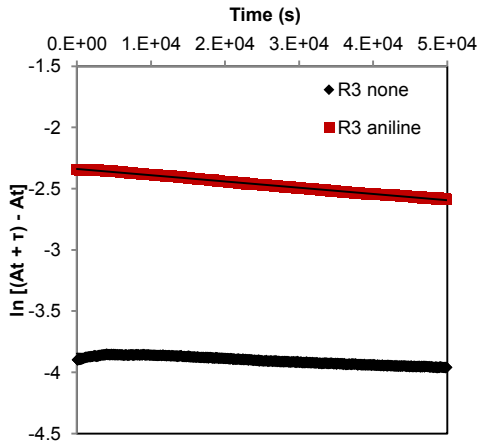

d

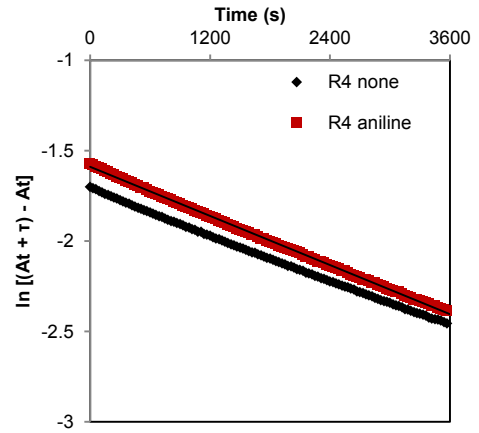

e

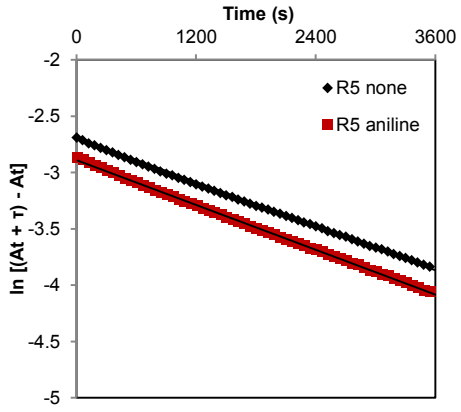
Time (s)
0
1200
2400
3600
-2
-2.5
-3
-3.5
-4
-4.5
-5
ln [(At + τ) - At]
R5 none
R5 aniline

f

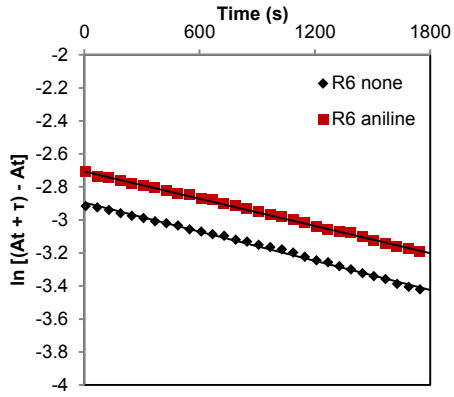
Time (s)
0
600
1200
1800
-2
-2.2
-2.4
-2.6
-2.8
-3
-3.2
-3.4
-3.6
-3.8
-4
ln [(At + τ) - At]
R6 none
R6 aniline

g

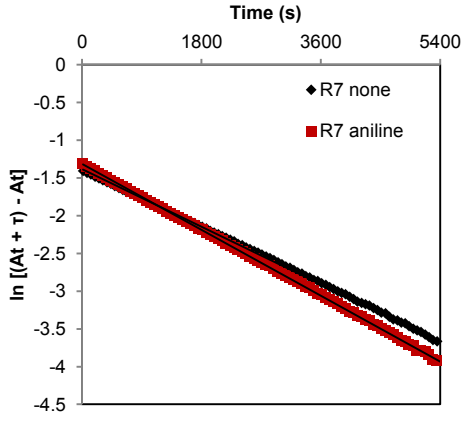
Time (s)
0
1800
3600
5400
0
-0.5
-1
-1.5
-2
-2.5
-3
-3.5
-4
-4.5
ln [(At + τ) - At]
R7 none
R7 aniline

h

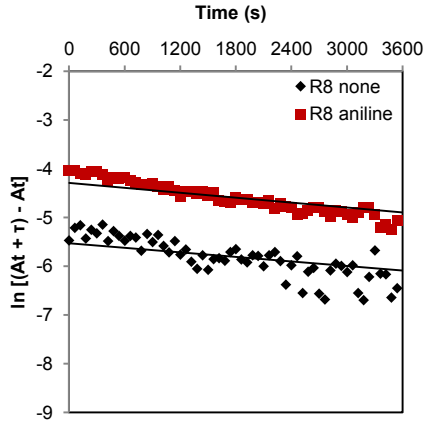
Time (s)
0
600
1200
1800
2400
3000
3600
-2
-3
-4
-5
-6
-7
-8
-9
ln [(At + τ) - At]
R8 none
R8 aniline

i

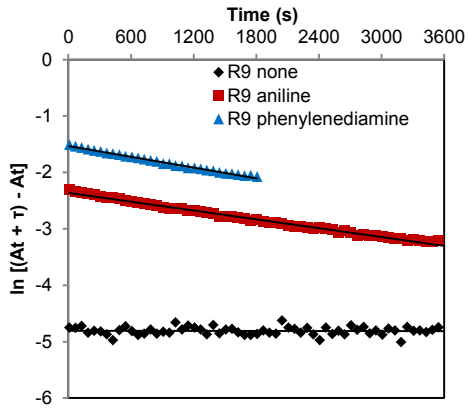
Time (s)
0
600
1200
1800
2400
3000
3600
0
-1
-2
-3
-4
-5
-6
ln [(At + τ) - At]
R9 none
R9 aniline
R9 phenylenediamine

j

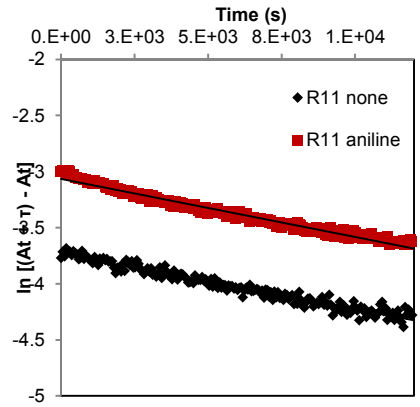
Time (s)
0.E+00
3.E+03
5.E+03
8.E+03
1.E+04
-2
-2.5
-3
-3.5
-4
-4.5
-5
ln [(At + τ) - At]
R11 none
R11 aniline

k

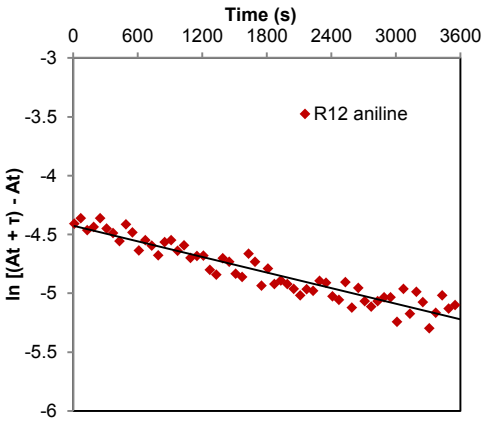
Time (s)
0
600
1200
1800
2400
3000
3600
-3
-3.5
-4
-4.5
-5
-5.5
-6
ln [(At + τ) - At)
R12 aniline

l

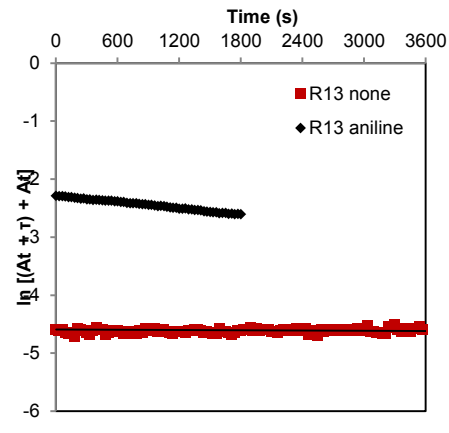
Time (s)
0
600
1200
1800
2400
3000
3600
0
-1
-2
-3
-4
-5
-6
ln [(At + τ) + At]
R13 none
R13 aniline

m

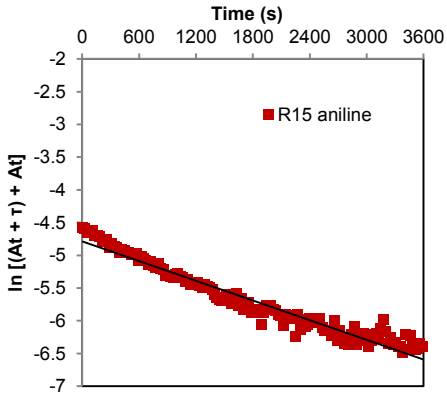

n

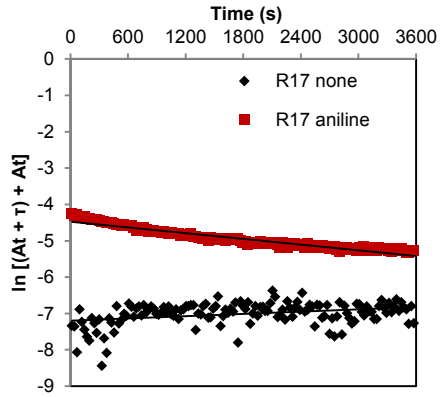

Supplementary Fig. 5.3: Fitting the Guggenheim time lag ln[(At + τ) – At] versus time gives $-k_1$ (the pseudo-first order rate constants), reactions without catalyst (black) and with aniline **1** (red). Reaction conditions: 0.020 mM hydrazide, 0.5 mM aldehyde, 0.5 mM aniline **1** or 0.5 mM 1,3-phenylenediamine·2 HCl **15** in 20% DMF in 100 mM sodium phosphate buffer pH 7.4. (**a**) Reaction 1 between hydrazide **3** and aldehyde **4**, (**b**) reaction 2 between hydrazide **3** and aldehyde **5**, (**c**) reaction 3 between hydrazide **3** and aldehyde **6**, (**d**) reaction 4 between hydrazide **7** and aldehyde **8**, (**e**) reaction 5 between hydrazide **7** and aldehyde **5**, (**f**) reaction 6 between hydrazide **7** and aldehyde **9**, (**g**) reaction 7 between hydrazide **7** and aldehyde **10**, (**h**) reaction 8 between hydrazide **11** and aldehyde **4**, (**i**) reaction 9 between hydrazide **11** and aldehyde **5**, (**j**) reaction 11 between hydrazide **13** and aldehyde **4**, (**k**) reaction 12 between hydrazide **14** and aldehyde **4**. Without aniline there is no detectable conversion. (**l**) Reaction 13 between hydrazide **14** and aldehyde **5**, (**m**) reaction 15 between hydrazide **11** and aldehyde **8**. Without aniline there is no detectable conversion, (**n**) Reaction 17 between hydrazide **14** and aldehyde **8**.

Change of absorbance of pro-aniline 2 with two different hydrazides

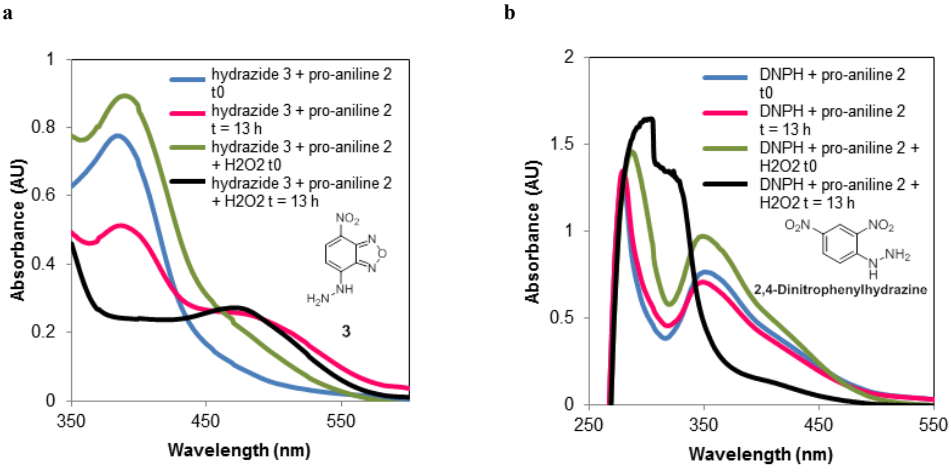

Supplementary Fig. 5.4: Change in absorbance of pro-aniline **2** and two examples of hydrazides with a nitro-group. (**a**) Pro-aniline **2** in the presence of hydrazide **3** at t0 (blue line) and at t = 13 h (magenta line), pro-aniline **2** in the presence of hydrazide **3** and H_2O_2 at t0 (green line) and at t = 13 h (black line). (**b**) Pro-aniline **2** in the presence of 2,4-dinitrophenylhydrazine (DNPH) at t0 (blue line) and at t = 13 h (magenta line), pro-aniline **2** in the presence of 2,4-dinitrophenylhydrazine and H_2O_2 at t0 (green line) and at t = 13 h (black line). Conditions: 0.045 mM hydrazide **3**, 0.045 mM 2,4-dinitrophenylhydrazine (DNPH), 2.5 mM pro-aniline **2**, 45 mM H_2O_2 in 20% DMF in 100 mM sodium phosphate buffer pH 7.4.

Change of absorbance over time of hydrazides 7 and 12

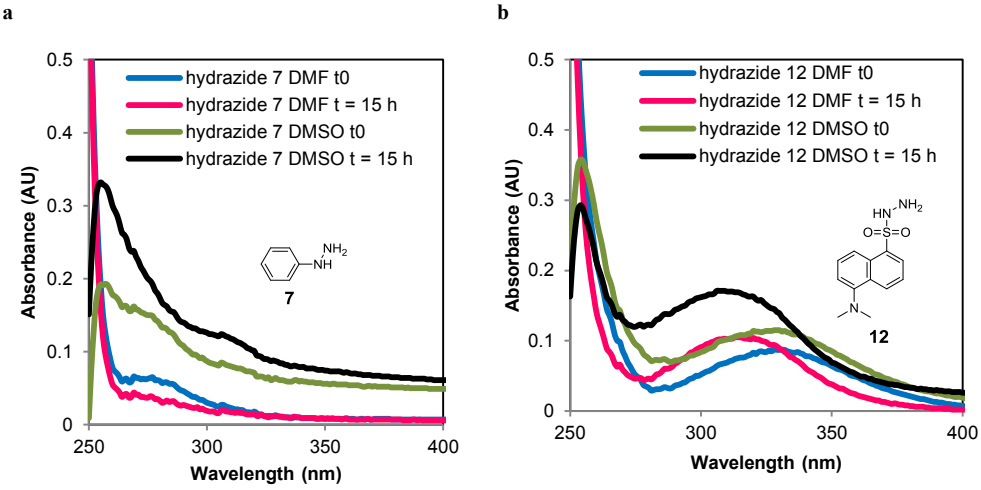

Supplementary Fig. 5.5: Change in absorbance of hydrazides in DMF and in DMSO. (**a**) Hydrazide **7** in DMF at t0 (blue line), hydrazide **7** in DMF at t = 15 h (magenta line), hydrazide **7** in DMSO at t0 (green line) and hydrazide **7** in DMSO at t = 15 h (black line). (**b**) Hydrazide **12** in DMF at t0 (blue line), hydrazide **12** in DMF at t = 15 h (magenta line), hydrazide **12** in DMSO at t0 (green line) and hydrazide **12** in DMSO at t = 15 h (black line). Conditions: 0.020 mM hydrazide in 20% DMF or 20% DMSO in 100 mM sodium phosphate buffer pH 7.4.

Overview of reaction rate constants of all hydrazone reactions

Supplementary Table 5.1: Overview of reaction rate constants of all hydrazone reactions. Reaction conditions: 0.020 mM hydrazide, 0.5 mM aldehyde, 0.5 mM aniline **1** or 0.5 mM 1,3-phenylenediamine · 2HCl **15** in 20% (v/v) DMF (dimethylformamide) in 100 mM sodium phosphate buffer pH 7.4. k_1 is the pseudo-first order rate constant of the uncatalysed reaction, reported with the standard error of mean (SEM, n ≥ 2), $k_{2\,(app)}$ is de calculated second order rate constant, calculated with $k_{2\,(app)} = k_1$ / [aldehyde], k_{rel} is the ratio of the rate constant of the reaction catalysed by aniline **1** and the rate constant of the uncatalysed reaction ($k_{rel} = k_{cat} / k_{uncat}$).

Reaction	k_1 (s^{-1})	SEM	$k_{2\,(app)}$ ($M^{-1}\,s^{-1}$)	SEM	k_{rel}
R1 none	1.1E-06	2.2E-07	2.1E-03	4.3E-04	
R1 aniline	1.8E-06	1.5E-08	3.7E-03	3.0E-05	1.7
R2 none	1.5E-05	5.0E-09	3.0E-02	1.0E-05	
R2 aniline	5.0E-05	2.0E-05	1.0E-01	3.9E-02	3.3
R3 none	1.8E-06	3.2E-07	3.6E-03	6.5E-04	
R3 aniline	6.7E-06	1.1E-06	1.3E-02	2.1E-03	3.7
R4 none	2.1E-04	4.1E-07	4.2E-01	8.2E-04	
R4 aniline	2.3E-04	4.5E-05	4.6E-01	9.0E-02	1.1
R5 none	3.2E-04	1.3E-04	6.5E-01	2.6E-01	
R5 aniline	3.2E-04	7.8E-06	6.4E-01	1.6E-02	1.0
R6 none	4.2E-04	1.3E-04	8.5E-01	2.6E-01	
R6 aniline	4.3E-04	1.6E-04	8.6E-01	3.1E-01	1.0
R7 none	5.7E-04	1.5E-04	1.1E+00	2.9E-01	
R7 aniline	5.4E-04	5.7E-05	1.1E+00	1.1E-01	1.0
R8 none	1.4E-04	1.1E-05	2.8E-01	2.1E-02	
R8 aniline	3.7E-04	2.1E-05	7.3E-01	4.1E-02	2.6
R9 none	6.7E-06	4.0E-06	1.3E-02	8.1E-03	
R9 aniline	3.1E-04	2.0E-05	6.2E-01	4.0E-02	47
R9 1,3-phenylenediamine · 2HCl 15	5.0E-04	5.0E-07	9.9E-01	1.0E-03	74
R10 none	0	-	0	-	
R10 aniline	0	-	0	-	-
R11 none	4.4E-05	5.5E-06	8.7E-02	1.1E-02	
R11 aniline	5.2E-05	6.5E-07	1.0E-01	1.3E-03	1.2
R12 none	0	-	0	-	
R12 aniline	2.1E-04	1.2E-05	4.2E-01	2.4E-02	-
R13 none	7.8E-06	4.3E-07	1.8E-04	1.1E-03	
R13 aniline	1.8E-04	1.3E-06	4.6E-01	3.3E-03	24

Reaction	k_1 (s^{-1})	SEM	$k_{2\,(app)}$ ($M^{-1}\,s^{-1}$)	SEM	k_{rel}
R14 none	0	-	0	-	
R14 aniline	0	-	0	-	-
R15 none	0	-	0	-	-
R15 aniline	5.0E-04	-	1.0E-00	-	-
R16 none	0	-	0	-	
R16 aniline	0	-	0	-	-
R17 none	0	-	0	-	
R17 aniline	2.5E-04	-	5.0E-01	-	-
R18 none	0	-	0	-	
R18 aniline	0	-	0	-	-

Overview of control experiments performed for reaction 9

Supplementary Table 5.2: Overview of control experiments performed for reaction 9. In all cases, the absorbance at 330 nm was followed during the reaction and spectra between 250 – 450 nm were taken at the $t = 0$ and at $t = 15$ h.

#	Hydrazide **11**	Aldehyde **5**	Pro-aniline **2**	H_2O_2	Aniline **1**	Boric acid	Results
1	x						no change in absorbance, stable for 15 h
2	x			x			no reaction 15 h
3	x		x				no reaction 15 h
4	x		x	x			no reaction 15 h
5	x				x		no reaction 15 h
6	x	x		x			same as uncatalyzed reaction
7	x	x		x	x		same as reaction with aniline **1**
8	x	x	x		x		same as reaction with aniline **1**
9	x	x	x	x	x		proportional increase in reaction rate
10		x					no change in absorbance, stable 15 h
11		x		x			no reaction 15 h
12		x	x				no reaction 15 h
13		x	x	x			no reaction 15 h
14		x			x		iminium formation negligible at 330 nm
15				x	x		stable for 15 h
16			x				stable for 15 h
17			x	x			no change in absorbance at 330 nm
18	x	x			x	x	same as reaction with aniline **1**
19	x	x		x	x	x	same as reaction with aniline **1**

NMR spectra of new compounds

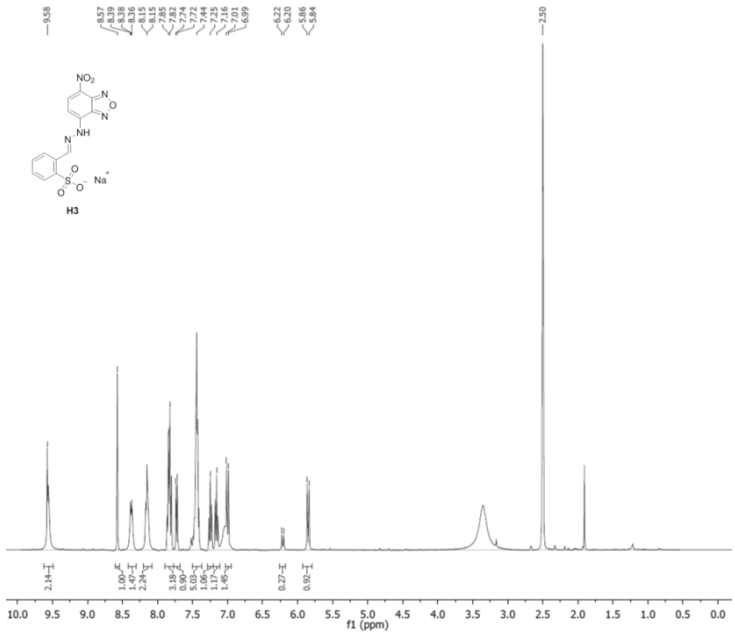

[1]H NMR H3 in DMSO-D6

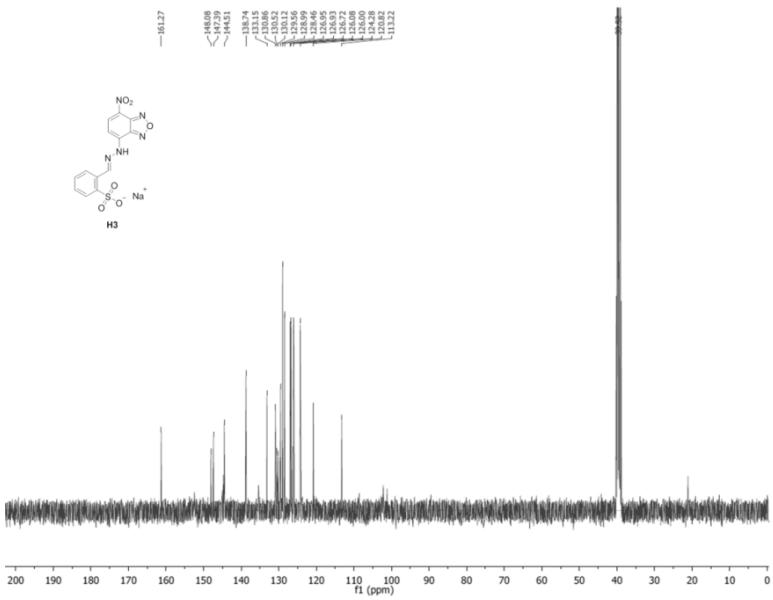

[13]C NMR H3 in DMSO-D6

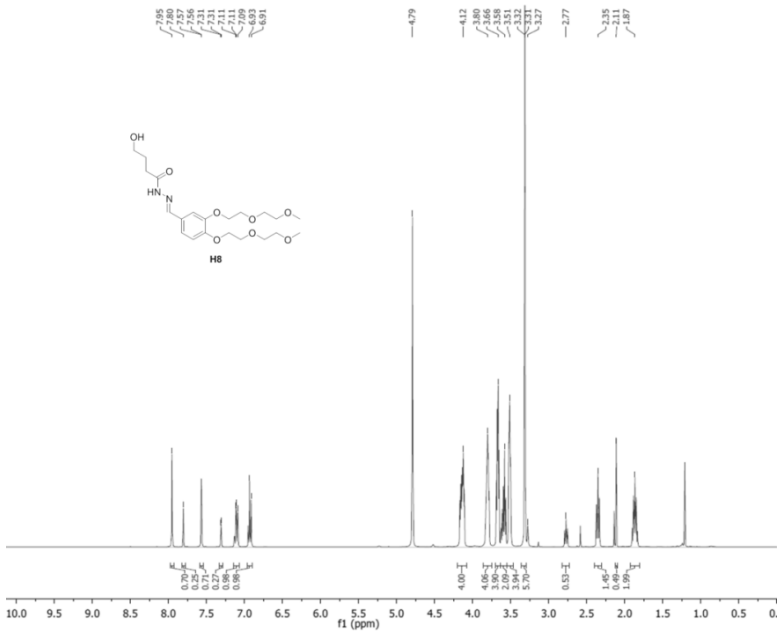

^{1}H NMR H8 in CD_3OD

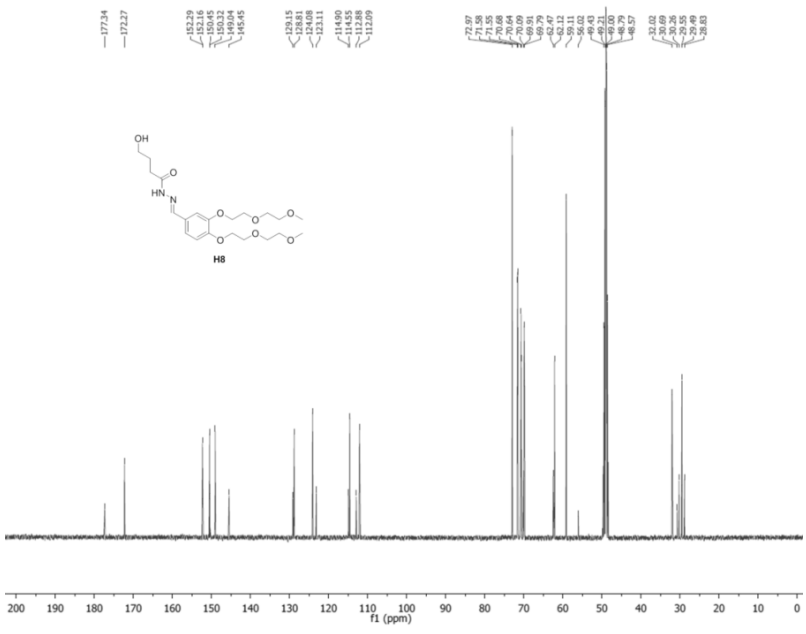

^{13}C NMR H8 in CD_3OD

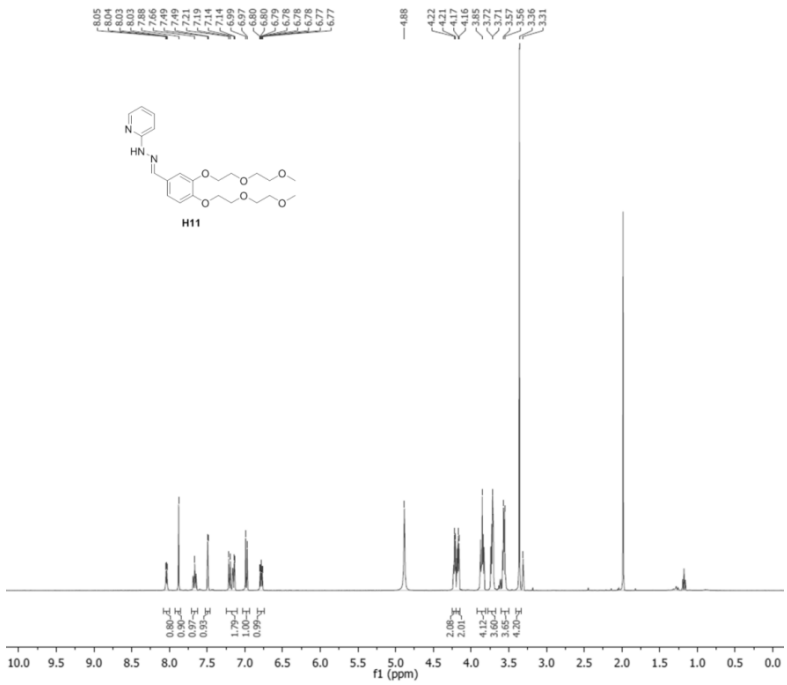

^{1}H NMR H11 in CD_3OD

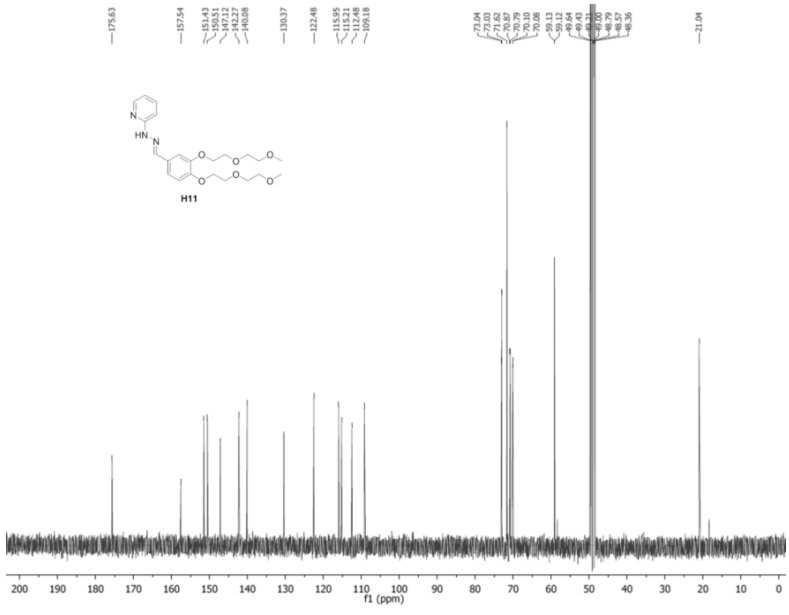

^{13}C NMR H11 in CD_3OD

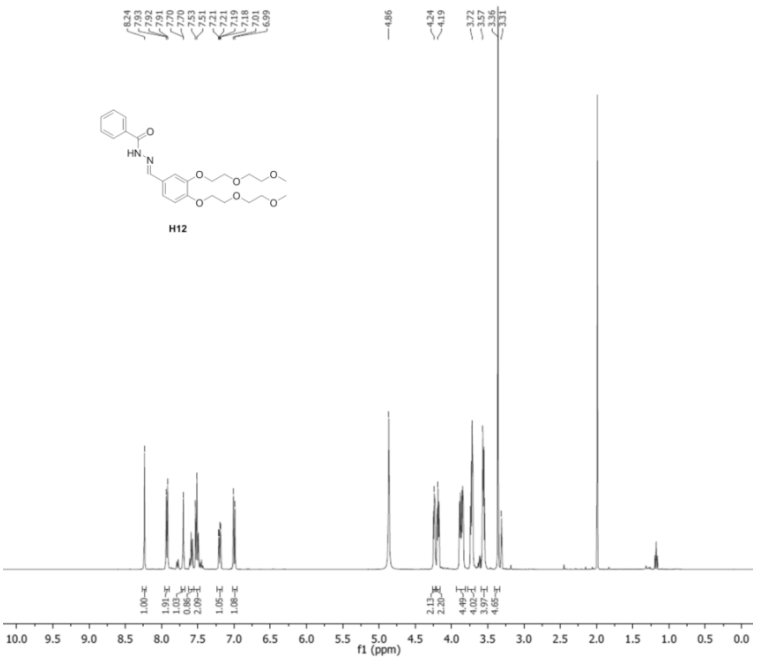

^{1}H NMR H12 in CD_3OD

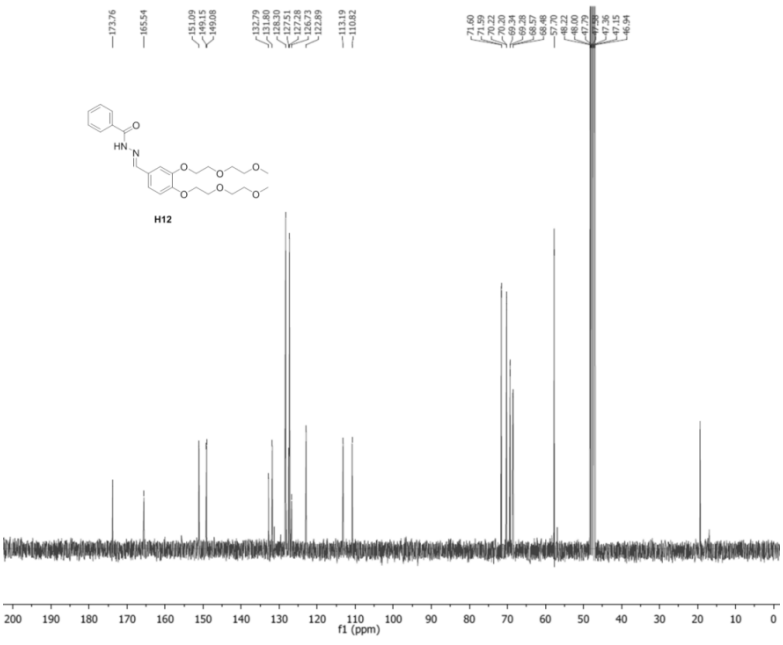

^{13}C NMR H12 in CD_3OD

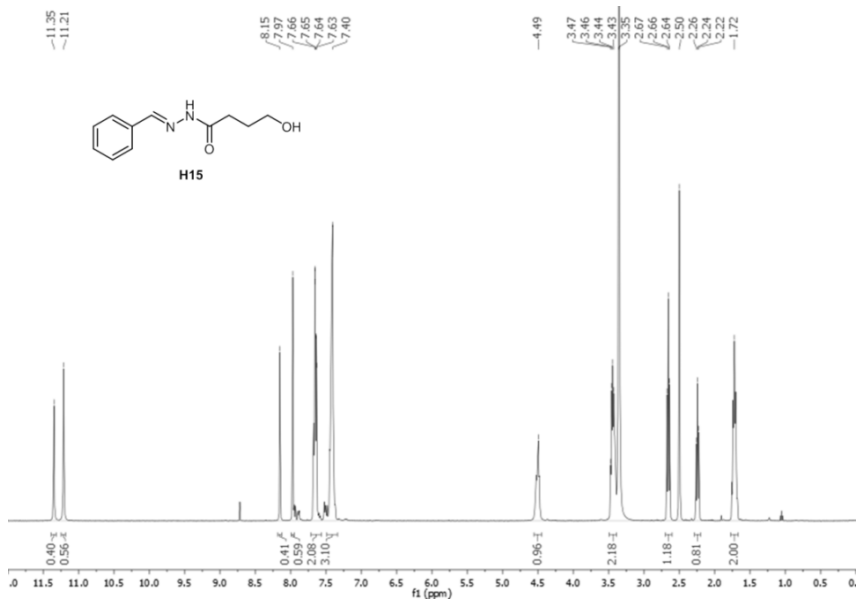

[1]H NMR H15 in DMSO-D6

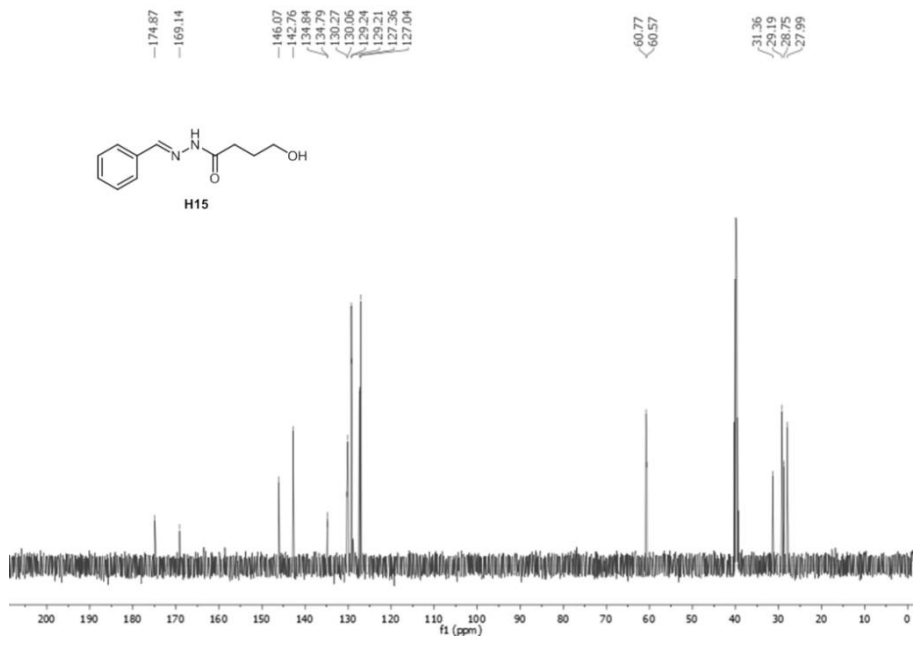

[13]C NMR H15 in DMSO-D6

HPLC traces of new compounds

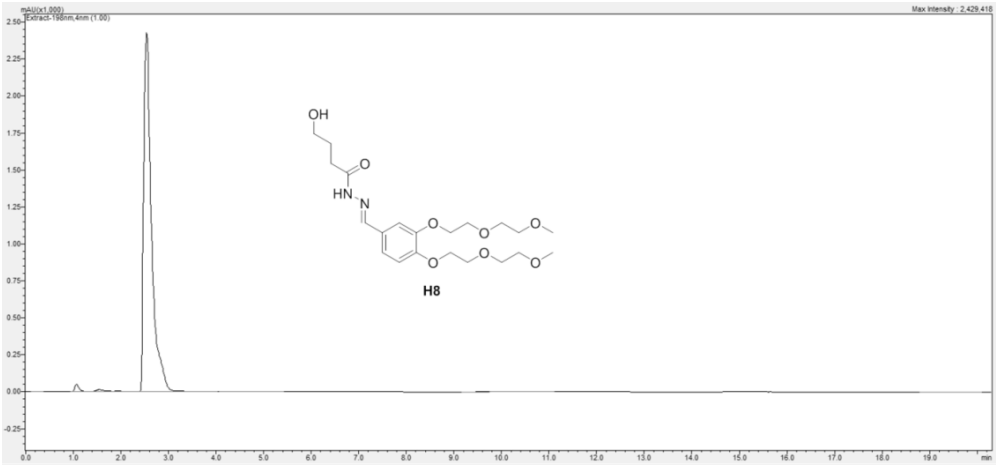

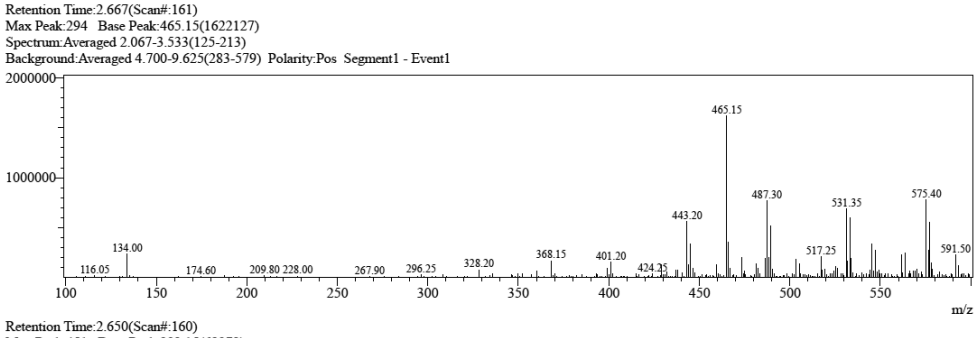

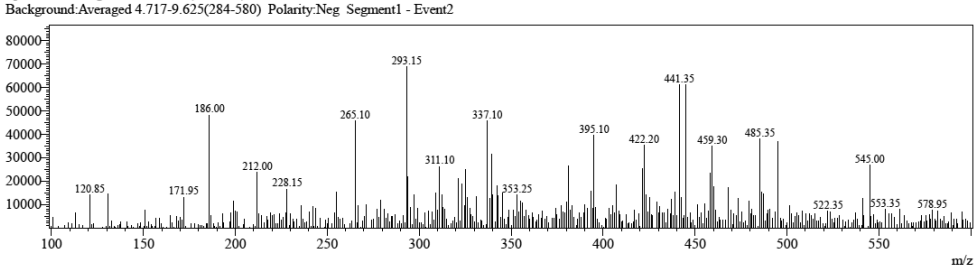

HPLC of H8

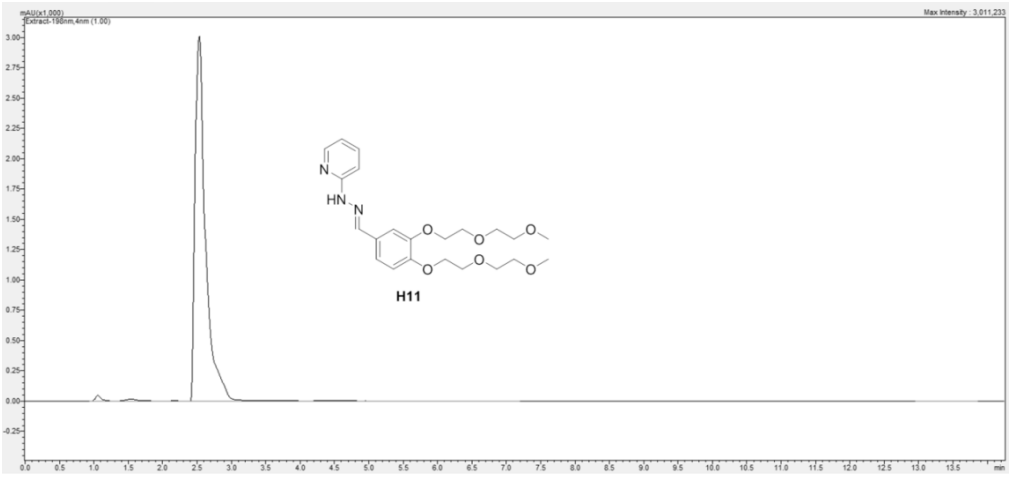

Retention Time:0.633(Scan#:39)
Max Peak:769 Base Peak:456.05(3194885)
Spectrum:Averaged 0.400-0.833(25-51)
Background:Averaged 1.333-2.378(81-143) Polarity:Pos Segment1 - Event1

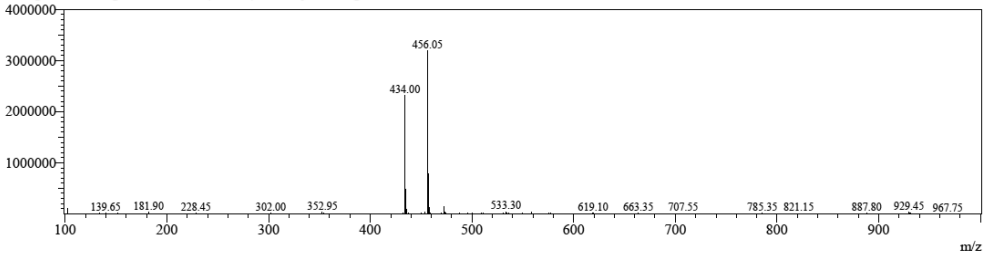

Retention Time:0.617(Scan#:38)
Max Peak:658 Base Peak:249.00(15725)
Spectrum:Averaged 0.417-0.850(26-52)
Background:Averaged 1.350-2.378(82-144) Polarity:Neg Segment1 - Event2

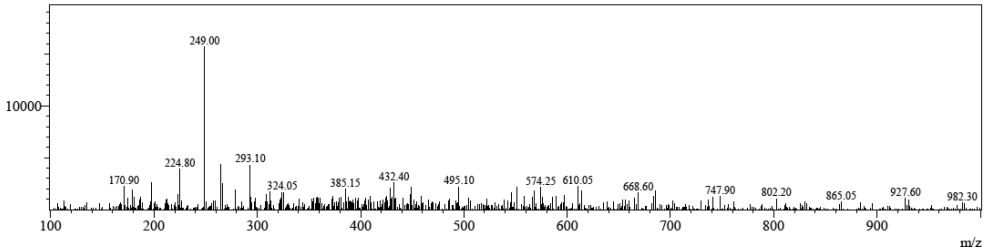

HPLC of H11

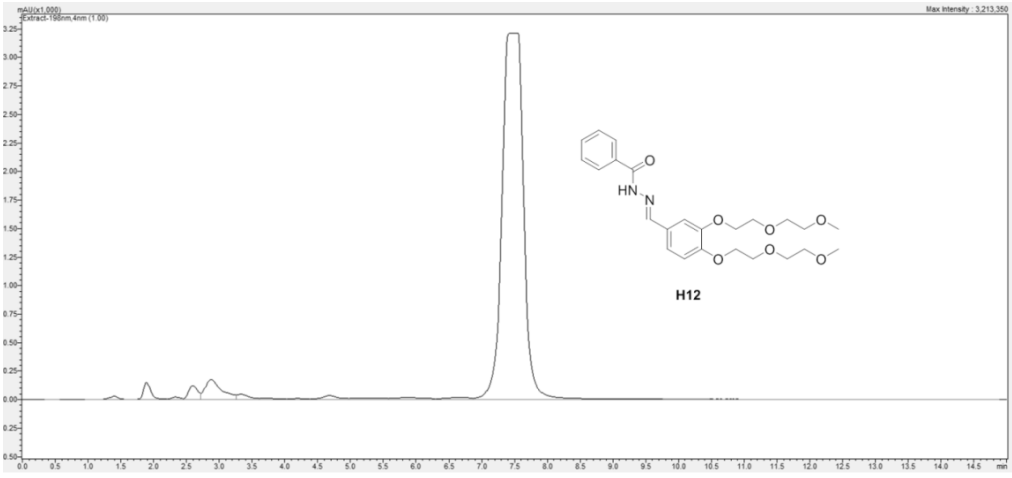

Retention Time:7.367(Scan#:443)
Max Peak:541 Base Peak:483.10(1507506)
Spectrum:Averaged 6.500-9.133(391-549)
Background:None Polarity:Pos Segment1 - Event1

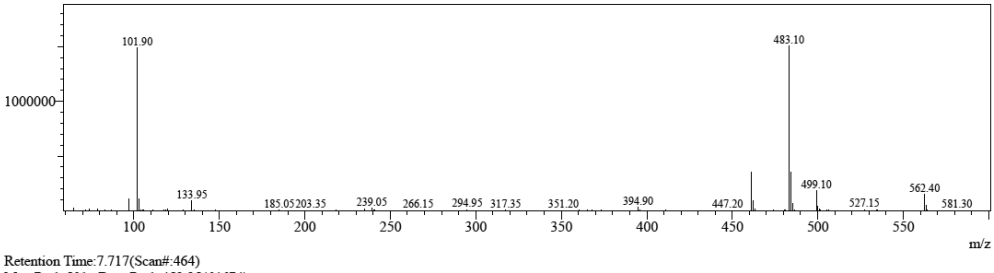

Retention Time:7.717(Scan#:464)
Max Peak:501 Base Peak:459.25(64674)
Spectrum:Averaged 6.517-9.150(392-550)
Background:None Polarity:Neg Segment1 - Event2

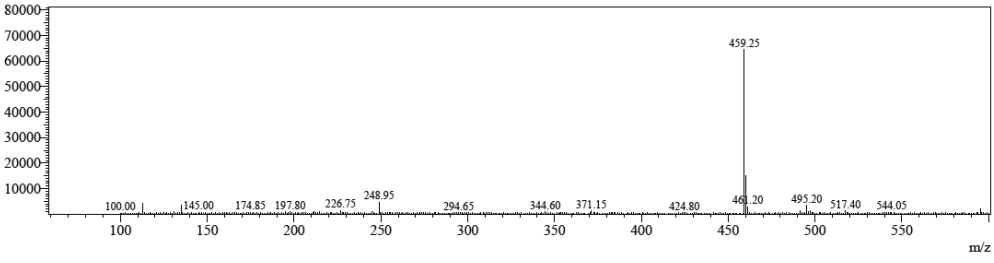

HPLC of H12

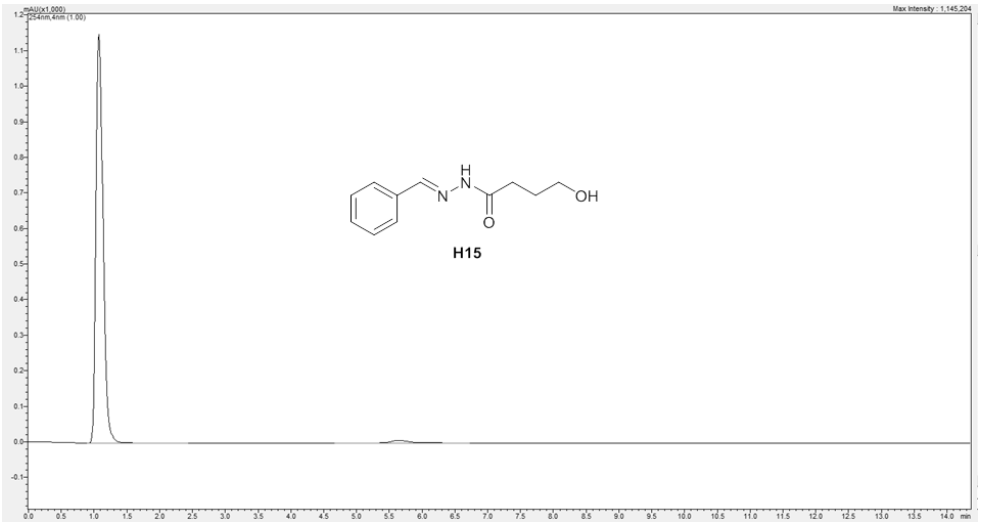
H15

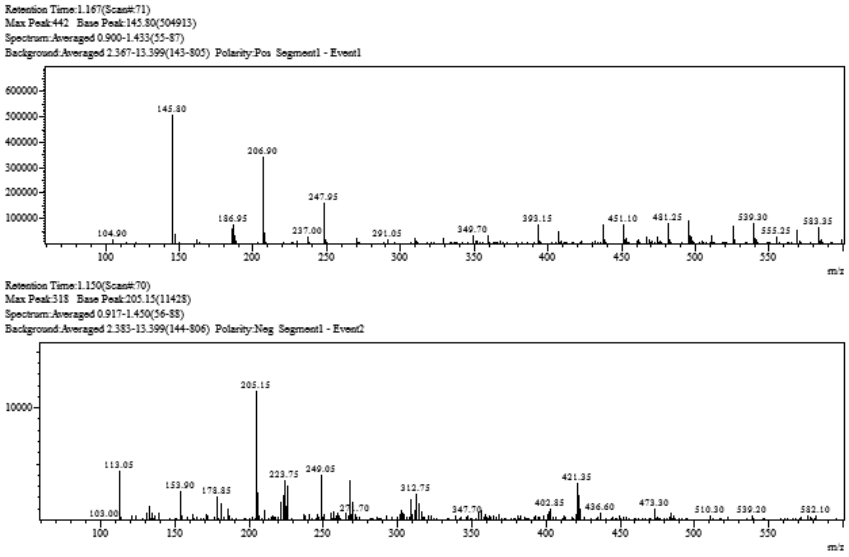
Retention Time:1.167(Scan#:71)
Max Peak:442 Base Peak:145.80(504913)
Spectrum:Averaged 0.900-1.433(55-87)
Background:Averaged 2.367-13.399(143-805) Polarity:Pos Segment1 - Event1
145.80
206.90
247.95
104.90
186.95
237.00
291.05
349.70
393.15
451.10
481.25
539.30
555.25
583.35
m/z
Retention Time:1.150(Scan#:70)
Max Peak:318 Base Peak:205.15(11428)
Spectrum:Averaged 0.917-1.450(56-88)
Background:Averaged 2.383-13.399(144-806) Polarity:Neg Segment1 - Event2
205.15
113.05
153.90
178.85
223.75
249.05
312.75
421.35
103.00
347.70
402.85
436.60
473.30
510.30
539.20
582.10
m/z

HPLC of H15

Supplementary References

1. Trausel, F., Maity, C., Poolman, J. M., Kouwenberg, D. S. J., Versluis, F., van Esch, J. H., Eelkema, R. Chemical signal activation of an organocatalyst enables control over soft material formation. *Nat. Commun.* **8**, 879 (2017).
2. Key, J. A., Li, C., Cairo, C. W. Detection of cellular sialic acid content using nitrobenzoxadiazole carbonyl-reactive chromophores. *Bioconjugate Chem.* **23**, 363-371 (2012).
3. Poolman, J. M., Boekhoven, J., Besselink, A., Olive, A. G. L., van Esch, J. H., Eelkema, R. Variable gelation time and stiffness of low-molecular-weight hydrogels through catalytic control over self-assembly. *Nat. Protoc.* **9**, 977-988 (2014).
4. Versluis, F*., et al.* Negatively charged lipid membranes catalyze supramolecular hydrogel formation. *J. Am. Chem. Soc.* **138**, 8670-8673 (2016).
5. Crisalli, P., Kool, E. T. Water-soluble organocatalysts for hydrazone and oxime formation. *J. Org. Chem.* **78**, 1184-1189 (2013).
6. Zhang, M., Shang, Z.-R., Li, X.-T., Zhang, J.-N., Wang, Y., Li, K., Li, Y.-Y., Zhang, Z.-H. Simple and efficient approach for synthesis of hydrazones from carbonyl compounds and hydrazides catalyzed by meglumine. *Synth. Commun.* **47**, 178-187 (2017).
7. Ru, Hwu J., Chieh Lin, C., Hsien Chuang, S., Yung King, K., Su, T.-R., Tsay, S.-C. Aminyl and iminyl radicals from arylhydrazones in the photo-induced DNA cleavage. *Bioorganic Med. Chem.* **12**, 2509-2515 (2004).
8. Deng, X., Mani, N. S. Regioselective synthesis of 1,3,5-tri- and 1,3,4,5-tetrasubstituted pyrazoles from n-arylhydrazones and nitroolefins. *J. Org. Chem.* **73**, 2412-2415 (2008).
9. Vantomme, G., Jiang, S., Lehn, J.-M. Adaptation in constitutional dynamic libraries and networks, switching between orthogonal metalloselection and photoselection processes. *J. Am. Chem. Soc.* **136**, 9509-9518 (2014).
10. Guggenheim, E. A. Xlvi. On the determination of the velocity constant of a unimolecular reaction. *Philos. Mag.* **2**, 538-543 (1926).
11. Hemalatha, M. R. K., Noorbatcha, I. An undergraduate physical chemistry experiment on the analysis of first-order kinetic data. *J. Chem. Educ.* **74**, 972 (1997).

Summary

Cells react to the environment by changing the activity of enzymes. Catalysts, such as enzymes, speed up reaction rates by lowering the activation energy of the reaction. Changing reaction rates by altering enzyme activity is used to temporarily increase the production of, for instance, a hormone or to change the mechanical properties of a cell. Control over enzyme activity is achieved in two different ways: by covalent modifications (e.g. phosphorylation) and by non-covalent interactions (allosteric enzymes). In this thesis we describe how we designed signal-responsive catalysts and used them to introduce signal response in artificial materials. Inspired by nature we developed a covalent and a non-covalent method to design catalysts that can react to signals from their environment. To design covalently protected catalysts we used self-immolative chemistry. A self-immolative molecule contains a signal-labile functional group. When this group reacts with the signal, the molecule fragments and releases a molecule of interest, in our case a catalyst.

In Chapter 2 we describe an organocatalyst that is activated by a chemical signal and that allows control over reaction rates and the formation of materials. Specifically, we designed a pro-catalyst that is activated by the chemical signal hydrogen peroxide and that releases the organocatalyst aniline that catalyses hydrazone formation. Activating the catalyst results in an immediate 10-fold increase in hydrazone formation rate. The responsive catalyst allows control over the formation rate and the properties of a supramolecular gel, as well as a polymer gel featuring hydrazone bonds.

In Chapter 3 we provide a generic strategy to design organocatalysts that can be activated by specific signals. To demonstrate the versatility of the design, we show three examples of organocatalysts that can be activated by three different signals and that can be used to control two different reactions. We synthesized three different protected proline catalysts: the first was activated by the chemical signal hydrogen peroxide, the second by light and the third by the enzyme Penicillin Acylase. The pro-prolines were used to control an aldol reaction between a ketone and an aldehyde and a Michael reaction between an nitro-olefin and an aldehyde. The pro-prolines did not show any catalytic activity without activation, whereas activating the pro-catalysts resulted in an immediate response in reaction rate. For

the aldol reaction, activating the pro-prolines resulted in a 2.5-fold increase in reaction rate: this increase was only modest because of a large background reaction. For the Michael reaction, activating the pro-proline had a more convincing result: without active catalyst, the reaction does not take place and activating the pro-proline initiated the reaction almost instantly.

In Chapter 4 we describe a non-covalent method to control the activity of organocatalysts, using host-guest chemistry. With the host molecule cucurbit[7]uril (CB[7]) we were able to decrease the catalytic activity of one organocatalyst by 3.5-fold, whereas we induced an 3-fold increase in activity for another catalyst. Addition of a stronger binding guest liberates the catalysts and restores the catalytic activity back to the original value. CB[7] enables precise control over the rate of hydrazone formation by adjusting the ratio of catalyst and CB[7]. We developed a kinetic model that can predict the reaction rates based on the concentrations of catalyst and CB[7].

Because we used hydrazone formation reactions in the design of supramolecular and polymer gels that are controlled by catalysis, we describe in Chapter 5 how we investigated a number of hydrazone formation reactions and their response to aniline catalysis. We found hydrazone formation reactions that are suitable for UV/vis analysis. The reaction rates differed with orders of magnitude and some reactions do not benefit from aniline catalysis whereas for other reactions the reaction rate increases up to 50-fold.

In conclusion, catalysts that can be activated by signals can be used to introduce signal response in chemical reactions and in materials. Self-immolative chemistry provides a generic strategy to protect a variety of organocatalysts that can be activated by different signals. Host-guest chemistry can be used to control the activity of organocatalysts and addition of a stronger binding guest can reverse this effect. Control over catalyst activity forms a promising strategy to design systems and materials that can respond to signals from the environment and can ultimately lead to communication between artificial chemical systems.

Samenvatting

Cellen reageren op de omgeving door de activiteit van enzymen te veranderen. Katalysatoren, zoals enzymen, verhogen reactiesnelheden door de activeringsenergie van de reactie te verlagen. Het veranderen van reactiesnelheden door de activiteit van enzymen aan te passen wordt gebruikt om bijvoorbeeld tijdelijk de productie van een hormoon te verhogen of om de mechanische eigenschappen van een cel aan te passen. De activiteit van enzymen kan op twee manieren worden beheerst: door covalente aanpassingen (bijvoorbeeld fosforylering) en door non-covalente interacties (allosterische enzymen). In dit proefschrift beschrijven we hoe we signaal-responsieve katalysatoren hebben ontworpen en hebben gebruikt om signaal-respons te introduceren in kunstmatige materialen. Geïnspireerd door de natuur hebben we een covalente en een non-covalente methode ontwikkeld om katalysatoren te ontwerpen die kunnen reageren op signalen uit de omgeving. Om covalent-beschermde katalysatoren te ontwerpen hebben we gebruik gemaakt van zelf-immolatieve chemie. Een zelf-immolatief molecuul bevat een signaal-labiele groep. Wanneer deze groep reageert met het signaal, fragmenteert het molecuul en wordt er een functioneel molecuul, in ons geval een katalysator, afgegeven.

In Hoofdstuk 2 beschrijven we een organokatalysator die wordt geactiveerd door een chemisch signaal en die het mogelijk maakt om reactiesnelheden en de vorming van materialen te beheersen. Om precies te zijn hebben we een pro-katalysator ontworpen die wordt geactiveerd door het chemische signaal waterstofperoxide en die de organokatalysator aniline vrijgeeft die hydrazoneformatie katalyseert. Het activeren van de katalysator heeft een 10-voudige versnelling van hydrazoneformatie tot gevolg. De responsieve katalysator maakt beheersing van de formatiesnelheid en de eigenschappen van zowel een supramoleculaire gel als een polymeergel met hydrazonebindingen mogelijk.

In Hoofdstuk 3 tonen we een generieke strategie om organokatalysatoren te ontwerpen die kunnen worden geactiveerd door specifieke signalen. Om de veelzijdigheid van het ontwerp te demonstreren laten we drie voorbeelden van organokatalysatoren zien die door drie verschillende signalen worden geactiveerd en die kunnen worden gebruikt om twee verschillende reacties te beheersen. We hebben drie verschillende beschermde proline-katalysatoren gesynthetiseerd: de eerste wordt geactiveerd door het chemische signaal

waterstofperoxide, de tweede door licht en de derde door het enzym Penicillin Acylse. De pro-prolines zijn gebruikt om een aldolreactie tussen een keton en een aldehyde te beheersen en een Michaelreactie tussen een nitro-olefin en een aldehyde. De pro-prolines vertonen geen enkele katalytische activiteit zonder activatie, terwijl de activatie van de pro-katalysatoren leidt tot een onmiddellijke respons in reactiesnelheid. Bij de aldolreactie leidt de activatie van de pro-prolines tot een 2.5-voudige toename in reactiesnelheid: de toename is bescheiden vanwege de hoge achtergrondreactie. Bij de Michaelreactie leidt de activatie van de pro-proline tot een overtuigender resultaat: zonder actieve katalysator verloopt de reactie niet en als de pro-proline wordt geactiveerd start de reactie meteen.

In Hoofdstuk 4 beschrijven we een non-covalente methode om de activiteit van organokatalysatoren te beheersen, met behulp van gastheer-gast chemie. Met het gastheermolecuul cucurbit[7]uril (CB[7]) waren we in staat de katalytische activiteit van een organokatalysator met een factor 3.5 te verlagen, terwijl we de katalytische activiteit van een andere organokatalysator juist met een factor 3 verhoogden. Het toevoegen van een sterker bindend gastmolecuul zorgt ervoor dat de katalysatoren weer worden vrijgegeven en brengt de katalytische activiteit terug naar de oorspronkelijke waarde. CB[7] maakt het mogelijk om de reactiesnelheid van hydrazoneformatie gecontroleerd te beheersen door de verhouding katalysator en CB[7] aan te passen. We hebben een kinetisch model ontwikkeld dat de reactiesnelheden kan voorspellen op basis van de concentraties katalysator en CB[7].

Omdat we hydrazonereacties gebruiken in het ontwerp van supramoleculaire gels en polymeergels die beheerst kunnen worden door katalyse, beschrijven we in Hoofdstuk 5 hoe we een aantal hydrazonereacties hebben onderzocht en hebben gekeken naar de respons op aniline-katalyse. We hebben hydrazonereacties gevonden die geschikt zijn voor UV-vis analyse. De reactiesnelheden verschillen met ordegroottes en sommige reacties hebben geen enkele baat bij aniline-katalyse terwijl andere reacties wel 50-keer worden versneld.

Concluderend, katalysatoren die geactiveerd kunnen worden door signalen kunnen worden gebruikt om signaalrespons in chemische reacties en materialen te introduceren. Zelf-immolatieve chemie vormt een generieke strategie om een verscheidenheid aan organokatalysatoren, die geactiveerd kunnen worden door verschillende signalen, te ontwerpen. Gastheer-gastchemie kan worden gebruikt om de activiteit van organokatalysatoren te beheersen en dit effect kan ongedaan worden gemaakt door een sterker bindend gastmolecuul toe te voegen. Het beheersen van katalysatoractiviteit vormt

een veelbelovende strategie om systemen en materialen te ontwerpen die op signalen uit de omgeving kunnen reageren en kan uiteindelijk leiden tot communicatie tussen kunstmatige chemische systemen.

Samenvatting voor een breder publiek

Een van de kenmerken van leven is het kunnen reageren op signalen uit de omgeving. Bacteriën kunnen bijvoorbeeld de aanmaak van eiwitten aanpassen aan de voedingsstoffen die aanwezig zijn in de omgeving, zonnebloemen kunnen zich naar het licht buigen en sommige soorten schimmel reageren op licht, zwaartekracht, wind en zelfs op de aanwezigheid van objecten.

Een van de manieren waarop organismen reageren op de omgeving is door de activiteit van enzymen te veranderen. Enzymen zijn speciale eiwitten die reacties katalyseren, het zijn natuurlijke katalysatoren. Katalysatoren verlagen de energie die je nodig hebt om een reactie te laten starten, de activeringsenergie, zonder dat ze daar zelf bij worden opgebruikt. Hierdoor versnellen ze die reacties: gekatalyseerde reacties die een paar minuten duren, zouden er soms anders duizenden jaren over doen. Als je de activiteit van enzymen, of andere katalysatoren, verandert, verander je dus ook de snelheid van de reactie die wordt gekatalyseerd.

De natuur maakt gebruik van regulerende enzymen die geactiveerd of juist gehinderd worden door bepaalde signalen uit de omgeving. Hierdoor kan een cel op de omgeving reageren door bijvoorbeeld meer hormoon te produceren, zijn membraan doordringbaarder te maken voor bepaalde stoffen, of zich te gaan delen. Enzymen worden op twee manieren geactiveerd of gedeactiveerd: op een covalente manier (met behulp van fosforylering) en op een niet-covalente manier (allosterische enzymen). Covalente verbindingen zijn de bindingen tussen de atomen die een molecuul vormen. Een molecuul water bestaat bijvoorbeeld uit twee atomen waterstof en een atoom zuurstof die met een covalente verbinding aan elkaar vast zitten. Een voorbeeld van een non-covalente interactie is de interactie tussen keukenzout en water dat er aan vastgeplakt zit als je het zoutvaatje te lang open hebt laten staan.

Het doel van het onderzoek dat beschreven wordt in dit proefschrift is om signaalrespons te introduceren in materialen met behulp van katalysatoren. Materialen die op de omgeving kunnen reageren zouden in de toekomst gebruikt kunnen worden om medicijnen naar bepaalde plekken in het lichaam te brengen en alleen af te geven op het moment dat dit nodig is. Als we een systeem zouden kunnen ontwikkelen waardoor kankermedicijnen

alleen afgegeven worden in tumors, zouden mensen gezond haar kunnen houden terwijl ze een chemokuur ondergaan. Andere toepassingen kunnen zijn het maken van sensoren en van zachte robots die gebruikt kunnen worden in operaties, als exoskelet of om tomaten te verpakken.

Om signaalrespons in materialen te introduceren met behulp van katalysatoren staan we voor twee uitdagingen. Ten eerste hebben we materialen nodig waarin de verbindingen vatbaar zijn voor katalyse: alleen reacties die versneld worden door katalysatoren zijn geschikt. Ten tweede hebben we katalysatoren nodig die je aan (en wellicht ook weer uit) kan zetten met behulp van een signaal.

Laten we het eerst eens hebben over die materialen. De materialen die we gebruiken zijn hydrogels. Hydrogels bestaan voor 99% uit water en voor 1% uit een netwerk van verbindingen die dit water bij elkaar houdt. Inderdaad, haargel is ook een hydrogel, maar andere voorbeelden zijn de bolletjes die in luiers zitten, zachte contactlenzen en pudding. Polymeergels bestaan uit hele lange moleculen die op twee manieren een gelnetwerk kunnen vormen: als de polymeermoleculen in de knoop raken, is het een fysische gel en als de polymeermoleculen covalente cross-linkverbindingen maken, is het een chemische gel (Figuur 1a). Als je de vorming van die covalente cross-linkverbindingen kan katalyseren, is dit een goede kandidaat om als signaalresponsief materiaal te gebruiken. Een ander type hydrogel wordt gemaakt van kleine moleculen die een non-covalente interactie met elkaar aangaan: dit zijn de supramoleculaire gels (Figuur 1b). Deze kleine moleculen, gelators genoemd, lossen niet graag op in water: ze zijn een beetje hydrofoob. Omdat moleculen altijd in beweging zijn, bewegen de gelatormoleculen naar elkaar toe en stapelen ze zich zo op dat de binnenkant van de moleculen, die het meest hydrofoob is, afgeschermd wordt van het water: zo bouwen de gelatormoleculen uit zichzelf een georganiseerde structuur: dit wordt zelf-assemblage genoemd. De gelatormoleculen vormen een gel doordat ze zich opstapelen tot lange draden die in de knoop raken en zo een gelnetwerk vormen. In onze groep is een twee-componenten gelator ontwikkeld: als deze twee wateroplosbare stoffen met elkaar reageren wordt de gelator gevormd. De reactiesnelheid tussen deze twee stoffen kan je beïnvloeden met katalysatoren.

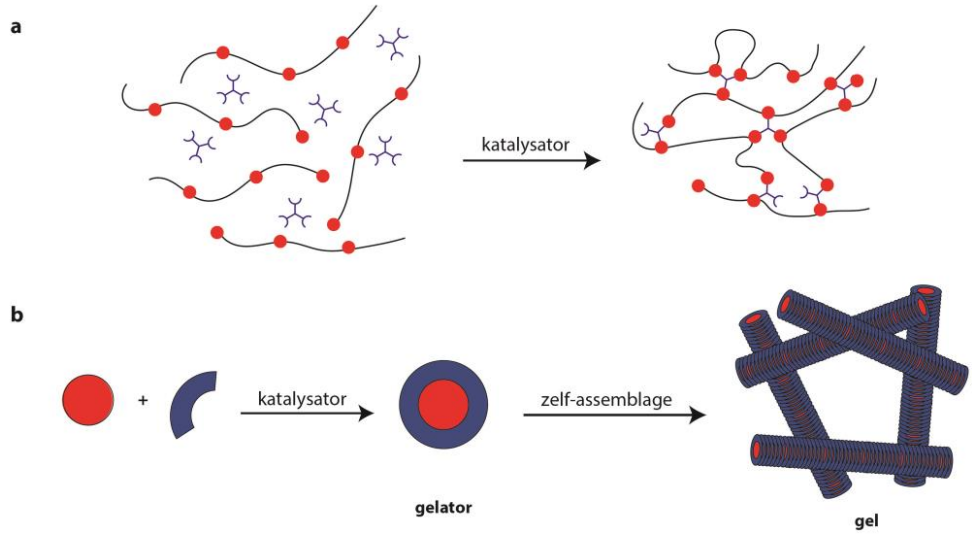

Figuur 1: Hydrogel netwerken. (**a**) Een polymeergel die covalente cross-links aangaat en op die manier een gelnetwerk vormt. (**b**) Twee wateroplosbare stoffen reageren met elkaar onder invloed van een katalysator en vormen een gelator. Deze gelator stapelt zich op en vormt zo een gelnetwerk.

Nu blijft de vraag: op welke manier kan je katalysatoren maken die je aan of uit kunt zetten en welke soorten katalysatoren bestaan er eigenlijk? Voor katalysatoren wordt er onderscheid gemaakt op basis van of ze wel of niet oplossen. Als ze niet oplossen worden ze heterogene katalysatoren genoemd: deze worden veel in de industrie gebruikt omdat je ze gemakkelijk kan terugwinnen. Homogene katalysatoren lossen wel op: deze worden weer onderscheiden in twee soorten: de organometaalkatalysatoren en de organokatalysatoren. Organometaalkatalysatoren bestaan uit een combinatie van een metaal en organische stoffen die een non-covalente verbinding met elkaar hebben. Organokatalysatoren bestaan uit kleine organische moleculen. Omdat organokatalysatoren de meest simpele katalysatoren zijn, hebben we ervoor gekozen om dit soort katalysatoren signaalresponsief te maken. Geïnspireerd door de natuur hebben we, zowel op een covalente manier als op een non-covalente manier, organokatalysatoren gemaakt die kunnen reageren op signalen uit de omgeving. Ik zal eerst de covalente en daarna de non-covalente manier bespreken.

In de natuur worden enzymen op een covalente manier geactiveerd of gedeactiveerd door er stukken molecuul op te zetten of af te halen. Met dit idee hebben we een signaal-labiele blokkerende groep op een organokatalysator gezet. Deze blokkerende groep zorgt ervoor

dat de katalysator niet meer werkt. De signaal-labiele groep reageert met een specifiek signaal uit de omgeving en zorgt ervoor dat de blokkerende groep eraf valt en de katalysator weer beschikbaar is om te katalyseren. De signaal-labiele blokkerende groepen zijn speciaal ontworpen om snel met een signaal te reageren en gemakkelijk uit elkaar te vallen: het wordt zelf-immolatieve chemie genoemd, omdat de stoffen zodra de signaal-labiele groep eraf is uit zichzelf uit elkaar vallen. Om ervoor te zorgen dat de zelf-immolatieve stoffen gemakkelijk uit elkaar vallen, worden ze vaak zo ontworpen dat er een gas vrijkomt als ze fragmenteren. Zelf-immolatieve chemie wordt nu vooral gebruikt om pro-drugs te maken: dit zijn medicijnen met een signaal-labiele groep erop die pas actief worden als er een bepaalde stof in het lichaam aanwezig is die deze blokkerende groep eraf haalt. Er zijn signaal-labiele groepen die eraf vallen onder invloed van licht, anderen worden eraf geknipt door bepaalde enzymen of door specifieke chemische stoffen. Voor zover we weten zijn wij de eerste die signaal-labiele stoffen gebruiken om pro-katalysatoren te maken die op de omgeving kunnen reageren (Figuur 2).

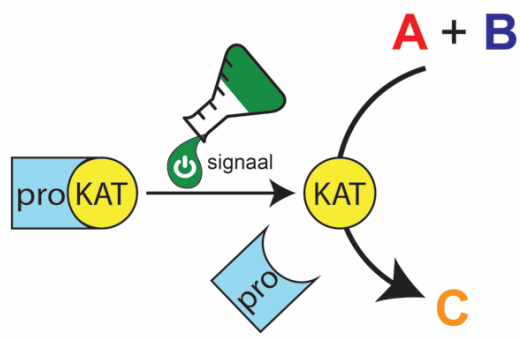

Figuur 2: Een pro-katalysator wordt geactiveerd met een signaal en kan dan een chemische reactie katalyseren.

In hoofdstuk 2 beschrijven we hoe we een organokatalysator hebben gemaakt die je kunt activeren met een chemisch signaal en die je kan gebruiken om de reactiesnelheid en de eigenschappen van twee soorten hydrogels te beïnvloeden. We hebben een zeer simpele organokatalysator gemodificeerd die de vorming van de supramoleculaire gelator (Figuur 1a) en van de gecrosslinkte polymeergel (Figuur 1b) katalyseert. We hebben deze katalysator geblokkeerd met een signaal-labiele groep: deze groep reageert met het chemische signaal waterstofperoxide. Waterstofperoxide wordt aangemaakt als cellen zich ziek voelen en zou dus gebruikt kunnen worden om ziektes te detecteren. De signaal-labiele

blokkerende groep werkt goed: zonder de aanwezigheid van het chemische signaal werkt de pro-katalysator niet, pas als we waterstofperoxide toevoegen wordt de actieve katalysator vrijgegeven. Als we de reactie volgen met de pro-katalysator en we voegen het signaal toe, zien we dat de reactie meteen 10 keer sneller verloopt.

Om te kijken wat voor invloed de pro-katalysator heeft op de vorming van gels hebben we gebruik gemaakt van de 'omgedraaide potjes test' (Figuur 3). Voordat de gel is gevormd zijn alle stoffen nog in oplossing: pas als het netwerk is gevormd ontstaat er gel. Om te zien of er een gel vormt kan je simpelweg kijken of het oplosmiddel nog stroomt of dat het juist bij elkaar gehouden wordt in een gelnetwerk door het potje ondersteboven te zetten: alleen een gel zal aan de bodem blijven plakken. Op die manier zagen we dat de supramoleculaire gel alleen vormt met een actieve katalysator. De polymeergel vormt zowel met als zonder actieve katalysator: maar met katalysator vormt de gel ongeveer 2 keer zo snel.

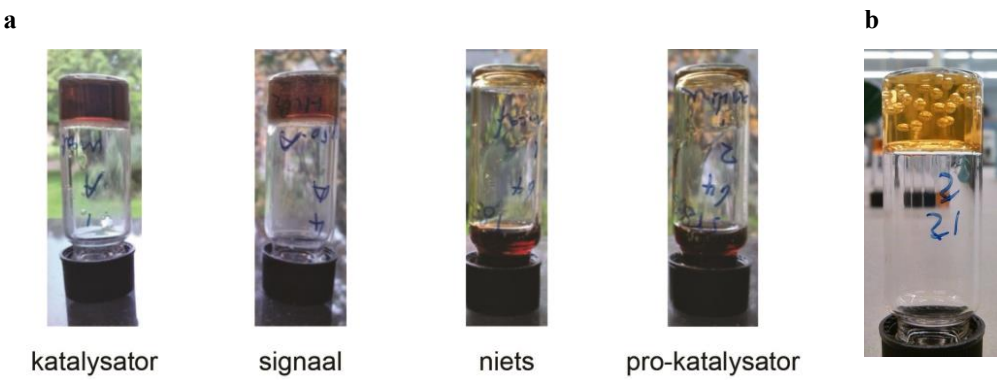

Figuur 3: Omgedraaide potjes test om te kijken of we de polymeergel hebben gevormd: als het materiaal op de bodem blijft plakken is het een gel en als het naar beneden stroomt is het (nog) een vloeistof. (**a**) Van links naar rechts: met katalysator (gel), met pro-katalysator en het signaal (gel), zonder katalysator (geen gel), met pro-katalysator zonder het signaal (geen gel). (**b**) Als we de pro-katalysator activeren met het signaal komt hier CO_2 gas bij vrij, dat kan je zien aan de bubbels in de gel. Een close-up van deze foto is gebruikt voor de kaft van dit proefschrift.

De vorming van de polymeergel hebben we op een meer kwantitatieve manier onderzocht, namelijk met een rheometer. Op een rheometer kan je de vorming van een gel volgen en meten wanneer je een gel vormt en hoe stijf deze gel is. Dit doen we door een plaat zachtjes te laten oscilleren op het mengsel waarin de gel vormt. Zolang het nog een vloeistof is zal

alles meebewegen met de oscillatie, maar een gel zal een beetje tegen gaan werken: de kracht waarmee de gel de vervorming tegenwerkt is een maat voor de stijfheid van de gel. Met behulp van rheologie hebben we gemerkt dat de polymeergel niet alleen sneller vormt met een actieve katalysator, maar ook resulteert in een stijvere gel: de snelheid waarmee de cross-links vormen bepaalt dus ook hoeveel cross-links er vormen.

a **b**

Figuur 4: De rheometer. Het mengsel waarin de gel vormt wordt op de onderste plaat gegoten. De bovenste plaat ligt op de gel en oscilleert zachtjes. De kracht waarmee het materiaal het oscilleren tegenwerkt is een maat voor de stijfheid van de gel. (**a**) De rheometer in gebruik. (**b**). De gel is gevormd op de rheometer.

Nu waren we benieuwd of we de pro-katalysator konden gebruiken om een materiaal te maken dat kan reageren op een chemische verandering in de omgeving. Daarom volgden we de vorming van de gel met de pro-katalysator op de rheometer en voegden we na een bepaalde tijd het chemische signaal waterstofperoxide toe. Omdat we zagen dat de snelheid waarmee de gel werd gevormd meteen toenam en dat de resulterende stijfheid van de gel ook was toegenomen, kunnen we concluderen dat het materiaal uit zichzelf reageerde op de aanwezigheid van het chemische signaal.

De methode die we gebruikten om de pro-katalysator van hoofdstuk 2 te maken is algemeen toepasbaar: je kunt de methode gebruiken om een grote verscheidenheid aan organokatalysatoren te maken die weer door allerlei verschillende signalen worden geactiveerd. In hoofdstuk 3 bespreken we deze algemene manier om pro-katalysatoren te maken. Om te laten zien dat de methode inderdaad algemeen toepasbaar is hebben we drie verschillende pro-katalysatoren gemaakt die door drie verschillende signalen worden geactiveerd en die vervolgens twee verschillende chemische reacties katalyseren. De eerste

pro-katalysator wordt geactiveerd door het chemische signaal waterstofperoxide, de tweede door licht en de derde door een enzym. Nadat we hadden gecheckt of de pro-katalysatoren inderdaad de actieve katalysator vrijgeven als we het goede signaal aanbrengen, hebben we gekeken hoe ze de snelheid van de twee reacties beïnvloeden. De reacties met de ongeactiveerde pro-katalysator waren even langzaam als wanneer we geen katalysator gebruiken. Als we de pro-katalysator activeren zien we dat de reactie meteen sneller verloopt. Het algemene ontwerp voor pro-katalysatoren kan de basis vormen om meer systemen te maken die op signalen uit de omgeving kunnen reageren.

Nu hebben we laten zien hoe we op een covalente manier katalysatoren kunnen maken die op signalen kunnen reageren, maar dit kan ook met non-covalente interacties: bijvoorbeeld met gastheer-gast chemie. Een gastheer molecuul is een groot molecuul met een holte erin waar een of meerdere gastmoleculen kunnen worden vastgehouden. Het is bekend dat de reactiviteit van gastmoleculen verandert als ze door een gastheer worden vastgehouden. Daarom vroegen wij ons af of de activiteit van organokatalysatoren als ze binden met een gastheer ook verandert. Een gastheermolecuul dat er om bekend staat dat hij in water sterk bindt aan een grote verscheidenheid aan gastmoleculen is de cucurbituril. De cucurbituril heeft zijn onuitspreekbare naam te danken aan het feit dat hij qua vorm op een uitgeholde pompoen (Cucurbita) lijkt. We hebben ontdekt dat de cucurbituril (CB) sterk bindt aan de katalysator uit hoofdstuk 2 (katalysator 1) en aan een andere katalysator voor dezelfde reactie (katalysator 2). Als we dezelfde soort reactie volgen als die we in hoofdstuk 2 hebben gebruikt met katalysator 1, zorgt CB ervoor dat de reactie langzamer verloopt (Figuur 5). Met katalysator 2 zien we juist het tegenovergestelde: als we CB toevoegen aan de reactie met katalysator 2 gaat de reactie juist sneller. Door te binden hindert CB de katalytische activiteit van katalysator 1 terwijl deze voor katalysator 2 juist wordt versterkt.

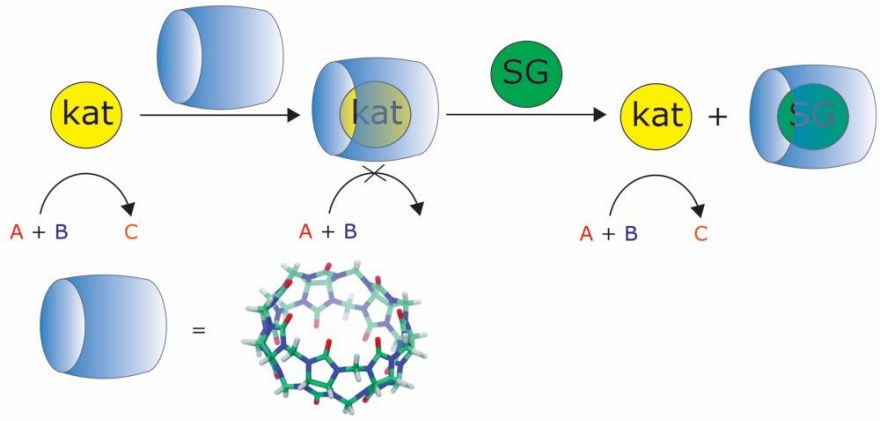

Figuur 5: Cucurbituril (CB) bindt aan katalysator 1 en hindert daarmee de katalyse. Als we een sterker bindende gast, de supergast (SG) toevoegen dan neemt die de plek in van de katalysator, zodat de katalysator weer beschikbaar is om de reactie te katalyseren.

De pro-katalysatoren uit hoofdstuk 2 en 3 hebben het nadeel dat je ze aan kan zetten, maar niet meer uit: de activeringsstap is irreversibel. We stelden ons voor dat we de niet-covalente interactie tussen CB en de katalysator daarentegen wellicht wel ongedaan konden maken door een gastmolecuul toe te voegen dat nóg sterker bindt: de supergast neemt dan de plaats in van de katalysator waardoor die weer vrij in oplossing is. Inderdaad, als we de reactie volgen met katalysator 1 en we voegen CB toe, dan gaat de reactie meteen 3,5-keer zo langzaam. Als we vervolgens de supergast toevoegen gaat de reactie weer even snel als in het begin. De reactie met katalysator 1 kunnen we dus uitzetten met CB en weer aanzetten met de supergast. Met katalysator 2 is het precies andersom: als we CB toevoegen gaat de reactie meteen 3-keer zo snel en als we vervolgens de supergast toevoegen gaat de reactie weer even langzaam als in het begin. De reactie met katalysator 1 kunnen we dus juist aanzetten met CB en weer uitzetten met de supergast.

Nu zal je je waarschijnlijk afvragen waarom CB de ene katalysator hindert en waarom het de andere katalysator juist activeert. Dit vragen wij ons ook af en op dit moment weten we niet precies hoe dit komt. Een mogelijke verklaring kan zijn dat katalysator 1 een kleiner molecuul is en daarom helemaal ingepakt wordt door CB. Katalysator 2 is groter en kan daarom misschien een beetje uit de CB uitsteken. We hebben onderzocht of we door de concentratie katalysator 1 of 2 en de concentratie CB te variëren, precies kunnen bepalen welke reactiesnelheid we krijgen. Als we de concentratie katalysator 1 constant houden en

we voegen meer CB toe, dan gaat de reactie steeds langzamer. En als we de concentratie CB constant houden en we voegen meer katalysator 1 toe, dan gaat de reactie steeds sneller. Wat er gebeurt met katalysator 1 en CB kunnen we volledig theoretisch verklaren. Met katalysator 2 is het daarentegen een heel ander verhaal. Als we de concentratie katalysator 2 constant houden en we voegen meer CB toe, verwachten we dat de reactie sneller zal verlopen, en dit gebeurt ook. Als we de concentratie CB constant houden en we voegen meer katalysator 2 toe, verwachten we ook dat de reactie sneller zal gaan, en dit gebeurt ook. Wat we alleen niet kunnen verklaren, is dat de reactiesnelheid veel harder omhoog gaat dan we verwachten. Het lijkt erop dat CB, katalysator 2, en katalysator 2 die gebonden is aan CB elkaar als katalysator versterken: dat er sprake is van een synergistisch effect. Het zou interessant zijn om te onderzoeken hoe dit precies komt en of we dit synergistische effect ook voor andere katalysatoren kunnen vinden. Hoe dan ook, door de concentratie katalysator 1 of 2 en de concentratie CB te variëren, kunnen we precies bepalen welke reactiesnelheid we krijgen. De non-covalente manier met gastheer-gast chemie lijkt dus ook een veelbelovende methode om de activiteit van katalysatoren te beïnvloeden.

In hoofdstuk 2 en 4 maken we gebruik van hetzelfde soort reactie (hydrazoneformatie). Uitleggen hoe deze reactie precies werkt gaat buiten de strekking van deze samenvatting. Het volstaat om aan te geven dat het om een reactie gaat die zeer geschikt is om hydrogels mee te maken. In hoofdstuk 5 bespreek ik een overzicht van dit soort reacties. We hebben reacties onderzocht waarvan je de reactie met UV/vis (ultra violet / visible) spectroscopie kunt volgen. UV/vis is een techniek waarmee je kijkt welke kleur licht wordt geabsorbeerd: iets dat er groen uit ziet absorbeert bijvoorbeeld alle kleuren behalve groen. Een chemische reactie waarvan het product een andere kleur heeft dan de beginstoffen kan je met UV/vis volgen. In Figuur 6 zie je cuvetten met daarin reactiemengsels: voor deze reactie geldt, hoe roder het mengsel, hoe meer product er is gevormd.

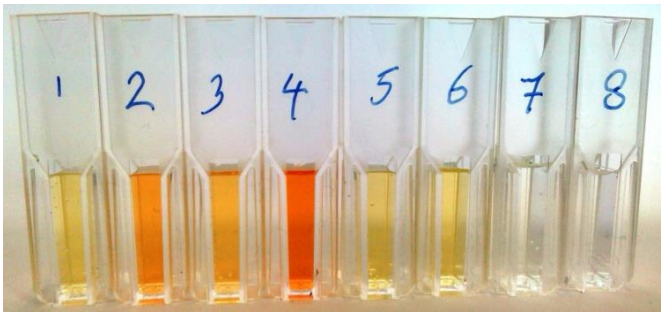

Figuur 6: Reactiemengsel in cuvetten voor UV/vis analyse.

We hebben getest hoe snel de reacties verlopen en hoe ze reageren op katalysator 1. We hebben gemerkt dat sommige reacties helemaal niet sneller gaan als we katalysator 1 toevoegen, terwijl andere reacties juist tot 50 keer worden versneld. Het lijkt erop dat reacties die van zichzelf al snel zijn, weinig baat hebben bij katalyse, maar dat de reacties die van zichzelf langzaam zijn, wel sterk versnellen met katalysator. Zo'n overzicht van reactiesnelheden en de invloed van katalyse is belangrijk om de juiste reactie te kiezen als je bijvoorbeeld een materiaal wilt maken dat kan reageren op de omgeving.

Concluderend, katalysatoren die geactiveerd worden door signalen kunnen worden gebruikt om materialen te maken die op de omgeving reageren. Het functionaliseren van katalysatoren met signaallabiele groepen vormt een breed toepasbare methode om katalysatoren te maken die worden geactiveerd door signalen uit de omgeving. Met gastheer-gast chemie kunnen katalysatoren op een niet-covalente manier geactiveerd of juist gedeactiveerd worden en dit effect kan ongedaan worden gemaakt door een sterker bindend gastmolecuul toe te voegen. Katalysatoren die op signalen kunnen reageren zijn veelbelovend voor de ontwikkeling van nieuwe responsieve materialen. Zo zijn we een stap dichter bij medicijntransport naar tumors, kweekmaterialen voor weefsels en nieuwe zachte robots.

Acknowledgements

None of the work you read about in this thesis would have been accomplished without the help of others. In this important part of the thesis you will meet the people who helped in any way with my PhD. How I longed to write the acknowledgements. It means that the thesis is almost finished. Now that I have reached this point, I feel a bit at a loss, because it also means that I have to say goodbye to all my colleagues who have become my dear friends over the last four years. When I was making an NMR sample a few months ago it suddenly occurred to me that it might be my last NMR sample I was making. Many days in the lab I hoped my lab work would soon be finished, but now that it is, I know I will miss it. Not that I will miss the 9 out of 10 failed experiments, especially now that I realize it was usually my own mistake they failed. I will mostly miss experiments number 10, the ones that are successful. Luckily, these are the experiments that we will remember. Fortunately as well, this is not only the ending of an eventful chapter in my life, but also the beginning of an exciting new one.

First of all I would like to thank Rienk, my daily supervisor and promotor. Thank you for giving me the opportunity to do my PhD. Despite being incredibly busy, somehow you always found time to check my papers. I learned a lot from you, especially how to be a good researcher and about communicating in a clear way. Dear Jan, thank you for being my promotor and teaching me how to become a good scientist, to learn which questions to ask and to be critical of results. Eduardo, you always remind me to use my curiosity as a scientist, sometimes our conversations left me utterly confused and I am grateful for everything you taught me. Ger, thank you for your wise words, I can still remember how thermodynamics seemed amazingly easy when you explained it to us as first year students. Stephen, thank you for letting me help you with the Electrical Cabinet. It is fun to see all those excited faces when you fire up the Tesla coil. I would also like to thank my committee members Tim, Ulf, Sylvestre, Syuzanna, Leonard, Freek and Stephen for taking the time to read my thesis and for challenging me during the defence. And because there is

no such thing as a free lunch (okay, except for lunch colloquia) I would like to thank NWO (Nederlandse Organisatie voor Wetenschappelijk Onderzoek) for funding the research.

Bowen, thank you for your help with the hydrazones. I will miss your endless enthusiasm to learn.
Susan, het was altijd gezellig om met je op kantoor te zitten ook al hield ik je soms van je werk. Het was leuk om samen met je naar Glasgow te reizen. Soms moest ik zuchten als ik je kritische opmerkingen over het hydrazone paper en het cucurbituril paper las, maar de artikelen zijn er wel een stuk beter van geworden. Bedankt dat je paranimf wilt zijn ook al ben je waarschijnlijk net zo zenuwachtig als ik tijdens verdediging.
Jos, de lunchpauzes zijn een stuk saaier en braver zonder jouw ongepaste grapjes. Bedankt dat je me wegwijs hebt gemaakt in het lab toen ik begon.
Dainius, I remember how overjoyed you were when you received your graduation date. Thank you for your help on my first days at ASM.
Emanuela, you serve as a great example, I rarely met anyone so purposeful as you.
Elena, thank you for brightening up my days in the lab.
Chandan, you can make any molecule one can possibly think of. Thank you for your endless patience to answer all my questions.
Ben, het was altijd gezellig bij de rheometer. Dank je wel voor je hulp.
Marcel, jij kunt als geen ander verhalen vertellen, of het nu over een avontuur gaat dat je hebt meegemaakt of over de uitvinding van buskruit. Bedankt voor je tips over woningen in Heemskerk, we hebben er een mooi huis gekocht.
Louw, soms kan je een beetje mopperen, maar zodra het over zeilen gaat begin je te stralen.
Mieke, jou moeten we voor altijd missen. Bedankt voor je geduld en voor de gezelligheid.
Stephen Eustace, ik ben jou ontzettend dankbaar. Dankzij jouw tomeloze inzet om de Agilent aan de praat te krijgen ben ik nu klaar met mijn PhD.
Verby, dank je wel voor je inzet en je hulp bij het verzamelen van handtekeningen voor alle formulieren.
Michelle, je bent niet alleen de beste student van de TU maar ook een gezellige collega. Je hebt me geïnspireerd om mijn werkaanpak te verbeteren. Ik vind het geweldig dat je verder gaat met de pro-katalysatoren.

Tobias, ik heb bewondering voor je eindeloze uithoudingsvermogen en je vindingrijkheid om moeilijke syntheses uit te voeren in het lab. Ik vind het leuk dat je verder gaat met de cucurbiturils.

Peggy, I only just met you, but I am impressed with your catching positivity and your moving story about Gandalf the seahorse.

Simge, you left ASM already a long time ago, but I still miss your kindness and your cooking.

Yiming, I am convinced you will become professor soon. Thank you for your wise counsel and interesting stories about China.

Fan, it was nice to be your office mate, even though it was only for one week or so.

Hendrik, thank you for your interesting stories.

Kai, I am very impressed how you managed to finish your PhD while you were doing a postdoc and raising a child.

Matija, drinks are much less eventful when you are not there. Thank you for your help when I was finishing my thesis.

Tomasz, you made me realize that it is important to keep a hobby, or two, or six. We had a lot of fun hiking. Thank you for letting us visit you in Glasgow and for being my paranymph.

Benjamin, we had a lot of fun during the survival run. I am impressed with your determination.

Vasu, you are always very attentive. I am very curious to see which career path you take. Just make sure you keep singing.

Serhii, you are always calm and wise. We miss your expertise in the lab.

Tonny, bedankt voor je hulp met de veiligheid en het inrichten van een goede werkplek.

Cansel, I will miss your cheerful personality. Thank you for your help in the lab.

Zenhu, thank you for your interesting stories about your background near Tibet. I have to remember to beware if you bring food that you find only a 'little' spicy.

Peter-Leon, bedankt voor het installeren van de ITC en dat je me op zo'n korte termijn nog het ITC programma kon geven. Hierdoor heb ik alles netjes op tijd af kunnen krijgen.

Angie, I will miss your calm kindness.

Dear Emma, you keep impressing me by raising two lovely daughters and still having time to do your PhD and to be a fun colleague.

Qian, you are always very wise and patient. Thank you for helping out with the survival run.

Wouter, het was gezellig om samen te helpen bij Stephen's elektrische kabinet, bedankt voor je tips voor mijn PhD.

Roman, you are always ready to join for drinks. We had a lot of fun canoeing.

Lars, bedankt voor je hulp in het lab. Ik heb je boeken nu wel gelezen, ze hebben geholpen bij mijn sollicitaties.

Sander, het was altijd gezellig. Bedankt voor je hulp met de PDMS. Ik heb veel geleerd van je doorzettingsvermogen.

Saida, bedankt voor je tips over solliciteren, het heeft me geholpen om een baan te vinden.

Qingzhu, as my student it was my job to teach you, but I learned just as much from you. Thank you for being always enthusiastic to learn and for showing such a great perseverance in the lab.

LO1 studenten, het was een groot genoegen om jullie les te mogen geven. Ik vind het geweldig dat sommige studenten ASM zo leuk vonden dat ze terug zijn gekomen. Anthea, leuk dat je terug kwam bij ASM en dat je mee deed met de survivalstrijd. Pepijn, ik heb het grootste vertrouwen erin dat je het goed zal doen.

Frank, van jou heb ik ontzettend veel geleerd. Je hebt me niet alleen geleerd hoe je goed schrijft, maar ook hoe je je experimenten op een goede manier uitkiest.

Katarzyna, it was fun being your office mate. I hope you are reunited more permanently with Lucas very soon.

Karolis, thank you for your advice about finishing my thesis.

Vincent, het was altijd gezellig in het lab. Bedankt voor je hulp.

Ruud en Ard-Jan, dankzij jullie heb ik de keuze gemaakt om een PhD te gaan doen. Bedankt voor jullie wijze lessen.

Alastair en Petra, bedankt dat jullie me aangenomen hebben. Mijn enthousiasme voor mijn nieuwe baan en de strikte deadline die het met zich meebracht hebben me geholpen om vlot mijn PhD af te maken.

Helpdesk, Edwin en Arco, bedankt dat jullie mijn computerproblemen altijd zo vliegensvlug hebben opgelost.

Annelies, bedankt dat je zo snel een mooie kaft voor me hebt ontworpen.

Alle trainers van Slopend, bedankt dat jullie altijd zulke afwisselende trainingen maken en ervoor zorgde dat ik boven op een opstakel even geen tijd had om me druk te maken over mijn metingen.

Jacqueline, bedankt voor je geduld om mijn pogingen tot fluiten aan te horen. Dankzij jou kan ik nu fluiten zonder de kat weg te jagen.

O'Panter, wat gezellig dat je altijd langs komt. Bedankt dat je af en toe op mijn toetsenbord gaat zitten om ervoor te zorgen dat ik pauze neem.

Lieve papa en mama, jullie steunen me altijd in wat ik ook onderneem. Bedankt dat jullie geduldig en met interesse alle ingewikkelde verhalen over mijn experimenten hebben aangehoord.

René en Agatha, bedankt dat jullie altijd begrip toonden als ik soms geen tijd had om langs te komen of bij jullie aan mijn artikelen door moest werken. Jullie hebben Harm een fijne jeugd bezorgd en hem opgevoed tot de man waar ik van houd.

Joppe, het blijft een spektakel om te zien hoe jij en Harm iets delen. Bedankt voor je interesse in mijn onderzoek en je hulp bij het zoeken naar een baan.

Oma, bedankt dat je het altijd gezellig vindt als ik langskom. Nu ga ik iets doen dat iets makkelijker uit te leggen is.

Harm, jij bent mijn ware liefde, de liefde van mijn leven, mijn wederhelft. Door jou ben ik een beter mens. Bedankt dat je me altijd steunt, zelfs als ik de gekkigheid in mijn hoofd haal om een PhD te gaan doen.

About the author

Fanny Trausel was born on the 2nd of December 1988 in Dordrecht, the Netherlands. She obtained her B.Sc. degree in Molecular Science and Technology (2011) in the combined education of Leiden University and Delft University of Technology. In 2013 she obtained her M.Sc. degree in Chemistry with a specialization on Design and Synthesis. Her Master Thesis was focussed on the synthesis of copper complexes as possible catalysts for the reduction of CO_2 in the Metals in Catalysis, Biomimetics & Inorganic Materials group. She also participated in a summer exchange internship with Williams College in Massachusetts where she worked on copper complexes for the atomic transfer radical polymerization of styrene. Furthermore, at TNO, she worked on the encapsulation of salt hydrates for thermochemical storage. In 2013 she started her PhD at Delft University of Technology in the group of prof. Jan H. van Esch under the supervision of dr. Rienk Eelkema. The work on responsive organocatalysis in soft materials resulted in the thesis you are reading now.

List of publications

1. Maity C., Trausel F., Eelkema R. Selective activation of organocatalysts by specific signals. *Chem. Sci.*, (2018).
2. Trausel F., Fan B., Rossum S. A. P. v., Esch J. H. v., Eelkema R. Aniline catalysed hydrazone formation reactions show a large variation in reaction rates and catalytic effects. *Adv. Synth. Catal.* **360**, 2571-2576 (2018).
3. Trausel F., Maity C., Poolman J. M., Kouwenberg D. S. J., Versluis F., van Esch J. H., Eelkema R. Chemical signal activation of an organocatalyst enables control over soft material formation. *Nat. Commun.* **8**, 879 (2017).
4. Versluis F.*, et al.* Negatively charged lipid membranes catalyze supramolecular hydrogel formation. *J. Am. Chem. Soc.* **138**, 8670-8673 (2016).
5. Trausel F., Versluis F., Maity C., Poolman J. M., Lovrak M., van Esch J. H., Eelkema R. Catalysis of supramolecular hydrogelation. *Acc. Chem. Res.* **49**, 1440-1447 (2016).
6. de Jong A.-J., Trausel F., Finck C., van Vliet L., Cuypers R. Thermochemical heat storage – system design issues. *Energy Procedia* **48**, 309-319 (2014).
7. Trausel F., de Jong A.-J., Cuypers R. A review on the properties of salt hydrates for thermochemical storage. *Energy Procedia* **48**, 447-452 (2014).